Pathological Epithelial Cell Apoptosis and Shedding in the Murine Small Intestine

Thesis submitted in accordance with the requirements of the University of Liverpool for the degree of Doctor in Philosophy by Jonathan Martin Williams

October 2013

Acknowledgements

I would firstly like to thank the Centre for Integrative Mammalian Biology for providing funding for my PhD project. The British Society of Toxicological Pathology, and The Comparative Pathology Educational Trust also provided much appreciated financial support to attend conferences. I would also like to thank collaborators Alastair Watson, Mark Frey, Jennifer Miguel, Lyndsay Hall, and Kevin Hughes for their contributions to this project, and Jorge Caamaňo, Mark Taylor, Alice Halliday, Simon Clare, Gordon Dougan and Shizuo Akira for the provision and generation of transgenic mice. Carrie Duckworth and Mike Burkitt, since the beginning of this project, have generously sacrificed their time in providing practical and theoretical teaching and advice, for which I am very grateful. I would also like to thank Dave Berry for his enthusiastic logistical help in the laboratories. My supervisors Mark Pritchard and Barry Campbell deserve special mention for providing scientific wisdom, guidance, and support throughout the project. Finally, I would like to thank Katie for her encouragement and support during my postgraduate studies.

Pathological Epithelial Cell Apoptosis and Shedding in the Murine Small Intestine

Jonathan Martin Williams

The intestinal epithelium represents a critical component of the gut barrier and is composed of a single layer of intestinal epithelial cells (IECs) held together by tight junctions. This epithelium prevents the entrance of harmful microorganisms, antigens and toxins from the gut lumen into the circulation. Small intestinal homeostasis is maintained by the rate of shedding of senescent enterocytes from the villus tip exactly matching the rate of generation of new cells in the crypt. However, in various localised and systemic inflammatory conditions, intestinal homeostasis may be disturbed as a result of increased IEC shedding. Such pathological IEC shedding may cause transient gaps to develop in the epithelial barrier and result in increased intestinal permeability. Although pathological IEC shedding has been implicated in the pathogenesis of inflammatory bowel disease, understanding of the underlying mechanisms remains limited. This thesis describes the development of a murine model to study this phenomenon, as IEC shedding in this species is morphologically analogous to humans. IEC shedding was induced by systemic lipopolysaccharide (LPS) administration in wild-type C57BL/6 mice, and mice deficient in TNF-receptor 1 (*Tnfr1*$^{-/-}$), *Tnfr2*$^{-/-}$, Nuclear Factor kappa B1 (*Nfκb1*$^{-/-}$) or *Nfκb2*$^{-/-}$. IEC apoptosis and cell shedding was quantified using immunohistochemistry for active Caspase-3 and gut lumen to systemic circulation permeability was assessed by measuring plasma fluorescence following fluorescein isothiocyanate-dextran gavage. LPS at doses ≥0.125mg/kg induced rapid villus IEC apoptosis and cell shedding which was maximal at 1.5h. This coincided with significant villus shortening, fluid exudation into the gut lumen and diarrhoea. A significant increase in gut to circulation permeability was observed at 5h. TNFR1 was essential for LPS-induced IEC apoptosis and shedding and the fate of the IEC was also dependent on NFκB, with signalling via NFκB1 favouring cell survival, and via NFκB2 favouring apoptosis. This model will enable investigation of the importance and regulation of pathological IEC apoptosis and cell shedding in intestinal and systemic diseases.

Contents

Abbreviations 10
1. GENERAL INTRODUCTION 15
1.1 The Small Intestine 16
1.2 Epithelial Turnover in the Small Intestine 16
1.3 Epithelial Cell Types of the Small Intestine 20
1.4 Epithelial Junctional Complexes 23
1.5 Intestinal Epithelial Cell Shedding 26
1.6 Small Intestinal Epithelial Gaps 31
1.7 Epithelial Cell Death and Shedding in the Small Intestine 34
1.7.1 Necrosis 35
1.7.2 Apoptosis 35
1.7.3 Necroptosis 40
1.7.4 Intestinal Epithelial Cell Shedding and Detachment 41
1.8 Stimuli Which Cause Intestinal Epithelial Cell Death 42
1.8.1 Tumour Necrosis Factor 43
1.8.2 Intestinal Ischaemia 45
1.9 Pathogenesis of Sepsis and Endotoxic Shock 46
1.9.1 The Role of Lipopolysaccharide 48
1.9.2 Intestinal Vascular Supply 55
1.9.3 Nuclear Factor kappa B Signalling in Endotoxic Shock 58
1.9.4 Inhibitors of NFκB 60
1.9.5 Activation of NFκB 61
1.9.6 Effects of Lipopolysaccharide on Enterocytes 63
1.10 Hypothesis, Aims and Objectives 66

2. MATERIALS AND METHODS 68
2.1 Experimental Design 69
2.2 Mice Examined 70
2.3 Generation of *Nfκb1*$^{-/-}$, *Nfκb2*$^{-/-}$ and *cREL*$^{-/-}$ mice 71
2.4 Generation of *Tlr4*$^{-/-}$ mice 72
2.4.1 Genotyping of *Tlr4*$^{-/-}$ mice 72
2.5 Generation of *Tnfr1*$^{-/-}$ and *Tnfr2*$^{-/-}$ mice 74
2.6 Generation of *vil-Cre Myd88*$^{-/-}$ mice 75
2.7 Lipopolysaccharide Administration 75
2.8 Recombinant TNF 76
2.9 Tissue Sampling and Processing 76
2.10 Transmission Electron Microscopy 79
2.11 Haematoxylin and Eosin (H&E) Staining 79
2.12 Active Caspase-3 Immunohistochemistry 80
2.12.1 Stage 1 of Immunohistochemistry 80
2.12.2 ABC Method for Active Caspase-3 Immunohistochemistry 81
2.12.3 Envision™ Method for Active Caspase-3 Immunohistochemistry 81
2.12.4 Immunohistochemistry Method Comparison 82
2.12.5 Active Caspase-3 Antibody Titration 82
2.13 Active Caspase-3 Scoring Criteria 83
2.13.1 Quantification of Active Caspase-3 Immunohistochemistry 85
2.14 Cell Positional Data for Active Caspase-3 Immunohistochemistry 86
2.15 Consistency of Active Caspase-3 Immunohistochemical Scoring 86
2.16 Consistency of LPS Induced IEC Apoptosis and Shedding Between Laboratories 88
2.17 Image Analysis of Active Caspase-3 Immunohistochemistry 90
2.18 Villus Height By Graticule Measurement 91

2.19 Measurement of Villus Height by Image J....91
2.20 Gut Permeability Assays....92
2.21 Tissue for RNA and Protein Extraction....93
2.22 RNA Extraction....93
2.23 Reverse Transcription....94
2.24 Real-time PCR (qPCR)....94
2.25 Protein Extraction and Western Blotting....96
2.26 Anaesthetic Protocol Evaluation....97
2.27 *In vivo* Confocal Microscopy....99
2.28 Data and Statistics....100

3. Effects of LPS on the Epithelial Cells of the Gastrointestinal Tract 101
3.1 Introduction....102
3.2 Systemic LPS administration caused clinical signs and gross pathological alterations from 1.5 hours....103
3.3 LPS caused small intestinal injury manifested by villus IEC shedding from 1.5 hours....104
3.4 LPS caused highly dynamic small intestinal epithelial cell apoptosis and cell shedding with concomitant activation of caspase-3....106
3.5 LPS did not cause significant apoptosis in the small intestinal crypts....110
3.6 LPS caused rapid villus atrophy in the duodenum, jejunum, and ileum....112
3.7 LPS induced apoptosis and cell shedding which increased in frequency towards the villus tip....116
3.8 *In vivo* confocal microscopy allowed identification of shedding cells in real time....119
3.9 LPS caused a significant increase in gut permeability by 5h....121

3.10 Ultrastructural examination of LPS induced IEC cell death and shedding 123

3.11 Effects of LPS dosage and purification on small intestinal epithelial apoptosis and cell shedding 124

3.11.1 LPS purity did not significantly affect IEC apoptosis and cell shedding in WT mice 125

3.11.2 Dose dependent effects of LPS on the small intestine 127

3.11.3 There was no significant gender difference in LPS response 130

3.12 Discussion 132

4. Mechanisms by which LPS Causes IEC Death and Cell Shedding .. 139

4.1 Introduction 140

4.2 IEC apoptosis and shedding is caused by systemic LPS but not by LPS administered within the intestinal lumen 142

4.3 LPS-induced apoptosis and cell shedding were significantly decreased in *Tlr4*$^{-/-}$ mice 143

4.4 Peripheral TLR signalling mediates LPS-induced IEC apoptosis and shedding 147

4.5 LPS induced changes in small intestinal cell death associated gene transcription 149

4.6 TNF caused small intestinal injury equivalent to LPS 152

4.7 *Tnfr1*$^{-/-}$ mice were completely resistant to LPS-induced apoptosis and cell shedding 155

4.8 Discussion 157

5. NFκB Regulation of Pathological IEC Apoptosis and Cell Shedding 169

5.1 Introduction 170

5.2 *Nfκb1*$^{-/-}$ mice were more sensitive, and *Nfκb2*$^{-/-}$ mice more resistant to LPS induced intestinal injury 171

5.3 *Nfκb1*$^{-/-}$ mice were highly sensitive, and *Nfκb2*$^{-/-}$ mice more resistant to TNF induced small intestinal injury 177

5.4 *Nfκb1*$^{-/-}$ mice exhibited crypt apoptosis in response to TNF 180

5.5 LPS caused small intestinal p100 processing to p52 in 1.5h 182

5.6 LPS treated *Nfκb2*$^{-/-}$ mice exhibited increased amounts of RelB by western blot 183

5.7 Positive RelB immunolabelling was detectable in villus IECs in LPS treated *Nfκb2*$^{-/-}$ mice 184

5.8 Discussion 186

6. DISCUSSION 196

6.1 Summary of Major Findings and Conceptual Advances 197

6.2 Limitations of the Study 200

6.3 Translational Impact 205

6.4 Future Investigations 206

6.5 Conclusions 210

7. BIBLIOGRAPHY 212

8. APPENDICES 227

8.1 Lipopolysaccharide Administration in Mice 227

8.2 Publications, Abstracts and Presentations during the Project 228

8.3 A Mouse Model of Pathological Small Intestinal Epithelial Cell Apoptosis and Shedding Induced by Systemic Administration of Lipopolysaccharide 231

Abbreviations

ABC: Avidin biotin complex

ANOVA: Analysis of variance

APES: 3-Aminopropyltriethoxylsilane

ATP: Adenosine-5'-triphosphate

BAFF: B-cell activating factor

Bak: Bcl-2 homology interacting-domain death antagonist protein

Bax: B cell associated X protein

BCL: B-cell lymphoma protein

Bid: Bcl-2 associated death promoter protein

Birc3: Baculoviral inhibitor of apoptosis repeat containing 3 protein

CBC: Crypt base columnar cells

CD: Crohn`s disease

c-FLIP: Cellular FLICE-like inhibitory protein

c-IAP: Cellular inhibitor of apoptosis

DAB: 3,3′-Diaminobenzidine

DAMPS: Damage associated molecular patterns

DIC: Disseminated intravascular coagulopathy

DSS: Dextran sodium sulphate

E. coli: *Escherichia coli*

EDTA: Ethylenediaminetetraacetic acid

ES: Embryonic stem cell

FADD: Fas associated death domain

FITC: Fluorescein isothiocyanate

GALT: Gastrointestinal associated lymphoid tissue

H&E: Haematoxylin and eosin

HIF1α: Hypoxia inducible factor 1 alpha

HSP70: Heat shock protein 70

IAP: Intestinal alkaline phosphatase

IBD: Inflammatory bowel disease

IEC: Intestinal epithelial cell

IE-LPS: Ion-exchange chromatography purified LPS

IFNγ: Interferon gamma

IgA: Immunoglobulin A

IgG: Immunoglobulin G

IgM: Immunoglobulin M

IHC: Immunohistochemistry

IκB: Inhibitor of NFκB

IKK: Inhibitor of NFκB kinases

IL: Interleukin

i.m.: Intramuscular

iNOS: Inducible nitric oxide synthase

i.p.: Intraperitoneal

IRAK: IL-1 receptor associated kinase

i.v.: Intravascular

kDa: Kilodaltons

LBP: Lipopolysaccharide binding protein

Lgr5: Leucine-rich repeat-containing G-protein coupled receptor 5

LPS: Lipopolysaccharide

MAPK: Mitogen-activated protein kinase

MDCK: Madin-Darby canine kidney cells

MHC: Major histocompatibility complex

MLCK: Myosin light chain kinase

MODS: Multiple organ dysfunction syndrome

MyD88: Myeloid differentiation primary response (88) protein

NEC: Necrotising enterocolitis

NEMO: NFκB essential modulator

NFκB: Nuclear factor kappa B

NIK: NFκB inducing kinase

NOD: Nucleotide-binding oligomerization domain-containing receptor

PAMPS: Pathogen associated molecular patterns

PBS: Phosphate-buffered saline

PCR: Polymerase chain reaction

PE-LPS: Phenol extracted lipopolysaccharide

PRR: Pattern recognition receptor

PUMA: p53 upregulated modulator of apoptosis

RHD: Rel homology domain

RIP: Receptor-interacting protein

ROCK: Rho-associated kinase

SEM: Standard error of the mean

SI: Small intestine

SIRS: Systemic inflammatory response syndrome

TACE: Tumour necrosis factor converting enzyme

TAD: Transcription activation domain

TBST: Tris-buffered saline, 0.1% Tween®20

TCA: Trichloroacetic acid

TEM: Transmission electron microscopy

TLR: Toll-like receptor

TNF: Tumour necrosis factor alpha

TNFR: Tumour necrosis factor receptor

TRADD: Tumour necrosis factor associated death domain

TRAFs: Tumour necrosis factor receptor associated factors

TRAIL: Tumour necrosis factor related apoptosis inducing ligand

TRIF: TIR-domain-containing adapter-inducing interferon-β

TUNEL: Terminal deoxynucleotidyl transferase dUTP nick end labelling

UC: Ulcerative colitis

Unt: Untreated

Wnt: Wingless-int

WT: Wild-type

XIAP: X-linked Inhibitor of apoptosis

ZO-1: Tight junction protein 1

1. GENERAL INTRODUCTION

1.1 The Small Intestine

The small intestine is lined on its inner surface by millions of villus projections covered by a single cell thick epithelium. This epithelium is highly specialised to efficiently digest, transport and regulate the absorption of nutrients and water into the circulation. It is also a critical component of the gut barrier, which as part of the innate immune system, precludes the entry of harmful microbes, toxins, and antigens from the intestinal lumen. The arrangement of this specialised epithelial monolayer minimises the distance that nutrients must be transported from the lumen into the immediately subjacent circulatory system of the villus. However, this also dictates that breaches of this delicate epithelium potentially expose the underlying tissue and vasculature to harmful luminal content. The intestinal epithelium is anchored to a basement membrane which overlies a lamina propria composed of myofibroblasts and a collagen framework. The basement membrane is composed predominantly of laminin and type IV collagen, which epithelial cells are capable of secreting *in vitro*, with contribution of interstitial collagens and procollagen 3 by myofibroblasts being required to produce a complete basement membrane (Hahn et al. 1987).

1.2 Epithelial Turnover in the Small Intestine

The small intestinal epithelium is constantly being renewed and replaced every 3-5 days in humans (and every 2-3 days in mice) by intestinal stem cells, and therefore has one of the most rapid cellular turnover rates of any fixed cell population. The intestinal stem cell compartment is contained within the flask like structures at the base of villi, known as the crypts of Lieberkühn.

Maintaining tissue homeostasis and a stable cell population is dependent on the loss of an equal number of cells as have been generated by cell division. Although early histological examinations of the small intestine allowed easy identification of mitotic activity in the intestinal crypts, it was not fully appreciated until 1948 (Leblond and Stevens), that the mechanism by intestinal epithelial cells (IECs) were lost, was by extrusion and shedding at the villus tip (Figure 1).

To put this cell loss into context, it is estimated that in mice up to 1400 mature enterocytes are shed from a single villus tip in a 24 hour period, equating to an estimated $2x10^8$ cells being shed per day from the small intestine. In humans, this daily loss has been estimated at 10^{11} cells (Potten 1990).

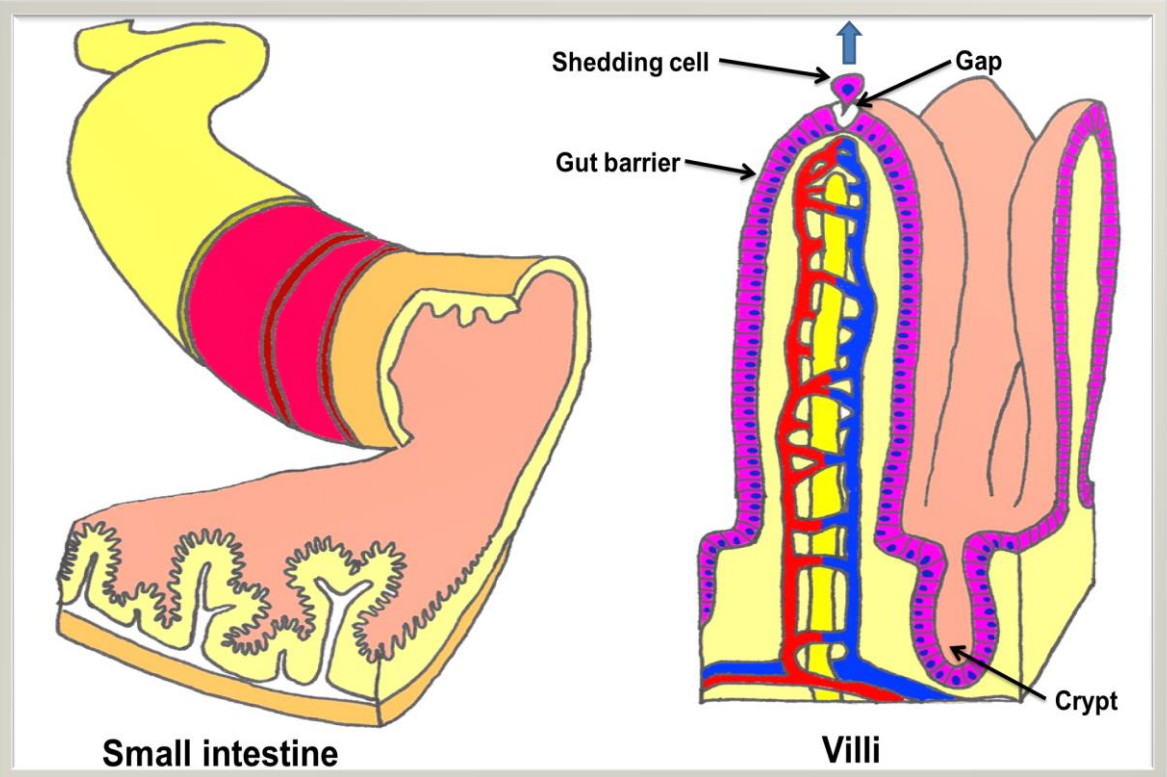

Figure 1: Illustration of intestinal epithelial cell turnover in the small intestine. New epithelial cells are generated in the crypt, and migrate up the villus until they are shed at the villus tip.

These estimates are based on investigation of crypt cell dynamics performed in male BDF1 mice (a hybrid strain resulting from crossing C57BL6 with DBA2 strains) (Potten 1990). In this study, it was found that there were approximately 6 crypts per villus, each containing around 250 cells per crypt. These crypts had a lifespan of approximately 2 years, with new crypts constantly being formed from fission of existing ones. Crypt cells were found to have an 11 hour cell cycle, with up to 60% of cells passing through the cell cycle each day.

These studies suggested that the crypt cell population contained approximately 4-16 actual stem cells (cell position 4-5 as counted from the crypt base) and up to 30-40 potential clonogenic stem cells which may become functional following perturbation of cell turnover. More recent studies have however suggested that the stem cell niche is substantially more complicated than this, with it being possible to further discriminate between proliferating progenitor stem cells, and transit amplifying cells which undergo further mitosis and differentiate into the four major types of intestinal epithelial cell. These cell types include enterocytes, goblet cells, enteroendocrine cells, and Paneth cells. These cells differentiate during their migration along the crypt-villus axis, with the exception of Paneth cells which migrate to the crypt base.

The location and identity of the definitive intestinal stem cell is still a matter of some debate. It has been recently suggested that crypt base columnar (CBC) cells, which reside below cell position 4 within crypts (Bjerknes and Cheng 1999), and express the stem cell marker leucine-rich repeat-containing G-

protein coupled receptor 5 (Lgr5) (Barker et al. 2007) are the actual stem cell population and give rise to transit amplifying cells. The *Lgr5* gene is a wingless-int (Wnt) target gene, and is expressed in stem cells at other sites apart from the intestine, including the hair follicle (Haegebarth and Clevers 2009), as well as in ovarian and hepatic neoplasia (Shaker and Rubin 2010). *In vivo*, the *Lgr5* expressing CBC cell has been demonstrated to fulfil the definition of the small intestinal stem cell; being capable of self-renewal, multipotency (Barker et al. 2007), and forming crypt-villus organoids in culture (Sato et al. 2009). Another quiescent stem cell population has been posited to reside at cell position 4, which positively label for B-cell lymphoma Mo-MLV insertion region 1 homolog (Bmi-1), homeodomain-only protein (Hopx), mouse telomerase reverse transcriptase (mTert), and leucine-rich repeats and immunoglobulin-like domains protein 1 (Lrig1). The control of proliferation and differentiation of IECs is dependent on the response of these cells to Wnt, bone morphogenic protein (BMP), notch, and epidermal growth factor (EGF) signalling. This has been reviewed by Sato and Clevers (2013).

The time it takes for an individual enterocyte to be generated in the crypt, migrate up the villus axis, and be shed at the villus tip is approximately 3-5 days in humans and 2-3 days in mice. Major questions remain surrounding what controls the migration of IECs towards the villus tip, their differentiation and maturation along this migration, and the cell death and shedding they undergo at the villus tip. It has been previously demonstrated that the migration of IECs is not dependent on forces generated by cell density

increases caused by mitosis in the crypt (Kaur and Potten 1986). Migration rate is however dependent on other influences, such as circadian rhythms (Kaur and Potten 1986), and intestinal flora. The importance of the intestinal flora in epithelial migration rate is illustrated in the context of gnotobiotic animals, where there is a slower turnover of enterocytes similar to that observed in the neonate, resulting in longer villi (Shanahan 2002). It has also been shown that gnotobiotic mice fail to absorb monosaccharides or to deposit adipose reserves as efficiently as conventionally housed mice. These effects were additionally found to be independent of lymphocyte responses (Backhed et al. 2004). By contrast, in animals that have achieved a maximum adult level of intestinal bacterial flora, epithelial turnover is much increased (Gelberg 2007). Differential epithelial expression of some integrins along the crypt-villus axis may also influence epithelial cell proliferation, migration and differentiation (Beaulieu 1992).

1.3 Epithelial Cell Types of the Small Intestine

Constituting the majority of villus epithelial cells, most new cells generated by the stem cell niche mature into absorptive enterocytes. These cells are responsible for absorbing and transporting amino acids, monosaccharides, electrolytes and water from the intestinal lumen into the intestinal capillaries, and lipids and lipoproteins into the central lacteal. Mature absorptive enterocytes of the villus possess a microvillus brush border at the apical pole with up to 3000, 1µm long microvilli, which greatly increase the surface area of the apical plasma membrane of the enterocyte. By contrast, immature crypt cells have sparse microvilli, little or no absorptive capacity, and are

considered to be the source of the secretory component of IgA (immunoglobulin A) and IgM (immunoglobulin M) and of chloride secretion (Gelberg 2007). Each microvillus has a central core of actin microfilaments arranged as a terminal web connected to the cytoskeleton which stabilises the apical membrane. Overlying the apical brush border, enterocytes are covered by a glycocalyx which contains glycoproteins, carbohydrates and enzymes projecting from the microvilli. Overlying and blending together with the glycocalyx, is the unstirred water layer consisting of goblet cell secreted mucus, acid mucopolysaccharides and trefoil factors. The enzymes attached to the microvillus brush border are responsible for the membranous phase of digestion, resulting in the breakdown of complex polymers into monomers and transcellular absorption through active transport (Herdt 1997).

Cells that make up the remainder of the population of the small intestinal epithelium include Paneth cells which are found together with stem cells within the crypts (Figure 2), enteroendocrine (neuroendocrine) cells, goblet cells, and microfold cells (also known as M cells). Goblet cells are found both in the crypt and villus regions and are involved in mucus secretion, and secrete trefoil factors which aid in epithelial gliding and restitution (Brown et al. 2007). Paneth cells complete their differentiation at the crypt base, and unlike other cell types, do not migrate along the crypt-villus axis. These cells are hypothesised to potentially protect the progenitor cells of the crypt from infection, and produce antibacterial peptides such as lysosyme, cryptidins and lysins, and other substances such as phospholipase, ribonuclease and tumour necrosis factor (TNF). In haematoxylin and eosin (H&E) stained

histological sections, Paneth cells possess abundant bright eosinophilic granules in their apical cytoplasm, and these cells are considered to have secretory and phagocytic functions (Gelberg 2007). Of note, Paneth cells are completely absent in certain species such as dogs, cats or pigs (Brown et al. 2007; Gelberg 2007), meaning that at least in some species, these cells are not an essential requirement for protection of the stem cell niche.

Enterochromaffin cells (a type of enteroendocrine cell) form part of the neuroendocrine system of the gut, producing hormones such as serotonin, catecholamines, gastrin, cholecystokinin, somatostatin, secretin, and enteroglucagon (Young 2006). Other specialised cell types include tuft cells which reside in the crypt, and are thought to be quiescent stem cells, expressing Lgr5 and doublecortin-like kinase (DCKL1) and have also been shown to produce opioids (Gerbe et al. 2011). M cells are far less common and overlie gastrointestinal associated lymphoid tissue (GALT). They are important in mucosal immunity as they perform immunosurveillance functions (Mabbott et al. 2013) and as such can be exploited by several pathogenic bacteria to invade into the subepithelial tissue.

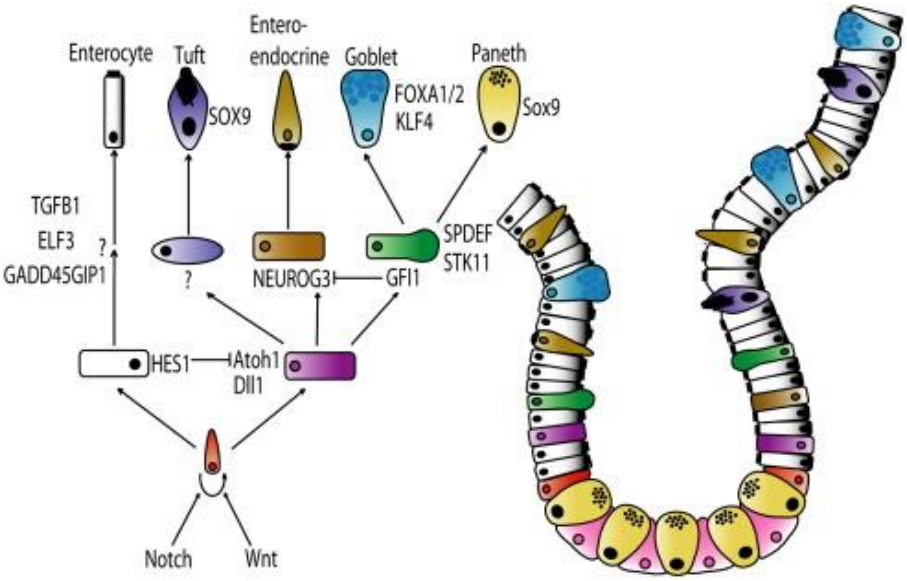

Figure 2: Schematic of possible differentiation pathways of the self-renewing intestinal stem cell (red and pink cell) under the influence of Wnt and Notch signalling. With the exception of Paneth cells, cells undergo migration out of the crypt base and onto the villus. Genes important in differentiation are indicated next to relevant cells. Notch signalling represses hairy and enhancer of split-1 (HES-1) and allows cells to differentiate into absorptive enterocytes. Reprinted from Experimental Cell Research 317(19): 2702-2710. Noah, T. K., B. Donahue and N. F. Shroyer (2011). "Intestinal development and differentiation." with permission from Elsevier.

1.4 Epithelial Junctional Complexes

Epithelial cells are attached to each other by a narrow continuous belt, or zonule, of tight junctions at their apical poles (Figure 3). This is fundamentally responsible for maintaining gut barrier function, i.e. occluding intestinal luminal content including bacteria, noxious substances, enzymes and foreign antigens from entering the lamina propria and the circulatory system. It is therefore also known as the *zonula occludens*. These tight junctions bring the plasma membrane of neighbouring enterocytes into extremely close proximity, being stitched together by sealing strands; consisting of a fusion of one molecule of the transmembrane protein claudin from each plasma

membrane. At their cytoplasmic aspect, these claudins are connected to the cytoskeleton.

Immediately deep to the *zonula occludens* is a belt of adhering junctions known as the *zonula adherens*, which connects to the actin cytoskeleton. Adhering junctions are composed of transmembrane proteins of the cadherin family. The cytoplasmic tail of cadherin proteins bind to anchor proteins such as catenins, vinculin, and α-actinin, which are respectively bound to cytoskeletal actin. *Macula adherens*/spot adhering junctions are positioned immediately deep to the *zonula adherens*, and although they form focal intercellular adhesions rather than a belt, they are otherwise similar to adhering junctions. They are composed of cadherin transmembrane proteins, anchored by desmoplakin and plakoglobin, which in turn connect to the cytokeratin intermediate filaments in neighbouring enterocytes. These cell junctions are generally considered together as a functional unit: the junctional complex. The junctional complex anatomically delineates the apical membrane of the epithelial cell superficial to the circumferential band of tight junctions, with the basolateral membrane being the portion of the epithelial cell that is located deep to the junctional complexes.

The narrow belt of junctional complexes tightly adhere neighbouring enterocytes to each other, essentially leaving the basolateral portion of the enterocyte unattached, except for at the hemidesmosome. This structure anchors the enterocyte to the basal lamina, thus creating the lateral space between neighbouring enterocytes. Hemidesmosomes are composed of transmembrane proteins of the integrin family, which are bound to laminins

via their extracellular component. These integrins are attached at their cytoplasmic tails to the anchoring protein plectin, which is in turn bound to cytokeratins (Young 2006).

The lateral space formed between neighbouring enterocytes is filled with extracellular fluid, which is separated from the lumen by tight junctions, and from the capillary network by the basal lamina. Tight junctions, whilst excluding macromolecules, are more permeable in the duodenum and jejunum, and do allow passive paracellular passage of small inorganic molecules such as electrolytes and water into the lateral space (Herdt 1997).

Gap junctions are also present where enterocytes share areas of closely apposed plasma membrane. These gap junctions are studded with transmembrane channels called connexons, which are aligned between neighbouring cells, each consisting of six transmembrane proteins of the connexin family. Connexons permit the passage of small molecules less than 1.5 nanometers (nm) in diameter, and exclude those of larger size or of negative charge. Gap junctions are hypothesised to be important in intercellular communication, the coordination of growth, development, differentiation, and electrical coupling (Young 2006). There are numerous different proteins that constitute the broad family of connexins, each conferring specific qualities to connexons. The connexons themselves may be open or closed depending on intracellular calcium concentrations, pH, or extracellular signals. In apoptotic cell death, when intracellular calcium is elevated, connexons become closed, which may prevent apoptotic related signals from influencing neighbouring viable cells (Dolowschiak et al. 2010).

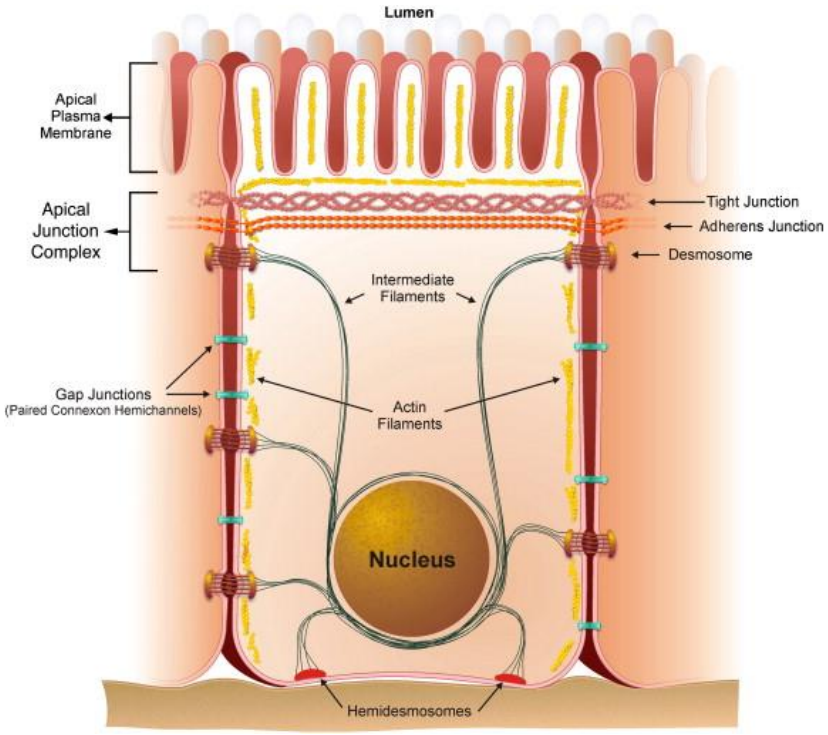

Figure 3: Diagram demonstrating intercellular and basement membrane adhesion of intestinal epithelial cells and the lateral spaces between cells which allow paracellular transport. Reprinted from Biochimica et Biophysica Acta (BBA) - Biomembranes, Volume 1788, Issue 4, Pages 832–841, (Guttman and Finlay 2009). © 2009, with permission from Elsevier.

1.5 Intestinal Epithelial Cell Shedding

Original observations in the rat small intestine suggested that enterocytes underwent shedding from the villus tip region into the gut lumen from what was termed the “extrusion zone” (Leblond and Stevens 1948). However, what dictates why mature enterocytes are shed at the villus tip is largely unknown, although it has been shown that the amounts of splice variant of acyl co-enzyme A synthetase 5 expressed in enterocytes increases towards the villus tip, which sensitises epithelial cells to TRAIL receptor mediated apoptosis (Gassler et al. 2007). Molecules of the extracellular matrix interact via β1-integrins and cadherins to provide constant survival signals through their associated adhesion mediated signalling pathways such as focal adhesion kinases, p125fak, PI3-K/Akt and Mitogen-activated protein kinase

(MAPK) to IECs, and have also been shown to show differential expression along the crypt-villus axis (Beaulieu 1992). In a *Cryptosporidium parvum* model of pathological epithelial cell shedding, it was also shown that infected enterocytes were prevented from shedding until reaching the villus tip by X-linked inhibitor of apoptosis (XIAP). An interesting alternative hypothesis is that cell shedding is induced by epithelial cells sensing cell crowding through stretch receptors such as Piezo1 (Eisenhoffer et al. 2012), which would explain the increased amounts of shedding observed at the villus tip.

Despite villus tip cell shedding occurring across species, the morphological features observed during the loss of senescent epithelial cells at the villus tip does show inter-species variation. In mice, whole enterocytes are shed, whereas in the guinea pig, apoptotic fragments are pinched off effete enterocytes leaving junctional complexes intact between neighbouring cells. In both reindeer and seals, fragments of shedding enterocytes are lost either by extrusion, or by phagocytosis performed by underlying macrophages (reviewed by Mayhew et al. 1999). Recent histological studies in humans have shown shedding to be of the whole cell extrusion type, and that shed enterocytes were not associated with lymphocytes or macrophages (Bullen et al. 2006). Therefore the mechanism of epithelial shedding in humans appears morphologically similar to the process in the mouse; suggesting that this is an appropriate species in which to study the process.

There are several hypothesised models for the process of extrusion of effete epithelial cells from the epithelial monolayer in whole cell extrusion. One of these is the zipper model, which is based on evidence from freeze-fracture

transmission electron microscopy studies. These showed that the enterocyte undergoing extrusion exhibits basolateral movement of tight junctions down the plasma membrane it shares with its neighbouring enterocytes (Figure 4). Neighbouring cells eventually extend processes underneath the shedding cell as it leaves the monolayer to reform tight junctions and maintain epithelial contiguity (Madara 1990).

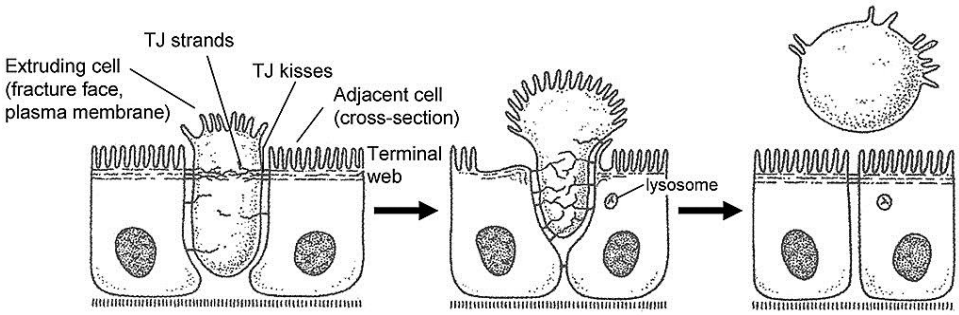

Figure 4: Diagram of a putative mechanism of epithelial cell shedding, showing rearrangement of the tight junctions and advancement of lamellipodia underneath the extruding cell in the “zipper model”. Reproduced from "Maintenance of the macromolecular barrier at cell extrusion sites in intestinal epithelium: physiological rearrangement of tight junctions." J Membr Biol 116(2): 177-184. Madara, J. L. (1990), Figure 8, with kind permission from Springer Science and Business Media.

In the context of *in vivo* studies of physiological enterocyte shedding in mice utilising confocal microscopy, it has been showed that one of the first events to be observed in an enterocyte which is destined to undergo shedding, is redistribution of tight junction protein 1 (ZO-1). This occurs approximately 15 minutes prior to cell shedding, first to the apical, then to the basolateral region of the shedding cell (Guan et al. 2011). In this study, it was also observed that permeation of the membrane impermeable marker; lucifer yellow, only extends around the shedding cell as far as redistributed ZO-1 protein, and that the whole process of extrusion lasted approximately 14 minutes. In 15% of these physiological shedding events, it was observed that

the neighbouring cells also underwent shedding within 5-10 minutes, suggesting that intercellular communication may take place.

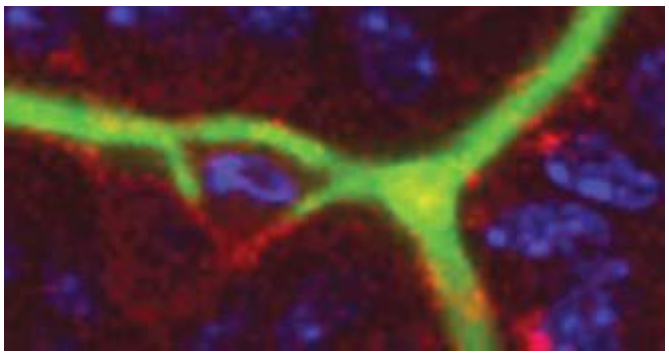

Figure 5: Confocal microscopy showing permeation of membrane impermeable dye lucifer yellow (green) to the limit of redistributed fluorescently tagged tight junction protein ZO-1 (red) around a shedding epithelial cell in the small intestine. Reproduced from Guan, Y., A. J. Watson, et al. (2011). "Redistribution of the tight junction protein ZO-1 during physiologic shedding of mouse intestinal epithelial cells." American Journal of Physiology.

In support of this, in human colonic epithelial cell culture and cultures of rat derived small intestinal phenotype IEC-6 cells, it has been shown that Toll-like receptor 2 (TLR2) ligation amplifies gap junction intercellular communication via connexin 43, and that TLR2 deficient mice exhibit reduced epithelial healing of erosions in DSS colitis. This study also showed that TLR2 agonists act to prevent spontaneous colitis in multi-drug resistance protein (MDR1α) deficient mice (Ey et al. 2009). TLR2 which recognises diverse pathogen associated molecular patterns (PAMPS) of Gram negative bacteria, Gram positive bacteria and yeast (such as lipoteichoic acid, peptidoglycan, bacterial lipoproteins and zymosan) has also been shown by others to aid mucosal healing (Cario 2008).

In vivo, studies of TNF induced intestinal epithelial cell shedding have shown with the aid of fluorescent tagged ZO-1 transgenic mice, that there is a

"funnel" that forms around shedding cells, with redistribution of ZO-1, and other tight junction proteins, including claudins. It was also found that E-cadherin, F-actin, myosin II, Rho-associated kinase (ROCK) and myosin light chain kinase (MLCK) were redistributed during the process. Both ZO-1 redistribution and MLCK activation have also been observed in neighbouring enterocytes in histological studies of cell shedding in humans (Bullen et al. 2006). In the Marchiando et al. 2011 study, caspase activity, myosin motor activity (dynamin) and microtubule rearrangement were all required for shedding, allowing refinement of the Madara "zipper" model (Figure 6).

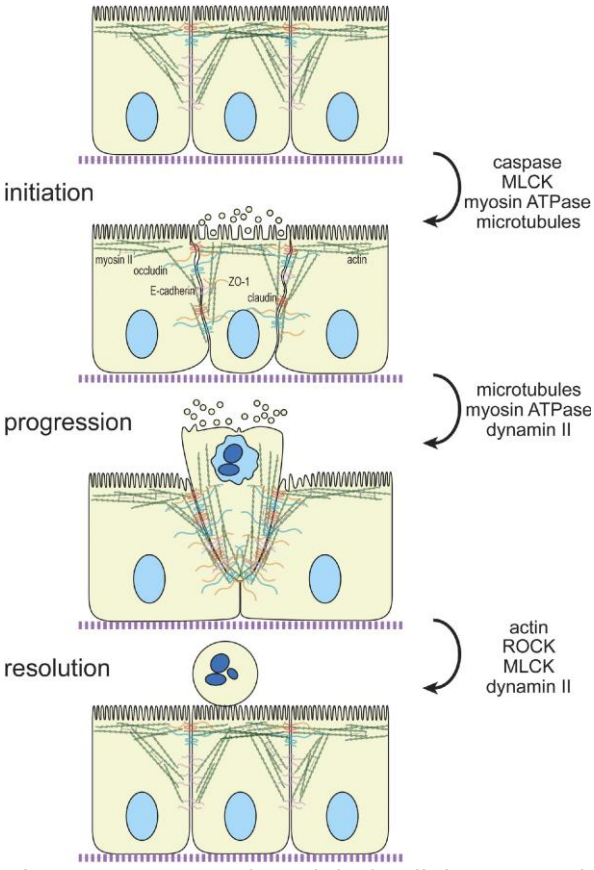

Figure 6: Proposed model of cellular events in epithelial shedding induced by TNF. Reprinted from "The Epithelial Barrier Is Maintained by *in vivo* Tight Junction Expansion During Pathologic Intestinal Epithelial Shedding" (Marchiando et al. 2011) Volume 140, Issue 4, April 2011, Pages 1208‑1218. © 2011 with permission from Elsevier.

It has been suggested through observations made *in vitro* from isolated villi, that actin rearrangement actually takes place only in the enterocyte undergoing shedding, rather than needing cooperation from neighbouring cells (Wang et al. 2011). By contrast, in observations made in chick embryo epithelium, apoptotic cells were extruded by actin myosin rings forming within both the cell that underwent shedding and in the neighbouring epithelial cells. This process was dependent on RhoGTPase, and it is hypothesised that the signal for extrusion precedes the activation of caspases with potassium channel blockers preventing extrusion (Rosenblatt et al. 2001). This study also demonstrated that when apoptotic cells were added to Madin-Darby canine kidney cells (MDCK) culture, they induced actin-myosin rings in the apical cytoplasm, close to where contact was established between apoptotic and viable cells. The plasma membrane of cells that underwent extrusion/apoptosis in MDCK cell culture remained intact until extrusion was complete, and these cells left the monolayer whilst retaining a long stalk of cytoplasm attached to neighbouring cells.

1.6 Small Intestinal Epithelial Gaps

The use of *in vivo* confocal microscopy has allowed the observation that after shedding of enterocytes from the apex of the villus, epithelial discontinuities or “gaps” develop (Watson et al. 2005; Kiesslich et al. 2007). These have also been shown by scanning electron microscopy (Figure 6). These gaps are sealed on average by 20 minutes after the extrusion process, and residual patches of ZO-1 are retained at the gap left by the departing cell (Guan et al. 2011). These gaps were shown to be filled with an unknown

substance that reflected laser light, were different to the "*en face*" appearance of goblet cells, which typically exhibit a targetoid appearance, and were still present in *Math 1*$^{-/-}$ mice deficient in goblet cells. When TNF was administered at 0.33µg/g, 20% of these gaps at shedding sites resulted in increased epithelial permeability.

The substance which plugs these gaps has been speculated to be secreted by adjacent enterocytes or by the underlying myofibroblasts. A candidate substance has been proposed as heparan sulphate, as congenital deficiency has been linked to protein losing enteropathy (Watson et al. 2005). It is uncertain whether these observable gaps represent true gaps in the gut barrier. However, it has been shown that despite the physiological formation of these discontinuities, the functional pore size has been determined to be far smaller than the diameter of a shed enterocyte, at less than 0.6nm (Fihn et al. 2000).

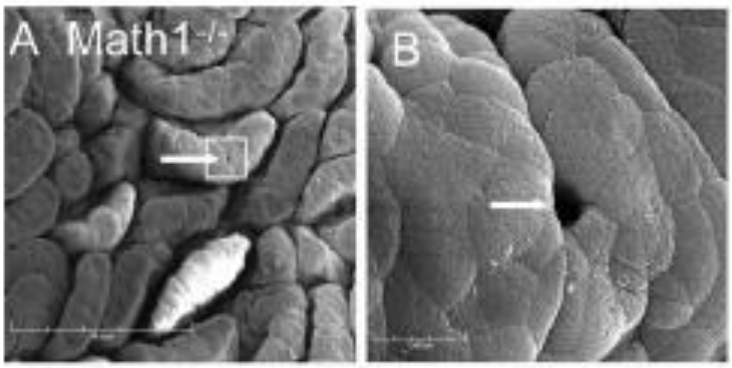

Figure 6: Scanning electron micrograph of small intestinal villi demonstrating the presence of epithelial gaps (white arrows) in goblet cell deficient (Math$^{-/-}$) mice. B represents magnified boxed area in A. Scale bars: A=30µm, B=5µm. Reprinted from "Identification of epithelial gaps in human small and large intestine by confocal endomicroscopy." Gastroenterology 133(6): 1769-1778 (Kiesslich et al. 2007).

Other *in vivo* studies have reported that physiological (Madara 1990; Watson et al. 2005) and pathologic enterocyte shedding (Marchiando et al. 2011) does not result in defective barrier function. However, in the context of pathological epithelial cell shedding during inflammatory bowel disease (IBD), it has been shown by confocal endomicroscopy that shedding events correlate with permeability defects and can aid prediction of disease relapse (Kiesslich et al. 2012). It has also been shown that epithelial gap density correlates with disease severity in IBD (Liu et al. 2011). There is also a strong association with increased intestinal permeability in patients at high risk of developing intestinal disease (reviewed by Meddings (2008)). Although a cause and effect relationship has not been established, this temporal relationship suggests that increased gut permeability is important in the pathogenesis and progression of these conditions. Increased intestinal permeability by measurement of urinary excretion of 99mTc-diethylenetriaminopentaacetic acid has been reported in intestinal diseases such as IBD (Casellas et al. 1986). However, probably the best evidence that gut permeability is directly implicated in the pathogenesis of intestinal disease, has been described by Arrieta et al. (2009). They showed that interleukin-10 (IL-10) knockout mice develop increased small intestinal permeability prior to developing spontaneous colitis. When these mice were administered AT-1001 (a synthetic peptide which blocks the zonulin receptor and reduces small intestinal permeability), they exhibited reduced colitis severity.

In vitro studies, albeit in monolayers of canine kidney epithelial cells (MDCK)

have also shown evidence of exploitation of epithelial “gaps” by bacteria, demonstrating that *Listeria monocytogenes* invades sites of epithelial cell extrusion via internalin A and E cadherin interaction (Pentecost et al. 2006).

1.7 Epithelial Cell Death and Shedding in the Small Intestine

The relationship between cell death and cell shedding in the intestine is incompletely understood. Without a robust animal model of this process, it is difficult to completely resolve whether cell death precedes loss of epithelial adhesion or extrusion, or vice versa.

From a historical perspective, although tissue and cell death had been recognised by Virchow, Weigert, and Flemming as early as the 1880s (reviewed by Majno and Joris 1995), making clearer distinctions between types of cell death only became well accepted when Kerr (1971) proposed that a morphologically distinct form of cell death occurred in the hepatocytes of rats when the hepatic vein was ligated, a process which he first dubbed “shrinkage necrosis”. The term “apoptosis” was later used (Kerr et al. 1972) and at this point its characterisation was based on histochemical stains, light microscopy and transmission electron microscopy.

However, apoptosis and necrosis rarely occur in a mutually exclusive manner, and further efforts to define the differences between necrosis and apoptosis by morphological features, biochemical markers, or genetic regulation, have shown there to be considerable overlaps between these processes. The discovery of various biochemical differences in cells

undergoing cell death according to the inciting stimulus, has further complicated this field by the development of designations such as oncosis, necroptosis, pyroptosis, and ever newer variations of cell death. The relevance of necrosis and apoptosis, and some of the newer developments in this field in the context of intestinal pathology will be briefly discussed in the following section.

1.7.1 Necrosis

Necrosis is the term given to spontaneous, non-programmed, non-energy dependent cell death in living tissue. It can be triggered by any noxious cellular insult that results in irreversible cell injury, including deprivation of oxygen, adenosine-5'-triphosphate (ATP), physical injury or toxins, and has therefore been described as accidental cell death (Majno and Joris 1995).

In the context of cell death in the intestine, necrosis can be broadly characterised on a histopathological basis by increased cell volume, cell membrane rupture, cytoplasmic hypereosinophilia, and nuclear pyknosis, karyorrhexis and karyolysis in large groups of adjacent cells (Myers and McGavin 2007).

1.7.2 Apoptosis

Apoptosis, or cell death by suicide (Majno and Joris 1995) is a programmed form of cell death and may be physiological or pathological. In H&E stained sections, apoptosis can be recognised by changes in cellular morphology in individual, usually non-adjacent cells. These include features such as cell shrinkage, cell rounding and condensation of cytoplasm and chromatin. Cytoplasmic fracturing and blebbing of the nucleus and cytoplasm lead

eventually to the formation of apoptotic bodies.

By transmission electron microscopy, the hallmark features of apoptosis are progressive cellular shrinkage with rounding and condensation of chromatin. Chromatin often marginates and forms peripheral crescents, and the nuclear membrane may become convoluted or invaginated. Autophagosomes accumulate which may contain membranous whorls (myelin figures). Cytoplasmic changes occur only in the very late stages of apoptosis, and mitochondria may appear small but structurally normal until this point (Cheville 1994). The biochemical events that lead to apoptosis have been extensively studied in the nematode *Caenorhabditis elegans*, and it was in this organism that caspases or cysteine-aspartic proteases were characterised as the critical enzymatic mediators of the process. Caspases exist as inactive pro-enzymes or zymogens, that when activated undergo proteolytic cleavage at conserved aspartate sites to form a larger and smaller subunit which then dimerise to form the functional enzyme (Figure 8). In general they consist of an N-terminal pro-domain followed by a large approximately 20kDa (p20) subunit and a smaller approximately 10kDa (p10) subunit, which in some procaspases may be separated by a small linker sequence.

The caspases are subdivided into those regarded as initiators of apoptosis (caspases 2, 8, 9 and 10), which trigger a cascade of events which bring about activation of effector or executioner caspases (caspases 3, 6 and 7). Through their proteolytic and DNAse properties, executioner caspases dismantle the cell cytoskeleton and organelles. The executioner caspase,

caspase-3 is encoded for by the CASP3 gene. It exists as a 32kDa zymogen which is then cleaved into 17kDa and 12kDa fragments (p17 and p12 subunits) which form a heterodimer. Two of these heterodimers then join together to form an active hetero-tetramer consisting of a twelve stranded beta-pleated sheet formed by hydrophobic interactions, surrounded by alpha helices (Lavrik et al. 2005). As a terminally activated executioner caspase, presence of cleaved caspase-3 is therefore usually interpreted as evidence of late stage apoptosis.

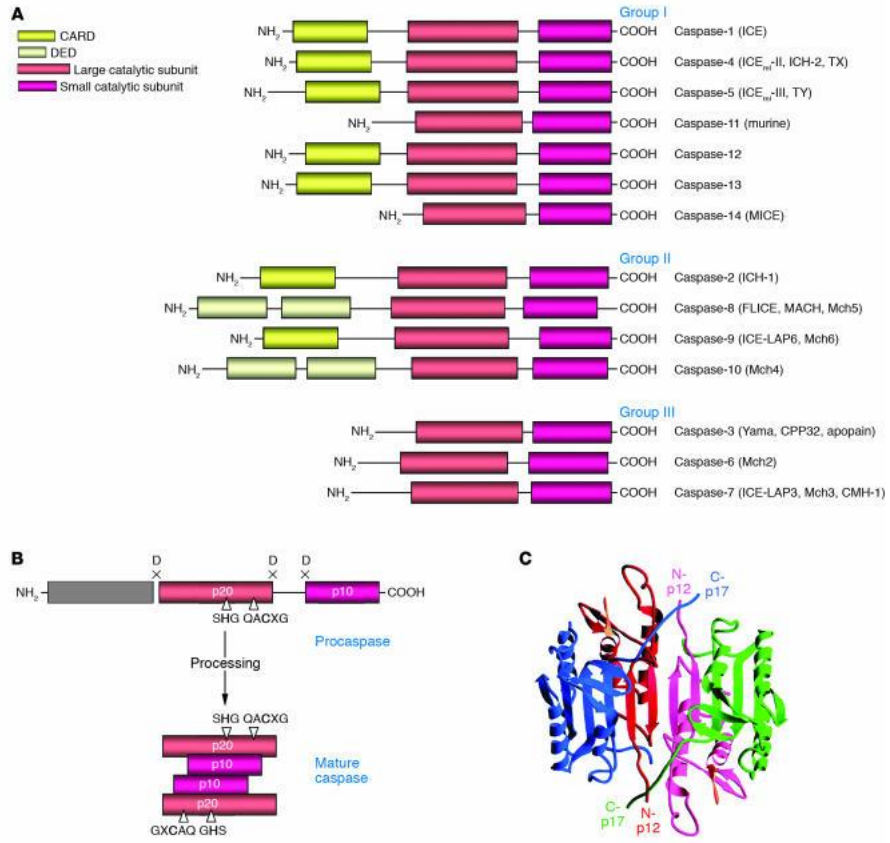

Figure 7: Schematic of the caspase family protein structures A). Group I includes inflammatory caspases, group II includes initiator caspases, and group III includes effector caspases. (B) Procaspase activation. Cleavage of the procaspase at the specific Asp-X bonds leads to the formation of the mature caspase, which comprises the heterotetramer $p20_2$–$p10_2$, and the release of the prodomain. (C) Three-dimensional structure of caspase-3 heterotetramer. Each heterodimer is formed by parallel β-sheets. Reproduced with permission of American Society For Clinical Investigation from “caspases: pharmacological manipulation of cell death” (Lavrik et al. 2005). J Clin Invest.

The mechanisms by which caspases are activated have led to two broad pathways being defined; these being the extrinsic pathway brought about by external cell signals, and the intrinsic pathway which is activated by internal cellular signals (Figure 9). The intrinsic pathway can be triggered by a variety of cell stressors or death signals such as withdrawal of growth factors, DNA damage, mitochondrial damage, lack of ATP production or failure of ion pumps. Death signals such as DNA damage work through p53 mediating transcription of PUMA (p53 upregulated modulator of apoptosis), which binds anti-apoptotic Bcl-2, and Noxa which is an anti-apoptotic member of the Bcl-2 family. The extrinsic pathway may be triggered by receptor ligand binding of FAS ligand to the FAS receptor (CD95 receptor), TNF to TNF receptor 1 (P55/P60) or TNF related apoptosis inducing ligand (TRAIL) to DR4 or DR5 receptors.

Both intrinsic and extrinsic pathways of apoptosis converge and culminate in the mitochondrial permeability transition via formation of the mitochondrial transition pore. This is mediated through death signals initiating the substitution of anti-apoptotic protein members of the B cell lymphoma (Bcl) family such as Bcl-x, Bcl-2, and Bcl-w from the outer mitochondrial membrane with pro-apoptotic proteins such as B cell associated X protein (Bax), Bcl-2 homology interacting-domain death antagonist protein (Bak), BH3 interacting-domain death agonist (Bid), Bcl-2-associated death promoter (Bad), and B-cell lymphoma 2 interacting mediator of cell death (Bim).

These events result in the release of cytochrome C from the intermediate space of the mitochondrial membrane. Cytochrome C goes on to form a

complex with apoptotic protease activator factor-1 (Apaf-1) and pro-caspase 9 to form the apoptosome, with pro-caspase 9 transitioning to active caspase-9 by autocatalytic cleavage, which then activates caspase-3.

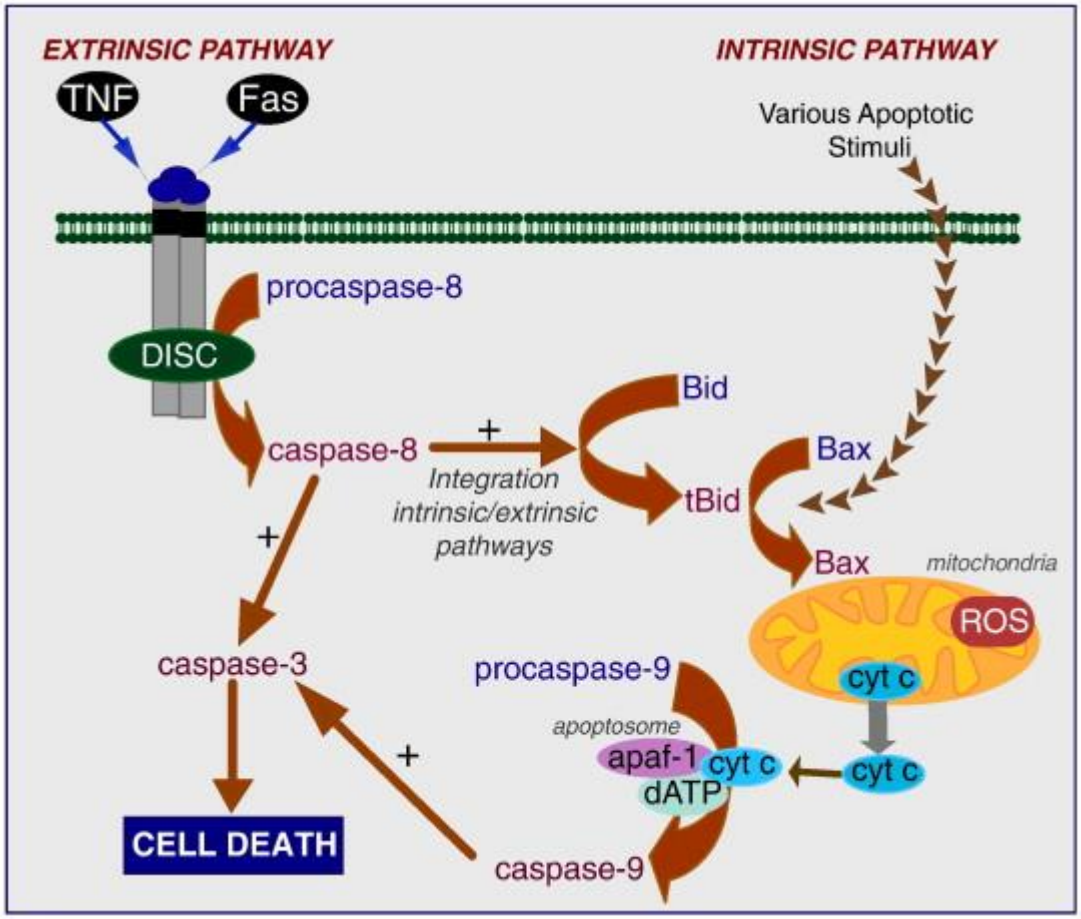

Figure 8: Diagram outlining the extrinsic and intrinsic pathways of apoptosis. Reprinted from Biochim Biophys Acta 1830(5) (Mari et al. 2013). Mitochondrial glutathione: features, regulation and role in disease" pages 3317-3328. © 2012 with permission from Elsevier.

Any of these events trigger the recruitment of TNFR1 Associated Death Receptor (TRADD) or FASL associated Death Domain (FADD), Mort1, and RIP, and the dimerisation of pro-caspase 8 to form active caspase-8. The activation of initiator caspases leads to a cascade and activation of executioner caspases. When considering the extrinsic pathway of apoptosis,

differentiation can be made between cell types. The anti-apoptotic protein Bcl-2 does not regulate apoptosis in type 1 cells such as thymocytes, but does regulate apoptosis in hepatocytes; designated type 2 cells, where Fas ligation results in activation of the intrinsic pathway through Bid and activation via caspase-3. Further differences between cell types are observed in their response to ligation of the TNF receptor, which may cause apoptosis in cells with a weak nuclear factor kappa B (NFκB) response, and stimulate proliferation in cells with a robust NFκB response. Different death signals also work by different pro-apoptotic factors; with Bid being activated by receptors of the extrinsic pathway, Bad responding to low glucose, and Bim responding to cytokines (reviewed by Watson 2004; Elmore 2007).

Biochemically, the most popular means by which apoptosis can be detected by means other than cellular morphology, is by terminal deoxynucleotidyl transferase dUTP nick end labelling (TUNEL) of cleaved DNA, or by immunohistochemical detection of activated caspase-3. However these techniques do not differentiate between activation of the intrinsic and extrinsic pathways.

1.7.3 Necroptosis

Recently it has been proposed that a third type of cell death referred to as necroptosis exists in certain cell types considered to be undergoing executioner caspase independent cell death. In this type of cell death, receptor mediated cell death is initiated, which is dependent on the formation of a protein complex termed the necrosome. This complex includes Fas associated death domain (FADD), tumour necrosis factor associated death

domain (TRADD), caspase-8, receptor interacting protein kinase 1 (RIP1) and RIP3. Necroptosis has been implicated as the mechanism of Paneth cell death in Crohn's disease (Gunther et al. 2011), when it was demonstrated that conditionally caspase-8 deficient mice lacked Paneth cells and exhibited depleted numbers of goblet cells. These mice developed terminal ileitis and were more susceptible to colitis. When TNF was administered to these mice, they exhibited increased TUNEL positive and caspase-3 negative cell death in the Paneth cell region of the crypt, with up regulated RIP3 expression. Mice exhibited a normal intestinal phenotype, suggesting that physiological IEC homeostasis is not dependent on extrinsic pathway apoptosis (reviewed in Han et al. (2011)).

1.7.4 Intestinal Epithelial Cell Shedding and Detachment

The relationship between intestinal epithelial cell shedding and cell death is incompletely understood, as it is not known whether cell death precedes detachment, or whether detachment triggers apoptosis in a process termed anoikis. Supporting the latter theory, Fouquet et al. (2004) showed that early loss of the *zonula adherens* protein E-cadherin in IECs resulted in rapid execution of a Bcl-2 and caspase-9 dependent apoptotic pathway in an *ex-vivo* mouse small intestine model. Other groups have shown via active caspase-3 immunostaining that the apoptotic pathway is activated prior to shedding, and that in detached IECs apoptosis begins by activation of initiator caspases 2 and 9, with subsequent activation of executioner caspases such as caspase-3 (Grossmann et al. 2002).

1.8 Stimuli Which Cause Intestinal Epithelial Cell Death

Despite the estimated physiological loss of massive numbers of enterocytes from individual villi, when H&E stained sections of the small intestine are examined, shedding events are observed relatively rarely, with recent studies into cell shedding in the human intestine finding a shedding cell in only 5.35% of villus sections (Bullen et al. 2006). For this reason, and the fact that physiological epithelial cell shedding does not appear to detrimentally affect gut barrier function, a number of varied stimuli have been investigated, and shown to increase IEC cell shedding. These include TNF administration (Garside et al. 1993; Piguet et al. 1998; Marchiando et al. 2011), ischaemia (Brown et al. 2007), ischaemia-reperfusion injury (Ikeda et al. 1998), burn injury (Song et al. 2008), trauma (Sodhi et al. 2011), increased lymphatic pressure (Lee 1977), cocaine or atropine induced villus contraction (Lee 1977), *Cryptosporidium parvum* infection (Foster et al. 2012), Galectin-1 administration (Muglia et al. 2011) and toxins such as *Bacteroides fragilis* toxin (Wu et al. 2007). The drawbacks encountered with these stimuli include technical difficulty, necessity of surgical procedures, animal welfare issues such as a need for anaesthesia and recovery, long intervals between the stimulus and shedding response, economic expense, and a lack of reproducibility. The ideal stimulus to study pathological epithelial cell shedding would therefore be one that is economically viable, rapid in onset, reproducible, technically simple without a requirement for anaesthesia or surgery, minimise detrimental effects on animal welfare, and clinically relevant. As this project aimed to investigate lipopolysaccharide as such a

candidate stimulus, TNF and ischaemia, as the most clinically related stimuli, will be discussed briefly.

1.8.1 Tumour Necrosis Factor

TNF is the abbreviation given to tumour necrosis factor alpha, which is predominantly produced in activated macrophages and to a lesser extent activated T cells, epithelial cells and myofibroblasts. TNF is part of the larger TNF family of cytokines, comprising of some 19 different pro-apoptotic cytokines which share structural and functional similarities. Other notable cytokines of this group include FASL and TRAIL.

TNF is synthesised as a pro-hormone, with an unusually long amino acid sequence, which is not present in the secreted mature cytokine. In mice TNF also exists in different glycosylation states. Both the secreted (17kDa) and membrane bound forms (18.5kDa) are capable of exerting biological effects (Sherry et al. 1990). Membrane bound pro-TNF is capable of juxtacrine signalling, but can become solubilised by action of ADAM17 (Black et al. 1997), otherwise known as TACE (TNF converting enzyme).

TNF acts via two known receptors: p55/TNFR1 or p75/TNFR2. The cellular response to TNF is highly context dependent, and varies according to cell type, the relative expression of the two receptors, and the downstream responses of these two receptors. Indeed, in cardiac myocytes and neurones, TNFR1 has been found to exert pro-death effects, and TNFR2 to pro-survival effects. In small intestinal enterocytes, both TNFR1 and TNFR2 have been alleged to be pro-death. Interestingly, it has been shown that TNFR1 deficient mouse strains are resistant to the lethal effects of

lipopolysaccharide (LPS) and superantigen (Pfeffer et al. 1993), suggesting that this receptor is responsible for the detrimental effects of TNF in this context.

TNFR1 is much more widely expressed than TNFR2, and it has been shown by immunohistochemistry that TNFR1 is present in intestinal epithelium (Song et al. 2005; Lau et al. 2011). It has also been shown that the response to TNF varies in the different regions of the small intestine, with a more rapid and greater extent of apoptosis being elicited in the duodenum, than the ileum. This correlates with TNFR1 being more highly expressed in the duodenum than the ileum, with the opposite situation being true for expression of TNFR2 (Lau et al. 2011). It has been shown in histological studies that intraperitoneal (i.p.) TNF administration in mice at 10^5 units per animal, caused duodenal villus atrophy that was significant at 60 minutes, and fully developed by 120 minutes, with shedding enterocytes being lost from the apex of villi (Garside et al. 1993). These findings have also been corroborated by others (Piguet et al. 1998), who observed similar effects from 0.5 hours after administration of 10µg of intravenous TNF. In the Garside et al. study, crypt elongation/hypertrophy was also reported from 15 minutes (although it would seem unlikely that this could be due to any proliferative response within this time frame) and at later time points in conjunction with the villus atrophy. Enterocyte loss with villus atrophy was also markedly enhanced by addition of interferon gamma (IFNγ), and to a greater extent than when either of these cytokines was administered alone. The Piguet et al. study also showed that apoptosis and detachment of enterocytes was

mediated by the TNFR1 receptor and was independent of the TNFR2 receptor and p53. It has been demonstrated that following acute TNF administration, epithelial specific expression of TNFR1 is necessary to induce this apoptosis and shedding, rather than indirect vascular dysfunction causing ischaemia/ischaemia-reperfusion. This was shown by analysing the small intestinal IEC loss and apoptosis in a *villin-Cre Tnfr1*$^{flxneo/flxneo}$ mouse model of acute TNF administration. These mice expressed a selectively reactivated *Tnfr1* allele only in IECs, and showed similar TNF induced cell shedding to WT. Interestingly, it was also found that this IEC specific expression of functional TNFR1 did not however mediate the Crohn's-like lesions associated with chronic epithelial specific TNF over-production in TNF$^{\Delta ARE/+}$ mice, which lack AU rich TNF regulatory elements within the intestinal epithelium (Roulis et al. 2011). What is not clear is whether parenteral or luminal TNF is the significant contributor to direct epithelial interaction, although it has been shown that direct instillation of TNF into the duodenal lumen can cause intestinal damage in rats (Jackson et al. 2000). Dramatically increased TNF production, and increased pulmonary inflammation has been shown in *Tnfr2*$^{-/-}$ mice in response to endotoxin administration, suggesting that this receptor may be responsible for suppressing TNF production (Peschon et al. 1998).

1.8.2 Intestinal Ischaemia

Intestinal ischaemia may be induced by any occlusive process of the vasculature such as thrombi, volvulus or torsion, or by compromise of perfusion in conditions such as cardiac insufficiency, sepsis, alpha

adrenergic administration (such as xylazine or medetomadine) or digitalis administration (Stoney and Cunningham 1993). It has been widely believed that ischaemia causes intestinal epithelial cell death by necrosis, but Ikeda et al. (1998) showed that ischaemia-reperfusion for 15-90 minutes in rats increased cell death by enterocyte apoptosis and necrosis. This study showed by a combination of light microscopy, transmission electron microscopy, and examination of DNA fragmentation, that apoptosis was the predominant form of cell death, although this occurred in conjunction with necrosis. Prior to this, Wagner et al. (1979) performed a transmission electron microscopy study on rat small intestine subjected to ischaemia. They found that after only 15 minutes of ligation of the vascular arcades of the jejunum, there was development of cytoplasmic blebs at the basal aspect of enterocytes which led to loss of cell adhesion and shedding. There was also accumulation of an amorphous substance beneath subepithelial spaces which was hypothesised to be oedema fluid. More recently it has been shown that some of these effects are mediated through hypoxia inducible factor 1 (HIF-1α) (Feinman et al. 2010).

1.9 Pathogenesis of Sepsis and Endotoxic Shock

The effects of TNF and ischaemia have been implicated as highly important in the multiple organ dysfunction syndrome (MODS) that is encountered in sepsis. Sepsis is the clinical term given to the systemic inflammatory response syndrome (SIRS) which results from infection, whereas septicaemia is more specifically the presence of pathogenic organisms in the bloodstream. Evidence suggests that the fundamental mechanisms by which

this inflammatory state is induced are via pattern recognition receptors (PRRs), especially TLRs of the innate immune system recognising pathogen associated molecular patterns (PAMPs). One of the most important clinical syndromes encountered in medicine is septic shock as a result of bacterial infection. This condition has 25-50% mortality and accounts for ~200,000 deaths per annum in the United States (Angus et al. 2001). Approximately 70% of these cases are referred to as “endotoxic shock”, as they are caused by Gram negative bacteria which produce endotoxin/lipopolysaccharide (LPS) (Mitchell 2004). LPS has been implicated as one of the most important molecules in initiating this type of shock (Beutler and Rietschel 2003).

LPS as a stimulus for intestinal epithelial cell shedding has not been previously investigated *per se*, but it is well established that gut mucosal injury and increased gut permeability occur in the latter stages of endotoxic shock. As the gut represents an extremely large reservoir of bacteria, including Gram negative bacteria and LPS, this has led to the development of the gut origin of sepsis hypothesis (Pastores et al. 1996). This proposes that endotoxic shock initiates failure of the gut barrier, which in turn allows bacteria and/or endotoxin into the circulation in a positive feedback loop (summarised in Figure 9 and reviewed by Gatt et al. (2007)). Previous studies have shown extensive gut injury with crypt apoptosis, several hours after induction of endotoxic or septic shock (Coopersmith et al. 2002; Coopersmith et al. 2003; Guma et al. 2011). Additionally, increased intestinal permeability has been shown in the ileum, but not the jejunum of rats 2 hours after LPS administration, and in mice, bacterial translocation has been

detected 24 hours post-LPS administration (Deitch et al. 1991).

Although the mechanisms of gut injury have not yet been established, it is thought to be initiated by the hypoxic and ischaemic conditions brought about by blood maldistribution during endotoxic shock; although in reality it is highly likely to be a multifactorial process.

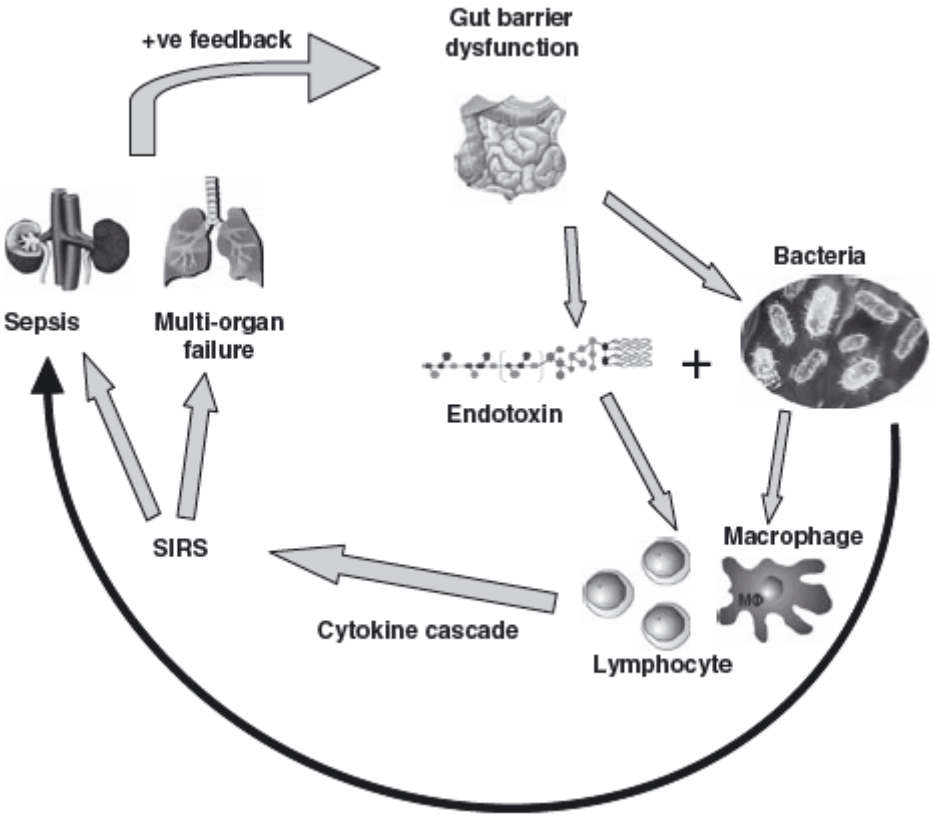

Figure 9: Diagram outlining the gut origin of sepsis hypothesis from “Bacterial translocation in the critically ill – evidence and methods of prevention” Alimentary Pharmacology & Therapeutics 25(7): 741-757. (Gatt et al. 2007). Reprinted by permission of John Wiley & Sons, Inc. © 2007.

1.9.1 The Role of Lipopolysaccharide

The lipopolysaccharide (LPS) molecule is an integral structural component of the Gram negative bacterial cell wall which may interact with the host’s

immune system either directly in bacterial cell associated form, or as a cell free form when liberated. LPS may be liberated when Gram negative bacteria replicate, and when they are lysed. This occurs when anti-bacterial proteins or plasma complement bind bacteria directly or via antibody adhesion, causing bacterial lysis.

The high level of immunological challenge presented by Gram negative bacteria within the gut, therefore represents a fascinating and far from understood host-microbial relationship. A typical Gram negative bacterium such as *E.coli* contains approximately $3.5x10^{6}$ LPS molecules, equating to 10^{-15}g of LPS. As lipopolysaccharide is a structural component of the bacterial cell membrane, it is necessary to employ various extraction methods to separate it from other bacterial components and purify it. Commonly used methods include phenol extraction, butanol extraction, trichloroacetic (TCA) extraction, and ion-exchange chromatography.

The LPS molecule itself consists of three distinct domains (Figure 11) including a lipid A domain, an oligosaccharide core, and an O-antigen. The lipid A domain confers much of the toxicity of the LPS molecule, and consists of a phosphorylated glucosamine disaccharide backbone with multiple hydrophobic fatty acids. The O-antigen is a variable polysaccharide side chain which extends from the oligosaccharide core domain, and confers antigenic specificity to LPS of different bacteria (reviewed by Van Amersfoort et al. 2003).

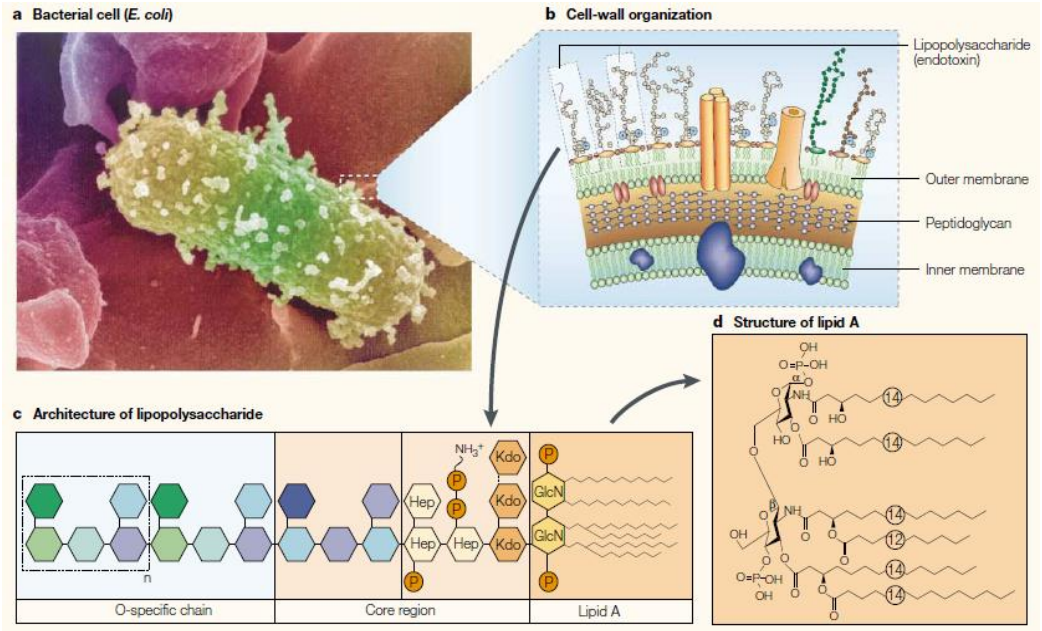

Figure 10: LPS is a critical structural component of the Gram negative bacterial cell wall. Reprinted by permission from Macmillan Publishers Ltd: Nature Reviews Immunology: Innate immune sensing and its roots: the story of endotoxin." 3(2): 169-176. Beutler, B. and E. T. Rietschel © 2003

The mechanism for LPS toxicity was not identified until a spontaneous mutation resulted in a genetic resistance in the C3H/HeJ mouse to the effects of LPS, (Watson and Riblet 1974). This was identified as the *Lps* locus. It was subsequently demonstrated that myeloid lineage immune cells were necessary to cause morbidity in endotoxic shock, as mice that were unresponsive to LPS were rendered sensitive by bone marrow transplantation from LPS responsive C3H/HeN mice (Michalek et al. 1980). The *Lps* gene was eventually cloned and the gene product; TLR4, convincingly demonstrated to be the conduit for LPS signalling (Beutler et al. 2001).

However, LPS signalling via TLR4 ligation was found to be additionally dependent on several other molecules. Investigations into the dynamics of acute LPS administration *in vivo*, were performed by administering LPS

systemically to rabbits and mice. These experiments showed that LPS was quickly bound in the circulation by lipopolysaccharide binding protein (LBP), discovered by Tobias et al. (1986). LBP catalyses the transfer and subsequent removal of LPS from the circulation to cells of the mononuclear phagocyte system bearing surface CD14, including Kupffer cells of the liver, and splenic macrophages (Mathison and Ulevitch 1979). This is followed by binding of LPS to Toll-like receptor 4 (TLR4), which is a member of the larger family of Toll-like receptors, which act as pattern recognition receptors to recognise a diverse range of PAMPS. TLR4 is variably expressed within many cell populations, but is highly expressed in monocytes and macrophages. After surface ligated TLR4 has dimerised, in conjunction with the essential adapter molecules CD14 (Wright et al. 1990) and MD-2 (Shimazu et al. 1999), cytoplasmic myeloid differentiation primary response gene 88 (MyD88) is recruited as an adapter protein (Pålsson-McDermott and O'Neill 2004). IL-1 receptor associated kinase (IRAK) is then recruited, undergoes autophosphorylation and activates TNF-receptor associated factor-6 (TRAF-6), which in turn activates the inhibitor of kappa B (IκB) kinase cascade and nuclear transcription factor kappa B (NFκB) activation. This activation leads to the production of TNF, IL-1, IL-6 and IL-8. In endothelial cells, activation of TLR4 eventually leads to down regulation of tissue factor pathway inhibitor (TFPI) and thrombomodulin, upsetting the balance of haemostasis in favour of thrombosis and disseminated intravascular coagulopathy (DIC). TLR4 activation also promotes the synthesis of type 1 interferons and inducible nitric oxide synthase (iNOS) in immune cells and vascular tissue (Mitchell 2004). It should be noted

however, that the signal transduction events subsequent to cell surface binding of LPS do not occur immediately, and it has been shown to take 15-30 minutes for monomeric LPS to become internalised (Detmers et al. 1996).

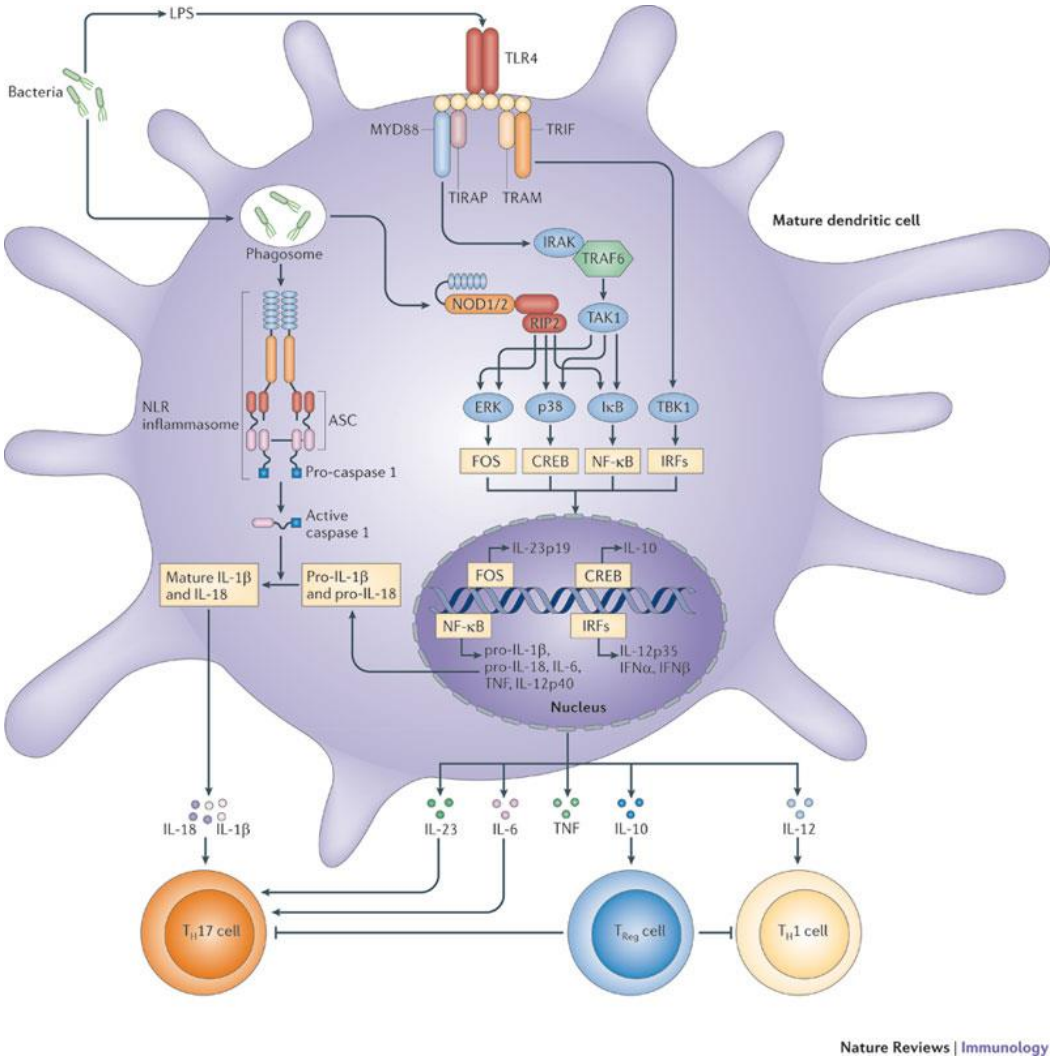

Figure 11: Signalling pathways induced in dendritic cells in response to Gram negative bacteria. All TLRs use myeloid differentiation primary response protein 88 (MyD88) as an adaptor protein, with the exception of TLR3. Phosphorylation of NFκB inhibitor (IκB), leads to activation of nuclear factor κB (NFκB) and consequent transcription of a range of genes coding for pro-inflammatory cytokines, including tumour necrosis factor (TNF), interleukin-6 (IL-6), pro-IL-1β and pro-IL-18. Reprinted by permission from Macmillan Publishers Ltd: Nature Reviews Immunology. "TLR-dependent T cell activation in autoimmunity." 11, 807-822. Kingston H. G. Mills © 2011

Investigations into the extraction methods of LPS from *E.coli* O111:B4 have shown that the immunogenic properties of LPS are also dependent on the purification technique, as LPS extracted by the phenol method elicited a strong mitogenic response in splenic cells of LPS responsive (C3H/St) mice, compared to splenic cells from LPS resistant (C3H/Hej) mice. By contrast, when LPS was extracted using butanol or TCA, similar mitogenic responses were observed in the splenic cells derived from these two strains (Skidmore et al. 1975).

In terms of dosage, an acute systemic inflammatory response may be induced by relatively small dosages of LPS, with intravascular (i.v.) doses of 2ng/kg of *E.coli* O113 LPS in humans and intraperitoneal (i.p.) doses of 500ng/kg in mice causing peaks in IL-6 and TNF expression at 2 hours after administration. This study also showed that i.v. and i.p. administration in mice caused comparable cytokine induction profiles (Copeland et al. 2005). It has also been shown that small amounts of oral LPS can stimulate interferon production in mice (Youngner 1972). When administered by oral gavage however, LPS appears to be minimally toxic, with a lack of clinical or pathological evidence of toxicity in mice at doses up to 1,000,000 endotoxin units (EU) of LPS from *E.coli* BL21 (DE3), equivalent to approximately 3.3 mg/kg (Harper et al. 2011). An earlier study found that an intraperitoneal injection of 100mg/kg LPS was lethal in mice and other species, whereas if this dose was administered directly into the duodenum, these animals survived (Berczi et al. 1966). This is in contrast to LPS derived from *Salmonella enterica* serovar Typhimurium, which does produce toxicity when

given orally in mice, albeit with a 10 fold reduced toxicity compared to the i.v. route (Youngner 1972). The lack of response caused by LPS within the intestinal lumen, has been suggested to be due to the presence of alkaline phosphatase at the small intestinal brush border, which has been shown to be able to detoxify some forms of LPS (Yang et al. 2012).

To put exogenous LPS administration into context, in healthy individuals, plasma LPS concentrations of up to 0.2ng/ml have been measured. Other physiological factors such as stress, heat, and high fat diets can cause physiological plasma concentrations of up to 2ng/ml. In patients with impaired gut barrier function, such as those suffering from necrotising enterocolitis (NEC), acute pancreatitis, alcoholic liver disease, and other forms of critical illness, LPS plasma concentrations of up to 10ng/ml have been recorded. In mice, it has been shown that basal plasma LPS is approximately 0.017ng/ml. When LPS is administered at 0.1mg/kg by i.p. injection, this can induce a measurable increase in peak plasma LPS of 2.2ng/ml at 1 hour (Guo et al. 2013). Estimates of the amount of endotoxin with the gut lumen are relatively scant in the literature, but it has been estimated to be approximately 1.8µg/ml in the distal ileum of rats.

Tracking studies have shown that following intravenous administration of LPS, the first cells to effectively interact with and phagocytose the molecule are tissue macrophages and especially the Kupffer cells of the liver. By immunohistochemical labelling, LPS has also been detected from 1 hour to beyond 28 days in the macrophages of the intestinal lamina propria, and in enterocytes from 8 hours to 7 days (Ge et al. 2000). This led to the authors of

this study to suggest the interesting possibility that epithelial cell shedding may represent an elimination route for LPS.

1.9.2 Intestinal Vascular Supply

One of the major hypothesised mechanisms for gut damage induced by endotoxic shock, is through ischaemia and hypoxia induced by cytokine storm induced blood maldistribution and reduced cardiac output. In a physiological context, the gut receives approximately 20-25% of cardiac output, which rises to approximately 30% postprandially. Vascular supply to the small intestine is via the gastroduodenal artery (arising from the hepatic branch of the coeliac artery) for the duodenum, while the jejunum and ileum are supplied by the jejunal and ileal intestinal arteries respectively (arising from the superior mesenteric artery) and these are interconnected by straight anastomotic arcades within the mesentery.

The extramural vessels of the serosa enter the submucosa at right-angles to form arterioles, the majority of which continue up through the centres of villi (Figure 13) and arborize at the villus tip to form a dense, fenestrated capillary plexus immediately subjacent to the basal lamina of the intestinal epithelium (Vollmar and Menger 2011). The remainder of these arterioles branch into capillary plexuses around the crypts of Lieberkühn. One to several venules drain the villus and crypt capillary plexuses, flowing into larger submucosal veins, mesenteric veins and eventually the hepatic portal vein (Brown et al. 2007). The venules draining the villus run parallel and in very close proximity to the central arteriole, allowing countercurrent exchange of oxygen. This has important implications during hypoperfusion, as when flow velocity

decreases, more oxygen is transferred from the arteriole to the adjacent venules in the basal portion of the villus, exacerbating the sensitivity of the villus tip to perfusion deficits (Vollmar and Menger 2011). The endothelium of the central lacteal of each small intestinal villus is permeable enough to allow the entry of macromolecules and chylomicrons and represents the main route of lipid absorption (Brown et al. 2007). The central lacteal drains into the lymphatic system and eventually into the thoracic duct and back into the bloodstream via the subclavian vein.

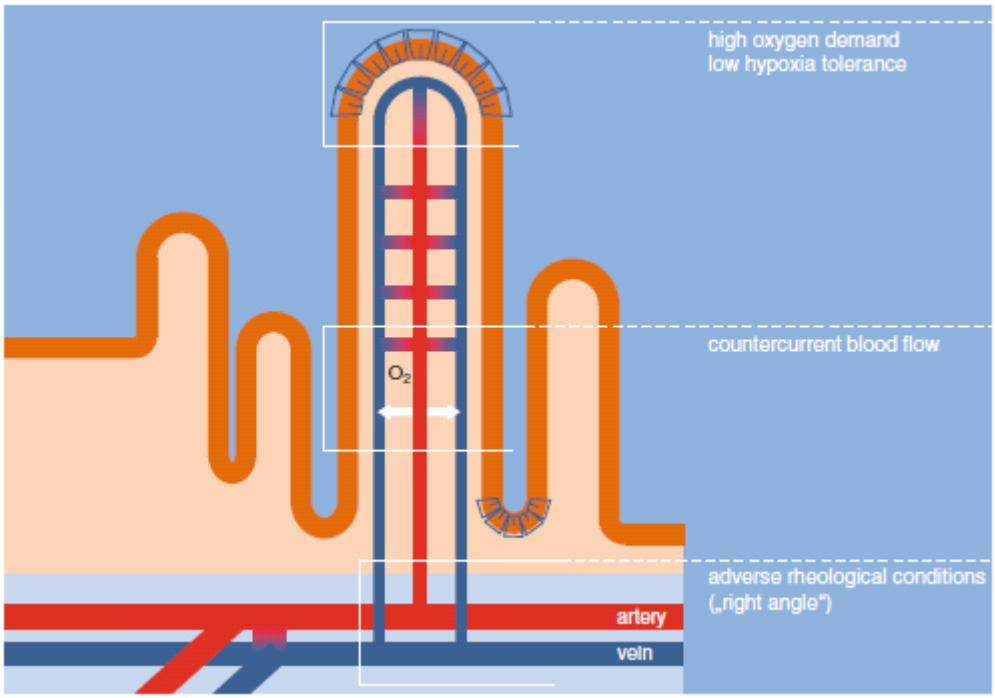

Figure 12: Diagram illustrating the vascular supply of the villus and the countercurrent exchange mechanism from "Intestinal ischemia/reperfusion: microcirculatory pathology and functional consequences". Langenbeck's Archives of Surgery" 396(1), 2011, Vollmar, B. and M. Menger, 13-29, figure 3. © Springer-Verlag 2010 with kind permission from Springer Science and Business Media

In a porcine model of endotoxic shock, it has been shown that there is a drop in arterial oxygen partial pressure after induction of endotoxaemia, with acidosis and increased hypoxanthine (a degradation product of adenosine

triphosphate via adenosine monophosphate) being found in many tissues and blood especially in the gut, increasing to significant levels by 2.5 hours and showing a 2.7 fold increase in endotoxaemic animals by 5 hours (Oldner et al. 1999).

The gut also has very high concentrations of xanthine dehydrogenase which increase towards the villus tip (Granger 1988). It has been speculated that this may contribute to the gut's sensitivity to ischaemic conditions, through xanthine dehydrogenase metabolising hypoxanthine to xanthine and uric acid. This causes the formation of hydrogen peroxide and superoxide. The generation of these reactive oxygen species results in free radical damage and ischaemia reperfusion injury (Kumar et al. 2004). This mechanism was advocated by Deitch et al. (1991) who showed that pre-treatment of endotoxaemic rats with allopurinol prevented increased gut permeability.

Inducible nitric oxide synthase (iNOS) has also been implicated in endotoxic shock induced intestinal injury (Han et al. 2004), although after LPS administration in cats, increased iNOS levels and apoptosis were only present after four hours, despite the observation of intestinal epithelial necrosis at two hours in the ileal mucosa by transmission electron microscopy (TEM) (Crouser et al. 2000). Interestingly, during this study, blood flow and oxygen levels in the blood perfusing the ileum over the course of the experiment were relatively unchanged. This has also been shown by comparing fluid resuscitation and superior mesenteric artery ligation in anaesthetised endotoxaemic rabbits (Lobo et al. 2004). These findings suggest that gut injury in endotoxic shock is independent of blood flow

alterations and blood oxygenation.

In endotoxaemic mice, iNOS has been implicated in tight junction failure in the ileum and colon (Han et al. 2004), with redistribution of the tight junction proteins ZO-1, 2, and 3 and occludins being observed in a time dependent manner from 6 hours after intraperitoneal administration of LPS. These effects were ameliorated in iNOS knockout mice, and by pharmacologic blockade of iNOS in wild-type mice with an inhibitor of iNOS; N6-(1-iminoethyl)-L-lysine, dihydrochloride (L-NIL). In this study, endotoxaemia was also associated with increased gut permeability as assessed by fluorescein and increased bacterial translocation from 12 hours. However, it has been shown that mice lacking iNOS are not resistant to LPS induced death from endotoxaemic shock (Laubach et al. 1995). Other transgenic mouse strains also show differing sensitivity to septic shock, with survival in a polymicrobial model of sepsis (surgical puncture of the caecum) being increased in bcl-2 over-expressing mice (Husain and Coopersmith 2003).

1.9.3 Nuclear Factor kappa B Signalling in Endotoxic Shock

NFκB is the umbrella term for a family of highly evolutionarily conserved cytosolic proteins. On activation, these proteins dimerise in various combinations and shuttle to the nucleus. Here they act as transient transcription factors to regulate the transcription of a very large array of genes. These include genes involved in inflammation, cell stress, apoptosis, cell adhesion and many other cellular processes. All the NFκB family subunits share an N-terminal Rel homology domain (RHD) which mediates dimerisation, and specific DNA binding. Traditionally, these proteins have

been broadly categorised into two broad pathways by their initiating stimulus and interactions with other NFκB subunits. These are the canonical pathway, and the non-canonical, also known as the alternative pathway (Table 1). However it is becoming increasingly evident that due to the extent of cross-talk between these pathways, this probably represents a gross simplification of the system. Additionally complicating matters, NFκB signalling appears to show profound differences between cell types, as in Sertoli cells, B cells, some neurones and T cells, and in many cancers, NFκB is constitutively located within the nucleus.

	Protein/gene	Aliases
Canonical Pathway	NF-κB1	p105 → p50
	RelA	p65
	cRel	
Non-canonical Pathway	NF-κB2	p100 → p52
	RelB	

Table 1: NFκB protein subunits by their traditional classification into canonical or non-canonical pathway signalling and their aliases. Arrows indicate the processed form of the protein.

NFκB1 (p105) is considered part of the canonical pathway and is constitutively processed to its active DNA binding protein p50, which is

contained within the N-terminal half of the larger inactive p105 protein. p105 also contains the inhibitor of NFκB: IκBγ in its C-terminal half (Sha et al. 1995). Whereas NFκB1 is constitutively processed to its active form, NFκB2 exists as the p100 subunit unless activated, whereupon it is processed to p52. However, both p50 and p52 are unable to regulate gene transcription independently, and rely on dimerisation with RelA, RelB and c-Rel, which possess a C-terminal transcription activation domain (TAD) which facilitates gene transcription. The Rel family members are all also capable of forming either homodimers or heterodimers, with the exception of RelB which can only form heterodimers (www.nf-kb.org (accessed July 2013)).

1.9.4 Inhibitors of NFκB

NFκB family subunits are kept within the cytoplasm in an inactive form by another family of proteins referred to as inhibitors of NFκB (IκB). Classical IκB members include IκBα, IκBβ and IκBε. These proteins possess terminal ankyrin repeats, which mediate their function through binding with NFκB dimers and preventing their nuclear localisation. Each of the IκB members exhibits preferential binding to certain NFκB dimers, with IκBα usually binding RelA:p50 dimers, and IκBε binding RelA:RelA and cRel:RelA dimers. It should also be noted that both p105 and p100 proteins additionally possess C-terminal ankyrin repeats, which exert inhibitory activity on these subunits prior to their removal during processing to their active forms of p50 and p52 respectively.

1.9.5 Activation of NFκB

NFκB dimerisation, nuclear translocation and DNA binding generally occurs following any of a great multitude of inducing signals which result in the activation of an enzymatic complex of serine specific IκB kinases (IKK) which include IKKα, IKKβ and IKKγ (also known as NFκB essential modulator or NEMO). These phosphorylate IκB, resulting in the release of NFκB subunits from inhibition.

In the canonical pathway (initiated by Th1 cytokines such as TNF or TLR4 receptor ligation amongst others), NEMO is recruited onto activated adapter molecules such as tumour necrosis factor receptor associated factors (TRAFs). Activated IKK (IκB kinase) complexes (consisting of two NEMO molecules, one IKKα and one IKKβ molecule) phosphorylate the inhibitory protein IκBα, which is targeted for proteosomal degradation by E2 ligases (Figure 13). This allows the release of NFκB family members p50:RelA and cRel:RelA dimers in the cytoplasm. They subsequently undergo nuclear translocation to bind to DNA binding sites and regulate the transcription of target genes.

Non-canonical NFκB pathway activation is generally thought to occur during B and T cell development, through ligation of B-cell activating factor (BAFF), or CD40 to their respective receptors, although others have shown that the non-canonical pathway can also be activated by the TNF receptor (Kim et al. 2011). In this pathway, adapter molecules first activate NIK (NFκB inducing kinase) which activates two IKKα molecules. These proteins go on to cause activation of the p100:Rel B complex, with the p100 molecule being

processed to p52, and the p52/RelB dimer translocating into the nucleus (reviewed by Vallabhapurapu and Karin (2009) and at www.nf-kb.org (accessed July 2013)).

LPS has traditionally been viewed as activating the canonical NFκB activation pathway via ligation of TLR4. However, evidence suggests that there may also be simultaneous activation of the non-canonical pathway by production of free radicals and heat shock protein 70 (HSP70). This was shown to occur in colonic epithelial cells stimulated by LPS *in vitro* (Bhattacharyya et al. 2008) via BCL10 serine 138 and NIK phosphorylation (Bhattacharyya et al. 2010). Guma et al. (2011) showed that constitutive canonical NFκB activation, specifically within the intestine, does not trigger destructive intestinal inflammation unless there is simultaneous activation of mitogen-activated protein kinase (MAPK). In this study, constitutively active canonical NFκB signalling resulted in increased production of TNF mRNA. However, MAPK activation was required to produce TNF. These mice were exquisitely sensitive to LPS administration, which resulted in shock and villus injury, and crypt apoptosis at 4h.

Previous studies have shown that *p50*$^{-/-}$ mice are much more sensitive to the enteropathy induced by LPS. *p50*$^{-/-}$ mice lacking lymphocytes (3XRAG) also developed an enteropathy, and this was shown to be TNF mediated (Gadjeva et al. 2007), suggesting that the effector cells were within the innate immune cell compartment. It has also been shown that NFκB signalling is of great importance in endothelial cells in the context of endotoxic shock, where blockade of NFκB signalling significantly reduced LPS induced hypotension,

vascular expression of TNF and endothelial nitric oxide synthase (eNOS) (Ding et al. 2009). Despite these observations and broad mechanistic studies, very little is understood about how NFκB signals in these situations.

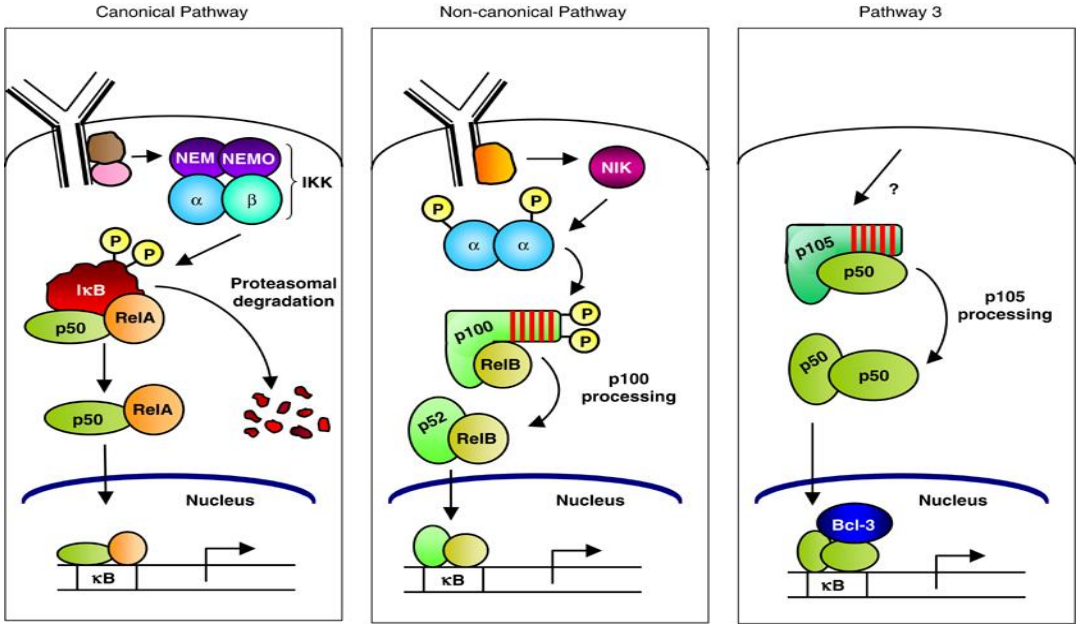

Figure 13: Diagram summarising NFκB signalling pathways. Reprinted by permission from Macmillan Publishers Ltd: Nature Reviews Immunology. Gilmore, T. D. (2006). "Introduction to NF-kappaB: players, pathways, perspectives." Oncogene 25(51): 6680-6684.

1.9.6 Effects of Lipopolysaccharide on Enterocytes

The mechanisms by which LPS causes gut injury during endotoxic shock have not been clearly defined. However, it has been shown that when gut commensals are depleted in mice by giving prolonged courses of oral antibiotics, enterocyte TLR4 expression in the intestine is reduced and increased apoptotic cells are observed within the intestinal epithelium after ischaemia-reperfusion injury (Chen et al. 2008). This study concluded that commensals and LPS reduce the susceptibility of IECs to apoptosis in an ischaemia-reperfusion model. *In vitro*, in IEC-6 cells (of neonatal rat small intestinal lineage), it has also been found that LPS stimulates growth,

whereas in cell culture models of non-transformed human intestinal epithelial cells, it has been found to be growth inhibiting (Ruemmele et al. 2002). These effects were demonstrated to be TNF dependent, and observations such as this have led to an argument by some for LPS to be viewed less as a detrimental molecule to the host, but as a necessary hormone for healthy physiological function of the gut and other organs (Marshall 2005). The myeloid differentiation primary response gene 88 (MyD88) molecule, which is the adapter molecule critical for TLR4 signalling, has also been shown to be important in suppressing the intestinal inflammatory response. Indeed, in murine dextran sodium sulphate (DSS) induced colitis, *Myd88*$^{-/-}$ mice developed more severe colitis compared to wild-type mice, implying that TLR signalling plays an important protective role in suppressing an over exuberant inflammatory response in the development of colitis (Araki et al. 2005).

There is also some evidence that LPS signalling may differ in enterocytes when compared to leukocytes. For example, it has also been shown *in vitro*, that in LPS treated M-IC$_{c12}$ cells (a murine intestinal epithelial cell line derived from L-PK/Tag1 transgenic mice), LPS became internalised into a perinuclear location, co-localising with TLR4 (Hornef et al. 2002). Increased transient CD14 expression with internalisation was shown in response to LPS in IEC-6 cells, and this was also observed *in vivo* after 3 hours of LPS treatment in mice (Mollen et al. 2008). In this study, it was also shown that there was increased activation of p38-MAPK with IL-6 production in the ileum. It has also been shown that myofibroblasts may also respond to LPS with up regulated cytokine secretion (Walton et al. 2009).

Enterocytes, as part of the innate immune system, may also amplify the cytokine response through intercellular communication. Free radicals generated by nicotinamide adenine dinucleotide phosphate (NADPH) oxidase 4 (NOX4) have been shown to represent a potential communication between enterocytes when infected with *Listeria monocytogenes*. NOX4 was shown in this study to mediate intercellular communication between neighbouring epithelial cells, and to coordinate synthesis and release of increased quantities of proinflammatory chemokines CXCL2 and CXCL5 (Dolowschiak et al. 2010).

Interestingly, there may also be differences in epithelial sensitivity to LPS between the small and large intestine. This has been demonstrated in colon explants cultures, where IL-10 and TGFβ were shown to play crucial roles in the relative unresponsiveness of the colon to LPS (Jarry et al. 2008). It has also been shown that the colon of weaned rats is more resistant to injury induced by systemically administered LPS, with significantly less IL-6, IL-4 and IL-10 production compared to suckling rats (Adams and Tepperman 2001).

1.10 Hypothesis, Aims and Objectives

The hypothesis for this PhD project is:

- That systemic administration of lipopolysaccharide causes increased small intestinal epithelial cell apoptosis and shedding in a mouse model

The aims of this project are to test this hypothesis, and to attempt to establish:

- Whether LPS may be used as a simple, consistent, and more economical stimulus of small intestinal epithelial cell shedding than other methods currently available
- The mechanism by which LPS induces cell shedding
- The sites in the gastrointestinal tract which are affected
- The parts of the villus which are affected
- The time course of this phenomenon
- The dose required to cause this effect, and whether there is a dose response relationship
- Whether this effect results in increased gut permeability
- Genetic, and other factors that may influence this process

The objectives of the project include:

- Performing a time course study and carrying out a histopathological assessment of H&E stained sections of the small intestine and other organs to characterise the effects of LPS
- Establishing a quantification method based on histopathological or immunohistochemical methods to measure the effects of LPS on the gut
- Quantifying and comparing the time dependent effects of LPS in the different segments of the gastrointestinal tract
- Establishing appropriate time points and LPS dosages for statistical comparisons to be made between transgenic mice
- Comparing and quantifying the severity of LPS-induced intestinal injury between transgenic mice
- Investigating changes in mRNA and protein expression following LPS administration using qPCR, IHC and western blotting
- Performing *in vivo* confocal microscopy studies in LPS dosed mice under an appropriate anaesthetic regimen
- Determining whether LPS-induced cell shedding causes altered gut permeability by performing gut permeability assays

2. MATERIALS AND METHODS

2.1 Experimental Design

Prior to designing the first experiments of this project, an extensive literature review was performed to investigate the most suitable mouse strains for LPS experiments. This also included review of the most suitable type of LPS to induce the systemic responses that might induce IEC shedding (selected literature summarised in an Appendix, section 8.1).

The most appropriate LPS was deemed to be that from *Escherichia coli* serotype O111:B4 as this was the most commonly utilised serotype for inducing endotoxic shock responses in mice, with dose response parameters having been relatively well investigated. This serotype also has a well characterised LPS molecule (Campos et al. 1994), due to its reported association with outbreaks of infant gastroenteritis (Tawil and El-Kholy 1959).

An initial dose of 10mg/kg LPS was chosen, as in the literature this dose was generally reported to cause a robust endotoxic shock response, but was non-lethal. The preparation used was phenol-extracted, as this was the most commonly utilised form used in the literature, and in the quantities required for a full scale study, higher grade ion exchange chromatography extracted LPS would have represented a large escalation in the cost of the study. Based on the literature review, and that the transgenic mice to be used in later experiments would be on this genetic background, it was decided that the most suitable mice to use would be the C57BL/6 strain.

Intraperitoneal injection was initially selected instead of intravenous as the route of systemic administration, as it is technically a much easier procedure for larger animal numbers, and results in a very comparable cytokine induction profile (Copeland et al. 2005).

2.2 Mice Examined

Wild-type (WT) C57BL/6 female mice were purchased from Charles River laboratories (Margate, UK) and transferred to the Biomedical Services Unit facility at the University of Liverpool (a conventional non-specific pathogen free unit) at 8-9 weeks of age. Mice were housed in groups of 3 or 4 per cage with *ad libitum* food and water, and maintained on a 12 hour light:dark cycle. Mice were given at least a 1 week acclimatisation period, prior to being used for experiments at a minimum age of 9-10 weeks. Procedures were all performed under UK Home Office approval on project license 40/3392, and personal license 40/10000. Transgenic mice including *Nfκb1*$^{-/-}$, *Nfκb2*$^{-/-}$ and *cREL*$^{-/-}$ mice were donated by Jorge Caamaňo of the University of Birmingham, UK. *Tlr4*$^{-/-}$ mice were kindly provided by Mark Taylor and Alice Halliday (The Molecular and Biochemical Parasitology Group, Liverpool School of Tropical Medicine). *Tnfr1*$^{-/-}$ and *Tnfr2*$^{-/-}$ mice were provided by Mark Frey and maintained at the Saban Research Institute at Children's Hospital Los Angeles. Procedures were performed by Jennifer Miguel and monitored by the Children's Hospital Los Angeles Institutional Animal Care and Use Committee. *vil-Cre Myd88*$^{-/-}$ mice were maintained at the Disease Modelling Unit, University of East Anglia, UK. Procedures were performed by Kevin Hughes with UK Home Office approval.

2.3 Generation of *Nfκb1*$^{-/-}$, *Nfκb2*$^{-/-}$ and *cREL*$^{-/-}$ mice

Nfκb1$^{-/-}$ mice were originally generated by Sha et al. (1995) on a C57BL/6 background. This was achieved by targeted disruption of the *Nfκb1* gene by electroporated insertion of a linearised pp50KO construct with a 3-phosphoglycerate kinase (PGK) neo cassette into exon 6 of the *Nfκb1* gene of embryonic stem (ES) cells. This disruption of p105 prevents production of functional p105 and p50, but allows production of functional IκBγ. These mice, although phenotypically normal, exhibit defective B cell responses, including defective antibody production, failure of LPS induced B cell mitogenic responses, and failure to clear *Listeria monocytogenes* infection *in vivo*, specifically failing to clear intracellular bacteria. They are also more prone to sustained bacteraemia following *Haemophilus influenzae*, infection but not *E. coli* infection, and are more resistant to cytopathic encephalomyocarditis infection than WT mice. Further studies of macrophage function have showed that phagocytosis, TNF and IL-1 production were normal in this strain, but IL-6 production was reduced.

Nfκb2$^{-/-}$ mice were generated by insertion of a PGK-neo cassette into exon 4 of the *Nfκb2* gene by electroporation into ES cells. It was confirmed that mutant mice did not express p100 or p52. These mice exhibit abnormalities confined to the lymphoid organs, with reduced B cell populations in the bone marrow, spleen and lymph nodes, with lack of organised lymphoid follicles or germinal centres. These mice also exhibited reduced proliferative responses in B cells to LPS, CD40 and anti-IgD-dextran and reduced antigen specific immunoglobulin production, although immunoglobulin class-switching in B

cells was normal. They also showed reduced T-cell dependent and T-cell independent immunological responses (Caamaño et al. 1998).

c-REL$^{-/-}$ mice were generated by replacing exons encoding amino acids 145-588 of the *c-REL* gene with a PGK-neo cassette by electroporation of a linearised pC-REL construct. This resulted in a truncated cREL protein that was incapable of dimerisation, DNA binding, or transcriptional activation (Kontgen et al. 1995). These mice show normal haematopoiesis and lymphocyte development, but do show proliferative defects in stimulated B and T cells, and deficient IL-2 production. Mice were on a C57BL/6 genetic background. All genotypes were previously confirmed by PCR by Dr. Michael Burkitt (Gastroenterology Department, University of Liverpool).

2.4 Generation of *Tlr4*$^{-/-}$ mice

Tlr4$^{-/-}$ mice were generated by Shizuo Akira by targeted disruption of the *Tlr4* gene by electroporation of a targeting vector which replaces a 2.54-kbp genomic fragment with a neomycin resistance cassette into ES cells. Macrophages from these mice were confirmed to be hyporesponsive to LPS (*E. coli* O55:B5) (Hoshino et al. 1999). Mice were on a C57BL/6 genetic background. The genotype of this strain was confirmed by PCR (Figure 15).

2.4.1 Genotyping of *Tlr4*$^{-/-}$ mice

Genotyping was performed according to a previously published protocol (Truett et al. 2000). Briefly, 2mm of mouse tail-tip was removed with a sterile scalpel blade post-mortem into a 1.5ml Eppendorf tube to which 75µl of 25mM NaOH/0.2mM ethylenediaminetetraacetic acid (EDTA) was added

and maintained at 98ºC for 1 hour. The solution was cooled to room temperature, and 75µl of 40 mM Tris HCl (pH 5.5) was added. Centrifugation was performed at 13,400 x *g* for 3 minutes and aliquots used for PCR. Presence of the mutated *Tlr4*$^{-/-}$ allele was tested by performing a polymerase chain reaction (PCR) using the protocol published at http://hostdefense.ifrec.osaka-u.ac.jp/ja/other/index.html (accessed July 2012). Briefly, primers (supplied by Eurogentec) designated "A","B", and "C" (as per Table 2 below) were added to ThermoPrime 1.1x ReddyMix PCR Master Mix with 2.5 mM MgCl2 (Thermo Scientific: Loughborough, UK) in 25µL reaction volumes. Cycling was performed in a MultiGene™ OptiMax Thermal Cycler (Labnet; Woodbridge, USA).

Primer	**Vol. (µL)**	**Gene**	**Sequence**	**Master mix vol. (µL)**	**DNA vol. (µL)**	**H_2O Vol. (µL)**
“A”	0.25	Targeted portion of TLR4 gene	5'-cgt gta aac cag cca ggt ttt gaa ggc-3'	22.5	1	1
“B”	0.25	TLR4 gene upstream of targeting construct	5'-tgt tgc cct tca gtc aca gag act ctg-3'	22.5	1	1
“C”	0.25	Neomycin resistance gene	5'-tgt tgg gtc gtt tgt tcg gat ccg tcg-3'	22.5	1	1

Table 2: Reaction mixes for PCR. Primers A and B are used to detect the wild-type allele, and primers B and C used to detect the mutated *Tlr4* allele

Cycles	**Duration**	**Temperature**
1	5 min	85 ºC
35	30 sec 1 min 1 min	94ºC 67ºC 74ºC
1	10 min	74ºC

Table 3: Cycling conditions for TLR4 genotyping.

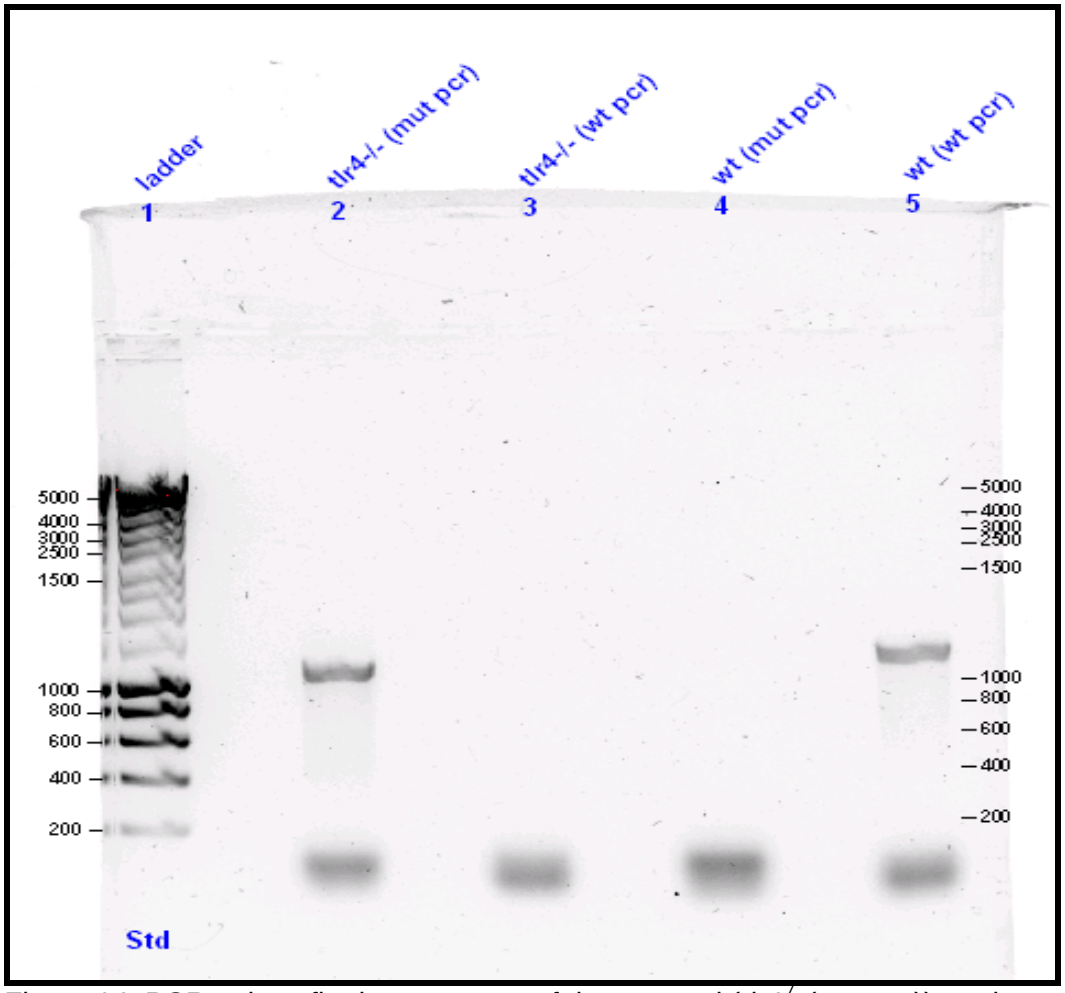

Figure 14: PCR gel confirming presence of the mutated (*tlr4*$^{-/-}$ (mut pcr)), and absence of the wild-type *Tlr4* allele (*tlr4-/-* wt pcr) in *Tlr4*$^{-/-}$ mice (lanes 2 and 3) compared to wild-type control mice (lane 4 and 5). Gene products are both approximately 1200 base pairs.

2.5 Generation of *Tnfr1*$^{-/-}$ and *Tnfr2*$^{-/-}$ mice

Tnfr1$^{-/-}$ mice were generated by targeting the *p55/Tnfr1* gene by homologous recombination. A targeting vector was constructed which replaces a 4-kb SpeI fragment encoding exons 2 to 5 (amino acids 30–184) with a PGK-neo cassette which was electroporated into ES cells. For *Tnfr2*$^{-/-}$ mice, targeting of the *p75/Tnfr2* gene by homologous recombination was achieved by replacing a 1-kb KasI-BamHI fragment encoding amino acids 3 to 26 with a

PGK-neo cassette which was electroporated into ES cells (Peschon et al. 1998). Mice were on a C57BL/6 genetic background.

2.6 Generation of *vil-Cre Myd88*$^{-/-}$ mice

Homozygous *Myd88*$^{fl/fl}$ that express a truncated mutant MyD88 protein following removal of the floxed region, were bred with *villin-Cre* mice which conditionally express Cre recombinase under control of the villin promoter (kindly provided by Simon Clare and Gordon Dougan, Wellcome Trust Sanger Institute, Cambridge). *vil-Cre* Mice heterozygous for the *Myd88* allele were used as controls. Offspring were genotyped for presence of the wild-type *Myd88*, mutated *Myd88*, and *Cre* alleles. Mice were on a C57BL/6 genetic background.

2.7 Lipopolysaccharide Administration

LPS from *Escherichia coli* O111:B4 purified by phenol-extraction (PE-LPS), or ion-exchange chromatography (IE-LPS) (Sigma-Aldrich: Gillingham, UK) was diluted in sterile phosphate-buffered saline (PBS) and administered to mice by i.p. injection. Briefly, LPS was weighed on a microbalance, and dissolved in autoclaved sterile phosphate-buffered saline (PBS) in a biosafety cabinet, at a solution concentration of between 2mg/ml and 12.5µg/ml to deliver appropriate dosages of between 20mg/kg and 0.125mg/kg body weight, in a delivered volume of 10µl/g. Solutions were aliquotted in a biosafety cabinet through a 0.2µm syringe filter into labelled Bijou containers. Aliquots were then frozen at -20°C. Prior to use, aliquots were thawed and warmed to room temperature, then vortexed. Mice were weighed, tail marked, and appropriate volumes of LPS solution or vehicle (PBS) were

injected into the peritoneal cavity with a BD microfine insulin syringe.

2.8 Recombinant TNF

Murine recombinant TNF (Peprotech Ltd: London, UK) was diluted in sterile water to a concentration of 33µg/ml and administered by intraperitoneal injection to mice at 0.33mg/kg in a delivered volume of 10µl/g body weight.

2.9 Tissue Sampling and Processing

After cervical dislocation, the abdominal skin was incised with scissors and retracted, a midline incision was made through the abdominal musculature with scissors and the intestines exteriorised. The small intestine was then separated from the large intestine, the lumen flushed with PBS to remove digesta, then fixed in 4% formaldehyde (Sigma–Aldrich) in PBS.

Stomachs were ligated around the cardia and pyloric sphincter with 4 metric sofsilk™ suture material, and instilled with 4% formaldehyde. Other organs including spleen and liver were routinely taken, together with brain, lung, heart, and kidney in initial studies. After 24 hours fixation, the proximal, middle, and distal third of the small intestine (referred to in this thesis as the duodenum, jejunum and ileum respectively) were separated, and chopped into short, approximately 10mm lengths. These lengths which were placed within a loop of 3M Micropore™ tape as a bundle, and cut cross-ways with a size 22 scalpel (Swann-Morton Ltd: Sheffield, UK) in order to achieve multiple cross-sectional intestinal circumferences for histopathological examination (Figure 15). This is an alternative to the “Swiss roll” method of embedding longitudinal intestinal sections (as described by Moolenbeek and Ruitenberg (1981)). This method was also evaluated for the study, but was

regarded as inferior due to the higher likelihood of tissue trauma during preparation and processing, and the lack of preservation of shed cells in the gut lumen.

Tissues were placed in histological processing cassettes and placed in 70% ethanol, before being processed routinely through serially increasing concentrations of ethanol solution (70%, 90% and 100%), on an overnight programme on a Shandon 2LE tissue processor (Table 4). Tissue was embedded in paraffin wax (Leica Surgipath Formula R) using a Shandon Histocentre embedder (Thermo Shandon Ltd: Runcorn, UK). Sections of 3-5µm thickness were prepared with a microtome and floated out on a heated waterbath onto glass slides for H&E or onto 3-aminoprpyltriethoxylsilane (APES) coated slides for immunohistochemistry. The latter were coated in 2% APES in acetone and allowed to air-dry. Slide mounted sections are dried in an oven at 37ºC prior to staining.

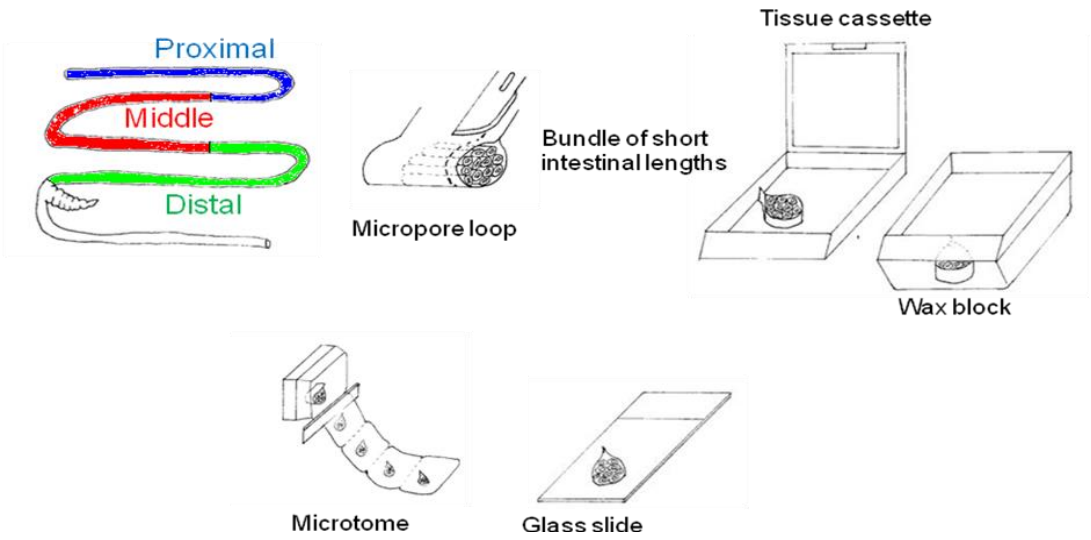

Figure 15: Tissue preparation, processing, embedding and sectioning to create a glass slide. The small intestine was first separated into thirds. These segments were then chopped into shorter 10mm lengths, placed as a bundle within a loop of Micropore™ tape and then placed within a tissue processing cassette. After dehydration, the tissue was placed in a mould and molten wax added. The original tissue cassette was set into the top of the wax block before the wax solidified. This wax block was then placed in the microtome to cut 3-5µm sections which were floated on a waterbath and onto a glass slide.

Step	Reagent	Temp	Immersion (hrs:min)
1	70% Ethanol	Room temp.	02:00
2	90% Ethanol	Room temp.	02:00
3	100% Ethanol	Room temp.	00:30
4	100% Ethanol	Room temp.	00:30
5	100% Ethanol	Room temp.	01:30
6	Xylene	Room temp.	00:30
7	Xylene	Room temp.	00:30
8	Xylene	Room temp.	00:40
9	Xylene	Room temp.	01:30
11	Wax	60	02:00
12	Wax	60	03:00

Table 4: Overnight tissue processing schedule.

2.10 Transmission Electron Microscopy

Small intestinal samples were fixed in 2.5% glutaraldehyde in 0.1 M sodium cacodylate buffer for transmission electron microscopy. Samples were then processed and imaged at the Electron Microscopy Unit, Veterinary Pathology, University of Liverpool, Leahurst Campus. Briefly, samples were washed in 0.1M sodium cacodylate buffer and secondarily fixed in 1% osmium tetroxide for 90 minutes. Tissues were washed in distilled water, stained *en bloc* with 2% uranyl acetate in 0.69% maleic acid for 90 minutes and dehydrated in ascending concentrations of ethanol, followed by acetone, then resin embedded. Semi-thin sections (0.5µm) and ultrathin sections (60 nm) were prepared with a diamond knife. The latter were mounted on copper grids, stained with Reynold's lead citrate and viewed with a Philips 208S electron microscope (Philips Electron Optics; Eindhoven, The Netherlands).

2.11 Haematoxylin and Eosin (H&E) Staining

Sections mounted on glass slides were placed in a slide rack, dewaxed in xylene for 10 minutes, followed by 5 minutes in 100% ethanol, 2 minutes in 90% ethanol, 2 minutes in 70% ethanol, and rehydrated in water for two minutes. Slides were placed in Gill no.1 haematoxylin (Sigma-Aldrich) for 2.5 minutes, then “blued” in running tap water for 10 minutes. They were then placed in eosin (Accustain:Sigma-Aldrich) for 3.5 minutes, followed by a rapid immersion in water for 5 seconds, then rapid dehydration in 70%, 90% and 100% ethanol each for 15 seconds, and finally transferred into xylene for 10 minutes. DPX mounting media was added to section surfaces and 22x50mm coverslips were applied.

2.12 Active Caspase-3 Immunohistochemistry

Two immunohistochemical methods were evaluated for the purpose of quantifying apoptotic cells. Both used antigen affinity purified, rabbit polyclonal anti-active caspase-3 primary antibody AF835 (R&D systems, Abingdon, UK). To produce this antibody, rabbits are immunised with keyhole limpet haemocyanin (KLH) coupled human caspase-3 synthetic peptide (CRGTELDCGIETD: corresponding to amino acids 163-175 of human caspase 3; accession number P42574). This antibody binds the p17 subunit of cleaved human or mouse caspase-3. These methods both followed stage 1 of immunohistochemistry, and were followed by either the avidin biotin complex (ABC) or Envision™ protocol as described. Sections were then counterstained with haematoxylin for 2.5 minutes, dehydrated and coverslipped as for H&E sections. All incubations were carried out in the dark.

2.12.1 Stage 1 of Immunohistochemistry

Sections underwent standard dewaxing from xylene to 100% ethanol, 5 minutes endogenous peroxidase block in 0.9% hydrogen peroxide (Sigma-Aldrich) in methanol followed by standard rehydration steps from 100% ethanol to water. Sections were microwaved at 800 Watts for 20 minutes in 0.01M pH6 citrate buffer to achieve heat induced antigen retrieval. Slides were allowed to cool slowly over twenty minutes, cold tap water was then added slowly and slides were washed in tris-buffered saline, 0.1% Tween®20 (TBST).

2.12.2 ABC Method for Active Caspase-3 Immunohistochemistry

The avidin biotin complex (ABC) method utilises a biotin labelled secondary antibody raised to bind to the fragment crystallisable (Fc) region of the primary antibody. Avidin conjugated with peroxidase has a strong affinity for the biotin label, and forms large avidin-biotin molecular complexes. The protocol following on from stage 1 for the ABC method was as follows: epitopes were blocked with 10% goat serum in TBST for 45 minutes, then incubated with primary antibody in 10% goat serum in TBST overnight at 4°C.

Slides were washed in TBST then incubated with 1/200 secondary polyclonal biotinylated goat anti-rabbit immunoglobulins (Dako: Ely, UK) in 10% goat serum in TBST for 30 minutes. Slides were again washed in TBST then incubated with Vectastain ABC elite (Vector Labs: Peterborough, UK) for 30 minutes. After slides had been washed in TBST, sections were incubated with 0.7mg/ml Sigmafast Diaminobenzidine (DAB) and 0.03% H_2O_2 (Sigma-Aldrich) in PBS in the dark for 5 minutes.

2.12.3 Envision™ Method for Active Caspase-3 Immunohistochemistry

This method utilises a polymer conjugated to multiple secondary antibodies and horse-radish peroxidase (HRP) molecules, thereby greatly improving sensitivity and specificity. This method avoids the need for blocking epitopes and is not affected by endogenous biotin. The protocol, following on from stage 1, was as follows: sections were incubated for 2 hours at room temperature with primary antibody. Slides were washed in TBST, then

incubated with Envision™ HRP labelled polymer anti-rabbit (Dako) for 30 minutes at room temperature. Slides were again washed in TBST then incubated with DAB chromogen and substrate liquid solution (Dako)

2.12.4 Immunohistochemistry Method Comparison

By assessing immunohistochemical labelling qualities of the two methods, it was possible to discern better definition of positive labelled epithelial cells with the Envision™ method, which also resulted in consistent labelling of morphologically apoptotic detached epithelial cells (Figure 17). This method also exhibited less background non-specific staining of sections compared to the ABC method, and provided considerably less labour and increased throughput.

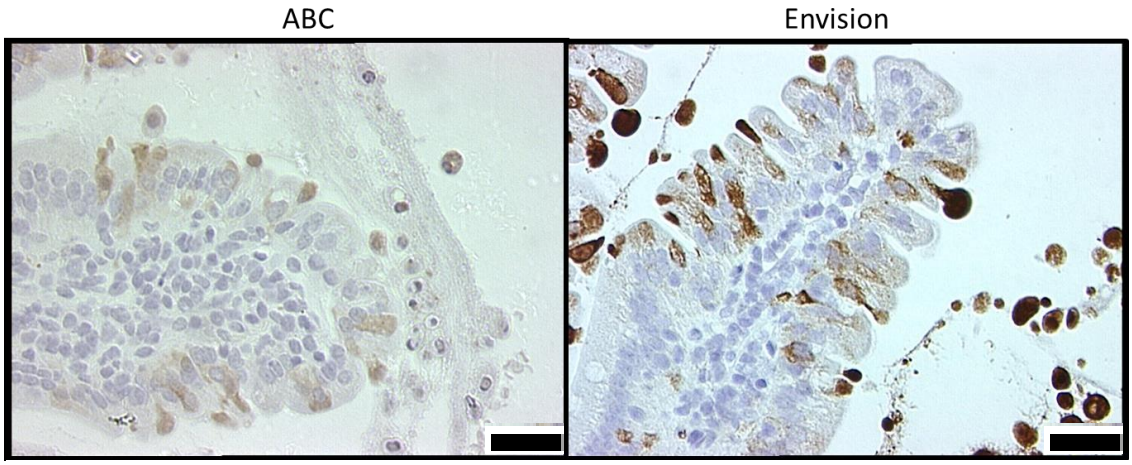

Figure 16: Immunohistochemistry was compared between the ABC method and Envision™ method using 1/800 concentration of anti-active caspase-3 primary antibody. The ABC method gave less consistent and less distinct immunostaining of apoptotic cells compared to the Envision™ method. Bars=25 µm.

2.12.5 Active Caspase-3 Antibody Titration

After selection of the Envision™ method, a titration was performed as the greater sensitivity of this staining system can often allow for more dilute primary antibody concentrations to be employed. However, concentrations

more dilute than 1/1000 resulted in more inconsistent immunolabelling (Figure 18). For the first study, including the time course and dose response, lot CFZ3207011 of the AF835 rabbit polyclonal anti-caspase 3 primary antibody was used at 1/800 dilution. For subsequent studies, titration was performed with a new batch of primary antibody (lot number CFZ3410111), for which it was found that 1/2000 gave optimal staining.

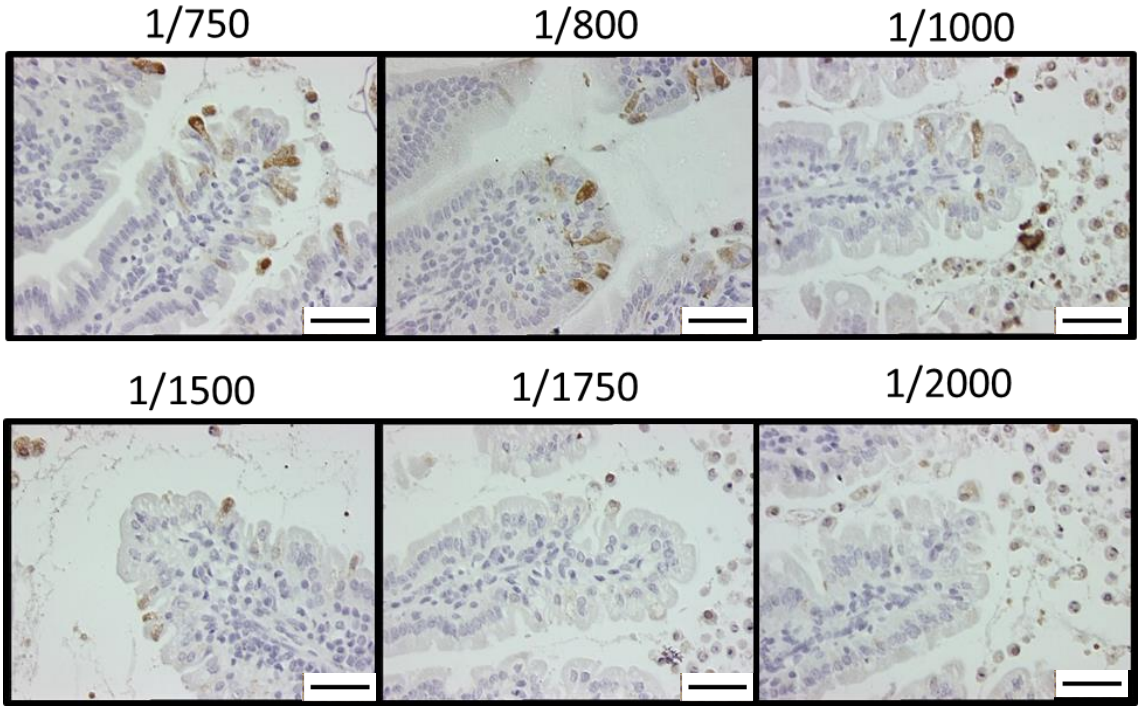

Figure 17: Titration of AF835 rabbit polyclonal anti-caspase 3 primary antibody (lot number CFZ3207011) showed greatest definition of positively labelled epithelial cells at 1/800, and more vague and inconsistent staining at concentrations more dilute than 1/800. Bars=50µm.

2.13 Active Caspase-3 Scoring Criteria

For quantification of apoptotic and shedding IECs, individual epithelial cells were counted from the base of the villus (above crypt level) to the mid-point of the villus tip in 18-20 well orientated “hemivilli” at 400x magnification (delineated by the red line in Figure 19). The hemivilli selected for scoring

were chosen based on the criteria that they were the first encountered during microscopic examination with correct orientation (similar to height of neighbouring villi, correct shape including shape of villus tip, continuous section) and that they exhibited a resolvable monolayer of epithelium along their axis. IECs were categorised according to the following criteria:

- “Normal” if there was no/weak diffuse non-specific brown staining and cells had a basally located basophilic nucleus.
- “Apoptotic” if there was defined positive staining which was confined to cytoplasmic or nuclear borders when compared to any background staining of neighbouring IECs.
- “Shedding” if there was defined positive staining which was confined to cytoplasmic or nuclear borders and in addition there was apical elevation of the cytoplasmic membrane, and/or an apically positioned nucleus.

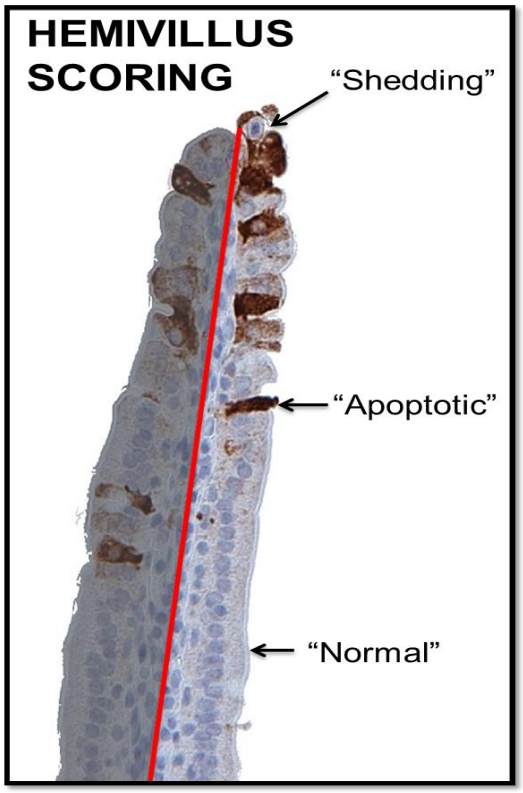

Figure 18: Active caspase-3 IHC. Duodenal villus tip, indicating the 3 possible categories into which cells are designated during counting. Arrows indicate active caspase-3 positive IECs with a "shedding" morphology, and IECs with positive immunolabelling for active caspase-3 with unaltered morphology, designated as "apoptotic". Unlabelled cells are designated as "normal".

Crypt IECs were similarly counted from the crypt base to the crypt-villus junction in 19-20 well-orientated duodenal hemicrypts per mouse. Crypt IECs were simply categorised as "normal" or "apoptotic" based on active caspase-3 staining.

2.13.1 Quantification of Active Caspase-3 Immunohistochemistry

A method for quantification of active caspase-3 positively immunolabelled cells by microscopic analysis was devised utilising SCORE software (Version 1, Beta 1, developed by Steve Roberts, at the Paterson Institute for Cancer Research, Manchester, UK 1996). This program allows categorised cell counting according to the scoring criteria described above. Cell category was

assigned a keyboard character on a cell positional basis in 18-20 well orientated villi from the duodenum, jejunum and ileum of the small intestine. IECs were counted with each keystroke from the base of the villus to the apex for each hemivillus or hemicrypt at 400x magnification. Individual files created in the score program were transferred to WinCrypts© software (Version 1.00, Release 1.9, Cancer Research Campaign 1999) for data analysis.

2.14 Cell Positional Data for Active Caspase-3 Immunohistochemistry

To allow comparison of cell positional data, villi were adjusted to a fixed length of 100 cells using WinCrypts© software. Data are then represented as percentage of villus length, with 0% therefore representing the villus base, and 100% representing the villus tip.

2.15 Consistency of Active Caspase-3 Immunohistochemical Scoring

There is an obvious degree of subjectivity to assessment of immunohistochemistry, as positive DAB labelling must be interpreted in relation to background non-specific staining levels, and by comparison to neighbouring cells. There is also unavoidable variability in section quality, and in different batches of immunohistochemistry in larger studies, which must be judged and interpreted to confirm that sections are suitable for further assessment. The author and principal observer (PO), as a trained veterinary pathologist has experience in the assessment of immunohistochemistry in the context of diagnostic histopathology. However,

the reproducibility of the scoring method, and both inter-observer, and intra-observer variation were tested (Figure 19). This was achieved by repeat scorings made on active caspase-3 stained duodenal sections on separate occasions. These data demonstrated relative consistency between repeated scoring by the principal observer, and relative agreement with the independent observer (IO) for individual slides at indicated time points post-LPS (Figure 20). There is also overall agreement between the independent observer and principal observer on the overall trend in peak apoptosis and shedding at 1.5h.

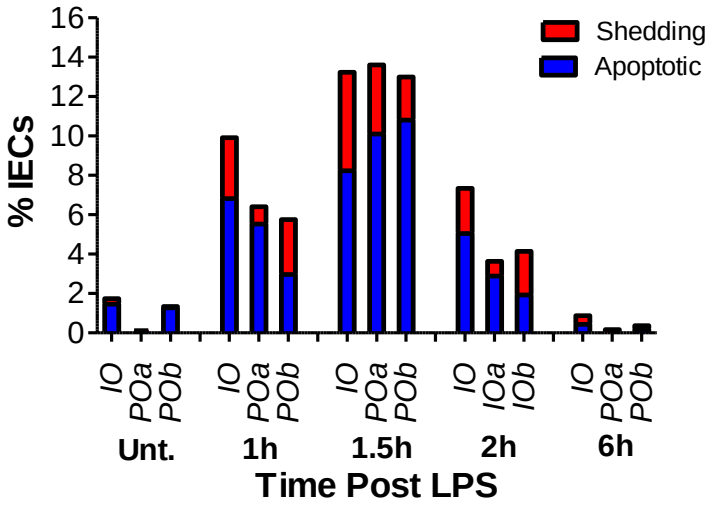

Figure 19: Bar charts demonstrating scoring consistency of active caspase-3 for the same set of 5 slides for duodenal sections at indicated time point post LPS by an independent trained observer (IO) compared with 2 separate scorings by the author (POa and POb). Unt=untreated.

2.16 Consistency of LPS Induced IEC Apoptosis and Shedding Between Laboratories

As well as confirming relative consistency and agreement between independent scorings and observers, it was necessary to confirm that LPS treated WT responses were consistent between different laboratories. LPS treated WT mice at the University of Liverpool (UoL) and University of Southern California (UoSC) were therefore compared. When administered 10mg/kg PE-LPS for 1.5h, mice at UoL and UoSC showed very similar duodenal villus height reduction to 260.5µm±15.0µm and 278.4µm±15.8µm respectively (Figure 20A). They also showed very comparable combined apoptosis and shedding indices (Figure 21B) at 12.8%±1.34% at UoSC compared to12.5%±1.7% at UoL.

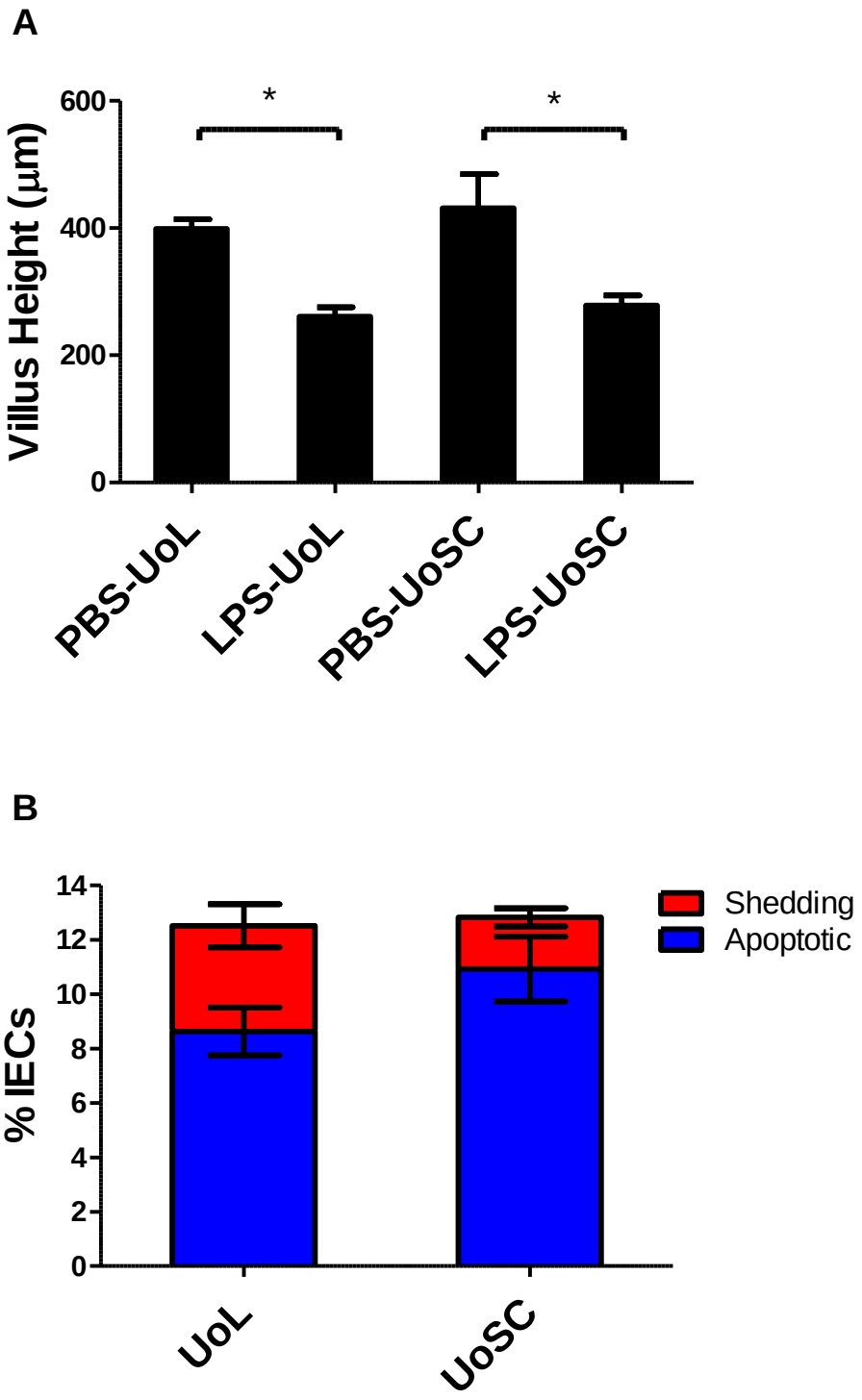

Figure 20: Villus heights (A) and percentage of apoptotic and shedding IECs (B) in vehicle (PBS) treated and LPS treated mice in University of Liverpool (UoL) and University of Southern California (UoSC) laboratories. n=3-6 mice per group. *N.B.* UoSC PBS treated mice represent mean villus height of n=1 for PBS treated WT, *Tnfr1*$^{-/-}$ and *Tnfr2*$^{-/-}$ mice. *=*P*<0.05 based on ANOVA with Holm-Sidak post-hoc test.

2.17 Image Analysis of Active Caspase-3 Immunohistochemistry

In an attempt to avoid the issues surrounding the effects of observer subjectivity in assessment of immunohistochemistry quantification, an automated IHC analysis method was also tested. This was achieved by utilising photomicrographs at 100x magnification and using ImageJ software (Schneider et al. 2012). Briefly photomicrographs were edited in ImageJ to remove positively labelled luminal content, and 10 well orientated villi were selected. Photomicrographs were then split into component red, green and blue channels. The blue channel image was then utilised as this largely cancelled out blue haematoxylin counterstaining and gave good contrast for brown DAB labelled cells. A threshold intensity for positive labelling was set manually, and the program was utilised to calculate the percentage of villus area positively labelled by DAB. The results for the time course experiment (Figure 21) showed broad agreement with the time course pattern assessed by human scoring, but with larger inter-animal variation. This method was also highly labour intensive, as it demanded a great deal of human intervention in villus selection, image editing, and setting threshold intensities, thereby introducing elements of human bias that were hoped to be avoided in computer based image analysis. It was therefore not pursued further as a suitable quantification method.

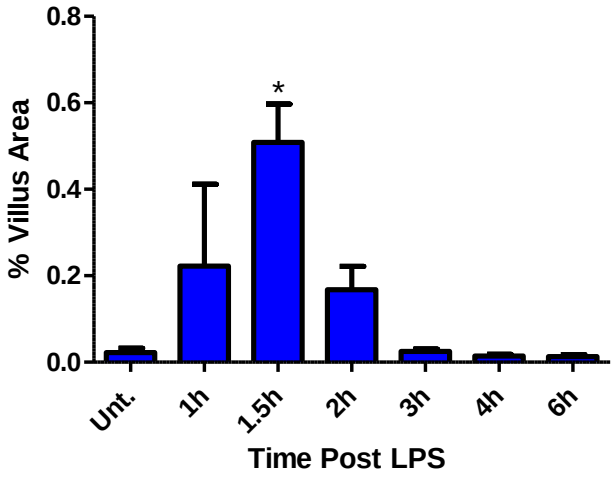

Figure 21: Bar chart of percentage duodenal villus area positively immunolabelled for active caspase-3 measured by ImageJ analysis at set time points post LPS, demonstrating maximum labelling at 1.5h. * =*P*<0.05 based on Kruskal-Wallis with Dunnett's post-hoc test. n=6, Unt.=untreated.

2.18 Villus Height By Graticule Measurement

An eyepiece graticule was calibrated by measurement against a 1x1mm haemocytometer, and length measurements made of 10 well orientated villi from the villus base to the villus tip. Data were inputted directly into Microsoft Excel. Mean villus length was calculated for the group of animals at each time point and for each intestinal segment.

2.19 Measurement of Villus Height by Image J

Image J was used to assess images captured by a Leica DMLA microscope, by setting the scale with a haemocytometer at 100x magnification. All images were captured at 100x magnification, and villi were measured by using the segmented line tool. Each segmented line was placed to originate at the base of the villus, above the level of adjoining crypts, and a segmented line extended to the villus tip, following any curvature of the villus. The mean of

these segmented line lengths for 10 well-orientated villi was calculated for each animal, and a mean value was then calculated for each group. The ImageJ assessment method was utilised for villus height measurements unless otherwise stated.

2.20 Gut Permeability Assays

Fluorescein isothiocyanate (FITC) conjugated dextran (FD4:Sigma-Aldrich) represents a fluorescent labelled dextran of molecular weight between 3-5KDa. This molecule should not in normal conditions be absorbed via the gastrointestinal tract into the circulation unless there is increased gut permeability. All animals were fasted overnight, then administered 22mg/ml FD4 in PBS at a dose of 20ml/kg by oral gavage with a blunted curved gavage needle. In order to allow the FD4 to be distributed throughout the intestinal tract, FD4 was administered 5 hours prior to them being euthanased via a rising CO_2 concentration, and blood taken by cardiac puncture. To assess the effect of LPS on permeability, it was administered at set time points prior to the end of the experiment, i.e. gut permeability at 1.5h post LPS was achieved by LPS administration at 1.5h prior to euthanasia. Plasma was separated from heparinised whole blood by centrifugation at 2000 x *g*. Plasma fluorescence was measured by an Infinite® F200 plate reader (TECAN: Reading, UK) at excitation wavelength 485nm, and emission wavelength 535nm, from blood collected post-mortem, 5h after gavage.

2.21 Tissue for RNA and Protein Extraction

Treated and untreated mice were euthanased by a Home Office approved method. The small intestine was removed at necropsy and flushed with chilled chelation buffer as described by Flint et al. (1991). Briefly, the small intestinal content was flushed out with chilled PBS, and the small intestine incised longitudinally with scissors. The small intestine was placed in chilled chelation buffer on ice for 20 minutes in 50ml Falcon™ tubes (Oxford, UK). Contaminated buffer was discarded and replaced with fresh solution, while the samples were maintained on ice with frequent agitation and vortexing. This was followed by centrifugation at 300 x *g* at 4ºC for 5 minutes to produce an epithelial enriched pellet containing crypt villus units. These samples were stored at -80ºC until further analysis.

2.22 RNA Extraction

RNA was isolated with a High pure RNA Tissue Kit (Roche; Burgess Hill, UK) from small intestinal epithelial enriched extracts isolated using the above method. Approximately 30mg of tissue was placed in denaturant/chaotropic guanidine hydrochloride solution and lysed by mechanical homogenisation. Homogenate was transferred into glass fleece containing spin columns, and in the presence of chaotropic salt solution, nucleic acids were selectively bound to this glass fleece. Nucleic acids were then eluted from the spin column into buffer and RNAse free water. The concentration of extracted RNA was quantified by absorbance spectrophotometry of a sample volume of 1µl using a Nanodrop Lite (Thermo Scientific: Loughborough, UK) at a wavelength of 260nm, and purity was assessed by the 260/280 absorbance

ratio. A ratio of ≥1.7 was considered adequate for further experiments.

2.23 Reverse Transcription

Reverse transcription was performed with 500ng RNA from individualised samples using a RT^2 First Strand Kit (SABiosciences; Crawley, UK) as per the manufacturer`s instructions. Briefly, samples were incubated with a genomic DNA elimination mix for 5 minutes at 42ºC in a heat block. Samples were then incubated with reverse transcriptase mix at 42ºC for 15 minutes and the reaction was stopped by incubation at 95ºC for 5 minutes. The resulting cDNA samples were stored at -20ºC.

2.24 Real-time PCR (qPCR)

cDNA sample quality was assessed by running individual samples on a murine RT^2 RNA QC PCR array plate (SABiosciences; Crawley, UK). Evaluation of these samples for transcription efficiency, genomic DNA contamination, and house-keeping gene expression concluded that the samples were of adequate quality for real-time PCR analysis. Two 89 gene Cell-Death Pathway Finder array (SABiosciences) plates were run, each with an n=4 pooled sample for untreated and 1.5 hour LPS treated samples. Reverse transcribed cDNA samples were equally weighted. Amplification was performed on a LightCycler 480 instrument (Roche: Burgess Hill, UK) as per the conditions outlined in Table 5, with quantification of SYBR green fluorescence.

Threshold cycle (Ct) values were calculated by the maximal second derivative algorithm using the 480 LightCycler software release 1.5.0. Gene

expression ratios were calculated by normalising genes to house-keeping genes, and using the ΔΔCt method via web based analysis software at www.sabiosciences.com/pcrarraydataanalysis.php (accessed October 2012) and comparing gene expression ratios between treated and untreated groups. Gene Primers for the following genes were included in this array:

Pro-apoptotic genes: *Abl1, Apaf1, Bcl2l11, Birc2 (c-IAP1), Casp1 (ICE), Casp6, Casp7, Casp9, Cd40 (Tnfrsf5), Cd40lg (Tnfsf5), Cflar (Casper), Dffa, Fasl (Tnfsf6), Gadd45a, Nol3, Tnfrsf10b*

Anti-apoptotic genes including: *Bcl2a1a (Bfl-1/A1), Birc3 (c-IAP2), Casp2, Igf1r, Mcl1, Tnfrsf11b, Traf2, Xiap*

Apoptosis and autophagy associated genes: *Akt1, Bax, Bcl2, Bcl2l1 (Bcl-x), Casp3, Fas (Tnfrsf6), Tnf, Trp53*

Apoptosis and necrosis associated genes: *Atp6v1g2, Cyld, Spata2, Sycp2, Tnfrsf1a*

Autophagy associated genes: *App, Atg12, Atg16l1, Atg3, Atg5, Atg7, Becn1, Ctsb, Ctss, Esr1 (ERa), Gaa, Htt, Ifng, Igf1, Ins2, Irgm1, Map1lc3a, Mapk8 (Jnk1), Nfkb1, Pik3c3 (Vps34), Rps6kb1, Snca, Sqstm1, Ulk1*

Necrosis associated genes: *9430015G10Rik, Bmf, Ccdc103, Commd4, Defb1, Dennd4a, Dpysl4, Eif5b, Foxi1, Galnt5, Grb2, Hspbap1, Jph3, Kcnip1, Mag, Olfr1404, Parp1 (Adprt1), Parp2, Pvr, Rab25, S100a7a, Tmem57, Txnl4b*

Triplicate samples were used to validate array plate findings for *Tnf* and *cd40*

using TaqMan® mouse gene expression assays (Life Technologies; Paisley, UK) for *β-actin* (Mm01205647_g1), *Tnf* (Mm00443260_g1) and *Cd40* (Mm00441891_m1;). cDNA and primers were added to TaqMan® Gene Expression Master Mix (Life Technologies; Paisley, UK). Amplification was also performed on the Roche 480 Lightcycler machine, with fluorescence measured for 6-carboxyfluorescein (FAM) probe. Cycling conditions were as above. The ΔΔCt method was again used in combination with REST© software for data analysis.

Cycles	Duration	Temperature
1	10 min	95ºC
45	15 sec 1 min	95ºC 60ºC

Table 5: Cycling conditions for qPCR analysis performed on Roche Lighcycler 480 with ramp rate of 1ºC/sec.

2.25 Protein Extraction and Western Blotting

Epithelial enriched extracts were isolated as previously described. Cell lysis was achieved by suspending cell pellets in radio immunoprecipitation (RIPA) buffer with 2x1mm diameter steel beads and performing cell lysis on a Qiagen Tissue Lyser II at 25hz for 2 minutes. Protein was quantified by Bradford assay against bovine serum albumin (BSA) at standard concentrations. Protein was denatured in Laemmli buffer at 95ºC for 5 minutes and loaded into 5% acrylamide stacking gel overlying a 10% acrylamide running gel (both used 30% acrylamide/bis-acrylamide solution; Sigma-Aldrich, UK). Samples were electrophoresed for approximately 90 minutes at 120V. Transfer and immobilisation of proteins onto nitrocellulose paper was achieved by electrophoresis at 100V for 60 minutes. Imaging was

performed with a Biorad Chemidoc Imager (Biorad; Hempstead, UK). Polyclonal rabbit antibodies for RelB (1:1000; SC-226 Santa Cruz, Heidelberg, Germany) and p100/p52 (1:1000; #4882 Cell Signaling Technologies, Danvers, USA) were incubated with nitrocellulose membranes overnight at 4ºC, and for 2 hours at room temperature with mouse monoclonal pan-actin (1:2000: ACTNO5; Neomarkers, Freemont, USA). This was followed by 2 hours incubation at room temperature with goat anti-rabbit horse-radish peroxidase (HRP) labelled immunoglobulins (1:10,000; SC-2004 Cell Signaling Technologies, Danvers, USA) or rabbit anti-mouse HRP labelled immunoglobulins (1:2000; P0161; Dako, Ely, UK) as appropriate. Nitrocellulose paper was then incubated with SuperSignal West solution (Thermo Scientific: Loughborough, UK).

2.26 Anaesthetic Protocol Evaluation

In order to perform confocal microscopy, it was necessary to establish an injectable anaesthetic protocol that did not cause any form of intestinal injury, and which also provided a stable surgical plane of anaesthesia to allow laparotomy. A combination of medetomidine (Domitor®; Pfizer, Germany) and ketamine (Vetalar®; Pfizer, Germany), was initially tested as a potential anaesthetic protocol. Medetomidine is an alpha 2 adrenoreceptor agonist, which binds with neuronal receptors predominantly in the pons and lower brainstem to prevent release of the excitatory neurotransmitter noradrenaline. This causes central nervous system depression and sedation, but also causes depressed sympathetic tone, reduced cardiac output and peripheral effects of systemic hypertension (Sinclair 2003). Ketamine represents a non-

competitive N-methyl D-aspartate (NMDA) receptor antagonist. The NMDA receptor is a cation gated channel receptor which is particularly important in cortical-cortical and cortico-subcortical interactions. Ketamine therefore causes dissociative anaesthesia and largely leaves reflexes intact (Bergman 1999).

A mixture of 0.16 mg/ml medetomidine and 20 mg/ml ketamine in sterile PBS was administered at a dose of 100µl i.p. for induction, and subsequent doses of 30µl were given intramuscularly (i.m.) every 30 minutes or as required to maintain surgical anaesthesia. This anaesthetic regimen did not provide a stable plane of surgical anaesthesia, with animals in general exhibiting inconsistent tail pinch and foot pinch reflexes, and gradually declining respiratory rate and perfusion as assessed by mucous membrane colour. These anaesthetised animals would frequently die prior to the predetermined time point. On analysis of the gut, the duodenum exhibited marked apoptosis and shedding, suggesting that this anaesthetic combination was highly unsuitable for further investigations. Instead, Hypnorm (0.315mg/ml fentanyl citrate; VetaPharma Ltd, Leeds, UK) and diazepam (5mg/ml; Hameln, Gloucester, UK) were tested as an alternative combination. Fentanyl at 13µg (0.04ml) with 150µg diazepam (0.03ml) were administered for induction by i.p. injection, followed by 6µg (0.02ml) fentanyl i.m. as required to maintain surgical anaesthesia. Fentanyl represents a potent and short-acting agonist of µ opioid receptors. Diazepam represents an agonist of $GABA_A$ receptors. It potentiates the inhibitory neurotransmitter γ-aminobutyric acid (GABA) causing central nervous system depression and muscular relaxation.

This combination gave stable surgical anaesthesia and histopathological analysis showed absence of apoptosis and cell shedding that were observed with the medetomidine and ketamine combination. This anaesthetic regimen was therefore utilised to perform confocal microscopy. Tests were also performed whereby anaesthetised animals were simultaneously administered LPS, followed by histopathology after euthanasia to confirm that similar apoptosis and shedding was caused in anaesthetised animals and in a similar time course to conscious animals.

2.27 *In vivo* Confocal Microscopy

Confocal microscopy is a technique whereby laser light at specific wavelengths is focused onto a specimen, stimulating electron excitation in fluorescent dyes which then emit photons of a specific wavelength. Photons at the specific emission wavelength are then collected by photomultiplier tubes to generate an image. By collecting only in focus and not scattered photons through a pinhole aperture, and using image deconvolution, this technique offers great benefits over traditional fluorescent microscopy by allowing three-dimensional optical sectioning through a thicker biological specimen.

Briefly, mice were administered fentanyl and diazepam i.p., with or without 10mg/kg LPS administered 10 minutes prior to induction. When a surgical plane of anaesthesia was considered to have been attained, the animal was placed on a heat mat in dorsal recumbency and a 1 cm midline abdominal incision made and laparotomy performed. The jejunum was externalised, and an approximately 2cm length segment was incised with a cauterizer along its

anti-mesenteric border and opened to expose the mucosal surface. The mouse was then transferred to a custom made metal stage insert in ventral recumbency, and the mucosal surface was then placed on a coverslip with a small amount 3.85mM acriflavine hydrochloride made up in Hank`s balanced salt solution (both Sigma-Aldrich, UK). Acriflavine stains both nuclei and cytoplasm and fluoresces on stimulation with laser light. Photons of laser light at approximately 416nm were used to stimulate emission of photons from acriflavine at approximately 514nm. Images were taken with a Leica True Confocal Scanner SP2 operated with Leica LCS software package at 200x magnification at scan speed of 400hz over a typical tissue depth of approximately 20µm.

2.28 Data and Statistics

Data represent mean±standard error of the mean (SEM). Comparisons were made between equivalent intestinal segments in treatment groups and controls using SigmaPlot 12© (Systat Software: London, UK). Normally distributed data were assessed by analysis of variance (ANOVA) with Holm-Sidak post-hoc test, and non-parametric data were analysed by ANOVA on ranks (Kruskal-Wallis) with Dunn's or Dunnett`s post-hoc test. $P<0.05$ was considered significant and indicated by an asterisk. REST© software was used for comparison of qPCR data from individualised samples by randomisation test as previously described (Pfaffl et al., 2002). n numbers indicate the total number of mice studied per group.

3. Effects of LPS on the Epithelial Cells of the Gastrointestinal Tract

3.1 Introduction

Characterisation of the cell death occurring in intestinal injury brought about by sepsis or endotoxic shock in mice has previously concentrated on intestinal pathology at time points beyond 4 hours (Alscher et al. 2001; Coopersmith et al. 2003; Han et al. 2004; Guma et al. 2011). Other animal studies in rats have given limited descriptions of the most acute lesions of endotoxic shock, having described small intestinal red streaks, which by *in vivo* microscopy appear to be congested vessels. These lesions have been reported as early as 20 minutes after intravenous injection of endotoxin, with haemoglobin leakage into the gut lumen (Shindo et al. 1996). One hour after the start of a constant intravenous infusion of endotoxin, gross evidence of "erosions, hyperaemia and haemorrhage" and histological evidence of "partial destruction of the upper part of the villi" have also been observed (Miura et al. 1996).

Intestinal permeability has previously been shown to increase in endotoxic shock in multiple studies, but the most rapid increase in intestinal permeability in a mouse model was recorded 2 hours after initiation of endotoxic shock by measurement of ^{51}Chromium labelled EDTA clearance (Deitch et al. 1991). This study implicated the ileum in this increased permeability but not the jejunum. Marginally increased levels of apoptosis (but primarily necrosis) have been observed at the villus tip in a feline model of septic shock within the ileum, also at 2 hours after LPS administration (Crouser et al. 2000).

Establishing when and where significant epithelial cell death and cell

shedding occur in the murine gastrointestinal tract following systemic LPS administration was therefore critical in order to study pathological villus epithelial shedding, and to develop this model for investigation of this phenomenon. We also aimed to characterise the early clinical signs in LPS treated mice, and compare the sensitivity of other organs compared to the gastrointestinal tract by taking additional visceral samples and examining them by histopathology. By ultrastructural and immunohistochemical study we aimed to characterise the cell death and/or shedding that occur in acute endotoxic shock. We also aimed to correlate pathological alterations in the gut with detrimental effects on gut barrier function by performing gut permeability assays.

3.2 Systemic LPS administration caused clinical signs and gross pathological alterations from 1.5 hours

Initial investigations focused on establishing the time dependent pathological effects of LPS. PE-LPS was administered at 10mg/kg by i.p. injection to adult female WT C57BL/6 mice, and they were euthanased by cervical dislocation at 1, 1.5, 2, 3, 4 and 6 hours later. Animals began to exhibit clinical signs such as crouching gait, piloerection and huddling behavior indicative of hypothermia, and ptosis anywhere between 15 minutes to 1.5 hours after LPS administration. Mucoid brown to yellow diarrhoea was observed in animals from 1.5-2 hours after LPS administration. At necropsy, gross pathological changes included serosal pallor of the small intestine (Figure 22B), which exhibited distension with watery yellow fluid. These observations showed that LPS caused acute onset diarrhoea in this murine model of

endotoxic shock, with gross evidence of fluid exudation into the small intestine.

3.3 LPS caused small intestinal injury manifested by villus IEC shedding from 1.5 hours

Histopathological examination of H&E stained sections was performed to characterise the intestinal injury following LPS administration. Small intestinal sections from animals euthanased at 1.5 hours (Figure 22D and F), and at 2 hours, demonstrated marked villus atrophy characterised by villus stunting, blunting, and clubbing. Large numbers of IECs were observed within the intestinal lumen, characterised by cell shrinkage and rounding, with hypereosinophilic cytoplasm, and a round, centrally located, pyknotic nucleus (consistent with apoptotic epithelial cells). IECs at the villus tip exhibited variable separation and detachment from neighbouring cells with either cytoplasmic swelling, vacuolation and an apically positioned nucleus (consistent with hydropic degeneration and shedding), or a teardrop morphology with cell shrinkage, hypereosinophilic cytoplasm, and an apical hyperchromatic nucleus (consistent with apoptosis and shedding). Large numbers of shed epithelial cells were present within the lumen. The small intestine also exhibited some patchy oedema of the lamina propria, and dilation of blood vessels with margination of neutrophils.

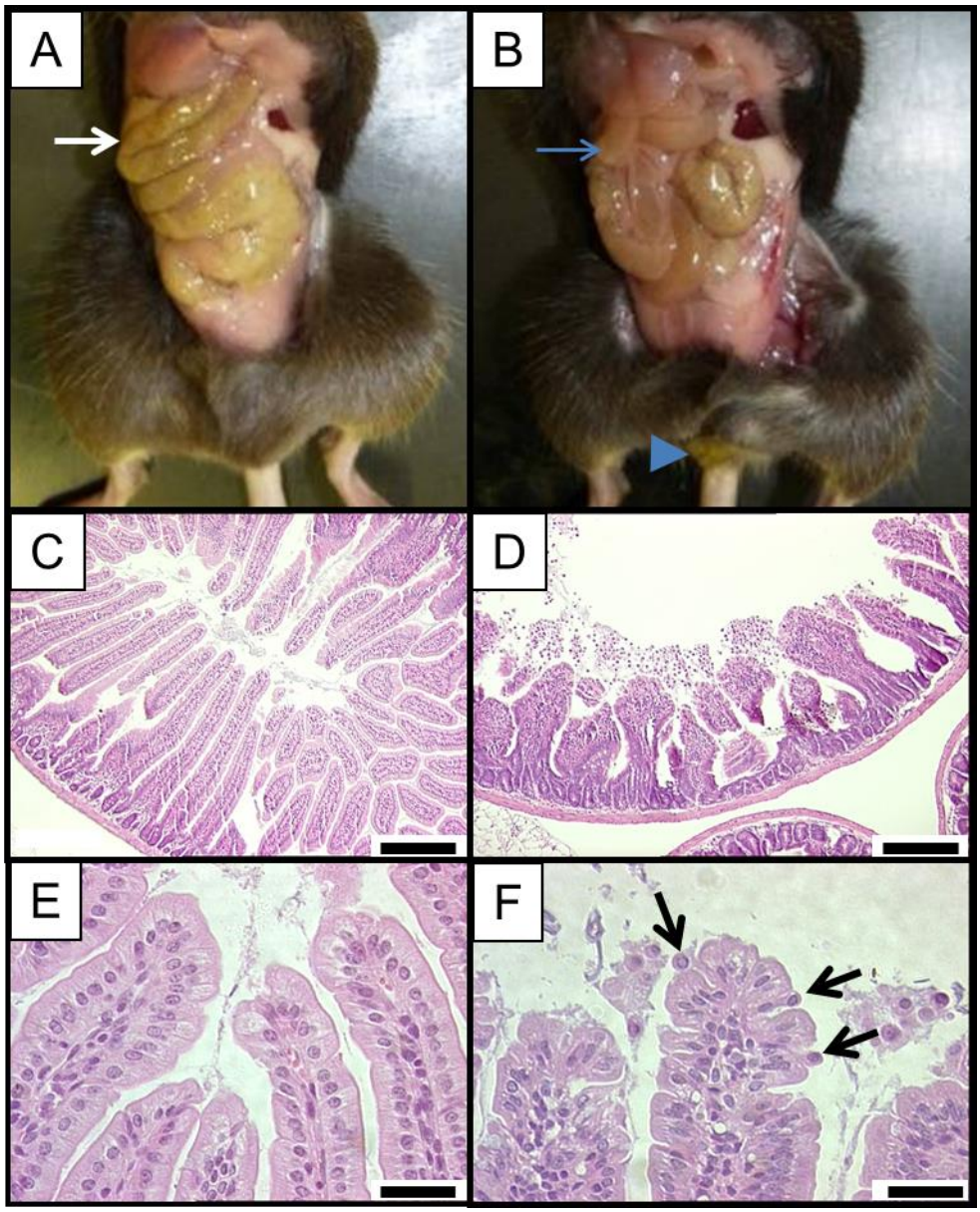

Figure 22: Untreated control (A) and 1.5h LPS treated WT mouse (B),exhibiting fluid filled small intestine devoid of digesta (blue arrow) with diarrhoeic faeces at anus (blue arrowhead). H&E stained sections of duodenum showing normal villi in untreated control (C) and shortened, blunted villi with shed IECs in lumen at 1.5h (D). Villus tips in untreated control (E) and shedding IECs (F) at 1.5h (arrows). Bars=200µm in (C) and (D), and 25µm in (E) and (F).

3.4 LPS caused highly dynamic small intestinal epithelial cell apoptosis and cell shedding with concomitant activation of caspase-3

After finding histopathological evidence of cell death and cell shedding, sections were examined for biochemical evidence of programmed cell death (apoptosis). Immunohistochemistry for active caspase-3 was therefore performed, which is a generally accepted method for detecting apoptosis in tissue sections. Active caspase-3 immunolabelled sections (Figure 24) demonstrated the amount of IEC apoptosis and shedding that was induced by LPS at the time points investigated. These representative photomicrographs demonstrate that the quantity of IECs positively immunolabelled for active caspase-3, was negligible in untreated animals, markedly increased at 1 hour post LPS administration (predominantly within the epithelium), was maximal at 1.5 hours (with many positively labelled IECs within the lumen), and declined markedly by the 3 hour time point, without further changes at 4 or 6 hours. At higher magnification (Figure 25) apoptotic IECs that were positively labelled for active caspase-3, and shedding IECs that were both positively labelled and undergoing extrusion from the epithelial monolayer were observed.

Quantification of this effect was achieved by manual counting (see Materials and Methods). Maximal active caspase-3 labelling of 12.5%±1.7% villus IECs was found in the duodenum 1.5 hours after LPS administration (Figure 26), representing a 21 fold increase compared to untreated mice (0.6%±0.2%, $P<0.05$: Kruskal-Wallis). Comparable IEC apoptosis and cell shedding were

also observed at 1.5 hours in the jejunum and ileum (12.1%±2.4% and 11.2%±1.3% respectively). Comparable apoptosis was not observed in the stomach, colon, liver, kidney, lung or brain 1.5h following LPS administration (Figure 26).

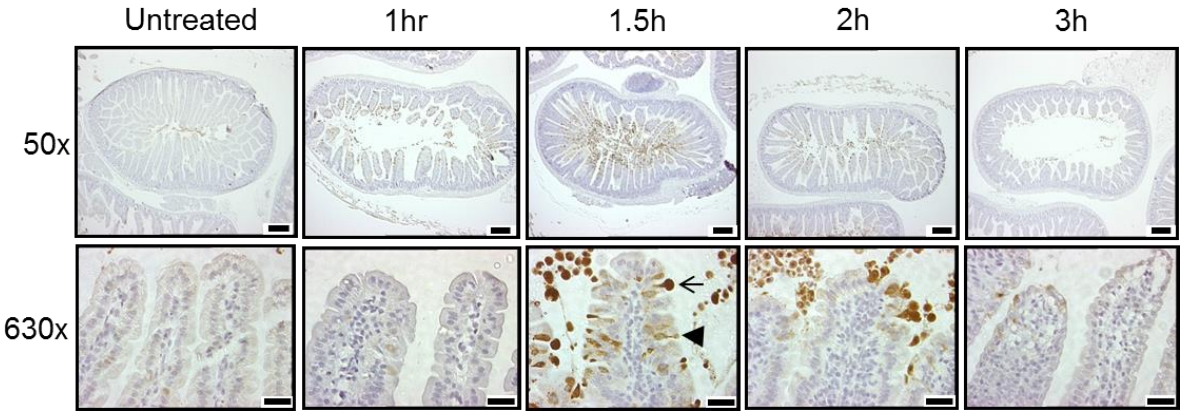

Figure 23: Active caspase-3 IHC in sections of duodenum, demonstrating negligible labelling in untreated mice, increased IEC labelling at 1 hour, and maximum positive labelling of IECs at 1.5 hours post LPS. Large numbers of positively labelled shed cells were present within the lumen. Minimal labelling was observed from 3 hours onwards. 50x bars=200µm, 630X=25 µm.

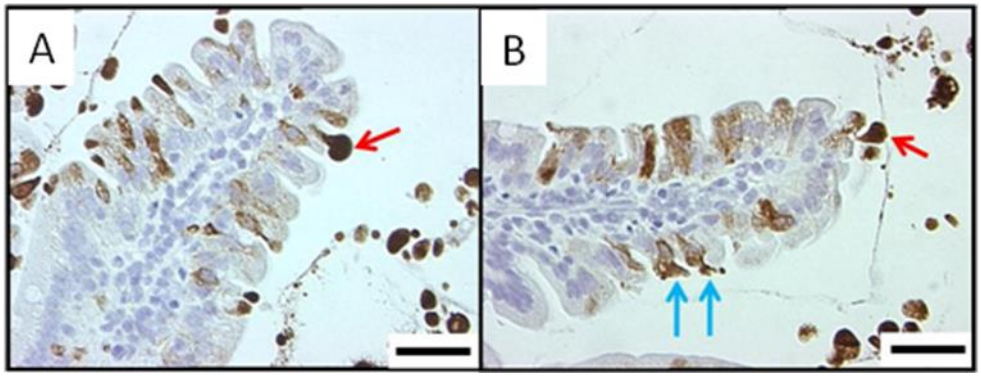

Figure 24: Active caspase-3 IHC showing typical duodenal villus tips at 1.5 hours post LPS. Red arrows indicate active caspase-3 positive IECs with a shedding morphology (A and B), blue arrows indicate IECs with positive immunolabelling for active caspase-3 with unaltered morphology (B), interpreted as apoptotic. Bars=25µm.

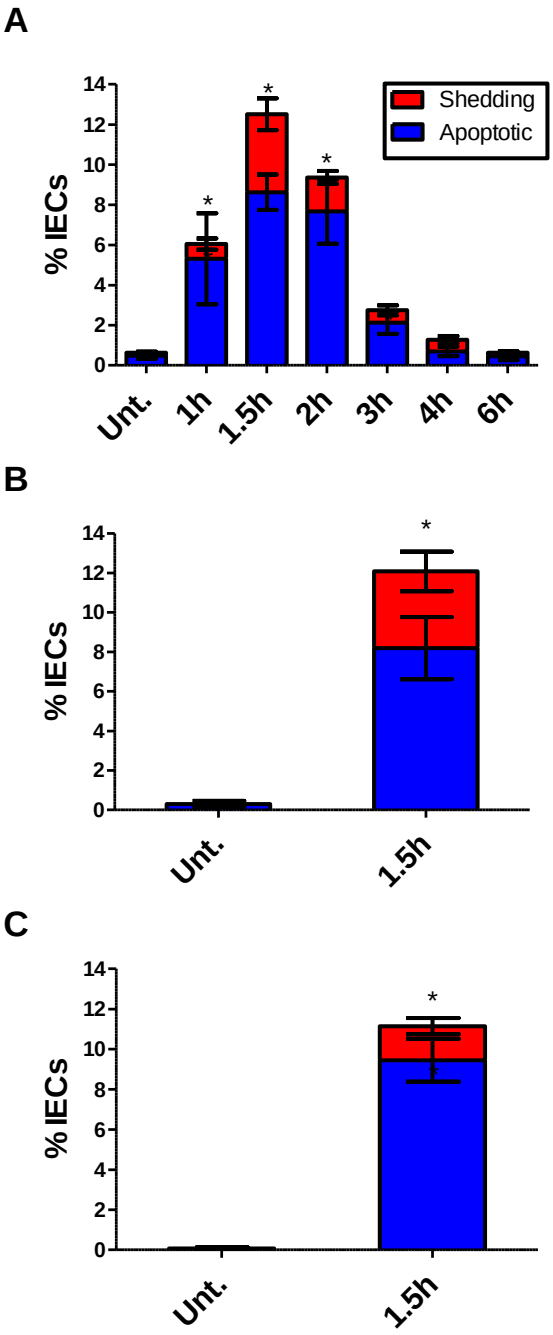

Figure 25: Quantification of categorised IECs by manual counts of active caspase-3 IHC at set time points post LPS in duodenum (A), jejunum (B), and ileum (C). *P*<0.05 based on Kruskal-Wallis comparison with Dunnett's post-hoc test. n=6 mice/time point. Unt.=untreated

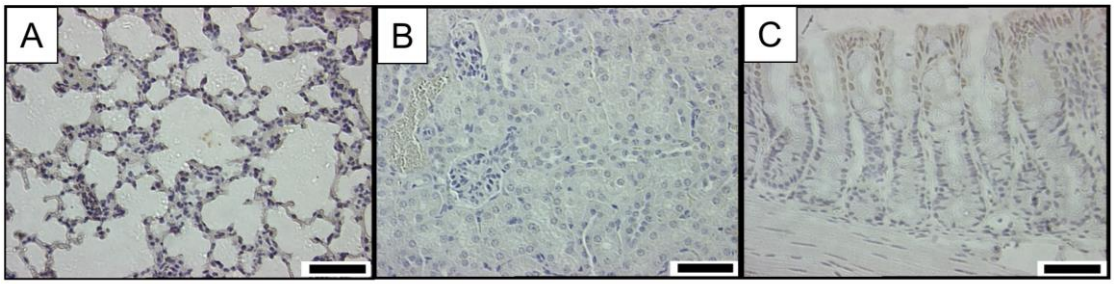

Figure 26: Other target organs commonly damaged in endotoxic shock did not show evidence of cell death**.** IHC for active caspase-3 shows lack of immunolabelling in lung (A), kidney (B), or other localisations of the gastrointestinal tract; colon (C) from 1.5h 10mg/kg LPS treated mice with confirmed apoptosis in the small intestine. Bars=50µm.

3.5 LPS did not cause significant apoptosis in the small intestinal crypts

From initial study of H&E stained sections of the small intestine, it was apparent that during the early phases of endotoxic shock in our model, the crypts did not exhibit the same magnitude of cell death as villi. However, as many studies of small intestinal injury induced by LPS have focused entirely on the effects caused in the crypts, generally from 4h onwards, investigation and quantification of the amount of apoptosis that occurred in the crypts was undertaken.

Crypt IEC apoptosis as interpreted by active caspase-3 IHC did not show a comparable magnitude of increase to that observed in villi at 1.5h (Figure 28A), although there was a ~3 fold increase by 6h post LPS compared to untreated mice (1.2%±0.3% versus 0.4%±0.1% in untreated). Accordingly, crypt counts did not alter significantly throughout the time course studied (Figure 28B), in contrast to villus IECs counts. Crypt apoptosis did not exhibit an obvious cell positional dependent pattern along the crypt axis (Figure 28).

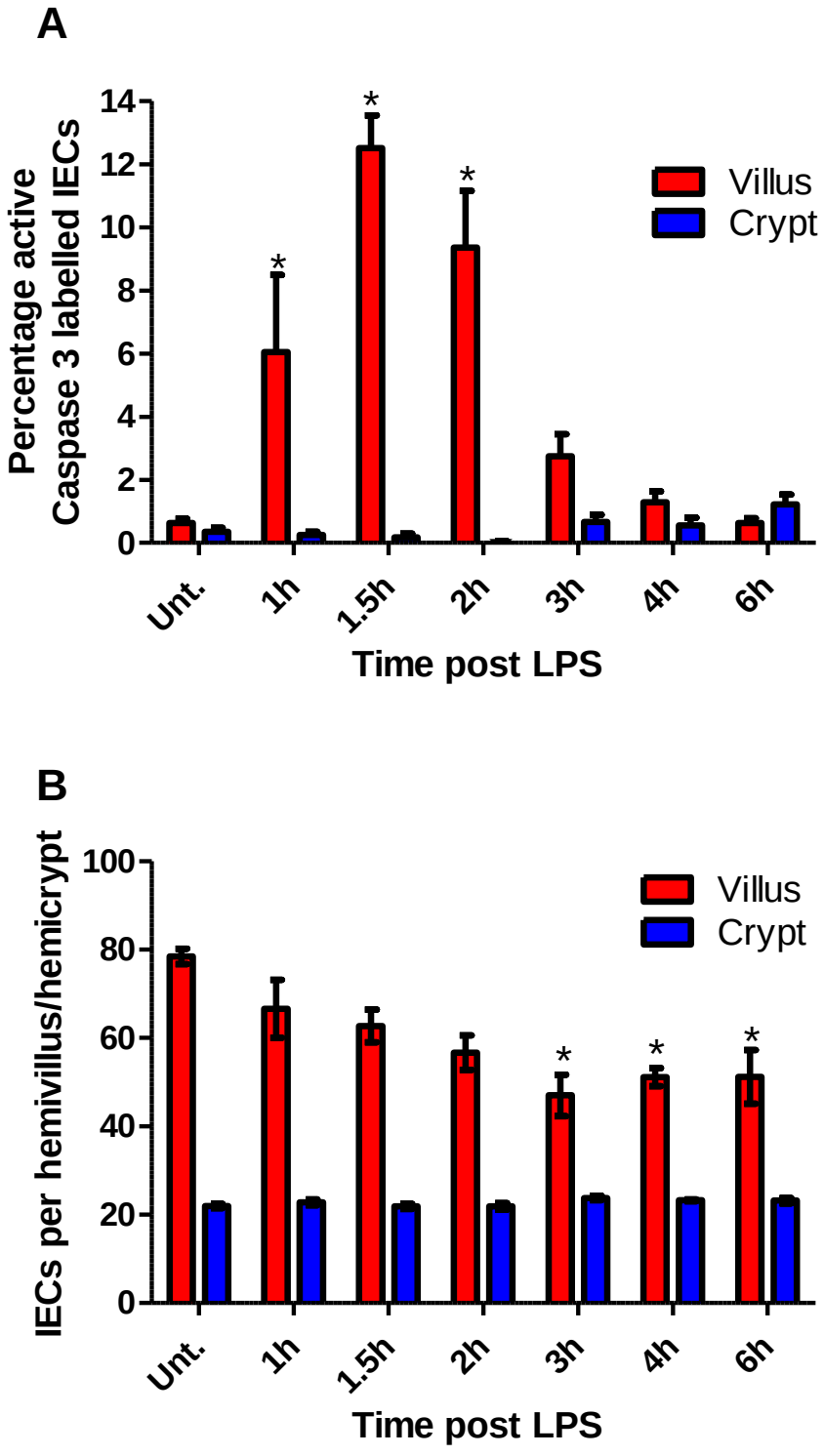

Figure 27: Quantification of active caspase-3 labelled IECs (A) and relative IEC counts in hemivilli compared to hemicrypts (B) in the duodenum at time points indicated after 10mg/kg PE-LPS.

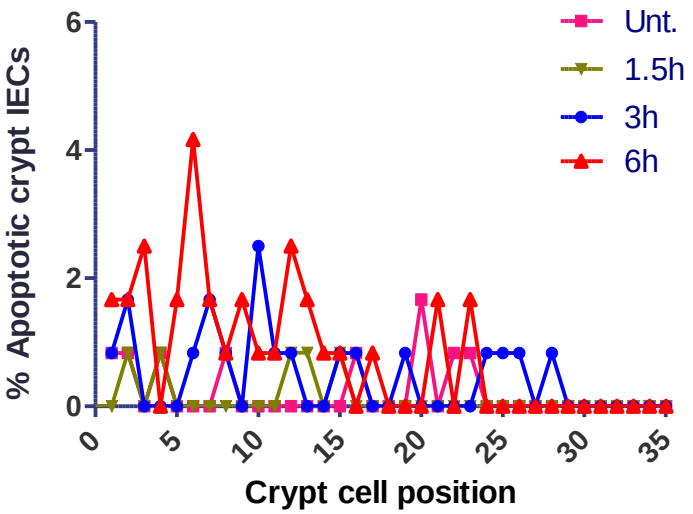

Figure 28: Crypt apoptosis quantification did not demonstrate an obvious pattern along the crypt axis at time points indicated after LPS administration. n=6 mice per group.

3.6 LPS caused rapid villus atrophy in the duodenum, jejunum, and ileum

As shortening of the villus (villus atrophy) is commonly observed in small intestinal damage, villus heights were measured as an additional means of assessing LPS induced injury. Villus height assessment was made by three different modalities, including IEC counts (Figure 29A), graticule measurement (Figure 29B), and ImageJ analysis (Figure 29C). The mean villus height was decreased in all intestinal segments from 1 hour post LPS, with the largest proportional and significant reduction in villus height being measured in the duodenum from 1.5 hours and minimum heights being observed at 3 hours. By ImageJ analysis (Figure 29C), mean villus height in the duodenum was reduced by 29% to 260.5µm±15.0µm, 1.5 hours after LPS administration, compared to untreated (365.9µm±6.6µm (P<0.01: ANOVA)). Maximal villus atrophy was also measured by this method at the 3

hour time point (252.2µm±22.2µm), representing a relative percentage reduction in villus height of approximately 31%. Villus heights did not exhibit further changes at the 4 and 6 hour time points.

Villus shortening was also associated with lower numbers of IECs lining the duodenal villi, with a 21% reduction in mean cell number observed at 1.5 hours post LPS administration (62.7±3.7 versus 78.5±1.8 cells in untreated mice), reaching significance at 3 hours, with a 40% decrease observed at 47.0±4.7 cells (P<0.05; Kruskal-Wallis: (Figure 30A)). This correlated with large numbers of shed IECs within the intestinal lumen, implying that cell shedding correlates with shortening of the villus and decreased villus IEC number.

ImageJ analysis was utilised to measure LPS induced villus atrophy in subsequent experiments, as this method can measure villus height to the nearest µm, and this can be done by measuring along the central core of the villus with the segmented line tool. This can take into account any subtle curvature of the villus when it is not perfectly straight or perpendicular to the muscularis. It was also considered superior to hemivillus IEC counts, as Wright et al. (1989) showed that although good correlation has been demonstrated between total villus population and villus height when counted by microdissection, this correlation was considerably diminished when there was altered villus morphology, such as we observed following LPS administration.

Taken in conjunction with the analysis of IEC apoptosis and shedding, these

data were utilised in selecting the duodenum at 1.5 hours as the most appropriate intestinal site and time point for comparisons to be made between LPS dosages and mouse genders, and genotypes in subsequent experiments.

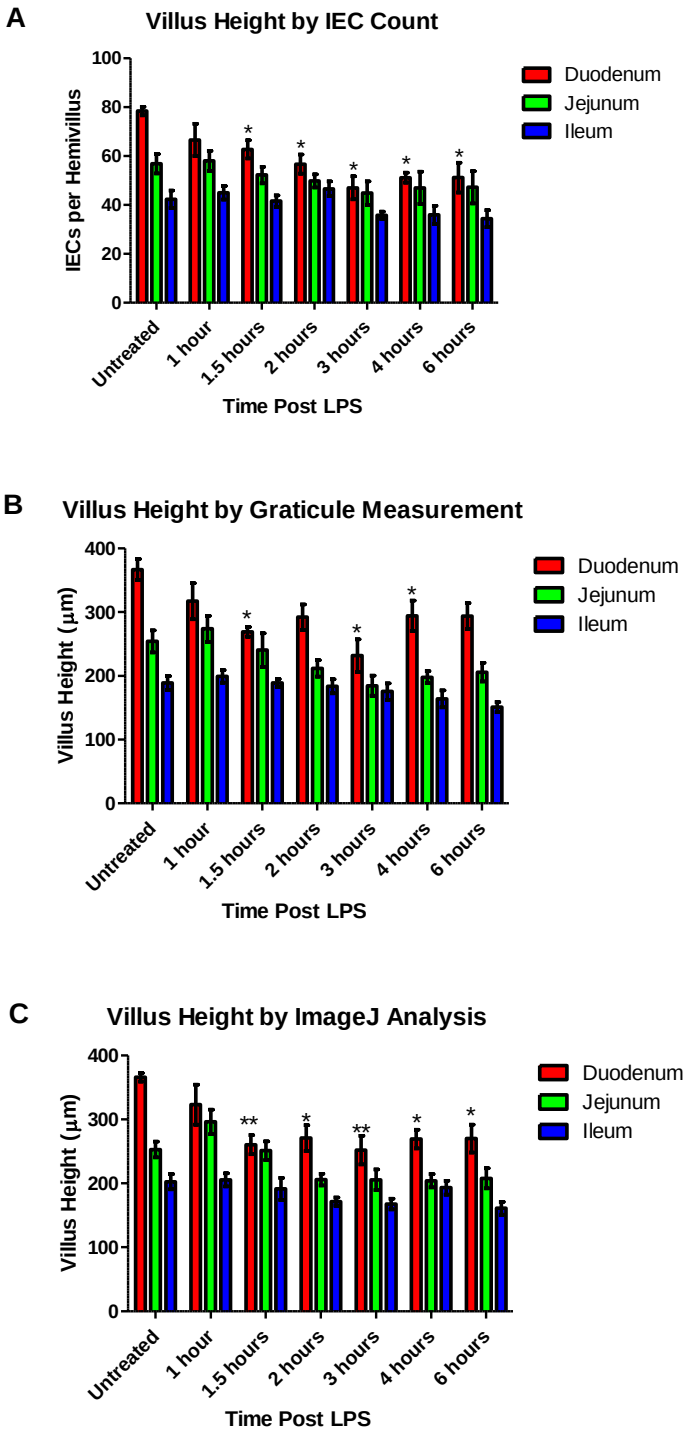

Figure 29: Villus heights for duodenum, jejunum, and ileum by IEC count (A), graticule measurement (B) and ImageJ analysis (C). n=6 mice per time point, statistical comparisons by Kruskal-Wallis with Dunnett`s post-hoc test in A and B, and by ANOVA with Holm-Sidak post-hoc test in C.*=P<0.05, **=P<0.01.

3.7 LPS induced apoptosis and cell shedding which increased in frequency towards the villus tip

Having measured the amount of IEC apoptosis and shedding that occurred in the duodenum, jejunum and ileum and the coexistent villus atrophy, cell positional data collected by IHC quantification was used to determine where along the villus axis IEC apoptosis and shedding occurred. These data showed that IECs positively immunolabelled for active caspase-3 without altered morphology, designated “apoptotic” (Figure 30), and “shedding” IECs (Figure 31), showed similar distributions along the villus axis at different time points in the duodenum. Similar distributions were also observed in the duodenum, jejunum and ileum at 1.5 hours. The duodenum, jejunum, and ileum exhibited broadly similar trends in the overall pattern of apoptosis and shedding along the villus axis. Both events markedly increased in frequency in the apical 50% of the villus at 1.5 hours, with increased IEC shedding being seen at the villus tip.

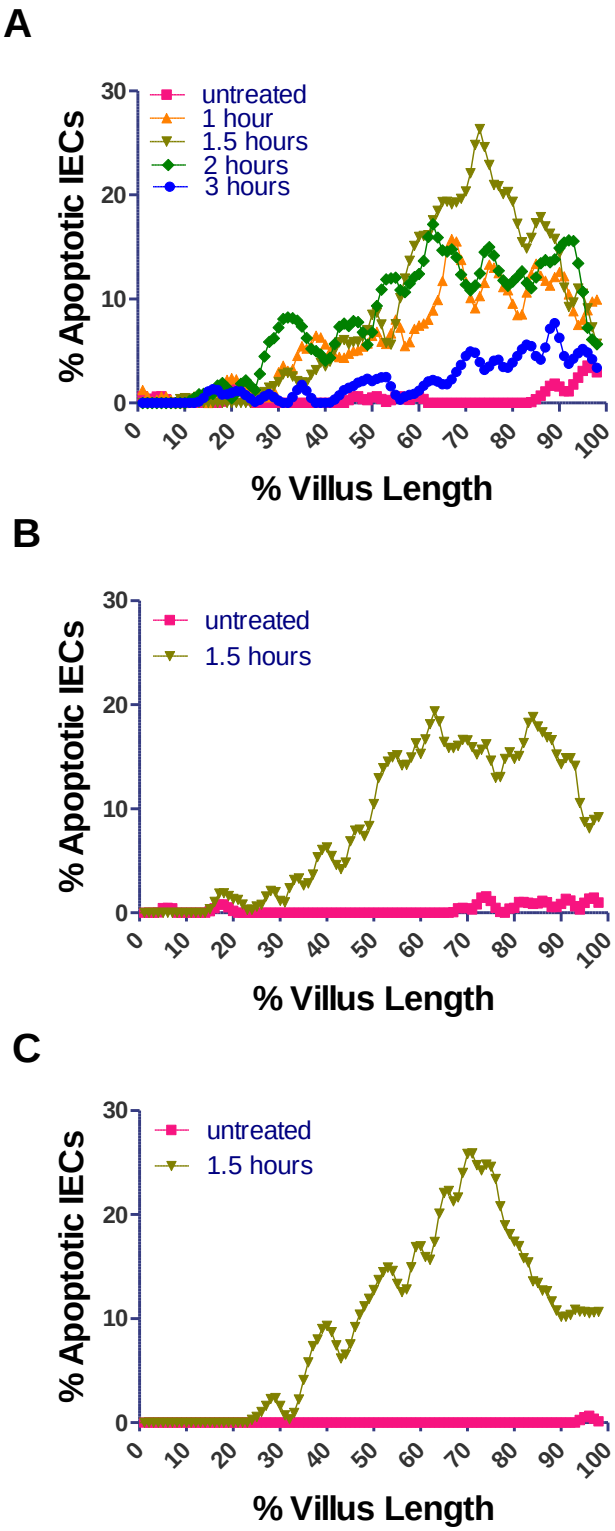

Figure 30: Cell positional graphs showing quantification of “apoptotic” immunolabelled intestinal epithelial cells along the villus axis for duodenum (A), jejunum (B) and ileum (C). All villi were artificially adjusted to 100 cells in length to allow comparison. n=6 mice per time point.

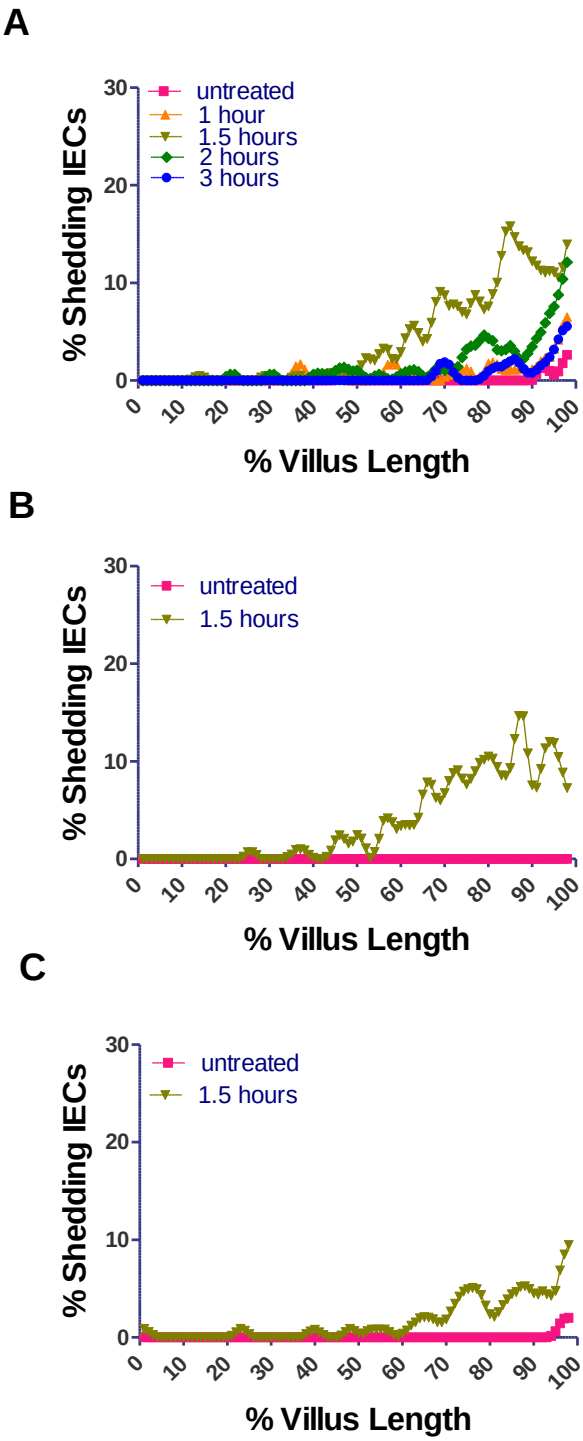

Figure 31: Cell positional graphs showing quantification of intestinal epithelial cells with “shedding” morphology along the villus axis for different intestinal segments. All villi were artificially adjusted to 100 cells in length to allow comparison. n=6 mice per time point.

3.8 *In vivo* confocal microscopy allowed identification of shedding cells in real time

In the context of investigating intestinal epithelial cell shedding, histological studies have been criticised as being inferior when compared to *in vivo* confocal microscopy, due to artefactual changes induced by tissue processing. The potential appeal of confocal microscopy is that tissue can firstly be resolved in the *x*, *y* and *z* directions to image through a limited depth of tissue, whereas traditional microscopy only allows examination of a 3-5µm tissue section in a single focal plane in the *x* and *y* dimensions. By repeatedly scanning a limited depth of tissue, confocal microscopy additionally allows cellular imaging over time, theoretically allowing a four-dimensional (*x,y,z* and *t*) imaging modality.

A protocol was therefore developed to image LPS induced small intestinal IEC shedding by confocal microscopy. Mice were administered 10mg/kg LPS i.p., anaesthetised with fentanyl and diazepam, and a midline laparotomy was performed. The jejunum was incised and the mucosal surface placed on a coverslip with acriflavine dye. Photons of laser light at approximately 416nm were used to stimulate the emission of photons from acriflavine at approximately 514nm (for further information see Materials and Methods).

Through utilisation of confocal microscopy during LPS induced IEC shedding, it was possible to identify shedding cells moving beyond the epithelial borders of individual villi when the villus tip was viewed *en face*. Figure 33 shows a time-lapse series of images from a 10mg/kg LPS treated mouse, taken in a single focal plane at approximately 3 minute intervals over 30

minutes. Several IECs moved centrifugally from the villus, being extruded from the epithelial monolayer and entering the lumen. This confirmed that this imaging modality could be used to capture the same cell shedding process that was observed by histopathological examination. However, achieving good quality images and videos by this method was extremely technically challenging for many reasons. These included performing surgery that was completely free of bleeding, maintaining adequate anaesthesia in mice undergoing imaging, finding a suitable part of mucosa and a suitable villus to image, optimising image capture settings, preventing z axis drift in the focal plane, and achieving images without movement blur, as in many experiments there was excessive tissue movement due to respiration and/or peristalsis. This imaging technique also represented an extremely poor modality in terms of the potential for measurement or quantification of shedding events, as image stacks had to be screened through the depth of the tissue in order to identify shedding cells. This imaging technique was therefore not extensively used during the remainder of the project.

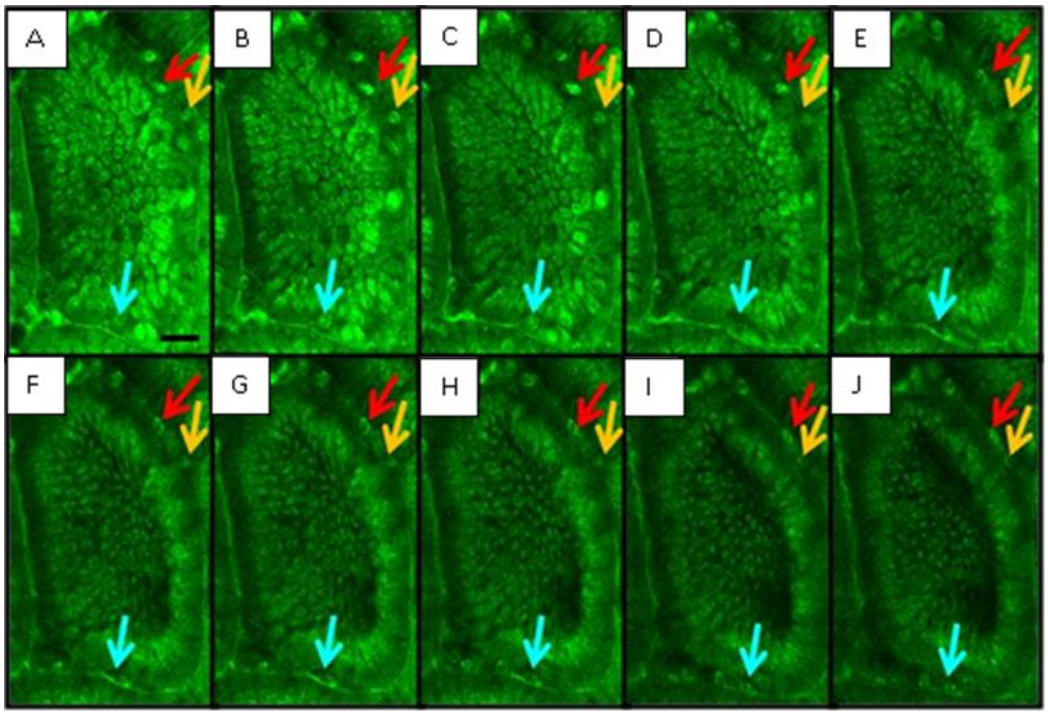

Figure 32: Confocal image series taken of the surface of a single jejunal villus tip viewed *en face* at approximately 3 minute intervals, from approximately 50 to 80 minutes after LPS administration (acriflavine staining). The red, yellow and blue arrows trace the movement of several individual IEC nuclei moving outwards and leaving the epithelial border of the villus. Bar (A)=20µm.

3.9 LPS caused a significant increase in gut permeability by 5h

Having established the pathological lesions induced by systemic LPS administration in mice, it was next investigated whether there was a correlation between small intestinal injury and increased intestinal permeability. Fluorescein-isothiocyanate-conjugated dextran (FD4) represents a fluorescent labelled dextran of molecular weight between 3-5KDa which should not, in normal conditions be absorbed via the gastrointestinal tract to any significant extent unless there is increased gut permeability. In order to allow the FD4 to be distributed throughout the intestinal tract, all animals were given FD4 by oral gavage for 5 hours prior to

them being euthanased by a rising CO_2 concentration, and blood taken by cardiac puncture. Untreated control mice received gavage only, and LPS treated mice received an i.p. injection of PE-LPS either 1.5h or 3h prior to the end of the experiment, or at the time of the gavage for the 5h time point (see Materials and Methods for further information). Plasma fluorescence was then measured. At 5h post-LPS (also 5h post FD4), there was a 5-fold increase in gut permeability (*P*<0.05: Kruskal-Wallis) with plasma fluorescence measured at 76.3±21.7 fluorescent units (Figure 33) versus 16.4±2.9 fluorescent units in untreated animals (5hrs FD4), suggesting that gut barrier dysfunction occurs at around 5h post-LPS administration.

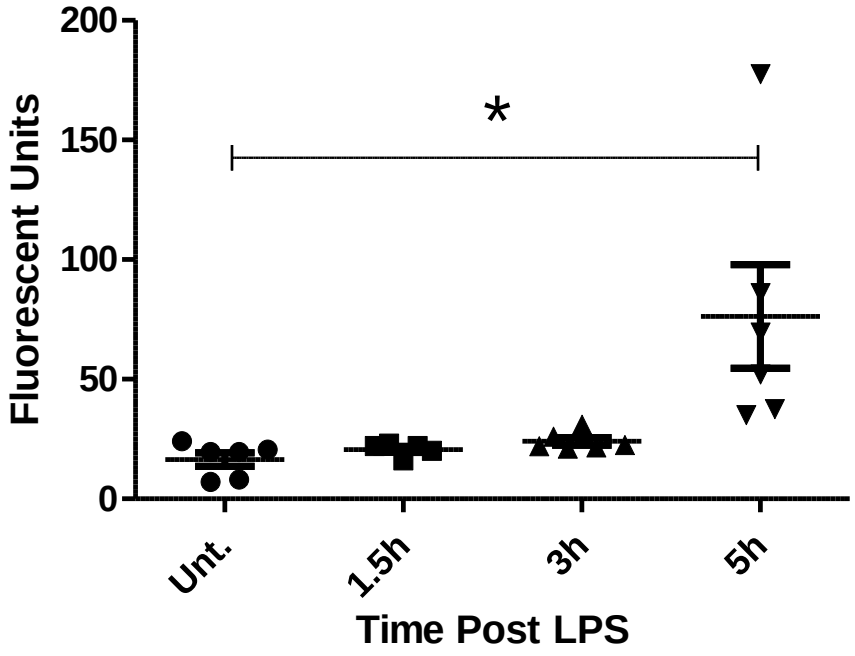

Figure 33: Plasma fluorescence measured after 10mg/kg PE-LPS and gavage of FD4. At 5h post-LPS (5hrs FD4), there was a 5-fold increase in gut permeability. *=*P*<0.05 (N=6, 1 outlier excluded at 1.5hr). Comparisons by Kruskal-Wallis.

3.10 Ultrastructural examination of LPS induced IEC cell death and shedding

In an attempt to examine the process of LPS-induced apoptosis and shedding in greater detail, transmission electron microscopy (TEM) was performed. Tissue was examined from the duodenum of a 10mg/kg LPS treated C57BL/6 female mouse 1.5 hours after administration, and compared against equivalent tissue taken from an untreated C57BL/6 (not shown). Adjacent small intestine was confirmed to exhibit extensive IEC apoptosis and cell shedding by active caspase-3 IHC. Transmission electron micrographs (Figure 34), showed several morphological changes in IECs at the villus tips consistent with apoptosis, but also features of cellular degeneration and necrosis with occasional examples of IEC detachment and shedding. Changes in morphology in individual epithelial cells included electron lucency of the cytoplasm without obvious changes in mitochondria, loss of surface microvilli, margination of condensed and clumped heterochromatin to the borders of the nuclear envelope, and increased electron lucency of central euchromatin. Changes more typically consistent with cellular degeneration and necrosis included increased cell volume, electron lucency of the cytoplasm and organelles (suggesting failure of ion exchange pumps and hydropic degeneration), detachment of ribosomes, mitochondrial swelling and membrane rupture.

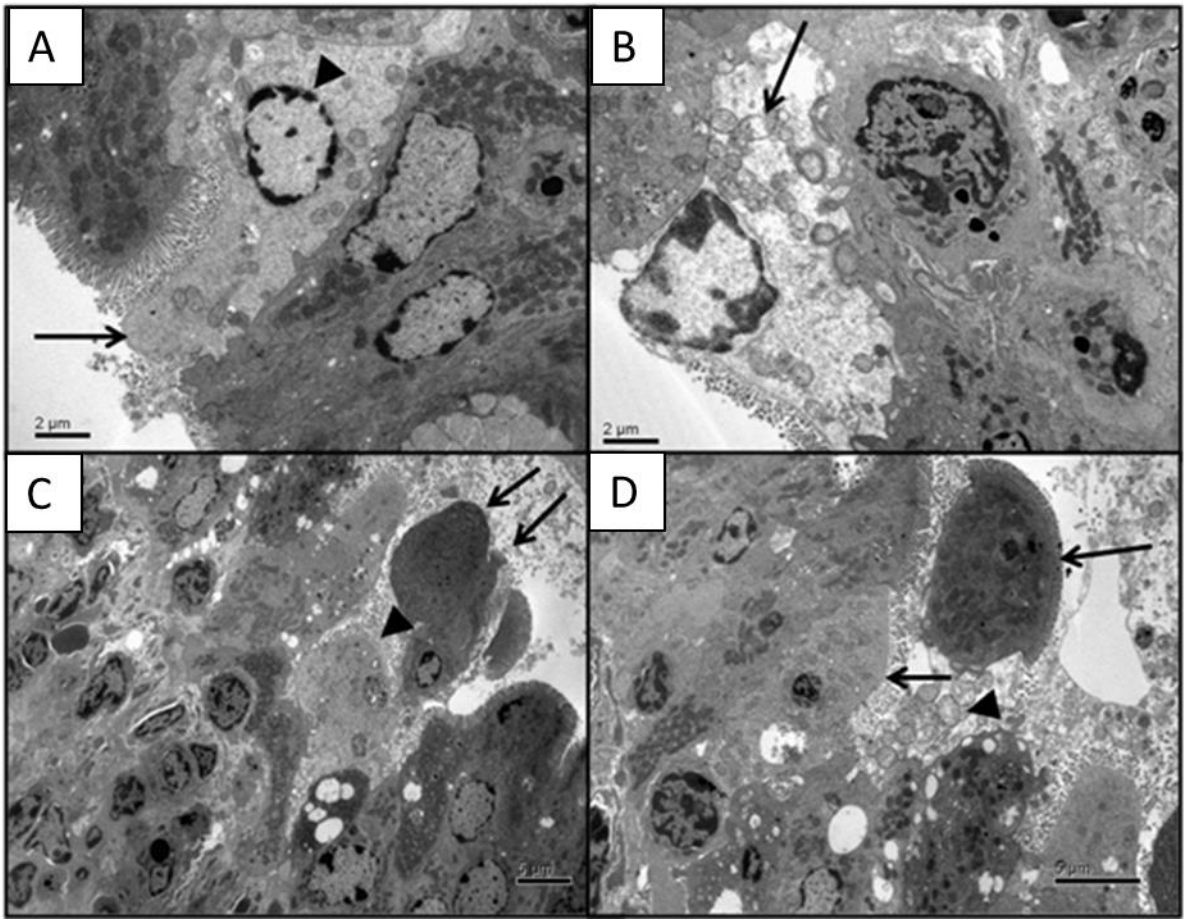

Figure 34: Transmission electron microscopy images from 10mg/kg 1.5h LPS treated C57BL/6 female mouse. A) IEC with loss of apical microvillus brush border (arrow), marginated and slightly clumped heterochromatin of the nucleus (arrow head). B) Deformed IEC with some apical microvilli still present, an eccentric apical nucleus, markedly electron lucent cytoplasm, and mitochondrial swelling (arrow). C) Marked disruption of epithelial monolayer with IECs showing detachment from neighbours with cell rounding and shrinkage (arrows) and ruptured cell membranes (arrow head). D) Fragmentation of IECs, with occasional IECs exhibiting shrunken electron dense nuclei or nuclear fragments (arrows), or cellular rupture and liberation of mitochondria (arrow head). Bar=2µm in A) & B), and 5µm in C) and D).

3.11 Effects of LPS dosage and purification on small intestinal epithelial apoptosis and cell shedding

Having characterised the time dependent small intestinal epithelial apoptosis and shedding within the small intestine caused by 10mg/kg phenol extracted LPS (PE-LPS), the dose response relationship of this effect, and method of LPS purification was tested. It was assumed that the time course for

apoptosis and shedding in the small intestine would not be affected by dosage, and therefore an endpoint of 1.5h was chosen for n=4-6 LPS administered adult female mice. Active caspase-3 immunohistochemically labelled duodenal sections were utilised to compare relative apoptosis and shedding between LPS dosage and LPS purification.

3.11.1 LPS purity did not significantly affect IEC apoptosis and cell shedding in WT mice

To assess whether the LPS purification/extraction method altered IEC apoptosis and cell shedding, 10mg/kg high-purity ion-exchange chromatography extracted LPS (IE-LPS) was administered to WT mice which were euthanased at 1.5h. The IE-LPS preparation caused similar villus shortening to that seen in 10mg/kg PE-LPS treated animals (298.0µm±39.1µm compared to 260.5µm±36.8µm) (Figure 36A). IEC apoptosis and cell shedding post IE-LPS administration were also significantly increased (10.8%±2.8%) as observed for PE-LPS (12.5%±1.7%) (Figure 35B).

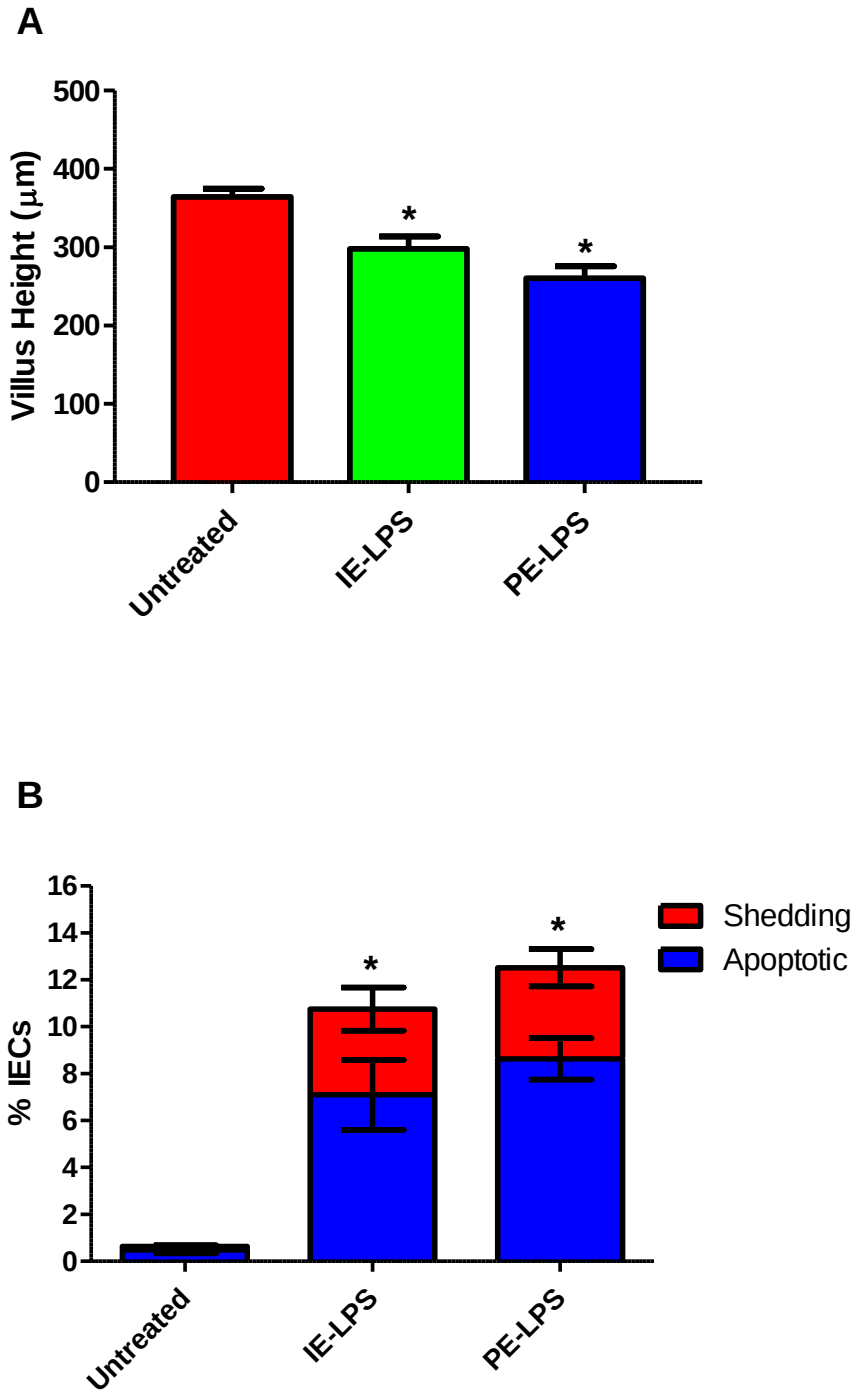

Figure 35: Bar chart demonstrating that both and ion exchange chromatography extracted LPS (IE-LPS) and phenol extracted LPS (PE-LPS) caused comparable villus atrophy (A) and IEC apoptosis and cell shedding (B) at 1.5 hours after administration of 10mg/kg i.p. n=6, *=*P* value<0.05 based on ANOVA against untreated with Holm-Sidak post-hoc test in (A) and by Kruskal-Wallis and Dunnett`s post-hoc test in (B). No statistical difference was detected between IE-LPS and PE-LPS in (A) or (B).

3.11.2 Dose dependent effects of LPS on the small intestine

As IE-LPS and PE-LPS caused similar amounts of small intestinal apoptosis and cell shedding, PE-LPS was utilised in the majority of further experiments, as this purification grade was considerably more economical. Dose dependent effects of PE-LPS on the small intestine were therefore quantified. A vehicle treated (PBS) control was also included to rule out intraperitoneal injection or handling stress in induction of observed intestinal injury. C57BL/6 female mice were administered with doses of 20, 5, 2.5, 1.25, 0.25 and 0.125mg/kg PE-LPS by i.p. injection (n=4-6/group) and were euthanased at 1.5h. Comparisons were made with the n=6 untreated groups, and 10mg/kg dosage groups from the prior time course experiment in an effort to reduce the animal numbers required.

LPS at 0.125mg/kg caused a 10-fold observed increase in IEC apoptosis and cell shedding compared to untreated mice at 6.0%±1.7% (P<0.05: ANOVA) (Figure 36A) but with a minimal (5%) reduction in villus height at 348.1µm±17.1µm versus 365.9µm±6.6µm in untreated control animals (Figure 36B). LPS at doses ≥0.25mg/kg caused ~30% reduction in villus height compared to controls, and IEC apoptosis and cell shedding of ~12%. These data suggest that the intestinal effects of LPS seem to be caused at a threshold dose, as all dosages greater than 0.125mg/kg caused comparable amounts of villus atrophy, apoptosis, and cell shedding. These results suggested that this threshold dose was approximately 0.125mg/kg, with the caveat that this was the lowest dose utilised, and the effect may be further abrogated by even lower doses. The comparison between apoptotic and cell

shedding indices with the villus height data, additionally suggested that IECs appear extremely sensitive to LPS induced apoptosis and cell shedding, whereas concomitant villus shortening only occurs following administration of higher dosages of LPS. In assessing small intestinal injury by these methodologies, it would also suggest that although apoptotic and cell shedding indices are a potentially more subjective means of assessment, this technique has greater sensitivity in detecting more subtle degrees of injury. These dose response data were also important in selecting a “low dose”, i.e. 0.125mg/kg for investigating differences between genotypes of mice in subsequent investigations. Dose response data for PBS treated mice also confirmed that small intestinal injury was not caused by intraperitoneal injection or by the stress of the procedure.

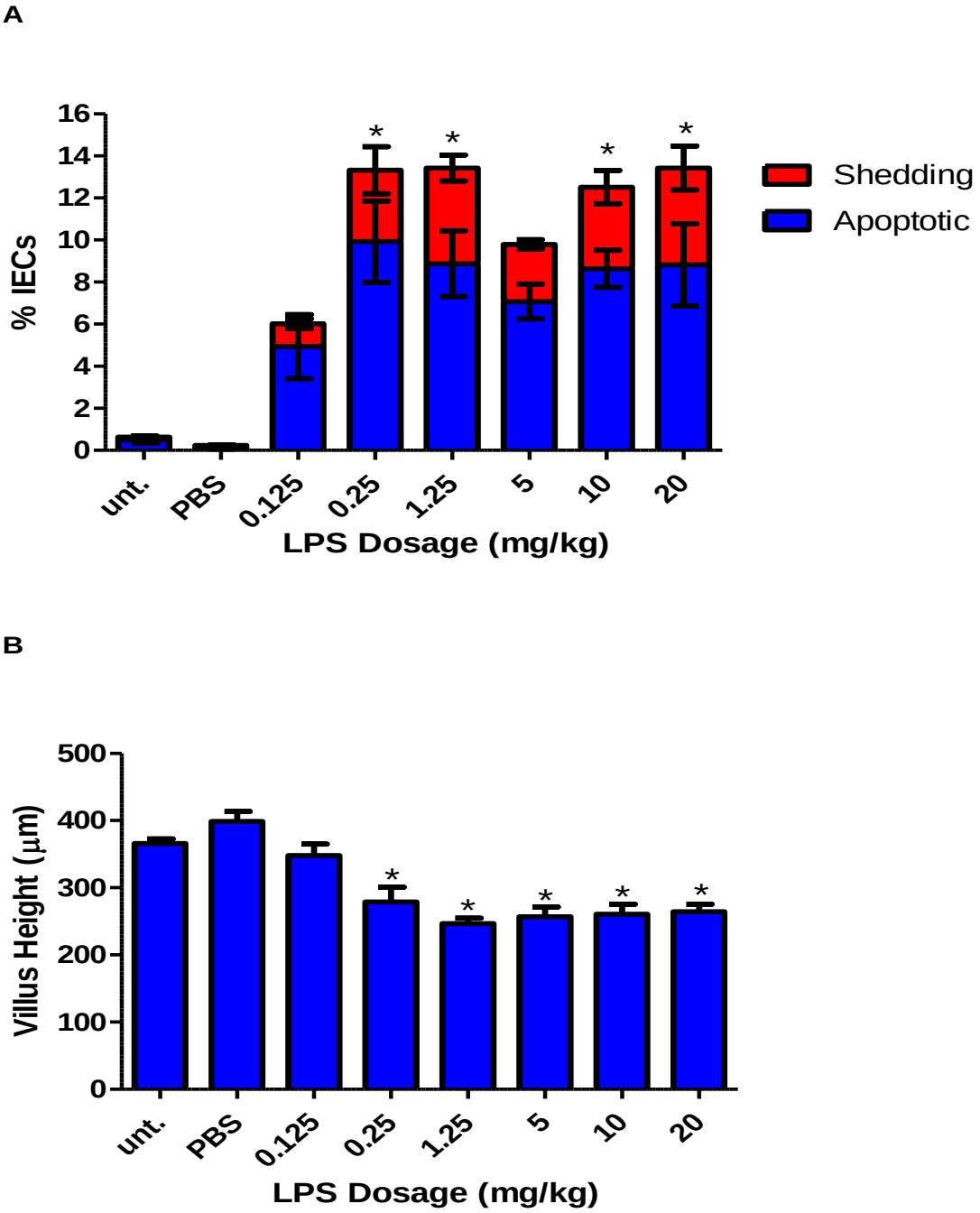

Figure 36: Dose response 1.5h post PE-LPS administration. Quantification of IEC apoptosis and cell shedding in active caspase-3 IHC labelled duodenal sections (A) and villus heights in duodenal sections (B). *=*P*<0.05, n=6 female mice/group for PBS, 0.125mg/kg and 10mg/kg, and n=4 female mice for all other groups.

3.11.3 There was no significant gender difference in LPS response

An important point to address in developing this model was whether gender had any influence on the small intestinal injury caused by LPS, as gender differences have been shown in the immunological responses to LPS in some studies (Aoyama et al. 2009). The amount of IEC apoptosis and cell shedding (Figure 38), and villus heights (Figure 38), in male and female WT mice following LPS administration were therefore compared. It was possible to ascertain that the extent of small intestinal injury induced by both low (0.125mg/kg) and high dose (10mg/kg) PE-LPS was broadly similar in both genders, with no significant differences being detected between genders within treatment groups. In both genders 0.125mg/kg LPS caused apoptosis and cell shedding in approximately 6% of IECs, whereas 10mg/kg LPS resulted in a marked increase in apoptosis and shedding (12.5% and 10.4% in females and males respectively). Villus heights showed a similar trend in males as already discussed in females, with 0.125mg/kg causing an approximately 5% reduction (384.7µm±30.0µm), and 10mg/kg causing an approximately 34% reduction (266µm±14.9µm) in villus height compared to untreated animals (405.4µm±19.7µm).

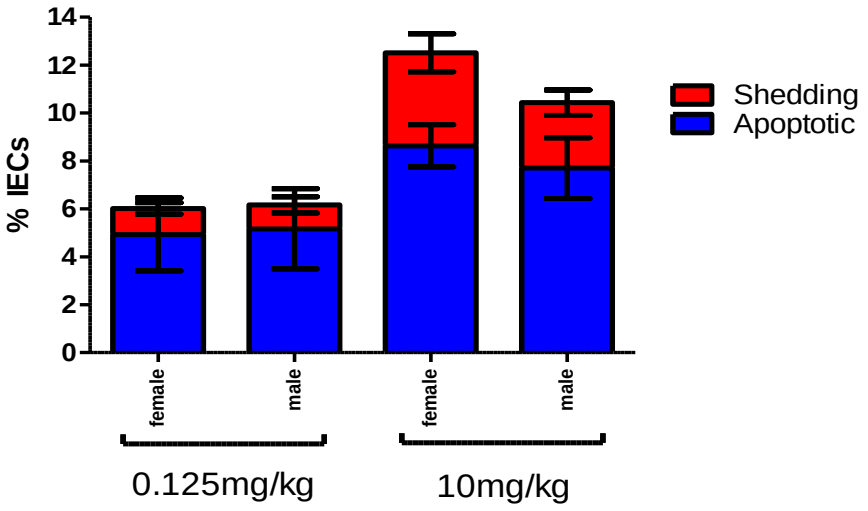

Figure 37: Bar chart of relative percentages of apoptotic and shedding IECs in the duodenal villi of male and female mice, at 10mg/kg and 0.125mg/kg of LPS. No significant difference was detected between genders based on comparisons by Kruskal-Wallis (n=6 per group).

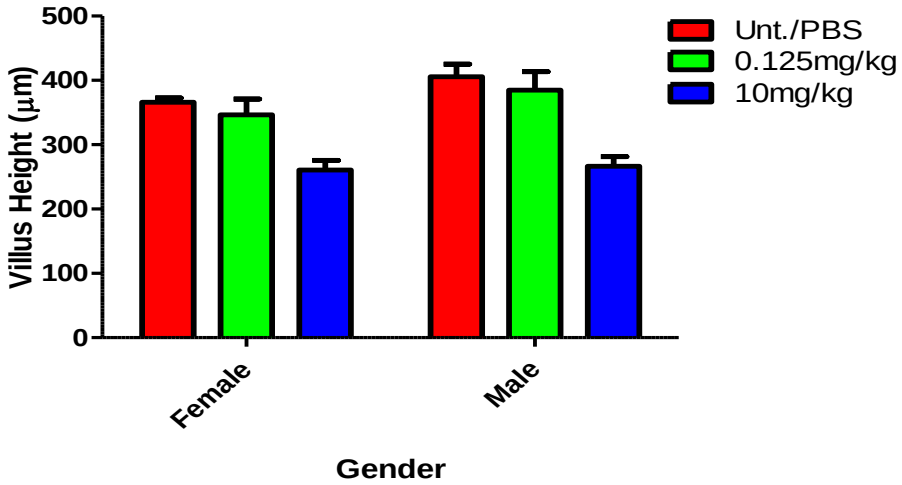

Figure 38: Bar chart of relative villus heights measured by ImageJ analysis in the duodenal villi of male and female mice, at 10mg/kg and 0.125mg/kg doses of LPS. No significant differences were detected between genders based on comparisons by Kruskal-Wallis (n=6 per group). Unt.=untreated.

3.12 Discussion

The data presented in this chapter provide a detailed characterisation of acute LPS induced intestinal injury in a murine model. Histopathological examination showed that systemic LPS administration caused rapid and specific small intestinal injury. No evidence of comparable cell death or injury was observed at any other location in the gastrointestinal tract, or any other organ systems examined, a phenomenon which has been partly investigated by others at later time points. For example, Julian et al. (2011) showed that the intestinal epithelium was indeed more susceptible to cytopathic injury and altered permeability than the pulmonary epithelium in acute sepsis. This group showed that in a feline model of *E.coli* induced sepsis, IECs exhibited evidence of mitochondrial injury by TEM. Intestinal epithelial cell death and degeneration in our own studies also appeared to show a mixture of morphological changes, including mitochondrial swelling, by TEM. They also showed that the intestinal epithelial cell death caused in this context was not related to intestinal hypoperfusion or hypoxia.

By assessment of cell morphology by light microscopy, TEM and by immunostaining for active caspase-3, the predominant form of cell death appeared to be apoptosis. Cell shedding appeared, on morphological and biochemical grounds to be dependent on the prior activation of apoptotic pathways, as both cells in the process of extrusion, and the vast majority of detached IECs were positively immunolabelled for active caspase-3. This supports the hypothesis that apoptosis precedes IEC shedding, at least in the pathological context. However, TEM findings such as membrane rupture, and

other features of necrosis, suggest that in some cases either a different cell death pathway is activated, or apoptosis; which is an energy dependent process, may degenerate to necrosis in instances where there is lack of ATP. A possible mechanism by which this may occur would be villus tip hypoxia due to the vascular disturbance caused by endotoxic shock. It was possible by *in vivo* confocal imaging to appreciate villus intestinal epithelial cell shedding in real time, and by this method it appeared that whole cells were being extruded without obvious membrane rupture. However examples of cytoplasmic “stalks” extending from IECs undergoing extrusion, which must presumably be ruptured during the process of cell shedding were frequently observed by IHC.

Consistent with observations made in physiological shedding, and shedding induced by TNF, a very small minority of intestinal epithelial cells appeared to undergo the conformational changes associated with cell shedding, but did not appear to be positively labelled with active caspase-3, or were only labelled very weakly. Similarly, in studies of physiological shedding in humans, 0.3% of shedding cells did not positively stain for activated caspase-3 (Bullen et al. 2006). In our own study, these cells were not recorded by cell counting, due to the rarity of their occurrence and difficulty in assigning them to pre-established categories of unaltered, apoptotic, or apoptotic and shedding. It is not entirely clear why these rarely observed cells do not stain for active caspase-3, but these cells may be undergoing necrosis, as has been observed by TEM in the perfused cat ileum model 2 hours after LPS administration (Crouser et al. 2000). Alternatively, necroptosis may be

occurring in these cells, as this form of cell death is not dependent on the activation of executioner caspases such as caspase-3.

Maximal intestinal epithelial apoptosis and shedding as assessed by active casapse-3 IHC occurred at around 1.5 hours after LPS administration. Terminal apoptotic pathways therefore appeared to be activated in a large percentage of IECs at 1 hour post LPS administration, whilst shedding was only beginning to occur in a small percentage of IECs at this early time point. When analysed on a cell positional basis, positively labelled IECs occurred with increased frequency approximately 50-90% along the villus length from the base of the villus, and cell shedding occurred from 60-100% along the length of the villus, with a sharp rise in shedding frequency being observed towards the villus tip.

Activation of executioner caspases is generally assumed to be a terminal event in apoptosis, and if this assumption is made it would be reasonable to suggest that all IECs that are positively labelled for active caspase-3 should be destined to undergo apoptosis and cell shedding. However, at least one mechanism by which cells may be rescued from apoptosis at this point is by X-linked inhibitor of apoptosis (XIAP), which is capable of completely blocking the activity of caspase-3 through structural changes in its active site (Eckelman et al. 2006). In *Cryptosporidium parvum* induced IEC shedding, it has been shown that XIAP binds to active caspase-3 and prevents apoptosis from occurring until IECs have reached the villus tip (Foster et al. 2012). It was also shown that XIAP, in conjunction with activation of NFκB and proteasome activity, were necessary to control cell shedding and restrict it to

the villus tip, and also to control intestinal barrier function.

The time course study also demonstrated that LPS caused villus shortening in association with IEC apoptosis and cell shedding, suggesting that active villus contraction is induced. Intestinal injury that induces cell death in various different situations usually occurs in conjunction with other rapid pathological changes in the mucosa. For example, after 5-10 minutes of intestinal ischaemia, subepithelial spaces referred to as Gruenhagen's spaces develop, with separation of the apical villus epithelium in sheets from the basement membrane, and contraction of the villus core (Brown et al. 2007). This is similar to what is observed *ex-vivo*, where there is energy dependent villus contraction with rapid restitution of the epithelium, and microfilament condensation of the underlying myofibroblasts in response to denudation of the overlying epithelium. Villus contraction has also been found to be dependent on neuronal action potentials, as tetrodotoxin blocked this phenomenon. This active contraction of the villus core during acute injury is hypothesised to aid epithelial restitution, as the process effectively reduces the size of the epithelial defect (Moore et al. 1989). Subsequently, epithelial cells adjacent to these defects undergo flattening and attenuation as they spread to cover defects, with complete restitution usually taking several days (Brown et al. 2007).

Small intestinal IEC apoptosis, cell shedding and shortening of the villus correlated temporally with fluid effusion into the small intestinal lumen and diarrhoea. This suggests that the pathophysiology of the diarrhoea that these mice exhibit may be caused directly by the rapid and uncoordinated shedding

of IECs, potentially in conjunction with increased vascular permeability, which may cause disruption of tight junctions and the paracellular space.

Supporting this hypothesis, Gadjeva et al. (2007) attempted to characterise this LPS-induced fluid effusion into the gut, and found that there was significant leakage of intravenously administered Evans blue dye and FITC labelled albumin into the gut lumen in p50 deficient mice 4 hours after LPS administration. This implies that the gut permeability that occurs in endotoxic shock is of a severity that allows passage of very large proteins, with the loss of albumin suggesting that there is accompanying loss of oncotic pressure further complicating fluid loss. This loss of oncotic pressure also suggests that fluid absorption into the intestinal vasculature will be reduced during this phase. Other possibilities to account for LPS-induced acute diarrhoea would include reduced villus absorption capacity due to lost absorptive enterocytes, although the very short time period between cell shedding and onset of diarrhoea suggests that this hypothesis is less plausible. Alternatively, increased epithelial secretion into the intestine may occur. It seems less likely that increased intestinal motility is responsible, as endotoxin is reported to cause ileus (Buchholz et al. 2009). Interestingly, it was also observed by periodic acid Schiff (PAS)/Alcian blue staining, that goblet cells are preferentially retained and do not undergo cell shedding to the same extent as absorptive enterocytes in this model (Luke Asquith, Physiology BSc honours student project, University of Liverpool), in agreement with observations in haemorrhagic shock (Chang et al. 2005) and following methotrexate administration to rats (Verburg et al. 2000). In this latter study,

the selective sparing of goblet cells at the villus tip was hypothesised to be an adaptive protective response following villus injury to preserve mucus secreting function and to aid restitution through trefoil factor 3 (TFF3). We also observed morphological changes in the goblet cell theca which suggested goblet cell secretion may occur in our model.

It is possible that goblet cells do not exhibit activation of cell death pathways in response to TNF receptor ligation, or to metabolic insults in the same way as enterocytes. In support of this, it was not possible to discern instances of active caspase-3 labelled goblet cells in our time course study. It may also be possible that goblet cells are more tightly bound to other epithelial cells or to the basement membrane by tight junctions and hemidesmosomes respectively.

It has previously been demonstrated in our laboratories that barrier loss in the intestine occurs at sites of excessive cell shedding in response to TNF (Kiesslich et al. 2012), and that the direction of fluid movement through epithelial defects is highly dependent on the osmotic and hydrostatic gradients across the epithelium. It was not until 5 hours after LPS administration in this model however, that we found movement of larger molecules (FD4) from the lumen to the plasma. This is in agreement with findings from *in vivo* confocal microscopy that from 5.5 hours after LPS administration, FD4 entered cell-free gaps and paracellular spaces (Lai et al. 2013). This may be a consequence of the net fluid and protein effusion into the intestinal lumen up until this point. Alternatively, it may be due to a later failure of tight junction regulation. In support of this latter concept, by staining

of small intestinal sections for junctional adhesion molecule A (JAM-A) by IHC, we observed tight junction redistribution at 4h and 6h post-LPS (Ross Fuller, Physiology BSc honours student project, University of Liverpool). This suggests that this later phenomenon may contribute to gut permeability defects.

In summary, these studies suggested that LPS represents a robust stimulus of pathological villus epithelial cell apoptosis and cell shedding throughout the small intestine. This response was initiated at a threshold dosage of ≥0.125mg/kg, and maximal apoptosis and cell shedding was observed at 1.5 hours after LPS administration.

4. Mechanisms by which LPS Causes IEC Death and Cell Shedding

4.1 Introduction

Having established the time and dose dependent effects of LPS on the small intestine, further experiments to investigate the mechanisms by which LPS caused cell death and shedding were performed. TLR4 signalling is critical in mediating the innate immune response to LPS (Beutler et al. 2001). It was therefore hypothesised that peripheral TLR4 ligation by LPS in immune cells (particularly macrophages and dendritic cells) leads to the production of cytokines, and it is these circulating cytokines that mediate and induce the apoptotic response either directly or indirectly within intestinal epithelial cells. To test this hypothesis, LPS was first administered by several different routes including direct intestinal instillation in WT mice, and the small intestinal response in terms of IEC apoptosis and cell shedding was analysed by immunohistochemistry for active caspase-3. The aim of these experiments was to exclude the possibility that LPS was acting directly on IECs, or that intraperitoneal LPS was somehow acting on the intestine in a localised transmural manner to induce epithelial apoptosis.

To test whether LPS-induced small intestinal apoptosis and cell shedding was TLR4 dependent, different purities of LPS from *E.coli* O111:B4 were then administered to *Tlr4*$^{-/-}$ mice, and the small intestinal response in terms of apoptosis and cell shedding was assessed by immunohistochemistry for active caspase-3.

TLR signalling (with the exception of TLR3) is further dependent on the MyD88 adapter molecule (Kawai and Akira 2011), as this molecule provides a critical link between TLR4 ligation, NFκB signalling and gene induction

(Hirotani et al. 2005). By using transgenic mice that lacked MyD88 specifically within intestinal epithelial cells, it was therefore possible to test whether intact intestinal epithelial TLR signalling was required to produce LPS induced IEC apoptosis and cell shedding. An understanding of whether LPS induced epithelial cell apoptosis and shedding were entirely epithelial regulated events could then hopefully be achieved by considering responses in *Tlr4*$^{-/-}$, and *vil-Cre MyD88*$^{-/-}$ mice in conjunction with those elicited by different routes of LPS administration in WT mice.

As it had been previously demonstrated by our own laboratories that systemic TNF administration caused IEC apoptosis and shedding, and it had been shown that TNF causes IEC apoptosis via TNFR1 (Piguet et al. 1998), it was also tested whether this same mechanism was the critical mediator of IEC apoptosis and cell shedding following systemic LPS administration. In collaboration with the University of Southern California, we investigated the response of mice deficient in TNFR1/p55 or TNFR2/p75 receptors to LPS.

By utilising quantitative PCR it was also aimed to further analyse and more specifically categorise the type of cell death occurring in our LPS model by investigating the expression of an array of genes involved in cell death pathways, including those involved in apoptosis, autophagy and necrosis.

By examining the effect of LPS purity, the importance of TLR signalling, the cytokines and cytokine receptors responsible, and type of cell death occurring, we hoped to gain important insights into how the immunological

response to LPS causes cell death and cell shedding in the murine small intestine.

4.2 IEC apoptosis and shedding is caused by systemic LPS but not by LPS administered within the intestinal lumen

To establish whether IEC apoptosis and cell shedding were initiated by epithelial, peritoneal, or peripheral innate immune responses, 10mg/kg PE-LPS was administered to C57BL/6 female mice intravenously (i.v.) as an alternative means of systemic administration, or subcutaneously (s.c.). These routes both caused IEC apoptosis at the 1.5 hour time point (Figure 39). To establish whether direct intestinal epithelial interaction with LPS was responsible, LPS solution (1mg/ml in PBS) was instilled into the ileum of mice which had been terminally anaesthetised with fentanyl and diazepam. This resulted in negligible amounts of IEC apoptosis and cell shedding at 1.5 hours post administration (Figure 39). It has been previously shown that ketamine suppresses TNF production in post-operative sepsis (Takahashi et al. 2010). To therefore exclude the possibility that anaesthetic agents were interacting to prevent LPS-induced apoptosis and shedding, systemic LPS was administered by i.p. injection to terminally anaesthetised mice. This again induced IEC apoptosis and cell shedding comparable to that observed in non-anaesthetised mice (Figure 40). These data supported the hypothesis that peripheral immunological signalling in response to LPS mediates small intestinal injury.

4.3 LPS-induced apoptosis and cell shedding were significantly decreased in *Tlr4*$^{-/-}$ mice

Toll-like receptor 4 (TLR4) is necessary for the innate immune system to respond to LPS (Beutler et al. 2001). To establish whether this was the critical signalling mechanism by which LPS induced IEC apoptosis and cell shedding, the small intestinal response to LPS was examined in *Tlr4*$^{-/-}$ mice. When 10mg/kg high-purity IE-LPS was administered to *Tlr4*$^{-/-}$ mice, it resulted in a negligible change in villus height at 375.3μm±21.9μm compared to untreated *Tlr4*$^{-/-}$ mice at 364.3μm±10.62μm, and a much reduced amount of IEC apoptosis and cell shedding at 1.4%±0.5% compared to WT mice at 10.8%±2.8% (Figure 41 and Figure 42). However, it should be noted that when *Tlr4*$^{-/-}$ mice were administered 10mg/kg of the lower purity PE-LPS, although this resulted in a negligible change in villus height at 365.4μm±17.1μm (Figure 42A), a moderate increase in IEC apoptosis and cell shedding of 7.0%±1.0% was seen (Figure 42B). These results suggested that while small intestinal injury due to highly purified LPS was almost entirely dependent on TLR4 signaling, other bacterial products present in PE-LPS were responsible for the difference between the response to IE-LPS (1.4%±0.5%) and PE-LPS (7.0%±1.0%). Additionally, even when administered IE-LPS, there was a small, although non-significant increase in IEC apoptosis and shedding at 1.4%±0.5% when compared to untreated *Tlr4*$^{-/-}$ mice at 0.2%±0.1%, which again points to some off-target effects either through impurities, or possibly by mechanisms alternate to TLR4, even when highly purified IE-LPS has been administered.

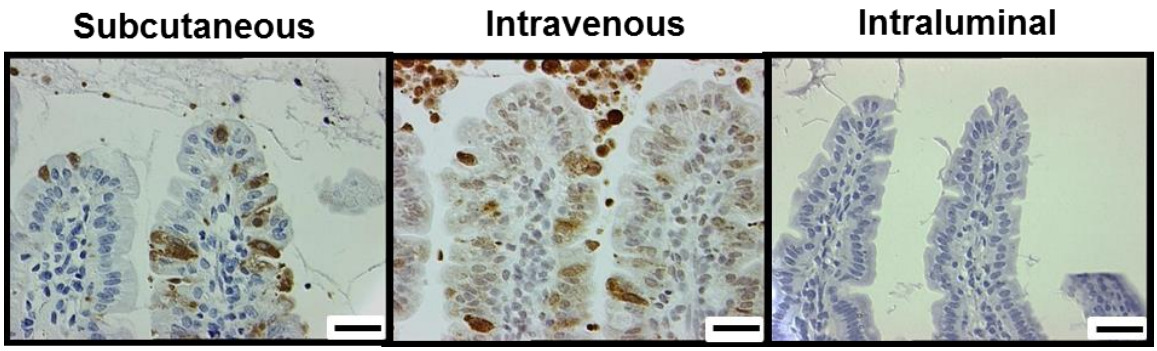

Figure 39: Photomicrographs of active caspase-3 IHC demonstrating villus tips of WT female mice 1.5h following PE-LPS administration by subcutaneous or intravenous routes exhibited villus IEC apoptosis and cell shedding. Negligible IEC apoptosis/shedding was seen when LPS was instilled intraluminally. Duodenum shown for s.c. and i.v. LPS (n=3 per group), ileum shown for intraluminal administration instilled with 1mg/ml LPS (n=4 per group). Bars=25µm.

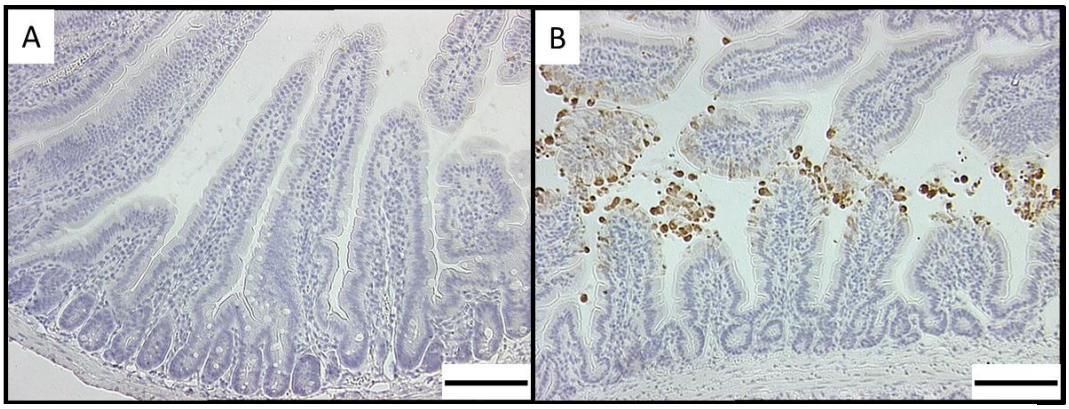

Figure 40: Photomicrographs of active caspase-3 IHC in duodenum from WT female mouse anaesthetised for 1.5h (A) demonstrating that IEC apoptosis and shedding was not caused by anaesthesia, and from a terminally anaesthetised WT mouse administered 10mg/kg PE-LPS for 1.5h (B), demonstrating that LPS induced IEC apoptosis and cell shedding was not inhibited by anaesthesia. Bars=100µm

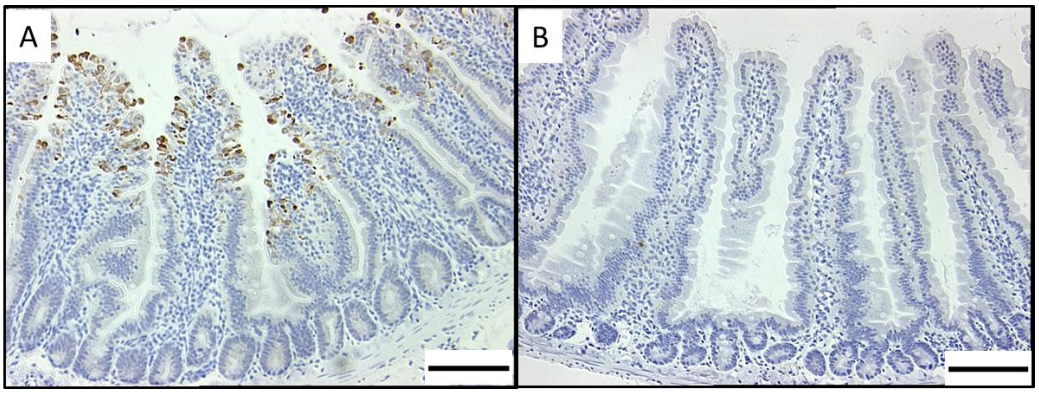

Figure 41: Photomicrographs of duodenal active caspase-3 IHC, 1.5h after treatment with 10mg/kg LPS purified by ion-exchange chromatography (IE-LPS). Whilst IEC apoptosis and shedding were induced in WT mice (A), the same dose given to *Tlr4*$^{-/-}$ mice failed to cause the same degree of IEC apoptosis and shedding (B). n=6 female mice per group, bars=100µm.

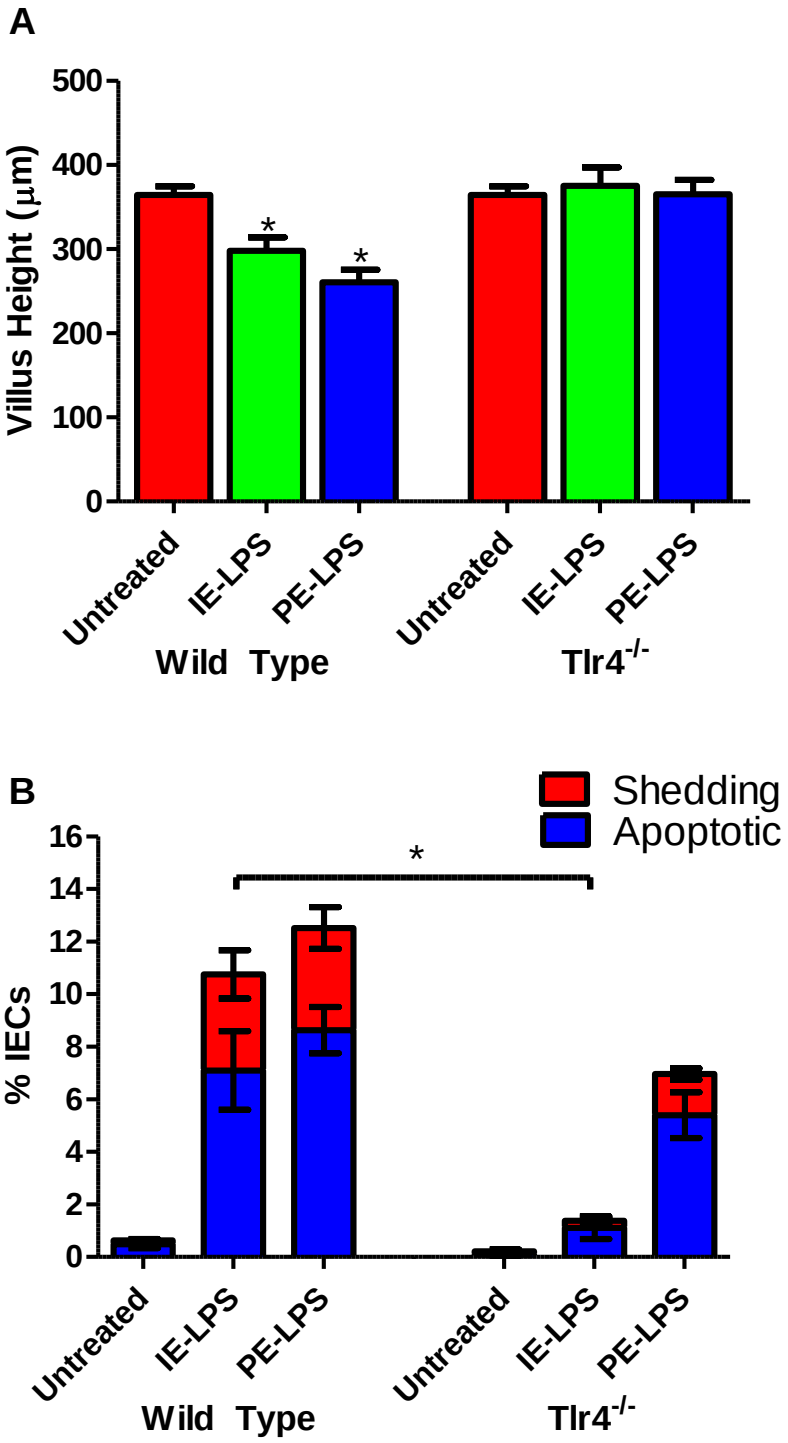

Figure 42: Villus heights in WT or *Tlr4*$^{-/-}$ mice 1.5h after phenol-extracted (PE-LPS) or ion exchange extracted (IE-LPS) at 10mg/kg i.p. (A). Quantification of IEC apoptosis and cell shedding in active caspase-3 IHC labeled duodenal sections (B). n=6 female mice/group. *=*P*<0.05, comparisons by ANOVA in (A) and by Kruskal-Wallis in (B).

4.4 Peripheral TLR signalling mediates LPS-induced IEC apoptosis and shedding

Villin represents a 92.5kDa protein which is expressed in cell lineages with a microvillus brush border, notably the intestinal and renal epithelium. It is an actin binding protein, which controls actin rearrangement (Friederich et al. 1999). Cre is a DNA recombinase enzyme that is capable of excising intervening DNA between floxed (loxP) sequences (Abremski and Hoess 1984). As villin represents a relatively tissue specific protein to the intestine, Cre expression can therefore be linked to the villin promoter in order to achieve relatively intestinal specific gene activation or deactivation in *vil-Cre* mice (El Marjou et al. 2004). *vil-Cre MyD88*$^{fl/fl}$ mice exhibit a non-functional truncated form of the MyD88 protein following removal of the intervening DNA between the floxed regions. These mice therefore lack functional TLR signalling within IECs. In collaboration with the University of East Anglia, the small intestinal response of these mice to LPS was tested.

Adult female *vil-Cre MyD88*$^{-/-}$ mice were administered 10mg/kg PE-LPS by intraperitoneal injection. Analysis of villus height in duodenal sections demonstrated similar villus atrophy in *vil-Cre MyD88*$^{-/-}$ mice at 232.8µm±12.42µm both compared to heterozygous *vil-Cre MyD88*$^{+/-}$ mice at 285.5µm±58.94µm (Figure 43A) and compared to LPS treated WT mice in our own laboratories at the University of Liverpool at 260.5µm±15.0µm. Active caspase-3 IHC showed that LPS caused comparable IEC apoptosis and shedding in *vil-Cre MyD88*$^{-/-}$ lacking IEC TLR signal transduction at 14.1%±0.61% compared to 13.7%±2.8% in heterozygous *vil-Cre MyD88*$^{+/-}$

mice (Figure 44B) which express wild-type MyD88 and therefore intact IEC TLR signalling. These data suggested that intact IEC TLR signalling is not required for LPS-induced villus IEC apoptosis and cell shedding.

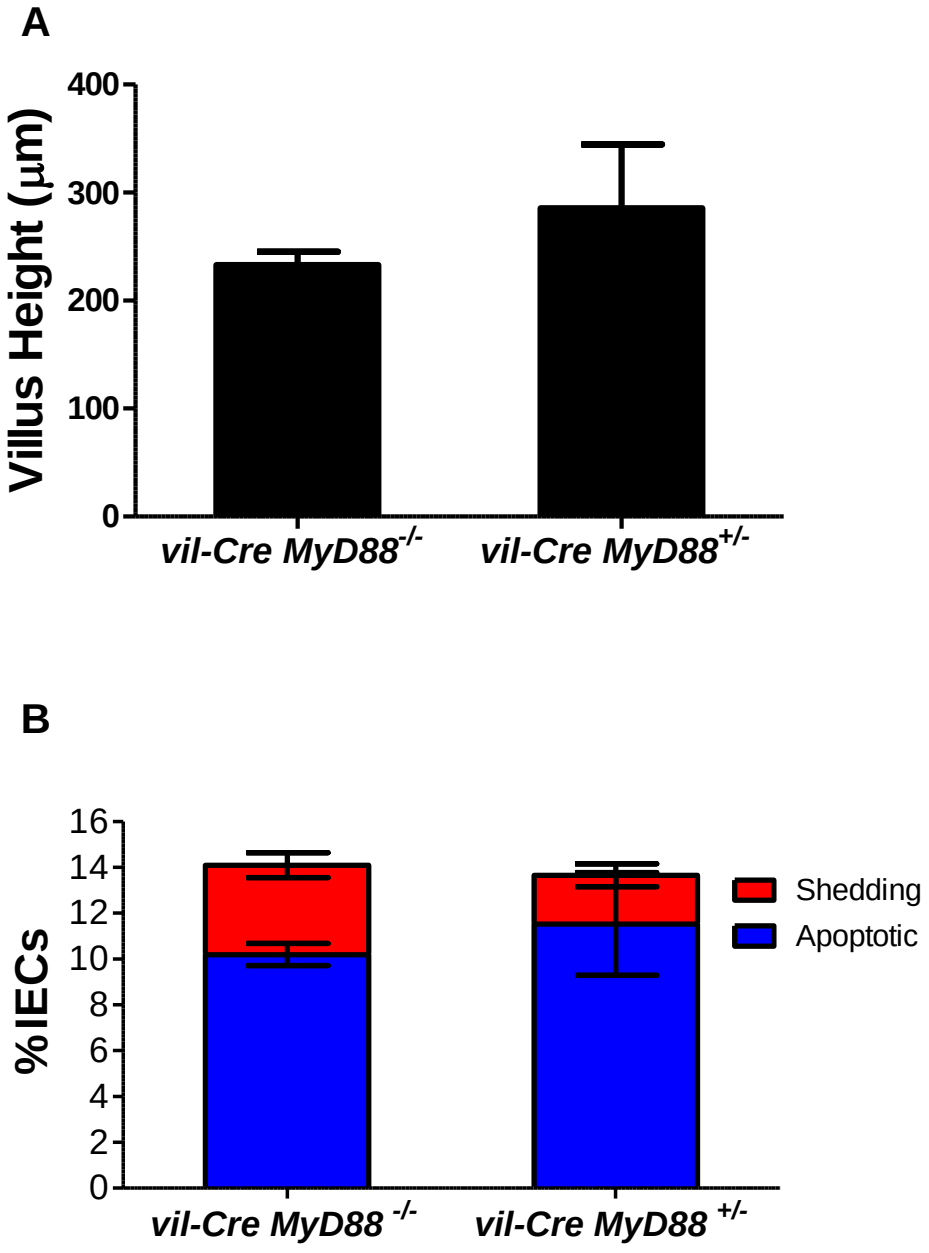

Figure 43: Intact intestinal epithelial TLR signalling is not required to mediate LPS induced small intestinal injury. Villus heights (A) and percentage apoptosis and shedding of villus IECs (B) in the duodenum of *vil-Cre MyD88*$^{-/-}$ mice and *vil-Cre MyD88*$^{+/-}$ mice 1.5h following 10mg/kg PE-LPS. n=3 female mice/group.

4.5 LPS induced changes in small intestinal cell death associated gene transcription

To further understand the type of cell death that was induced in the small intestinal epithelium in response to LPS, a gene array analysis of 89 genes associated with various cell death pathways was performed. These included genes that were classed as pro-apoptotic, anti-apoptotic, or associated with autophagy or necrosis. We performed this array on small intestinal epithelial enriched samples extracted as described in Materials and Methods. These extracts were taken from 10mg/kg 1.5h PE-LPS treated and untreated WT animals (pooled n=4 female C57BL/6 mice per group). Gene expression was then compared between LPS treated and untreated groups. The *Tnf* gene showed a marked +40.4 fold up regulation in mRNA expression (Figure 44) as did *Cd40* which exhibited a +37.4 fold increase. These two pro-apoptotic genes were therefore analysed further by qPCR using triplicate samples from individual animals. qPCR showed a mean normalised gene expression ratio of +32.0 in *Tnf* mRNA ($P<0.05$: randomization test). Real-time PCR however only showed a non-significant increase of +2.1 in *Cd40* expression.

Other genes that showed a greater than 2 fold change in regulation, included the down regulation of anti-apoptotic nucleolar protein 3 (*Nol3*) which encodes the apoptosis repressor with caspase recruitment domain (ARC) protein. This protein has been shown to interact with and down regulate the activities of caspase 2 and 8, and has been shown to be up-regulated in hypoxic SW480 cells (human colon cancer cell line) via transcriptional activation by HIF1α (Ao et al. 2012). The -3.8 fold down regulation of this

anti-apoptotic gene would tend to suggest an ultimately pro-apoptotic effect.

Bcl2l11 or BIM (O'Connor et al. 1998), which is part of the Bcl family and encodes for three protein isoforms which are activators of apoptosis, exhibited a +2.7 fold up regulation. Birc3 (baculoviral IAP repeat containing 3; also known as c-IAP2) which has been shown to be up regulated in conjunction with TNF, and to inhibit caspase-3 and caspase-6 activity in transected peripheral nerve Schwann cells (Wang et al. 2012) exhibited a +3.0 fold up regulation. Tumour necrosis factor receptor superfamily member 11B (TNFRSF11B) or osteoprotegerin, which is anti-apoptotic and a decoy receptor of receptor activator of nuclear factor kappa B ligand (RANKL), thereby inhibiting NFκB activity, exhibited a +2.9 fold up regulation. Polio virus receptor (*Pvr*), also known as CD155 exhibited a +2.8 fold up regulation. This gene has been shown to undergo increased transcription in cancer cell lines and is associated with increased proliferation and migration (Atsumi et al. 2013). These data, in conjunction with histopathological findings and activation of caspase-3, suggest that apoptosis is the predominant form of cell death occurring in the small intestine following systemic LPS administration. It also identified several genes which may play important roles in regulating LPS-induced IEC apoptosis and cell shedding. Additionally, these data suggest that the small intestinal epithelium itself may be an important source of TNF production in LPS induced IEC apoptosis and cell shedding.

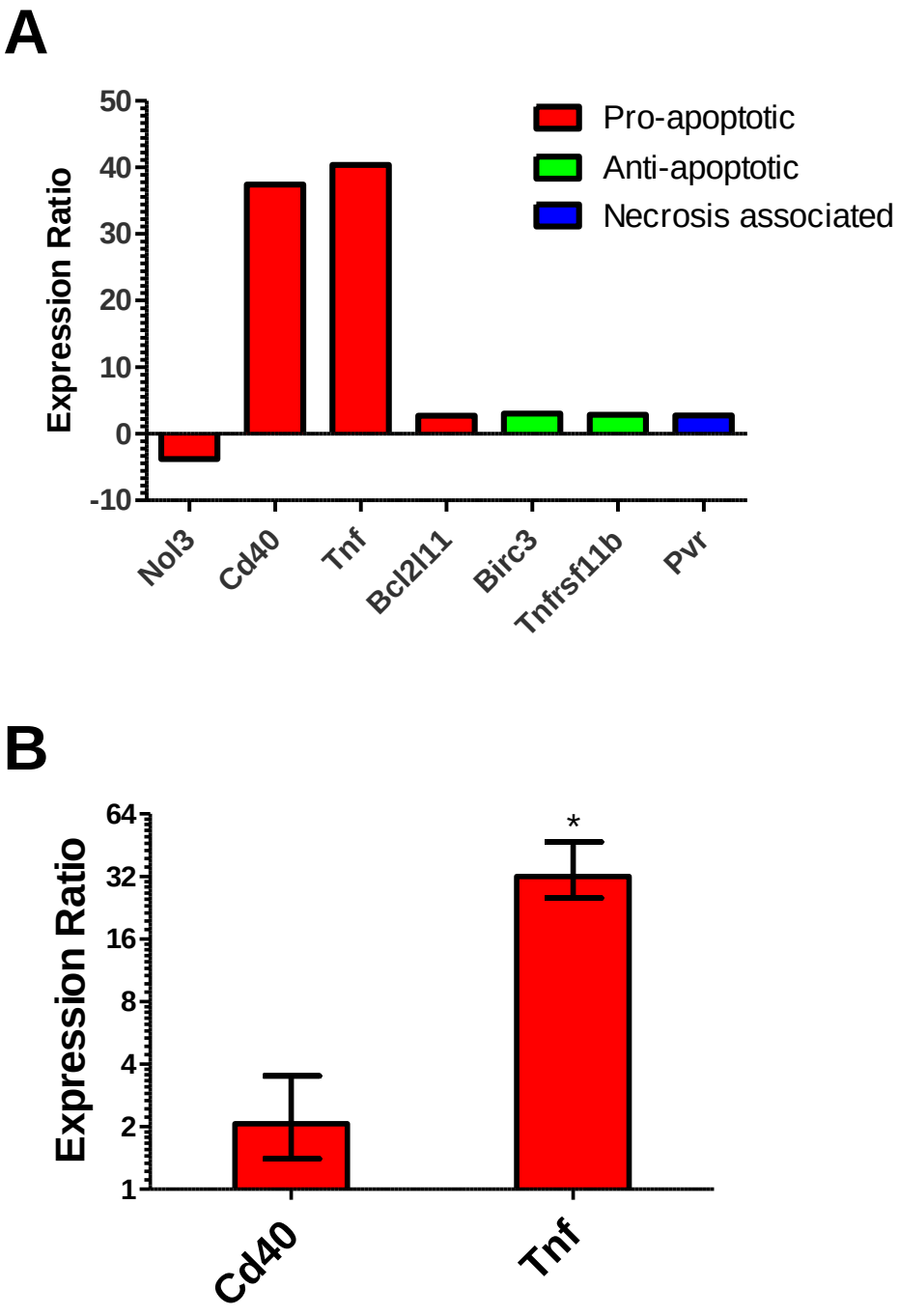

Figure 44: LPS induced genes predominantly involved with apoptosis in the small intestine. (A) selected qPCR array data for genes that exhibited ≥2-fold LPS-treated versus untreated expression ratios out of 89 genes examined in a cell-death pathway array. n=4 mice per group with pooled epithelial enriched extracts examined. (B) qPCR performed on Individualised samples in triplicate for *Cd40* and *Tnf* expression (n=4). *=*P*<0.05 based on randomisation test.

4.6 TNF caused small intestinal injury equivalent to LPS

As TNF is implicated as a key mediator of endotoxic shock, and following the finding of increased small intestinal *Tnf* mRNA in LPS treated animals, exogenous TNF administration was tested, to examine whether it caused equivalent IEC apoptosis and cell shedding to LPS. Adult C57/BL6 female mice were therefore administered murine recombinant TNF at 0.33mg/kg by i.p. injection. This dosage had been previously established as capable of inducing small intestinal epithelial cell shedding in mice (Kiesslich et al. 2007). TNF caused equivalent duodenal villus shortening at 268.4μm±20.9μm to that seen following 10mg/kg PE-LPS at 260.5μm±15.0μm (Figure 46A). Although less IEC apoptosis and cell shedding were observed following TNF, at 7.0%±1.0% compared to LPS-treated mice at 12.5%±1.7% (Figure 46B) this was attributed to a faster small intestinal response to TNF. This was confirmed by additionally administering TNF to WT female mice which were euthanased at 1h. This demonstrated that 0.33mg/kg TNF caused very similar amounts of IEC apoptosis and cell shedding at 1h, at 12.3%±1.0% (Figure 46C and Figure 47) compared to that seen 1.5h following 10mg/kg PE-LPS administration at 12.5%±1.7%. It is highly likely that the reason for this more rapid TNF induced IEC apoptosis and cell shedding compared to LPS, is that direct administration of exogenous TNF effectively bypasses TNF induction in cells of the innate immune system by LPS.

These data, together with significant induction of intestinal *Tnf* mRNA by LPS, suggest that TNF is the key mediator of LPS induced small intestinal injury.

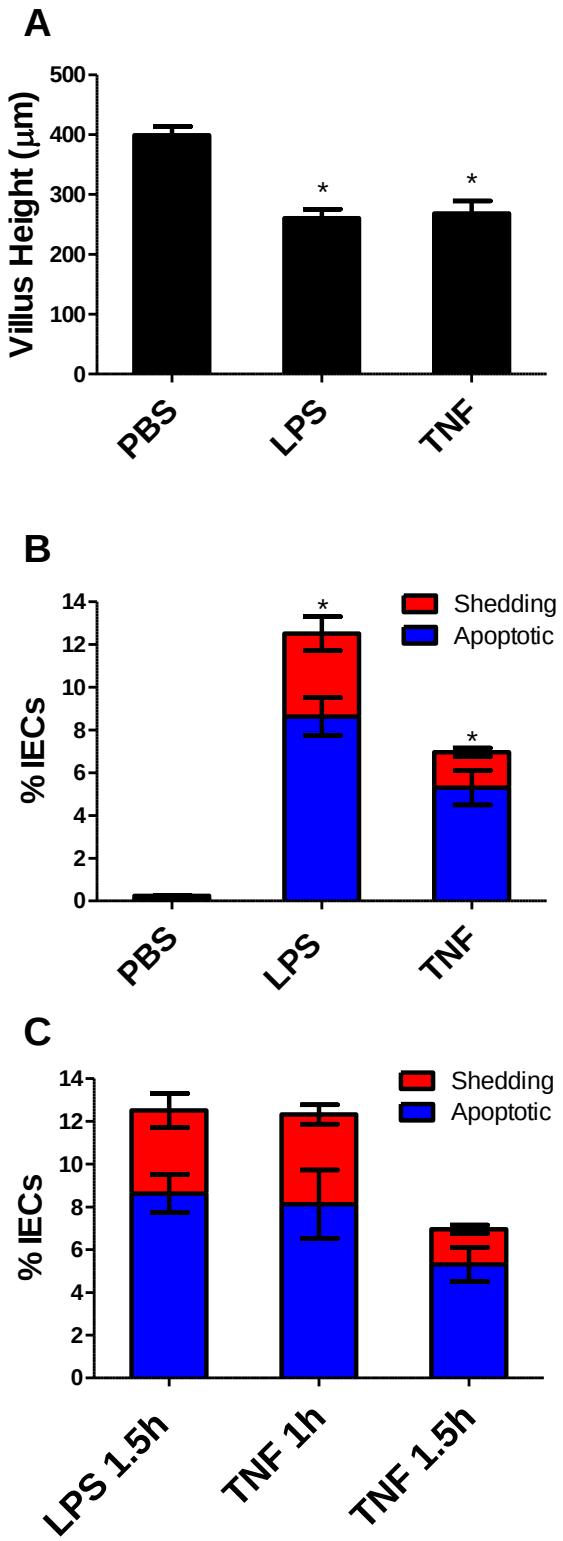

Figure 45: Villus heights and IEC apoptosis and cell shedding 1.5h after 10mg/kg PE-LPS or 0.33mg/kg TNF in WT mice (A, B) and after 1h of TNF in (C). n=4-6 female mice per group.

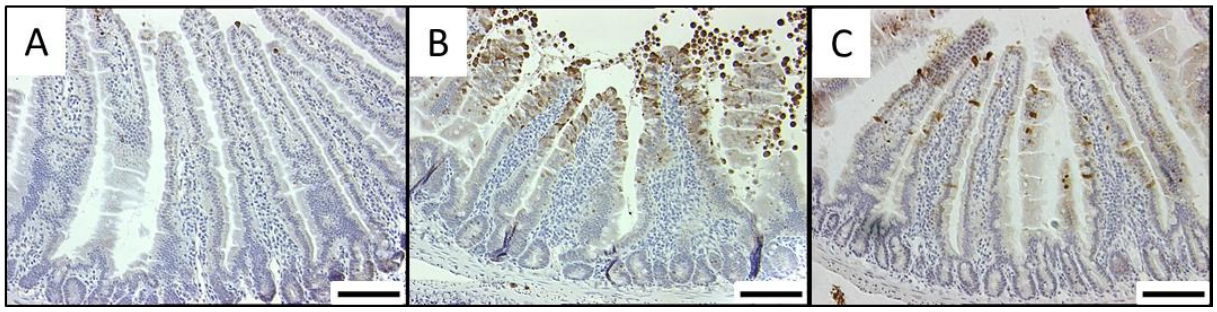

Figure 46: TNF caused more rapid small intestinal apoptosis and shedding than LPS. Photomicrograph of TNF treated female mice euthanased at 30 min (A) 1 hour (B) and 1.5 hours (C) post administration (bars=100µm). TNF caused very similar amounts of apoptosis and shedding at 1h to that caused by LPS at 1.5h. By 1.5h, maximum apoptosis and shedding had subsided in TNF treated animals (n=4-6).

4.7 *Tnfr1*$^{-/-}$ mice were completely resistant to LPS-induced apoptosis and cell shedding

To further examine the role of TNF in LPS induced IEC apoptosis and cell shedding, the small intestinal responses of mice deficient in TNF receptors TNFR1/p55 or TNFR2/p75 were tested. When *Tnfr1*$^{-/-}$ mice were administered 10mg/kg PE-LPS for 1.5h, there was significantly less villus shortening at 363.4µm±17.32µm (Figure 47A and Figure 48A) and IEC apoptosis and cell shedding by active caspase-3 IHC (Figure 47B) at 0.1%±0.1%, relative to WT animals (P<0.05:Kruskal-Wallis, Figure 48B). By contrast, the same dose administered to *Tnfr2*$^{-/-}$ mice caused 68% of the response caused in WT in terms of IEC apoptosis and cell shedding at 8.5%±1.0% (Figure 48B). These findings suggest that TNFR1 signaling is required to drive LPS induced IEC apoptosis and cell shedding, with potential enhancement by TNFR2.

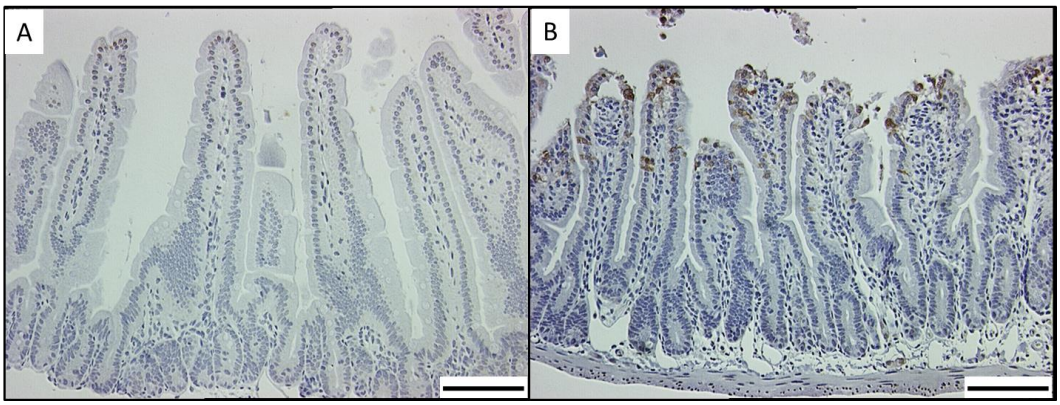

Figure 47: TNFR1 is required to produce LPS-induced IEC apoptosis and cell shedding. Photomicrographs of active caspase-3 IHC labelled duodenum demonstrating lack of IEC apoptosis and cell shedding in 10mg/kg, 1.5h PE-LPS treated *Tnfr1*$^{-/-}$ mice (A), and moderate IEC apoptosis and cell shedding in *Tnfr2*$^{-/-}$ mice (B). Bars=100μm

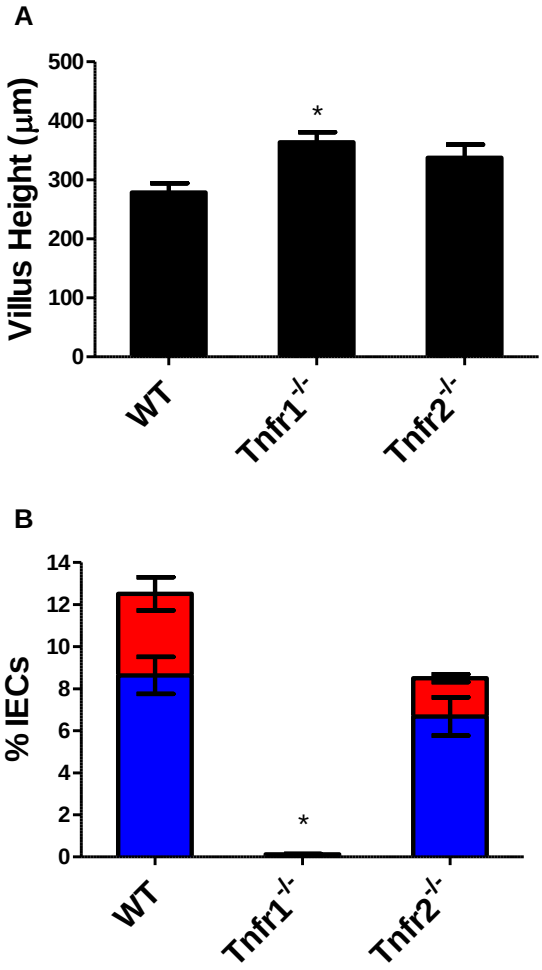

Figure 48: Bar charts of villus heights (A) and IEC apoptosis and cell shedding (B) in 1.5h, 10mg/kg PE-LPS treated WT, *Tnfr1*$^{-/-}$, and *Tnfr2*$^{-/-}$ mice. *=*P*<0.05, comparisons by Kruskal-Wallis and Dunn`s post-hoc test. n=6 female mice per group.

4.8 Discussion

Through the combination of experiments outlined in this chapter, important insights were gained into the mechanism by which LPS causes pathological IEC apoptosis and shedding in the murine small intestine. By demonstrating a lack of response when LPS was administered directly into the small intestinal lumen, this demonstrated that LPS-induced pathological IEC apoptosis and cell shedding was not mediated by direct apical epithelial LPS interactions. LPS additionally caused IEC apoptosis and cell shedding when delivered by i.v. or s.c. routes which also helped to demonstrate that this effect was not due to a localised peritoneal phenomenon following i.p. administration.

These data were further supported by testing LPS responses in *vil-Cre MyD88*$^{-/-}$ mice which lack intact TLR signalling within the intestine. These mice exhibited very similar amounts IEC apoptosis and cell shedding to WT mice, thereby further demonstrating the necessity of peripheral TLR signalling to mediate this affect in the small intestine. Similarly, Poly I:C, a synthetic viral RNA TLR3 agonist which signals independently of MyD88, has also been shown to cause IEC apoptosis and cell shedding when administered systemically, but not when given orally (McAllister et al. 2013).

The lack of direct epithelial response to LPS represents an important concept in immune tolerance and compartmentalisation of pathogen associated molecular patterns (PAMPS). Suppression of the immune response to the large intraluminal bacterial population and the bacterial products therein, is theoretically essential for preventing intestinal damage and establishment of

active inflammation. There are a number of potential mechanisms by which this prevention of microbial/microbial product interaction with the epithelium and/or the immune system may be achieved. They include: the intestinal mucus acting as a physical barrier, luminal or membrane associated proteins either enzymatically destroying or inactivating microbes/microbial products, compartmentalisation or mechanistically different PAMP recognition in the gut, or cytokine mediated suppression of mucosal immune responses in the subepithelial tissue.

Luminal and membrane associated defences which would reduce potential LPS interactions include mucus and IgA secretion, but an additional mechanism by which the intestinal mucosa may detoxify the abundant LPS within the lumen, is by the action of intestinal alkaline phosphatase (IAP). IAP has been shown to dephosphorylate and reduce the toxicity of the toxic lipid A component of LPS, but this enzyme is also highly important in dictating luminal pH, and in lipid metabolism. It is expressed at the brush border in the small intestine in well differentiated absorptive enterocytes in an increasing gradient towards the villus tip, and in a decreasing gradient from the duodenum to the ileum in rodents. It is minimally expressed in the stomach and colon. This pattern of expression therefore runs counter to the bacterial population of these localisations of the gastrointestinal tract (reviewed by Lalles (2010)). Intriguingly, IAP knock-out mice fail to establish a normal microbiome (Malo et al. 2010). These mice exhibit an abnormal intestinal bacterial flora which fails to be colonised by commensal *E.coli*, even when mice are orally supplemented with these bacteria. IAP knock-out mice

additionally exhibit metabolic endotoxaemia (a syndrome of sub-clinically increased circulating endotoxin) when fed on a high fat diet (Kaliannan et al. 2013) and exhibit more severe colitis in response to dextran sodium sulphate (DSS), which is attenuated by oral supplementation with calf IAP (Ramasamy et al. 2011). IAP expression has also been shown to be reduced in starvation, to inhibit NFκB expression *in vitro*, and also to reduce bacterial translocation *in vivo*, in an ischaemia reperfusion model (Goldberg et al. 2008). It could be therefore be hypothesised that stimuli which cause damage to the upper villus may result in reduced expression of IAP, as it is the well differentiated IECs in this region of the villus which predominantly express IAP. This could then predispose to increased bacterial growth or dysbiosis and chronic inflammation. In support of this concept, lower expression of IAP has been shown in the intestines of patients with ulcerative colitis (UC) and Crohn`s disease (CD) (Tuin et al. 2009).

LPS signalling is additionally dependent on delivery of LPS to the cell membrane in a bioactive form by lipopolysaccharide binding protein (LBP) and the adapter molecules CD14 (Wright et al. 1990) and MD-2 (Shimazu et al. 1999). TLR4 and CD14 have been found to be expressed throughout the gastrointestinal tract of the mouse, with an increasing expression gradient from the proximal to distal intestinal tract; the highest expression being found in the distal colon (Ortega-Cava et al. 2003). It has additionally been shown that TLR4 and CD14 are confined to the crypt base, suggesting a further microanatomical compartmentalisation of this pattern recognition receptor, to a site that may be more physically protected by both distance and mucus,

from exposure to the luminal bacterial content.

The high expression of TLR4 in the distal colon, possibly in conjunction with very low expression of IAP, may explain why it has been demonstrated that luminal LPS delivered by enema into the colon of CD-1 mice causes small intestinal damage 2 days after administration (Eunok et al. 2012). In these experiments, it was found that TLR4 signalling was required, but intriguingly LPS enema did not cause colitis. These findings could therefore point towards different TLR sensing in the colon as opposed to the small intestine, and/or a different immunological response in the two sites to LPS.

Immune tolerance to what would be constant stimulation by the luminal Gram negative bacterial population in the gut, may additionally be achieved through localisation of TLRs to the basolateral, rather than apical membrane of the IEC. In support of this, it has been shown in humans that both TLR2 and TLR4 are expressed on the basolateral side of foetal ileal crypt enterocytes (reviewed by Abreu (2010)). Alternatively, fundamentally different TLR signalling in small intestinal IECs may occur. Indeed, in cell culture of m-ICcl2 murine IECs, TLR4 was found to reside within the Golgi apparatus, rather than at the cell membrane (Hornef et al. 2002).

Although the healthy human gut predominantly contains Gram positive bacteria, there is often a shift towards a predominantly Gram negative bacterial population in IBD (Seksik et al. 2003). This is also accompanied by increased IEC TLR4 expression in IECs of IBD patients (Cario and Podolsky 2000), suggesting that the relative expression of this receptor may be

important in predisposing to the onset of inflammation.

At the subepithelial level, it has been shown that there may be important roles for intestinal dendritic cells in maintaining gut immune tolerance. In support of this, human intestinal dendritic cells of the lamina propria have been shown to lack the co-receptor molecule for TLR4; CD14 (Smith et al. 2001) further compartmentalising responses to luminal LPS.

Having established that luminal LPS did not appear to trigger IEC apoptosis and cell shedding (by 1.5h) in contrast to systemic LPS, it was demonstrated that high purity IE-LPS caused IEC apoptosis and shedding via an almost entirely TLR4 dependent mechanism. However, lower purity PE-LPS administered to *Tlr4*$^{-/-}$ mice caused a moderate amount of IEC apoptosis and cell shedding. This suggests that other constituents of the PE-LPS preparation may interact with the immune system and may also contribute to this effect.

Potential interactions could include the recognition of other bacterial products representing impurities in the PE-LPS preparation, by alternative TLRs. Such bacterial products likely to be present include bacterial RNA, which may represent a major constituent of the phenol extracted LPS. Bacterial RNA is recognised by TLR7 in murine plasmacytoid dendritic cells, but interestingly it has also been shown that other immunoreceptors may also be activated by this ligand to cause TNF secretion (Eberle et al. 2009).

Other impurities could also include lipopeptides which can be recognised via TLR2 (Buwitt-Beckmann et al. 2006), peptidoglycans which may also be

recognised by TLR2/TLR6, and intracellular nucleotide-binding oligomerization domain-containing (NOD) proteins NOD1 and NOD2 (reviewed by Royet and Dziarski (2007)). In support of other PAMPs causing this phenomenon, it has been demonstrated that in mice apoptosis in the intestinal villus can be triggered by the TLR3 agonist poly I:C (McAllister et al. 2013). TLR3, in contrast to other TLRs, signals exclusively via the TIR-domain-containing adapter-inducing interferon-β (TRIF) rather than MyD88 pathway (Kawai and Akira 2011). As such, this agonist represents an unusual TLR mediated inflammatory response. In the McAllister study, it was demonstrated that poly I:C caused apoptosis by a TRIF dependent and in contrast to our own model, TNF independent mechanism. IEC apoptosis peaked at 2h post administration, possibly reflecting delayed activation of the TRIF pathway compared to the MyD88 pathway (Pålsson-McDermott and O'Neill 2004). The authors of this study hypothesised that the apoptotic and shedding response may be some kind of host defence mechanism to eliminate pathogens. However, if this were the case, it perhaps would be expected that luminal pathogen sensing would be more effective, and in this model oral poly I:C failed to cause a response.

The rapid increase in plasma TNF concentration after LPS administration has been previously characterised (Copeland et al. 2005). In the current study, a large fold change in *Tnf* mRNA abundance in small intestinal epithelial enriched extracts 1.5h after LPS administration was demonstrated compared to untreated mice. These qPCR data also show that LPS administration caused changes in transcription of genes predominantly involved in

apoptosis. As the samples analysed by qPCR were epithelial enriched, this would suggest that the predominant cell type responsible for this increased transcription of *Tnf* mRNA is the intestinal epithelial cell. This is supported by research by Guma et al. (2011) who showed IEC TNF production in the small intestine by immunofluorescence, and increased *Tnf* transcription by *in situ* hybridisation, in mice with epithelial specific constitutively active IKKβ, when challenged with LPS for 4h. This TNF production was additionally dependent on MAPK activation. This suggests that once triggered, epithelial TNF production can proceed to autocrine and paracrine TNF signalling to cause severe IEC apoptosis and cell shedding. However, in our own experiments epithelial enriched extracts did not represent a purely epithelial population, and so it cannot be discounted that there could be contributions by intestinal dendritic cells, other leukocytes, endothelial cells, or myofibroblasts.

The significance of TNF as the critical mediator in our model was further demonstrated by TNF administration causing IEC apoptosis and cell shedding consistent with previous results (Garside et al. 1993; Piguet et al. 1998), and equivalent to that caused by LPS. Moreover, it was shown that lack of TNFR1 caused complete blocking of LPS induced pathological IEC apoptosis and cell shedding. Although it was hypothesised that TNF could be the most important mediator of LPS-induced apoptosis and cell shedding, we did not expect this cytokine, via TNFR1 to be entirely responsible for this effect.

Indeed, research conducted on endotoxic shock induced gut injury has implicated many other mediators such as platelet activating factor (PAF),

thromboxane, inducible nitric oxide synthase (iNOS), IL-1 and interferon gamma (IFNγ), the production of all of which should not be affected in *Tnfr1*$^{-/-}$ mice in response to systemic LPS administration.

However, this dependence on TNFR1 is in keeping with those that have investigated the mechanism of exogenous TNF mediated small intestinal apoptosis, where the effect is entirely mediated through TNFR1 (Piguet et al. 1998). This form of TNF induced apoptosis also appears to be critically dependent on dosage, as it has been shown that a dose of 5µg TNF in adult WT mice caused significant IEC apoptosis in the small intestine by 1h, whereas 1µg TNF did not (McAllister et al. 2013). This can be compared to the dose studied in this project of 0.33mg/kg TNF (equating to 6.6µg per mouse). In the McAllister study, when comparison was made after 1h between 20mg/kg LPS, 1µg TNF, and 5µg TNF, this resulted in serum TNF concentrations of around 10,000pg/ml, 20,000pg/ml, and 100,000pg/ml respectively. The 10 fold lower concentration of TNF induced by 20mg/kg LPS compared to 5µg TNF probably again reflects the early time point examined (1h), and presumably continues to increase further by 1.5h post administration.

Limitations do however exist in the interpretation of the LPS response in *Tnfr1*$^{-/-}$ mice, as they do not exhibit IEC specific absence of TNFR1. Although highly probable, and in keeping with other investigations (Jackson et al. 2000; Guma et al. 2011), it cannot be stated categorically in our model whether TNFR1 ligation is occurring at the level of the IEC or whether TNF is causing IEC apoptosis and shedding by indirect mechanisms distant to the

IEC. These could include effects of TNFR1 ligation at the level of myofibroblasts, leukocytes, neurones, or endothelial cells. In the case of the latter, this could contribute to serious haemodynamic disturbances, and reduced perfusion of the villus. However, strong evidence for direct IEC TNFR1 ligation initiating apoptosis and shedding comes from elegant experiments by Roulis et al. (2011). In this study, it was shown that following exogenous TNF administration, mice which express functional TNFR1 specifically within IECs, exhibited apoptosis and shedding at 1h after intravenous administration of 12µg TNF. This suggests that direct TNFR1 ligation does indeed occur at the level of the IEC.

It is well established that TNF binding with TNFR1 leads to multimerisation and autocleavage of caspase-8 in extrinsic pathway apoptosis. When the TLR3 agonist poly I:C is administered systemically, this results in activation of caspase-8 and caspase-3 in IECs. However, if poly I:C is administered to mice specifically lacking caspase-8 in IECs, caspase-3 is not activated and there is massive destruction of the villus, with complete loss of villus epithelium by 2.5h, and the death of these mice occurring by 6h post-treatment (McAllister et al. 2013). This cell death occurs by alternative cell death pathways, possibly culminating in necroptosis, as it does not seem dependent on executioner caspase activity. It is not entirely clear what the secondary mediator of IEC apoptosis was in the McAllister study, as it was concluded that although TLR3 and TRIF were required to cause villus apoptosis, this process was independent of all cytokines tested, including TNF, IL-1, IL-6, IFNγ and IL-15. It was also shown to be dependent on cells

of non-haematopoietic origin. It may therefore be speculated that in the case of TLR3 agonists, pro-apoptotic IEC signalling may arise from basolateral IEC TLR3 signalling, or possibly by endothelial, myofibroblast or neural TLR3 signalling.

LPS-treated mice specifically lacking caspase-8 in IECs also exhibit β1 integrin depletion in IECs (de Chambrun et al. 2013). It was shown in this study that in addition to obvious apoptotic functions, caspase-8 regulates clathrin dependent endocytosis. These mice were resistant to LPS-induced small intestinal damage when treated with an endocytosis inhibitor; chlorpromazine, or when crossed with mice lacking autophagy related protein 7 (Atg 7). These mice were also completely protected from LPS-induced damage by crossing with mice lacking *Tnfr1*$^{-/-}$.

In the intestinal epithelium, and in intestinal cell lines, TNFR1 is expressed to a greater extent than TNFR2 (Mizoguchi et al. 2002; Lau et al. 2011), although the latter can be induced by inflammatory cytokines (Mizoguchi et al. 2002). Although TNFR1 has well defined pro-apoptotic effects (Locksley et al. 2001), the role of TNFR2 has been less well characterised. Interestingly, the intestinal epithelial response to LPS was moderate in *Tnfr2*$^{-/-}$ mice, suggesting that this receptor does participate in LPS-induced IEC apoptosis, possibly by enhancement of TNFR1 signals through degradation of TRAF2, resulting in termination of NFκB signalling (Rodríguez et al. 2011). Interestingly, in the context of colitis, it has been shown that TNFR2 can induce myosin light chain kinase (MLCK) to cause tight junction dysregulation, which leads to colonic epithelial cell apoptosis and gut barrier

defects (Su et al. 2013). This may imply that the reduced apoptosis and shedding that was observed in TNFR2 deficient mice may be due to the lack of MLCK activation, and thereby reduced detrimental effects on tight-junctions. In a more chronic model of TNF induction, it has been shown in mice that lack the autoregulatory elements which control and suppress excessive TNF production, that a spontaneous intestinal inflammation similar to Crohn`s disease develops, which is TNFR1 dependent. In keeping with our model, this affect was enhanced by presence of TNFR2 (Kontoyiannis et al. 1999).

Although *Cd40* also showed marked up regulation in the array, this was not corroborated when individual replicate samples were analysed by qPCR. This was probably due to the fact that this increased transcriptomic abundance was measured at a late qPCR cycle number in both treated and untreated animals. This is consistent with very low level transcription found in both groups, and therefore reflects a more unreliable result. The array also did not detect significant transcriptional alterations to other caspases including caspases 1-3,6,7, and 9. This is perhaps not unsurprising, as the activation of these enzymes largely occurs at the protein level through cleavage, conformational changes, and dimerisation (see Introduction).

In summary, the findings outlined in this chapter suggest that LPS initiates a rapid process of peripheral TLR4 ligation, most likely within peripheral macrophages and dendritic cells. This triggers a cascade of pro-inflammatory gene induction.

Of the cytokines produced, it is TNF via TNFR1 which induces the rapid activation of caspase-3, likely via caspase-8, resulting in IEC apoptosis and cell shedding. It also seems likely that initial TNF production from the periphery stimulates epithelial TNF production.

5. NFκB Regulation of Pathological IEC Apoptosis and Cell Shedding

5.1 Introduction

Having established the mechanisms by which LPS induced IEC apoptosis and cell shedding in the small intestine of WT mice, the influence of NFκB signalling pathways downstream of LPS and TNF were investigated. As NFκB is a major transcriptional regulator downstream of TLR, it was first investigated whether mice lacking NFκB subunits, specifically *Nfκb1*$^{-/-}$ which lack p50 and its precursor p105 protein, *Nfκb2*$^{-/-}$ which lack p52 and its precursor p100 protein, and *cRel*$^{-/-}$ mice, would exhibit altered sensitivity to LPS induced IEC apoptosis and cell shedding. As NFκB is also a major transcriptional regulator downstream of TNFR1, the response of these mice to TNF would also be tested.

The relative sensitivities of these genotypes to LPS were investigated utilising previous data on time and dose responses to LPS in WT mice. By administering PE-LPS at high dose (10mg/kg) and low dose (0.125mg) by i.p. injection for 1.5h, it was hypothesised that by measurement of duodenal villus height, and IEC apoptosis and cell shedding by active caspase-3 IHC, that differing sensitivities between genotypes would be detected. By examining these differences between genotypes when administered TNF, it was hypothesised that this would effectively bypass the upstream influence of the differing innate immune response in these genotypes. This would thereby reveal events relating to regulation of apoptosis occurring downstream of TNFR1 (and possibly TNFR2) ligation. Finally, the role of NFκB proteins was also investigated by performing western blotting on small intestinal epithelial enriched extracts, and immunohistochemistry on

duodenal sections from treated and untreated mice of these genotypes, to further clarify the influence that these signalling pathways exert on pathological IEC apoptosis and cell shedding in the murine small intestine.

5.2 *Nfκb1*$^{-/-}$ mice were more sensitive, and *Nfκb2*$^{-/-}$ mice more resistant to LPS induced intestinal injury

PE-LPS was administered to male and female *Nfκb1*$^{-/-}$, *Nfκb2*$^{-/-}$, and *c-Rel*$^{-/-}$ mice. Data were analysed separately for males and females, and were combined following absence of observable, or statistically significant differences being detected between genders following either high dose (10mg/kg), or low dose (0.125mg/kg) PE-LPS, as had been established to be the case in WT mice (see 3.11.3). Results are therefore described for "combined genders" unless otherwise stated. This is with the exception of *c-Rel*$^{-/-}$ mice following 0.125mg/kg LPS, due to apparent and statistically significant differences between genders (discussed later).

Following 10mg/kg LPS for 1.5h, *Nfκb1*$^{-/-}$ mice exhibited a mean villus shortening of 31%; reduced to 261.1µm±24.6µm when compared to 384.9µm±12.9µm in untreated *Nfκb1*$^{-/-}$ mice (Figure 50). This was comparable to the 32% villus shortening observed following 10mg/kg LPS in WT mice, reduced to 263.6µm±10.1µm compared to 385.7µm±11.5µm in untreated animals (Figure 50). Following 10mg/kg LPS, *Nfκb1*$^{-/-}$ mice also showed similar amounts of IEC apoptosis and cell shedding at 12.3%±4.2% compared to WT mice at 11.5%±3.1% (Figure 51). In contrast, mean villus height was only reduced by 11% in *Nfκb2*$^{-/-}$ mice administered 10mg/kg LPS,

to 347.5µm±12.4µm compared to 389.7µm±14.0µm in untreated *Nfκb2*$^{-/-}$ animals.

This represented a significantly attenuated villus shortening when compared to the 32% observed in WT mice administered this dose (P<0.05: Kruskal-Wallis, Figure 51). *Nfκb2*$^{-/-}$ mice given 10mg/kg LPS also exhibited a trend towards reduced IEC apoptosis and cell shedding at 8.5%±4.2%, compared to similarly treated WT mice at 11.5%±3.1%, although this difference was not statistically significant (Figure 51).

Interestingly, when administered a low dose of LPS (0.125mg/kg), villus height in *Nfκb1*$^{-/-}$ mice was reduced by 27% to 283.6µm±19.6µm when compared to 384.9µm±12.9µm in untreated *Nfκb1*$^{-/-}$ animals. This represented almost the same degree of villus shortening as when administered 10mg/kg LPS (31%; Figure 50) and was significantly greater than the 5% villus shortening observed in 0.125mg/kg LPS treated WT mice [365.6µm±19.0µm when compared to 385.7µm±11.5µm in untreated WT animals (P<0.05: Kruskal-Wallis)]. *Nfκb1*$^{-/-}$ mice administered 0.125mg/kg LPS also exhibited significantly greater amounts of IEC apoptosis and cell shedding (Figure 51) at 12.9%±1.7% (P<0.05: Kruskal-Wallis) compared to WT mice at 6.0%±1.7%. By contrast, when administered this low dose (0.125mg/kg of PE-LPS), no villus shortening was observed in *Nfκb2*$^{-/-}$ mice (414.5µm±5.7µm compared to 389.7µm±14.0µm in untreated *Nfκb2*$^{-/-}$ animals; Figure 50), and negligible IEC apoptosis and shedding of 0.8%±0.2% was detected (P<0.05: Kruskal-Wallis; Figure 51).

Of note, when administered 10mg/kg LPS, *c-Rel*$^{-/-}$ mice showed villus shortening of 47%, to 230.1µm±12.7µm compared to 430.5µm±11.5µm in untreated *c-Rel*$^{-/-}$ animals (Figure 50). This represented the greatest degree of villus shortening observed in any of the genotypes. However, when *c-Rel*$^{-/-}$ mice were administered 0.125mg/kg PE-LPS, differences were detected between the responses of males and females, with females exhibiting greater sensitivity to LPS, comparable with *Nfκb1*$^{-/-}$ mice. This was firstly shown in terms of villus shortening (Figure 50) to 331.2µm±28.2µm compared to 430.6µm±16.0µm in untreated *c-Rel*$^{-/-}$ females (23%). By contrast, *c-Rel*$^{-/-}$ males exhibited a villus height reduction of only 4% to 415.3µm±17.4µm compared to 430.3µm±18.1µm in untreated *c-Rel*$^{-/-}$ male animals. *c-REL*$^{-/-}$ female mice treated with 0.125mg/kg LPS also exhibited greater amounts of IEC apoptosis and cell shedding at 10.57%±2.5% (Figure 51) compared to 3.7%±1.5% in males.

Together, these results suggest that LPS induced small intestinal injury is enhanced by intact alternative pathway NFκB2 signalling, while canonical NFκB1 signalling may be necessary to suppress IEC apoptosis and cell shedding. c-REL may also be important in suppressing IEC apoptosis, as demonstrated in 10mg/kg LPS treated mice of this genotype, however at 0.125mg/kg this seems to be the case only in female animals.

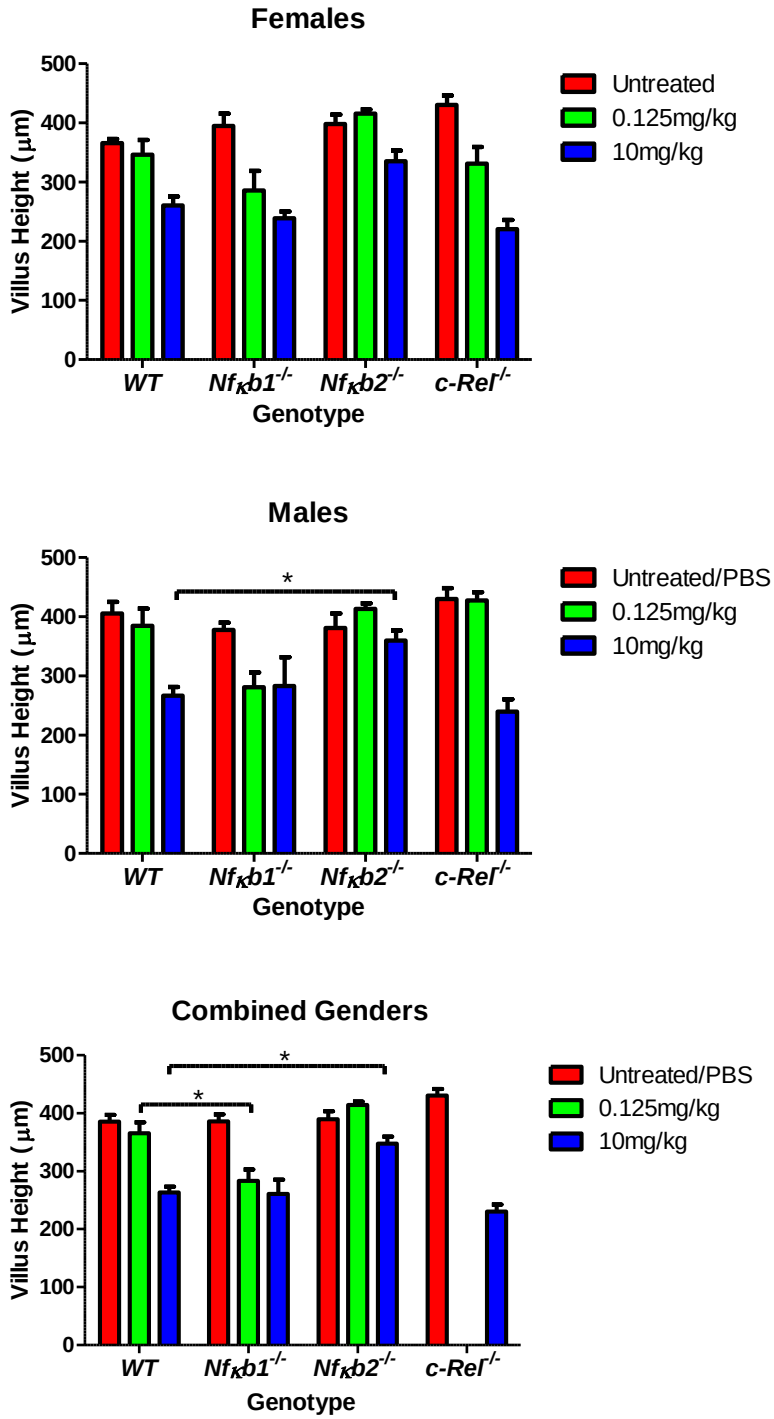

Figure 49: Bar charts of villus height measurements of duodenal villi for female, male, and combined gender groups, demonstrating the marked sensitivity of *Nfκb1*$^{-/-}$ mice to 0.125mg/kg LPS and relative resistance of *Nfκb2*$^{-/-}$ mice to 10mg/kg LPS-induced small intestinal injury. Comparisons are between genotypes within same dosage group against WT controls by ANOVA and Holm-Sidak post-hoc test. * =*P*<0.05, n=6 female and n=6 male mice per group. *N.B.* green bar representing combined genders for *c-Rel*$^{-/-}$ treated with 0.125mg/kg LPS is absent due to statistically significant differences between genders at this dose.

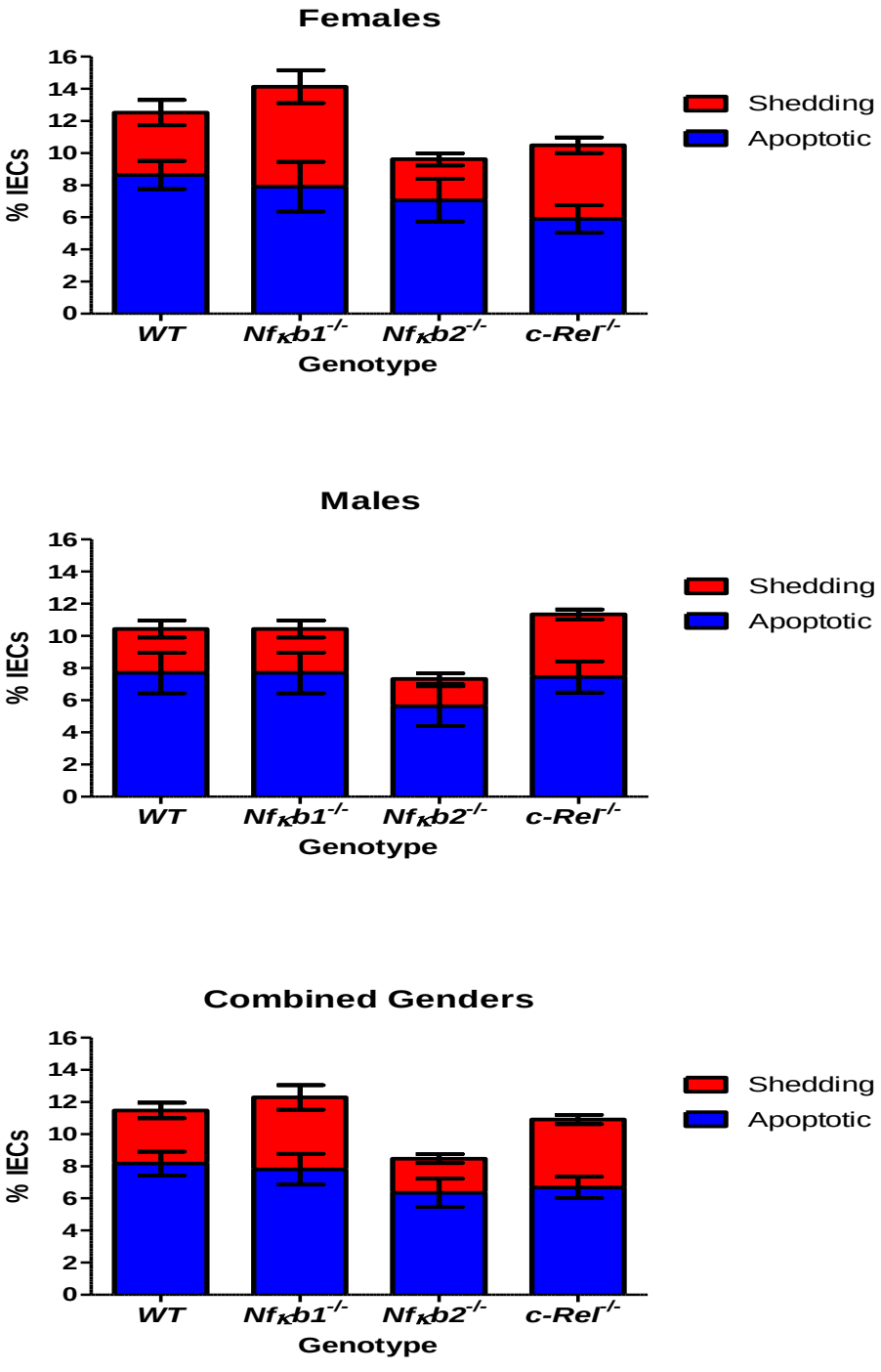

Figure 50: Bar charts of relative percentage of apoptotic and shedding IECs in the duodenal villi of high dose (10mg/kg PE-LPS) treated male, female, and combined gender transgenic mice, demonstrating that there was less IEC apoptosis and cell shedding (albeit not statistically significant) observed in the *Nfκb2*$^{-/-}$ genotype. n=6 female and n=6 male mice per group.

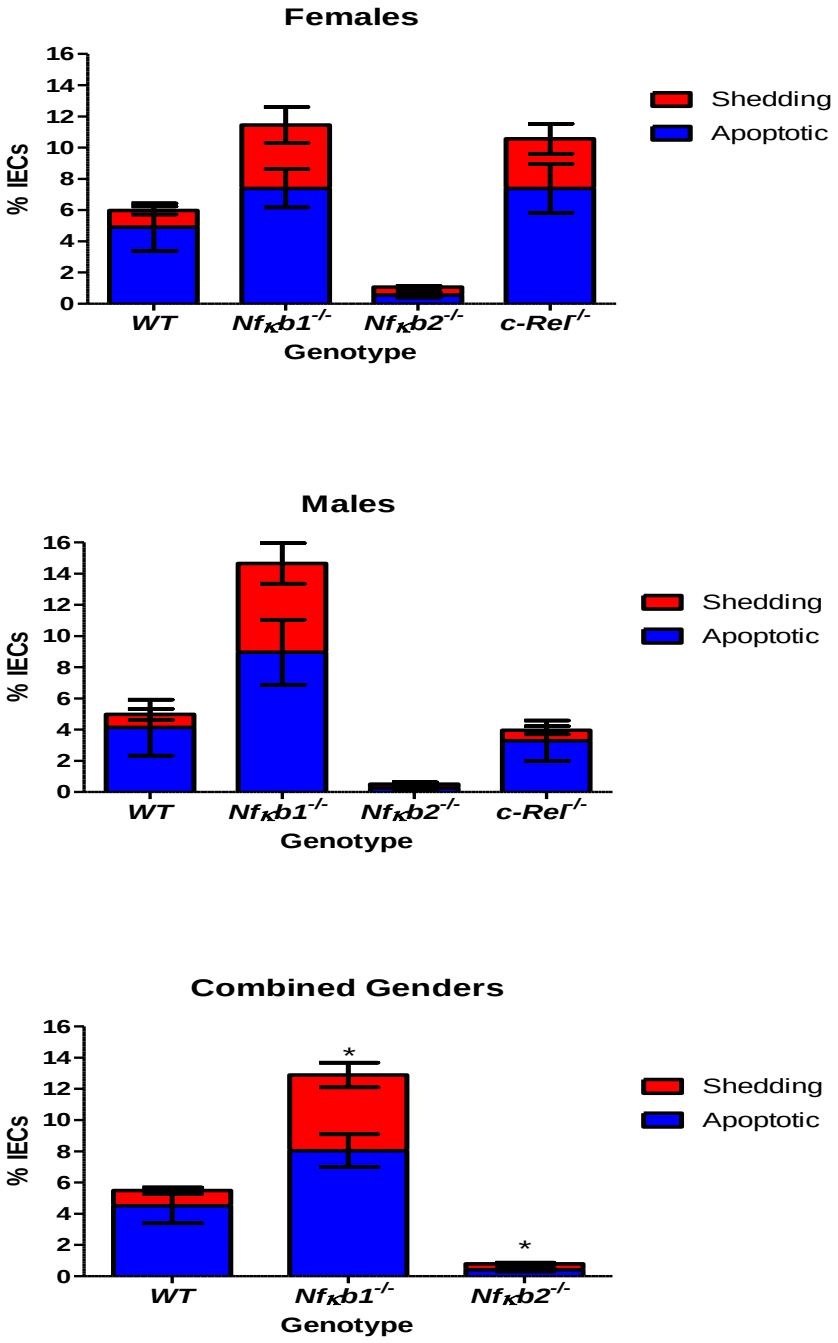

Figure 51: Bar charts showing relative percentage of apoptotic and shedding IECs in the duodenal villi of transgenic mice at 1.5h after low dose (0.125mg/kg) PE-LPS, showing significantly increased IEC apoptosis and cell shedding in *Nfκb1*$^{-/-}$, and significantly decreased IEC apoptosis and cell shedding in *Nfκb2*$^{-/-}$ mice. * =*P* value <0.05 based on ANOVA and Holm-Sidak post-hoc test. n=6 for females and n=6 for males except for *Nfκb1*$^{-/-}$ (n=7 males, n=7 females) and *c-REL*$^{-/-}$ (n=8 males, n=6 females). *N.B.* bar representing combined genders for *c-Rel*$^{-/-}$ treated with 0.125mg/kg LPS is absent due to statistically significant differences between genders at this dose.

5.3 *Nfκb1*$^{-/-}$ mice were highly sensitive, and *Nfκb2*$^{-/-}$ mice more resistant to TNF induced small intestinal injury

As well as acting as a transcriptional regulator downstream of TLR4 ligation, NFκB is also a major exponent of signalling downstream of TNFR receptor ligation. The responses of *Nfκb1*$^{-/-}$ and *Nfκb2*$^{-/-}$ female mice to TNF were therefore tested by administration of murine recombinant TNF by i.p. injection at 0.33mg/kg for 1.5h. This dose of TNF had been previously shown to induce IEC shedding by *in vivo* confocal microscopy in our own laboratories (Kiesslich et al. 2012). Duodenal villus heights, and villus IEC apoptosis and cell shedding were then quantified and compared between genotypes. *Nfκb1*$^{-/-}$ mice were highly sensitive to TNF induced small intestinal injury (Figure 53) with a significant reduction in villus height to 160.1μm±7.3μm compared to TNF-treated WT mice at 268.4μm±20.9μm (P<0.05: ANOVA; Figure 53A). This correlated with increased IEC apoptosis and cell shedding of 9.9%±0.7% in TNF-treated *Nfκb1*$^{-/-}$ mice compared to 7.0%±1.0% in WT (P<0.05: ANOVA; Figure 53B). Conversely, *Nfκb2*$^{-/-}$ mice were resistant to TNF induced reduction in villus height, with only a small measurable decrease in villus height to 340.1μm±15.1μm (Figure 53A) when compared to 398.2μm±15.7μm in untreated, and significantly reduced IEC apoptosis and cell shedding of 2.5%±0.7% (Figure 53B) compared to similarly treated WT animals at 7.0%±1.0% (both P<0.05).

These data suggest that in response to TNF administration, IEC apoptosis and cell shedding are suppressed by classical NFκB activation via NFκB1,

and promoted by alternative NFκB activation via NFκB2.

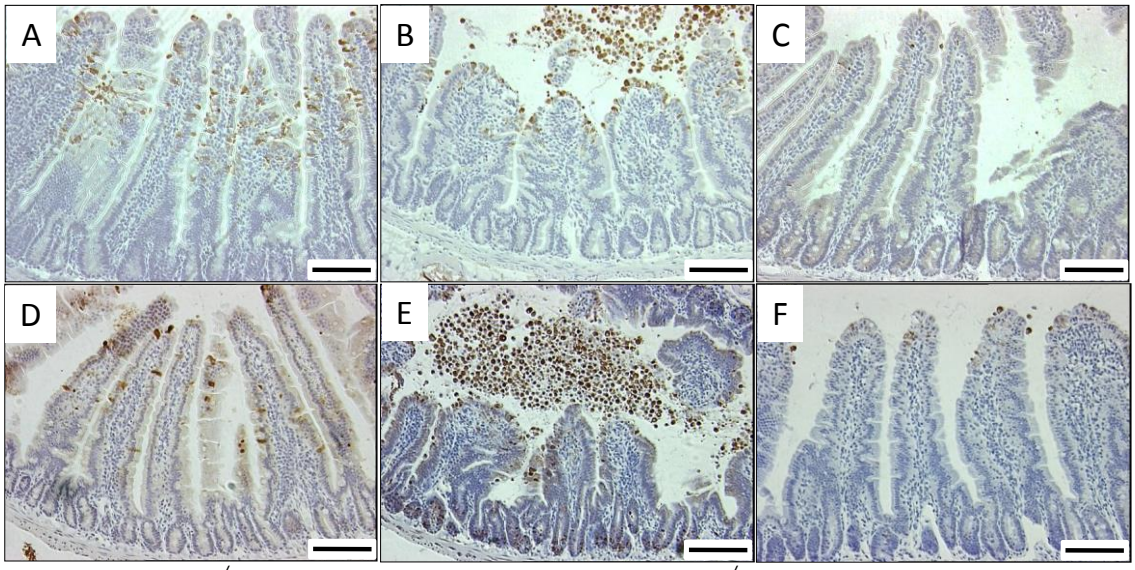

Figure 52: *Nfκb1*$^{-/-}$ mice were more sensitive, and *Nfκb2*$^{-/-}$ mice more resistant to LPS or TNF induced IEC apoptosis and cell shedding. Representative active caspase-3 IHC photomicrographs of LPS treated WT, *Nfκb1*$^{-/-}$, and *Nfκb2*$^{-/-}$ (A, B, and C) and TNF treated WT, *Nfκb1*$^{-/-}$, and *Nfκb2*$^{-/-}$ (D,E, and F). Enhanced IEC apoptosis and cell shedding was present in *Nfκb1*$^{-/-}$ mice, and reduced villus shortening and reduced IEC apoptosis and cell shedding in *Nfκb2*$^{-/-}$ mice. Bars=100μm.

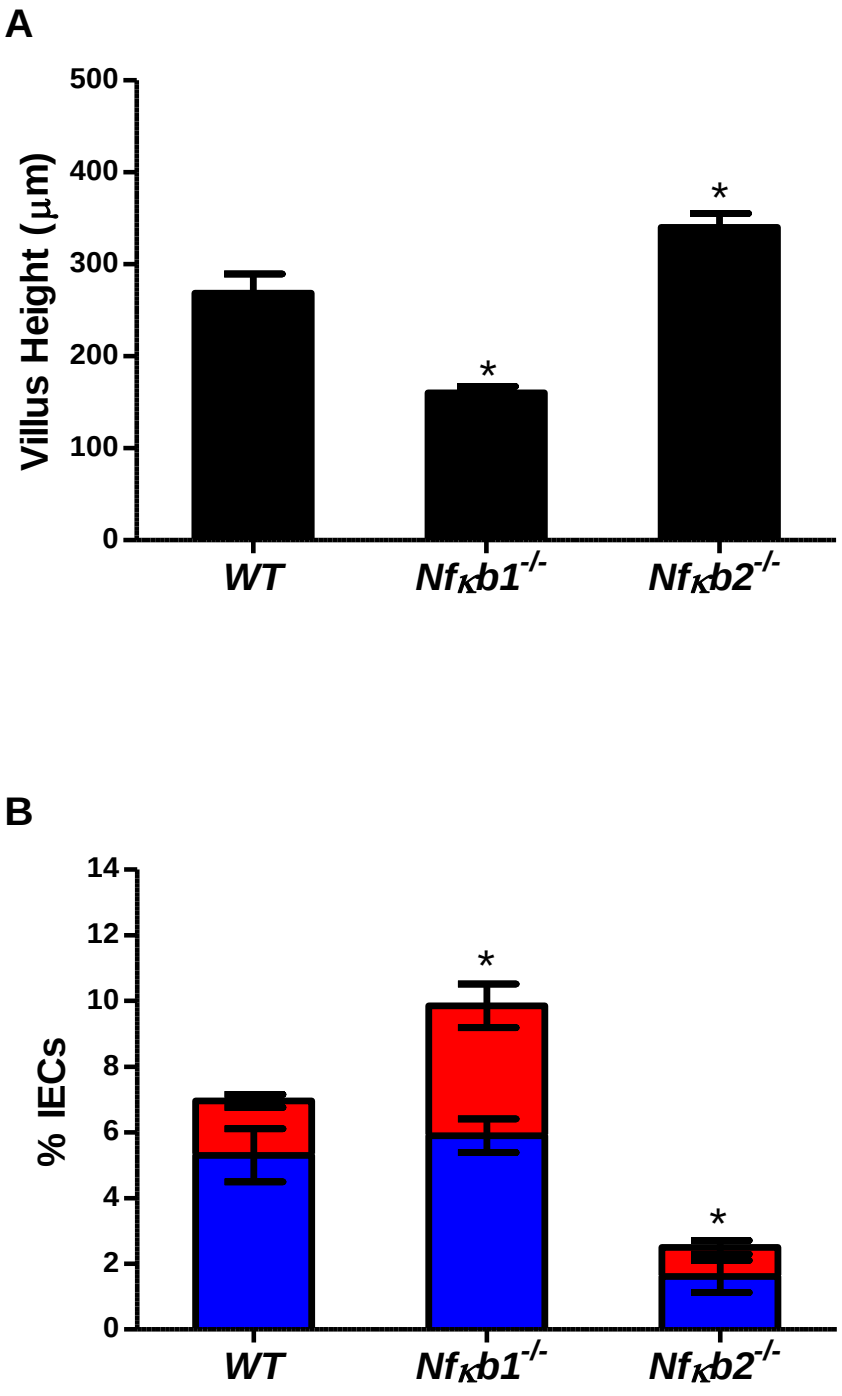

Figure 53: Villus heights (A) and IEC apoptosis and cell shedding (B) 1.5h after 0.33mg/kg TNF in WT, *Nfκb1*$^{-/-}$ and *Nfκb2*$^{-/-}$ mice. *=*P*<0.05. n=4-6 female mice per group, comparisons by ANOVA and Holm-Sidak post-hoc correction.

5.4 *Nfκb1*$^{-/-}$ mice exhibited crypt apoptosis in response to TNF

An interesting further observation in TNF treated *Nfκb1*$^{-/-}$ mice, was that in addition to the much greater villus IEC apoptosis and cell shedding seen in the duodenum of these mice, marked crypt apoptosis was also observed (Figure 54) when compared with WT and *Nfκb2*$^{-/-}$ mice. Quantification demonstrated significantly increased apoptosis within crypts of *Nfκb1*$^{-/-}$ mice, at 15.7%±2.9%, compared to 0.9%±0.5% in WT, and 1.4%±0.6% in *Nfκb2*$^{-/-}$ mice (Figure 56). This suggests that both villus and crypt IECs exhibit a pro-apoptotic phenotype in response to TNFR1 (and possibly TNFR2) ligation when canonical NFκB1 signalling is ablated. The inference from this finding is that NFκB1 is important in promoting survival of both villus IECs and crypt IECs when exposed to TNF. Interestingly, there is relative sparing of the IECs of the villus base to the mid-villus region, again perhaps pointing to villus IEC apoptosis and shedding not being caused indirectly by a TNFR1 mediated vascular phenomenon, as it would perhaps be expected that there should be relatively uniform cell death along the crypt:villus axis if this were the case. Crypt apoptosis was however mainly observed in the crypt base (Figure 57) and appeared to include Paneth cells (Figure 54B), with maximum between cell position 3-5. Frequency of apoptotic crypt cells observed declined towards the crypt villus junction.

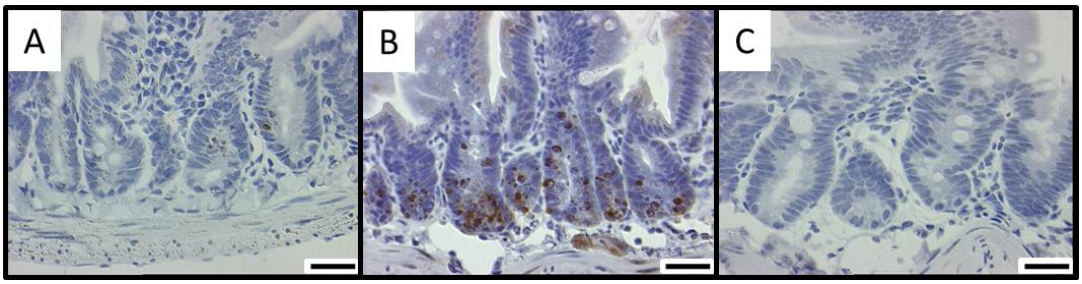

Figure 54: Photomicrographs of active caspase-3 immunohistochemistry in duodenal sections of WT (A), *Nfκb1*$^{-/-}$ (B) and *Nfκb2*$^{-/-}$ (C) female mice 1.5h following 0.33mg/kg TNF treatment. Large numbers of apoptotic crypt cells were observed in the crypt base of *Nfκb1*$^{-/-}$ mice, compared to negligible amounts in WT and *Nfκb2*$^{-/-}$ mice. Bars=25µm.

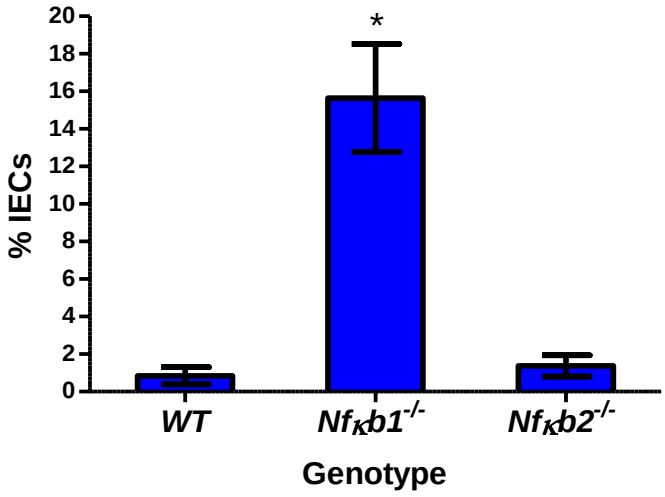

Figure 55: Quantification of crypt apoptosis induced by TNF (0.33mg/kg) in active caspase-3 IHC stained sections of duodenum, showing significantly increased crypt apoptosis in *Nfκb1*$^{-/-}$ mice. Comparisons made against WT by ANOVA and Dunnett`s post-hoc test. n=4 female mice per group.

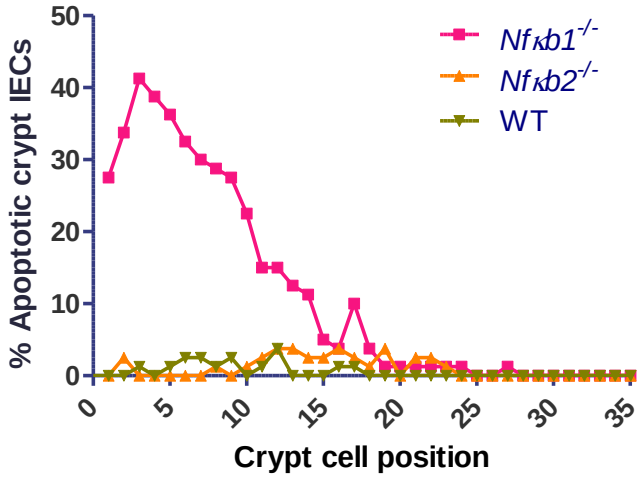

Figure 56: *Nfκb1*$^{-/-}$ mice exhibited greatest crypt apoptosis in the crypt base (with maximum between cell position 3-5) which declined along the crypt axis. n=4 female mice per group.

5.5 LPS caused small intestinal p100 processing to p52 in 1.5h

As the relative sensitivity of *Nfκb1*$^{-/-}$ and *Nfκb2*$^{-/-}$ mice to LPS and TNF had now been established, further investigation of cellular NFκB signalling events in the IEC following LPS stimulation was undertaken. From the phenotypic responses characterised, it appeared that NFκB1 and NFκB2 differentially regulated villus IEC apoptosis and shedding. It was therefore hypothesised that p100/NFκB2 processing to the derivative p52 subunit and nuclear translocation in IECs may result in apoptosis. This was investigated by western blotting for presence of these protein subunits in small intestinal epithelial enriched extracts from mice in 1.5h 10mg/kg PE-LPS treated and untreated WT, *Nfκb1*$^{-/-}$ and *Nfκb2*$^{-/-}$ mice. With the major caveat that this was performed successfully once for n=1 untreated and treated mice from each genotype, and has not been repeated to confirm the result due to time

constraints, this western blot showed a positive band at the expected molecular weight for p52 in the treated lanes for WT and *Nfκb1*$^{-/-}$ mice (Figure 57). These data suggest that there is processing of p100 (although band intensity for this protein was weak) to p52 after 1.5h of LPS treatment. It also supported the hypothesis that p52 dimers may translocate to the nucleus to promote IEC apoptosis and cell shedding.

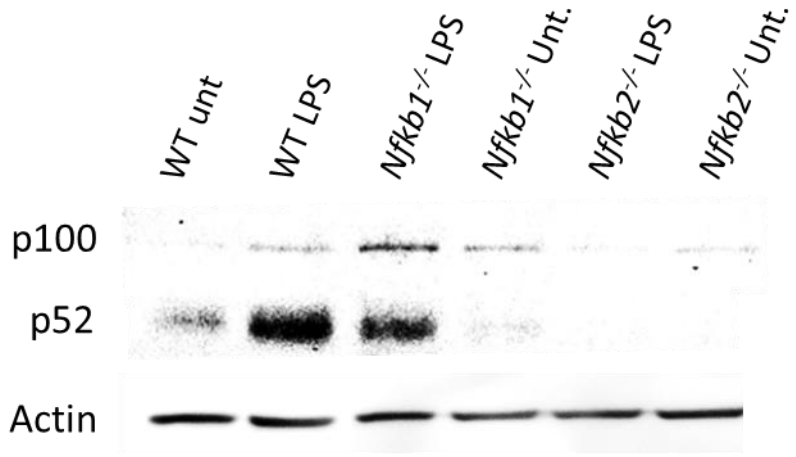

Figure 57: Western blotting demonstrated that there was processing of p100 to p52 in WT and *Nfκb1*$^{-/-}$ mice 1.5h following LPS administration. Unt=untreated. Please note lane order.

5.6 LPS treated *Nfκb2*$^{-/-}$ mice exhibited increased amounts of RelB by western blot

RelB is a member of the NFκB protein family which is the preferred binding partner of p100/p52. To further examine alternative pathway NFκB signalling, western blotting was again utilised to investigate relative protein abundance of RelB in 10mg/kg PE-LPS treated and untreated WT, *Nfκb1*$^{-/-}$ and *Nfκb2*$^{-/-}$ mice in epithelial enriched extracts. This showed the presence of a (double) band at the expected molecular weight for RelB protein of approximately 70kDa in both treated and untreated lanes of all genotypes, but with stronger

bands present in the *Nfκb2*$^{-/-}$ untreated lane, and particularly the treated *Nfκb2*$^{-/-}$ lane (Figure 58). These data suggest that RelB is present within the small intestine to a greater extent in *Nfκb2*$^{-/-}$ mice, and is also present in greater amounts 1.5h following LPS treatment. The inference is therefore that LPS treatment either promotes production of this protein at this site, or cells rich in this protein are infiltrating the intestine in response to LPS treatment.

Again, this is with the major caveat that due to time constraints this blot has been performed once for n=1 and requires repeating for confirmation.

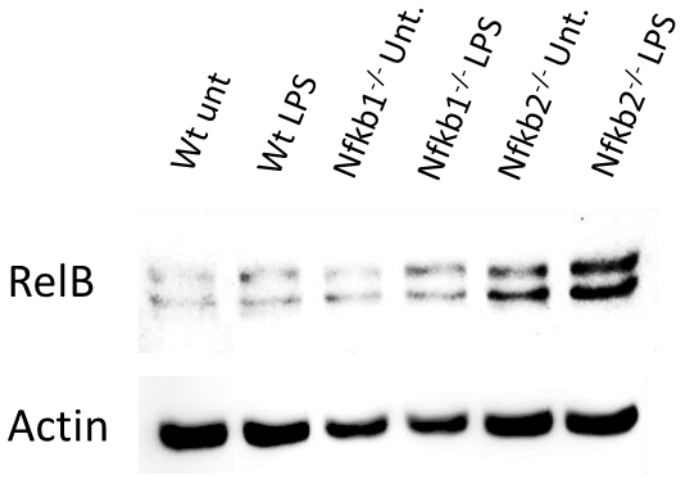

Figure 58: Western blot for RelB protein showing increased abundance in 10mg/kg PE-LPS treated, *Nfκb2*$^{-/-}$ small intestinal epithelial enriched extracts 1.5h after administration.

5.7 Positive RelB immunolabelling was detectable in villus IECs in LPS treated *Nfκb2*$^{-/-}$ mice

To further investigate the role of NFκB2 in LPS-induced IEC apoptosis and shedding, immunohistochemistry for RelB (1:500; SC-226 Santa Cruz Heidelberg, Germany) was performed on formalin fixed paraffin embedded sections of duodenum from 1.5h 10mg/kg PE-LPS treated (n=2 for 1.5h and

untreated) for WT, *Nfκb1*$^{-/-}$, and *Nfκb2*$^{-/-}$ female mice. Immunohistochemistry (performed by Envision™ method as detailed for active caspase-3 IHC), showed positive nuclear labelling of epithelial cells overlying lymphoid tissue (follicular associated epithelium), as has been reported previously (Yilmaz et al. 2003) and also some positive lamina proprial lymphocytes in duodenal sections of all genotypes examined. However, in LPS treated *Nfκb2*$^{-/-}$ mice, positive nuclear immunolabelling of villus IECs was also observed. These mice appeared to exhibit increased labelling along the crypt-villus axis, being particularly prominent in the apical 50% of the villus.

These findings suggest that the increased RelB protein expression detected by western blot, is more specifically correlated with activation of NFκB pathways that involve RelB in villus epithelial cells in *Nfκb2*$^{-/-}$ mice. Since *Nfκb2*$^{-/-}$ mice were shown to be more resistant to LPS-induced IEC apoptosis and cell shedding, this implies that RelB expression could be protective for IECs by preventing apoptosis and cell shedding. The relatively exclusive epithelial labelling again supports that it is the epithelial compartment in which NFκB signalling is critical in determining the fate of the IEC, rather than the immune or vascular compartment.

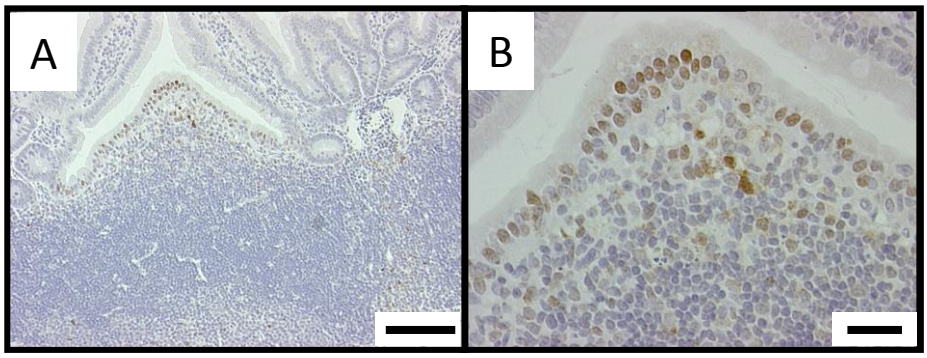

Figure 59: RelB immunohistochemistry in WT untreated mice demonstrated rare nuclear labelling of epithelial cells localised to follicular associated epithelium, and occasional lymphocytes. Bars=100 µm in A) and 25 µm in B).

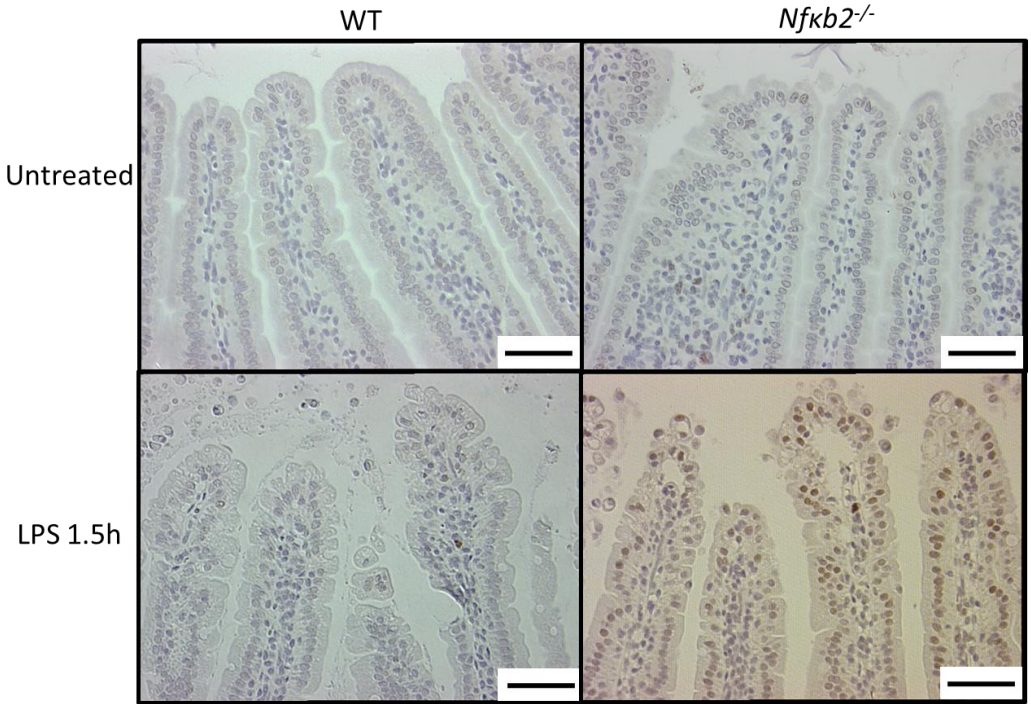

Figure 60: Immunohistochemistry for RelB protein in duodenal sections demonstrated increased nuclear staining in IECs of villus tips in 10mg/kg 1.5h PE-LPS treated *Nfκb2*$^{-/-}$ mice. Bars=50 µm

5.8 Discussion

Data presented in this chapter provide evidence that NFκB signalling plays important roles in regulating pathological small intestinal epithelial cell apoptosis and cell shedding. It was demonstrated that *Nfκb1*$^{-/-}$ mice exhibit greater sensitivity to LPS-induced IEC apoptosis and cell shedding than WT

mice. By contrast, *Nfκb2*$^{-/-}$ mice were more resistant to IEC apoptosis and cell shedding than WT mice. This implies that NFκB subunits differentially regulate pathological IEC apoptosis and cell shedding.

NFκB signalling in response to a diverse range of stimuli, results in increased transcription of hundreds of genes including inflammatory cytokines, and genes regulating apoptosis (www.nf-kb.org (accessed July 2013)). Much of the information regarding the activation of specific NFκB signalling pathways is derived from *in vitro* studies, and appears to conflict according to the cell-line examined. Additional layers of complexity are added to the system by the large number of possible NFκB protein dimer combinations which may be formed, and that oscillatory shuttling of NFκB proteins between the cytoplasm and nucleus is dictated by NFκB transcriptional negative feedback (Nelson et al. 2004). All of this means that any of the mechanisms proposed to account for the findings in this chapter, are therefore likely to represent a gross over-simplification of the vast complexity of NFκB signalling events that lead to pathological IEC apoptosis and cell shedding.

Further confounding this interpretation is the fact that the strains of mice examined in this study, represented whole organism rather than tissue specific transgenic models. Therefore the influence of NFκB signalling in different tissues cannot be easily separated.

However, as it had previously been established that LPS caused IEC apoptosis and cell shedding via TNFR1, it was possible to further clarify the relative sensitivity of *Nfκb1*$^{-/-}$ and *Nfκb2*$^{-/-}$ mice to LPS by administration of

exogenous TNF to these animals. This helped to separate the potential upstream NFκB mediated events in the innate immune cell compartment; such as LPS activation of TLR4 and TNF production in leukocytes, from downstream mechanisms involved in IEC apoptosis and cell shedding. By administering TNF directly, it was possible to theoretically disregard to some extent the differences in innate response to LPS between genotypes.

One possible explanation for the greater sensitivity of *Nfκb1*$^{-/-}$ mice to either LPS or TNF induced IEC apoptosis and cell shedding, is that these mice exhibit higher basal circulating TNF concentrations. The summation of endogenous and exogenous TNF therefore reaches a threshold and precipitates greater IEC apoptosis and cell shedding in this genotype. Indeed it has been shown that in untreated *Nfκb1*$^{-/-}$ mice, there is significantly increased abundance of TNF mRNA in the gastric mucosa (Burkitt et al. 2013). However, this would imply that unstimulated WT mice exhibit higher circulating or tissue TNF concentrations than *Nfκb2*$^{-/-}$ mice; a scenario which seems less plausible.

Alternatively, it could be that pathological IEC apoptosis and cell shedding is not caused directly by exogenously administered recombinant TNF, but that TNF caused rapid gene induction, or signalling pathway activation, and production of endogenous TNF by immune cells and intestinal epithelial cells.

This hypothesis would postulate that it is the failure of *Nfκb1*$^{-/-}$ to regulate exuberant stimulated TNF production, that results in the more severe phenotype observed in these mice. A potential mediator of this mechanism

could be the fact that p50 homodimer formation is necessary to produce TNF-alpha-inhibiting factor (TIF) and down-regulate TNF transcription (Baer et al. 1998). However, it may be that production of epithelial derived TNF is also heavily dependent on co-activation of other signalling pathways. Indeed, unchallenged mice with constitutive IκBα activity in the intestinal epithelium, also produce large amounts of intestinal TNF mRNA, 10-20 fold higher than WT mice (Guma et al. 2011). These mice do not exhibit increased circulating TNF or tissue damage until challenged, but exhibit exquisite sensitivity to low doses of LPS with severe small intestinal crypt apoptosis 4h following treatment. It was found that the transition from high transcriptomic abundance of TNF to epithelial production of TNF in these animals was dependent on additional activation of MAPK and p38 pathways. The authors speculated this was only provided on treatment with LPS or possibly LPS induced TNF. This study also provided some valuable insights into potential mechanisms by which NFκB may influence the fate of the IEC, and clinical outcomes in endotoxic shock. Firstly, the fact that the mice used in this study were epithelial specific transgenics again supports the hypothesis that TNF production and epithelial destruction can be epithelial dictated events, and not caused indirectly by vascular dysfunction. Secondly, these mice also had increased basal F4/80 positive dendritic cell populations and CD3 positive T-cells in the lamina propria, suggesting that constitutive epithelial NFκB activity results in greater recruitment of these cells, which are likely to also be involved in the initial inflammatory response; particularly in the case of dendritic cells. Thirdly, these mice suffered 100% mortality 24h following 5mg/kg LPS from *E.coli* O111:B4, compared to 100% survival in similarly

treated WT mice, demonstrating the importance of epithelial compartment NFκB signalling in preservation of small intestinal epithelial integrity and in dictating the outcome of endotoxic shock.

The key mediator of pathological IEC apoptosis and shedding in response to LPS was shown in the previous chapter to be TNF via interaction with TNFR1 (see 4.7). The sequence of events following TNFR1 ligation has been shown to include the formation of two separate complexes. Complex 1 is rapidly formed by TNFR1, TRADD, RIP, TRAF2, and c-IAP1, and induces the NFκB response. The second complex contains FADD, pro-caspase-10 and pro-caspase-8, and it is this complex that causes apoptosis in the absence of an adequate NFκB response (Micheau and Tschopp 2003). These investigators also showed reduced expression of the anti-apoptotic protein c-FLIP (which prevents caspase-8/caspase-10 interaction) if canonical NFκB signalling from complex 1 is blocked. This results in caspase-8 and caspase-10 interaction, activation and apoptosis. The relationship between TNFR complexes and NFκB signalling is therefore highly complicated and reliant on feedback, as NFκB is itself responsible for transcriptional regulation of anti-apoptotic TRAF2, c-IAP1, and c-FLIP. However, this represents another potential mechanism which may account for the apparent pro-apoptotic phenotype in TNF treated *Nfκb1*$^{-/-}$ mice, where canonical signalling and transcription of these anti-apoptotic proteins is blocked.

Interestingly, another protein involved with the anti-apoptotic response in TNFR signalling that is under transcriptional control of NFκB, is c-IAP2, also known as *Birc3*, the gene for which was found to be +3 fold up-regulated in

LPS-treated WT mice (see 4.5).

One of the unexpected findings to emerge from this study, was data to support a role for activation of the alternative pathway and p52 in pathological IEC apoptosis and shedding. Reports of this pathway being involved in apoptosis are scant in the literature. One study has however shown that a p100 death domain was essential for apoptosis induced by TNFR1 by complexing with this receptor, and mediating caspase-8 activation (Wang et al. 2002). Interestingly, it appeared from western blotting that there was a stronger band present for p100 in LPS treated *Nfκb1*$^{-/-}$ mice; in which there was greater IEC apoptosis than for similarly treated WT mice (Figure 57), perhaps supporting a hypothesis such as this. Activation of this pathway has nonetheless traditionally been associated with lymphocyte development and signalled exclusively by lymphotoxin B (LTβ) CD40L, and B-cell activating factor (BAFF)(Gilmore 2006). It has also been shown to exhibit delayed kinetics compared with canonical NFκB activation (Choudhary et al. 2013). However, it has recently been shown that in TNF stimulated cells, there is negative cross-talk between canonical and non-canonical pathways, with it being possible for RelA to form dimers with RelB. The formation of these dimers prevents RelB DNA binding which may have important implications for the fate of the IEC in our model (reviewed by Sun (2012)). Western blotting performed on epithelial enriched extracts suggested that LPS caused activation of small intestinal p100, and subsequent processing to p52, 1.5h following administration. As RelB is the preferred binding partner of p52, the inference is that p52:RelB dimers probably promote apoptosis in

IECs. A20 may potentially be implicated in acting as a molecular switch that suppresses canonical signalling and initiates non-canonical NFκB signalling through stabilisation of NFκB initiating kinase (NIK) (Yamaguchi et al. 2013).

Western blotting also showed increased small intestinal RelB expression in *Nfκb2*$^{-/-}$ mice, which was particularly increased 1.5h following 10mg/kg PE-LPS. Immunohistochemistry additionally showed increased nuclear labelling of RelB in villus IECs of LPS treated *Nfκb2*$^{-/-}$ mice. This suggests that RelB may promote survival in villus IECs in response to TNF. RelB is an unusual member of the NFκB protein family, in that it is reported to only be capable of forming heterodimers (www.nf-kb.org (accessed July 2013)). The formation of RelA:RelB heterodimers, preventing RelB DNA binding, or potentially the formation of RelB:p50 dimers may potentially prevent apoptosis, and/or reduce TNF production in IECs. Indeed, it has been shown that embryonic fibroblasts from *Relb*$^{-/-}$ mice exhibit dramatically increased TNF production following LPS stimulation (Xia et al. 1999). Moreover, RelB reduced TNF production by stabilising IκBα in this study.

It is however interesting that these results suggest RelB is important in suppressing IEC apoptosis and cell shedding, as generally it is considered that RelA is the critical subunit associated with the survival of IECs. This is because mice specifically lacking RelA in IECs have been found to exhibit profoundly increased IEC apoptosis, dysregulated IEC proliferation, and suffer spontaneous intestinal failure with loss of crypt:villus architecture (Steinbrecher et al. 2008). It has also been shown that nuclear translocation of RelA occurs in villus IECs that resist shedding in a *Cryptosporidium*

parvum model of IEC shedding in piglets (Foster et al. 2012). Additionally, evidence of the importance of canonical NFκB signalling has also been shown in mice specifically lacking IEC IKKα or IKKβ, which exhibit crypt apoptosis in response to either poly I:C (TLR3 agonist) or TNF (McAllister et al. 2013). This prompted the authors of this study to hypothesise that NFκB signalling does not protect villus IECs, but is required to protect crypt IECs. They speculated that this may be due to differing p50 isoforms or homodimer formation along the crypt:villus axis.

Our own studies suggest that p50 is indeed protective in both villus and crypt IECs in response to TNF, as large amounts of crypt IEC apoptosis were observed in p50 deficient *Nfκb1*$^{-/-}$ mice when compared to WT or *Nfκb2*$^{-/-}$ mice. This also suggests that alternative RelA containing dimers cannot rescue the IEC from TNF-induced cell death. The highest frequency of apoptosis in the crypts of *Nfκb1*$^{-/-}$ mice was observed within the crypt base, with maximum between cell position 3 and 5, and appeared to include Paneth cell apoptosis. This perhaps suggests particular sensitivity of stem-cell IECs and Paneth cells lacking canonical NFκB signalling within this compartment, to TNF induced cell death. Although here we demonstrate active caspase-3 dependent apoptosis, necroptosis has been shown in the crypt base in response to TNF in caspase 8 deficient mice, and these mice also lack Paneth cells (Gunther et al. 2011). Our findings may perhaps suggest that NFκB1 may be necessary to prevent a caspase-8 independent form of apoptosis in response to TNF in the crypt base.

Interestingly, in both male and female mice, the greatest villus injury caused

by 10mg/kg PE-LPS was in the *c-Rel*$^{-/-}$ genotype. However, at 0.125mg/kg PE-LPS, there appeared to be divergent sensitivity in male and female mice, with the latter appearing to be more sensitive to LPS induced IEC apoptosis and cell shedding. In another study which investigated the response of female *c-Rel*$^{-/-}$ mice to septic shock (by caecal ligation puncture), it was also found that these mice exhibit increased mortality compared to WT mice (Courtine et al. 2011). In this study *c-Rel*$^{-/-}$ mice exhibited sustained depletion of splenic dendritic cells from 24h following caecal ligation, and in the acute phase of the inflammatory response, exhibited enhanced secretion of inflammatory cytokines including TNF. This study also showed that there was activation of RelA, p50 and c-REL 2h following LPS stimulation *in vitro*, supporting the theory that both canonical and non-canonical pathways are simultaneously activated in response to LPS.

These investigators also performed microarrays in treated *c-REL*$^{-/-}$ mice, and found a failure to up regulate *Bcl-2l11* in *c-Rel*$^{-/-}$ mice compared to WT (consistent with qPCR data in Section 4.5), as up regulation of this gene is associated with “organism survival” in septic shock. The relative sensitivity of *c-Rel*$^{-/-}$ mice suggests that p50:c-REL dimers or RelA:c-REL dimers could also be important in suppressing apoptosis and/or TNF production. What is not clear, is why there was a divergent response in males and females at low dose. However, it has been shown that in mouse splenocytes, 17-β estradiol inhibits the nuclear translocation of RelA/p65, c-Rel, and RelB. The overall affect is thought to up regulate NF-κB signalling, as p50/p50 and p52/p52 may still signal in association with up regulated Bcl3 (Dai et al. 2007). This

could suggest that it is the inhibition of RelA containing dimers that increased susceptibility to IEC apoptosis and cell shedding in *c-Rel*$^{-/-}$ female mice.

6. DISCUSSION

6.1 Summary of Major Findings and Conceptual Advances

The initial aims of this study were to investigate LPS as a potential stimulus for inducing pathological epithelial cell shedding. This phenomenon has been poorly characterised, despite the fact that it probably represents the acute phase of many forms of epithelial injury in the small intestine, which result in villus atrophy. Indeed, the relationships between IEC cell shedding and gut permeability, gut immune defence, and tissue homeostasis, remain poorly understood.

It was demonstrated, that LPS-induced villus IEC apoptosis and cell shedding occurred far earlier and in much greater amounts than the crypt apoptosis which was observed at later time points. The first evidence of IEC apoptosis occurred at approximately 1 hour after LPS administration, was maximal at 1.5h following administration and showed a marked reduction from 3h onwards. LPS administration caused this effect via TLR4 ligation in cells peripheral to the intestinal epithelium, and induced marked intestinal TNF transcription. It was further established that LPS-induced IEC apoptosis and cell shedding were mediated by TNF and TNFR1. These data provided novel insights into the mechanisms of LPS-induced villus IEC apoptosis and cell shedding, as this effect had not previously been exclusively attributed to TNF and TNFR1 in WT mice. NFκB signalling downstream of TNFR was also important in determining the sensitivity of IECs to apoptosis and cell shedding, with NFκB2 (p100/p52) apparently promoting apoptosis and

NFκB1 (p105/p50) and c-REL apparently suppressing apoptosis (summarised in Figure 61).

Preliminary protein analysis data has suggested that p100 is processed to p52 within 1.5h of LPS administration, and that RelB activation may be involved in the resistance of *Nfκb2*$^{-/-}$ mice to LPS-induced small intestinal injury. Apoptosis occurred specifically, and relatively uniformly within different regions of the small intestine at the early time points examined. It was generally observed within the apical 50% of the villus, and occurred in conjunction with villus atrophy. This suggests that small intestinal epithelial cells are the most sensitive cells to LPS-induced apoptosis, and that other factors such as the length of the villus, proximity to lymphoid tissue, and blood flow do not seem to have major influences on this process.

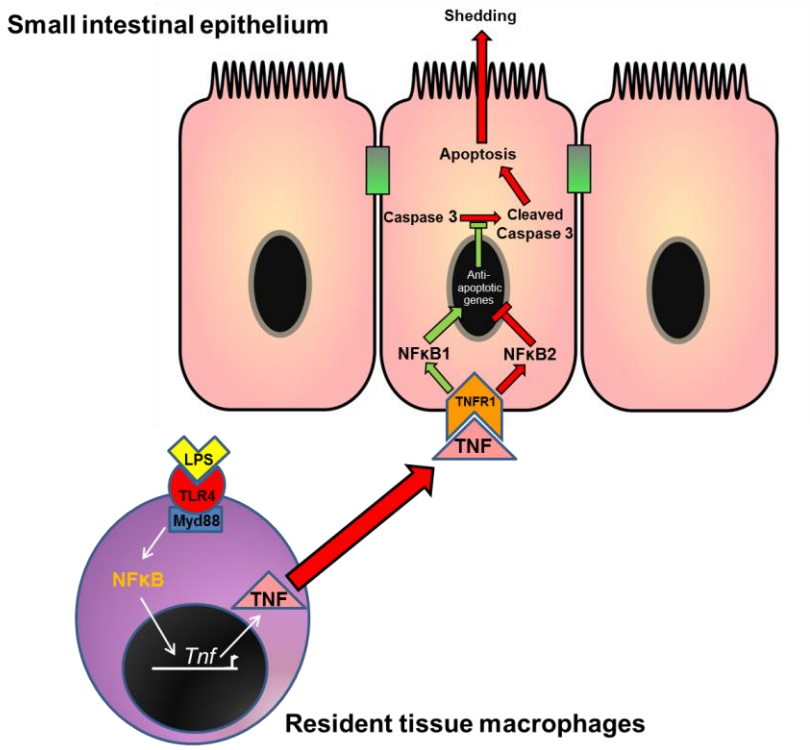

Figure 61: Diagram summarising putative mechanism by which LPS induces apoptosis in IECs. Systemically delivered LPS is first recognised predominantly by resident TLR4 expressing mononuclear cells (such as dendritic cells, macrophages, and monocytes) which produce TNF. TNF is released into the systemic circulation and binds with TNFR1 on intestinal epithelial cells, triggering IEC apoptosis and cell shedding if NFκB2 signalling dominates, or cell survival if NFκB1 (or c-Rel) signalling dominates.

The biological significance of LPS-induced IEC apoptosis and cell shedding was demonstrated by acute onset diarrhoea at 1.5h-2h. This correlated temporally, albeit with a slight time lag, with peak IEC apoptosis and cell shedding in LPS treated mice. Furthermore, resultant villus atrophy was seen, and gut permeability was significantly increased at 5h following LPS administration. These findings provided strong evidence that LPS-induced IEC apoptosis and cell shedding cause serious disturbances in fluid homeostasis within the gastrointestinal tract, and can allow entrance of molecules of at least 4kDa in size through the intestinal barrier at later time

points. The resultant villus atrophy may also lead to malabsorption over a longer time period than examined herein.

6.2 Limitations of the Study

Although mice were ideally suited to this study in terms of recapitulating the morphology of human IEC shedding (Mayhew et al. 1999), there are obvious limitations to utilising a mouse model of a human disease process. Apart from the obvious anatomical differences which exist in the structure and scale of the small intestine in the two species, humans are far more sensitive than mice in terms of their immunological responses to LPS (Copeland et al. 2005). The dosages of LPS that were utilised to induce endotoxic shock in mice were therefore larger than would be expected in a human physiological or pathological context. This has previously led to criticism of the clinical relevance of murine endotoxic shock models in the literature. An alternative model, more specifically of septic shock, would have been that of caecal-ligation puncture. In this model, individual animals are anaesthetised and ligation and puncture of the caecum via laparotomy is performed to induce a polymicrobial peritonitis, followed by recovery. Although more clinically relevant to septic shock, this model would have presented many disadvantages for the current area of study. The need for recovery of the animal and the serious morbidity and pain associated with this procedure would have had a serious negative impact on animal welfare and therefore be considered a severe procedure by the UK Home Office. The logistics would have also been extremely difficult, with confounding issues of serosal inflammation and tissue handling which could also affect the interpretation of

IEC apoptosis and cell shedding.

For the purposes of studying IEC apoptosis and cell shedding, the LPS model was therefore deemed to be more suitable. Ultimately, it was also established that the mediator of this process was TNF, which therefore negates the criticisms of the LPS model to some extent. This is because by utilising LPS (albeit in high doses), to initiate the acute inflammatory response, the resulting endogenous TNF production was within the capabilities and dynamics of the innate immune system. By contrast, the exogenous administration of recombinant TNF as a bolus injection, has the potential to grossly exceed the timescale and magnitude of endogenous pathophysiological TNF production.

Due to economic constraints, the majority of LPS utilised during the course of these experiments was phenol-extracted. This form also contains impurities, most notably bacterial RNA. Although this was the form of LPS commonly utilised in many published studies examining a murine model of endotoxic shock (see Appendix Table 8.1), ideally the highest purity grade of LPS should have been used for all experiments, as impurities could interact with other TLRs or cause other non-TLR mediated effects.

However, further experiments involving administering ion-exchange LPS to both WT and *Tlr4*$^{-/-}$ mice, confirmed that the effect of these impurities did not appreciably alter the findings of the project.

Another issue faced during the course of this project, was that with the exception of the *vil-Cre Myd88*$^{-/-}$ mice, the experimental animals were not

epithelial specific transgenics. This meant that it was not possible to categorically confirm whether the effects we observed were immune or epithelial mediated. Obviously, if epithelial specific transgenics had been available, these would have been preferable, and would be useful for conducting future studies of this phenomenon.

The technique ultimately chosen for quantifying and comparing LPS-induced apoptosis and shedding between genotypes was that of active caspase-3 immunohistochemical scoring. The advantages of this method were that it was relatively easy to interpret, and produced data on IEC apoptosis and shedding on a cell positional basis. However, disadvantages included the slowness of data collection, with it being necessary to count up to 80 cells per hemivillus amounting to up to 1600 cells per intestinal section. Due to time constraints, certain assumptions were therefore made during the course of this study. These assumptions were built upon findings of the time course study, and included the assumption that the duodenum would be representative of apoptosis and cell shedding across the entire small intestine. The duodenum was chosen as the representative segment, as it was also shown to exhibit detectable villus shortening, which could be used as an additional measurement parameter to further support IEC apoptosis and shedding data.

It was also assumed that the same dynamics, (i.e. that peak apoptosis and cell shedding would be observed at 1.5h following LPS administration), would hold true for different dosages and purifications of LPS, and between the

different mouse genotypes tested. This may not necessarily have been the case.

Potentially, after showing that the apoptosis and cell shedding were largely confined to the apical 50% of the villus, it may have been preferable to only count apoptotic/shedding IECs per villus, rather than including “normal” IECs and expressing positively labelled cells as a percentage of the total counted. This would have made for more expedient data collection, and therefore allowed counting of IECs in a greater number of villi, and potentially over more intestinal segments (i.e. jejunum and ileum). Another potential criticism of immunohistochemistry as a quantitative method, is that although most staining can be considered relatively categorically as positive or negative, and that scoring was based on scoring criteria (see Materials and Methods), there were instances where it was necessary to subjectively decide whether a cell was positively or negatively stained, which could potentially lead to variation in scoring. In the context of this study, these decisions were based largely on background staining of adjacent cells. A major weakness of hemivillus scoring, is that it quantifies only apoptotic or shedding IECs confined within the epithelium. Of course, this represents a massive under-representation of the number of apoptotic and shed IECs (see Section 3.3), as a much larger number of cells have been sloughed into the lumen by 1.5h after LPS administration. It was however thought necessary to disregard these cells from the quantification process, as it was considered to introduce greater variability between animals. This included variability in how efficiently the intestine had been flushed with saline prior to fixation, how much digesta

was present within the lumen, and potentially intestinal mucus quality or quantity. The role of intestinal mucus, which may also be important in preservation of the gut barrier during IEC apoptosis and shedding, has also been largely disregarded during this project due to the fixation and examination techniques employed, and may warrant further investigation.

Some studies have approached the problem of quantification of cell shedding differently, and have actually studied the flushed material for apoptotic cells (Piguet et al. 1998). There are therefore some possible alternative methods to traditional light microscopy for quantifying pathological epithelial cell shedding. These would include the analysis of flushed material for shed epithelial cells, potentially by cell counts, or by enzyme linked immunosorbent assay (ELISA) for active caspase-3. However, such methods would involve greater tissue handling and delay in fixation, and although they would potentially provide a better representation of epithelial cells sloughed into the intestinal lumen, they probably would not yield as much information as histopathological assessment. Confocal microscopy has also been advocated as a useful method for imaging IEC apoptosis and cell shedding, with the capability of imaging events over time in individual animals. This method was unfortunately poorly suited to maintaining a single field of view, or allowing quantification of shedding events. It may yet however prove to be a useful technique in the context of imaging mice that express fluorescent tagged proteins, to verify mechanisms underlying IEC apoptosis and cell shedding.

6.3 Translational Impact

With the major caveat that these findings have been made in a mouse model, important concepts derived from this study may be translatable to human pathology. The most direct implication is that IEC apoptosis and cell shedding, as a process, may be an important contributor to the pathogenesis of the acute inflammatory response during endotoxic or septic shock. It may be particularly important with respect to the disturbed fluid and electrolyte homeostasis that manifests as diarrhoea. IEC apoptosis and cell shedding, although studied over a short time course here, could also potentially lead to disturbed tissue homeostasis and gut barrier function in chronicity. Increased IEC shedding has been shown in the chronic disease processes of inflammatory bowel disease (IBD) including Crohn`s disease and ulcerative colitis, and TNF antagonists have been used successfully in the management of these conditions. Indeed, the importance of TNFR1 in initiating IEC apoptosis and cell shedding in this mouse model, potentially suggests that a common mechanism may underly this process in both species. It also suggests that better epithelial targeted prevention of TNFR1 signalling or TNF production, may allow a more focused therapeutic strategy to prevent IEC apoptosis and cell shedding.

Processes including dysregulated inflammatory responses to normal luminal flora, and increased gut permeability, have been heavily implicated in the development of chronic intestinal diseases such as IBD. The finding that increased gut permeability can occur following pathological IEC apoptosis and cell shedding in mice, suggests firstly that this process could lead to

disease, but also that it could initiate a positive feedback loop.

This scenario would mean that epithelial damage could lead to increased gut permeability, which could lead to failure of gut barrier function and exposure of the immune system to gut luminal antigens. This could then promote TNF secretion, further exacerbating pathological IEC apoptosis and cell shedding, leading to chronic inflammation. This also may predispose to bacterial translocation from the gut in acute inflammatory responses, as has been shown in LPS treated mice at later time points (Deitch et al. 1987). Findings from transgenic mice have also provided valuable insights into NFκB regulation of IEC apoptosis in response to TNF, particularly that NFκB2 inhibition could potentially be used to suppress this process.

6.4 Future Investigations

There are many intriguing questions which have been raised during the course of this study which remain unresolved. Although the work outlined herein establishes a robust animal model of IEC apoptosis and cell shedding, detailing the temporally associated diarrhoea and subsequent gut barrier dysfunction, cause and effect have not been definitively established. Although increased IEC shedding has been shown in IBD, it is also not clear whether this is simply an accompanying process of the disease, or whether it initiates or contributes to disease progression.

Some important questions that therefore remain include:

- Does excessive IEC apoptosis and cell shedding lead directly to increased intestinal permeability?

- Does the epithelium itself regulate this process?
- Can IEC apoptosis and cell shedding lead directly to development of chronic intestinal disease?
- Can bacteria exploit gaps in the epithelium *in vivo*, and how quickly can they do this?
- How can the process of IEC apoptosis and cell shedding be suppressed?
- Does blocking this process prevent intestinal/systemic disease?
- Does IEC apoptosis and cell shedding occur in acute disease in humans?

The first question which is currently unanswered is whether IEC apoptosis and shedding are the direct cause of gut barrier dysfunction in this endotoxic shock model. Investigators have implicated various cytokines, chemokines and reactive oxygen species (ROS) in the development of tight junction rearrangement and gut barrier failure in murine endotoxic shock. However, as these studies investigated later time points, the relationship with IEC apoptosis and shedding is not clear. This is a difficult question to address, as an experiment is required where the acute inflammatory response is elicited, but IEC apoptosis and cell shedding is blocked. An interesting possible way of addressing this would be to test gut barrier function in *Tnfr1*$^{-/-}$ mice at 5 hours after LPS administration. These mice should produce many of the cytokines, chemokines and ROS elicited in the inflammatory response, but

should exhibit little or no IEC apoptosis and cell shedding. A more focused experiment would utilise a *vil-Cre Tnfr1*$^{-/-}$ knockout mouse which would give even greater specificity to the blocking of purely epithelial events.

It would be fascinating to examine whether the blocking of epithelial TNFR1 preserves gut barrier function in this model, as this would potentially directly demonstrate that the process is orchestrated by the epithelium. However, to the author`s knowledge, these mice are not currently available.

Also yet to be established is whether a single episode of IEC apoptosis and cell shedding is capable of eliciting chronic inflammation of the intestinal tract. We could therefore potentially perform longer term experiments to establish whether full restitution to normal intestinal morphology and function occurs in all mice following LPS administration.

In addition to gut barrier function studies, it could also be tested whether bacteria can exploit gaps in the epithelium, and whether luminal bacteria may undergo translocation via these gaps. Again, this is a difficult question to address experimentally, but could involve testing whether green fluorescent protein (GFP) labelled bacteria administered by oral gavage enter either the blood, or translocate to peripheral organs after LPS administration. This however still does not conclusively demonstrate whether these bacteria exploit small intestinal epithelial gaps. Two other possible approaches would be to image bacterial invasion by *in vivo* confocal microscopy of the intestinal mucosa, or to examine by scanning electron microscopy the morphology of the mucosa following cell shedding, and whether bacteria are associated with

mucosal erosions.

With regards to potential suppression of IEC apoptosis and cell shedding, one of the most intriguing findings to emerge from this study was the apparent resistance of *Nfκb2*$^{-/-}$ mice to this process. It would therefore be very interesting to further characterise the mechanism of this resistance. Ideally this would again be tested in a *vil-Cre* epithelial specific knockout of p100/p52. It would then be tempting to test whether protection from IEC apoptosis and cell shedding is conferred to LPS treated WT mice by specific inhibitors of the alternative pathway of NFκB signalling. A potential enzyme of the non-canonical pathway that could be targeted, for which pharmacological inhibition is being developed (Li et al. 2013), is NFκB inducing kinase (NIK). Another interesting finding warranting further investigation was the enhanced crypt apoptosis induced by TNF in *Nfκb1*$^{-/-}$ mice. This suggests that NFκB is also important in determining the survival of crypt epithelial cells in the context of high TNF concentrations. Further experiments should firstly aim to address whether differences in TNF production underlie these variations between genotypes. Potentially, the role of the MAPK pathway in translating TNF transcription into TNF production could also be tested by administration of MAPK inhibitors. It would also be interesting to compare gene expression arrays between small intestinal epithelial extracts from untreated and treated NFκB transgenic strains, particularly to elucidate the genetic basis of the resistance of *Nfκb2*$^{-/-}$ mice to LPS.

Finally, efforts to establish by confocal endomicroscopy whether IEC shedding occurs in acute human diseases, such as acute pancreatitis, are

on-going. However, due to the very nature of the acute inflammatory diseases where this process might occur, justifying supplementary invasive investigations such as this without establishing the direct relevance to disease progression is difficult.

6.5 Conclusions

This project has studied in detail the very early time course of villus IEC apoptosis and cell shedding in response to systemic LPS administration. It has established a robust and reproducible animal model for the study of this phenomenon. It has refined the time course to be studied in mouse models of endotoxic shock for investigators interested in examining small intestinal apoptosis, and has provided the basic underlying mechanism. Intriguingly, despite the highly complex acute inflammatory response induced by LPS, and the many mediators implicated in gut barrier failure in endotoxic shock, it was TNF which was shown to be the critical mediator of this process. This additionally implies that any acute inflammatory response which elicits a threshold concentration of TNF in mice, is likely to cause this affect in the small intestine, and may therefore initiate the clinical manifestation of diarrhoea. This may also be true of humans, and could result from many different TLR agonists or acute infections that trigger inflammatory responses that include a threshold concentration of TNF.

In summary, the establishment of this mouse model is important not only because IEC shedding in this species reflects the morphology of shedding observed in humans, but also because of the vast number of transgenic mice which may be utilised to examine the regulation of this process further. It will

also now be possible to test potential new therapeutic interventions in this murine model. These interventions may in the future be applicable to the management of human diseases.

7. BIBLIOGRAPHY

Abremski, K. and R. Hoess (1984). "Bacteriophage P1 site-specific recombination. Purification and properties of the Cre recombinase protein." Journal of Biological Chemistry 259(3): 1509-1514.

Abreu, M. T. (2010). "Toll-like receptor signalling in the intestinal epithelium: how bacterial recognition shapes intestinal function." Nat Rev Immunol 10(2): 131-144.

Adams, J. K. and B. L. Tepperman (2001). "Colonic production and expression of IL-4, IL-6, and IL-10 in neonatal suckling rats after LPS challenge." Am J Physiol Gastrointest Liver Physiol 280(4): G755-762.

Alscher, K. T., P. T. Phang, T. E. McDonald and K. R. Walley (2001). "Enteral feeding decreases gut apoptosis, permeability, and lung inflammation during murine endotoxemia." AJP - Gastrointestinal and Liver Physiology 281(2): G569-576.

Angus, D. C., W. T. Linde-Zwirble, J. Lidicker, G. Clermont, J. Carcillo and M. R. Pinsky (2001). "Epidemiology of severe sepsis in the United States: analysis of incidence, outcome, and associated costs of care." Crit Care Med 29(7): 1303-1310.

Ao, J. E., L. H. Kuang, Y. Zhou, R. Zhao and C. M. Yang (2012). "Hypoxia-inducible factor 1 regulated ARC expression mediated hypoxia induced inactivation of the intrinsic death pathway in p53 deficient human colon cancer cells." Biochem Biophys Res Commun 420(4): 913-917.

Aoyama, M., J. Kotani and M. Usami (2009). "Gender difference in granulocyte dynamics and apoptosis and the role of IL-18 during endotoxin-induced systemic inflammation." Shock 32(4): 401-409.

Araki, A., T. Kanai, T. Ishikura, S. Makita, K. Uraushihara, R. Iiyama, T. Totsuka, K. Takeda, S. Akira and M. Watanabe (2005). "MyD88-deficient mice develop severe intestinal inflammation in dextran sodium sulfate colitis." J Gastroenterol 40(1): 16-23.

Arrieta, M. C., K. Madsen, J. Doyle and J. Meddings (2009). "Reducing small intestinal permeability attenuates colitis in the IL10 gene-deficient mouse." Gut 58(1): 41-48.

Atsumi, S., A. Matsumine, H. Toyoda, R. Niimi, T. Iino and A. Sudo (2013). "Prognostic significance of CD155 mRNA expression in soft tissue sarcomas." Oncol Lett 5(6): 1771-1776.

Backhed, F., H. Ding, T. Wang, L. V. Hooper, G. Y. Koh, A. Nagy, C. F. Semenkovich and J. I. Gordon (2004). "The gut microbiota as an environmental factor that regulates fat storage." Proceedings of the National Academy of Sciences of the United States of America 101(44): 15718-15723.

Baer, M., A. Dillner, R. Schwartz, C. Sedon, S. Nedospasov and P. Johnson (1998). "Tumor necrosis factor alpha transcription in macrophages is attenuated by an autocrine factor that preferentially induces NF-kappaB p50." Molecular and cellular biology 18(10): 5678-5689.

Barker, N., J. H. van Es, J. Kuipers, P. Kujala, M. van den Born, M. Cozijnsen, A. Haegebarth, J. Korving, H. Begthel, P. J. Peters and H. Clevers (2007). "Identification of stem cells in small intestine and colon by marker gene Lgr5." Nature 449(7165): 1003-1007.

Beaulieu, J. F. (1992). "Differential expression of the VLA family of integrins along the crypt-villus axis in the human small intestine." Journal of Cell Science 102(3): 427-436.

Berczi, I., K. Baintner Jr and T. Antal (1966). "Comparative assay of endotoxins by oral and parenteral administration." Zentralblatt fur Veterinarmedizin. Reihe B. Journal of veterinary medicine. Series B 13(6): 570-575.

Bergman, S. A. (1999). "Ketamine: review of its pharmacology and its use in pediatric anesthesia." Anesth Prog 46(1): 10-20.

Beutler, B., X. Du and A. Poltorak (2001). "Identification of Toll-like receptor 4 (Tlr4) as the sole conduit for LPS signal transduction: genetic and evolutionary studies." J Endotoxin Res 7(4): 277-280.

Beutler, B. and E. T. Rietschel (2003). "Innate immune sensing and its roots: the story of endotoxin." Nat Rev Immunol 3(2): 169-176.

Bhattacharyya, S., A. Borthakur, P. K. Dudeja and J. K. Tobacman (2010). "Lipopolysaccharide-induced activation of NF-kappaB non-canonical pathway requires BCL10 serine 138 and NIK phosphorylations." Exp Cell Res 316(19): 3317-3327.

Bhattacharyya, S., P. K. Dudeja and J. K. Tobacman (2008). "Lipopolysaccharide activates NF-kappaB by TLR4-Bcl10-dependent and independent pathways in colonic epithelial cells." Am J Physiol Gastrointest Liver Physiol 295(4): G784-790.

Bjerknes, M. and H. Cheng (1999). "Clonal analysis of mouse intestinal epithelial progenitors." Gastroenterology 116(1): 7-14.

Black, R. A., C. T. Rauch, C. J. Kozlosky, J. J. Peschon, J. L. Slack, M. F. Wolfson, B. J. Castner, K. L. Stocking, P. Reddy, S. Srinivasan, N. Nelson, N. Boiani, K. A. Schooley, M. Gerhart, R. Davis, J. N. Fitzner, R. S. Johnson, R. J. Paxton, C. J. March and D. P. Cerretti (1997). "A metalloproteinase disintegrin that releases tumour-necrosis factor-alpha from cells." Nature 385(6618): 729-733.

Brown, C. C., Baker, D. C. and Barker, I. K. (2007). Alimentary System. In M. G. Maxie (Ed.), *Jubb, Kennedy and Palmer`s Pathology of Domestic Animals* (5th ed. Vol 2, pp3-296). Philadelphia: Saunders.

Buchholz, B. M., R. S. Chanthaphavong and A. J. M. Bauer (2009). "Nonhemopoietic Cell TLR4 Signaling Is Critical in Causing Early Lipopolysaccharide-Induced Ileus." The Journal of Immunology 183(10): 6744-6753.

Bullen, T. F., S. Forrest, F. Campbell, A. R. Dodson, M. J. Hershman, D. M. Pritchard, J. R. Turner, M. H. Montrose and A. J. Watson (2006). "Characterization of epithelial cell shedding from human small intestine." Lab Invest 86(10): 1052-1063.

Burkitt, M. D., J. M. Williams, C. A. Duckworth, A. O'Hara, A. Hanedi, A. Varro, J. H. Caamano and D. M. Pritchard (2013). "Signaling mediated by the NF-kappaB sub-units NF-kappaB1, NF-kappaB2 and c-Rel differentially regulate Helicobacter felis-induced gastric carcinogenesis in C57BL/6 mice." Oncogene.

Buwitt-Beckmann, U., H. Heine, K.-H. Wiesmüller, G. Jung, R. Brock, S. Akira and A. J. Ulmer (2006). "TLR1- and TLR6-independent Recognition of Bacterial Lipopeptides." Journal of Biological Chemistry 281(14): 9049-9057.

Caamaño, J. H., C. A. Rizzo, S. K. Durham, D. S. Barton, C. Raventós-Suárez, C. M. Snapper and R. Bravo (1998). "Nuclear Factor (NF)-κB2 (p100/p52) Is Required for Normal Splenic Microarchitecture and B Cell–mediated Immune Responses." The Journal of Experimental Medicine 187(2): 185-196.

Campos, L. C., T. S. Whittam, T. A. Gomes, J. R. Andrade and L. R. Trabulsi (1994). "Escherichia coli serogroup O111 includes several clones of diarrheagenic strains with different virulence properties." Infect. Immun. 62(8): 3282-3288.

Cario, E. (2008). "Barrier-protective function of intestinal epithelial Toll-like receptor 2." Mucosal Immunology 1: S62-S66.

Cario, E. and D. K. Podolsky (2000). "Differential Alteration in Intestinal Epithelial

Cell Expression of Toll-Like Receptor 3 (TLR3) and TLR4 in Inflammatory Bowel Disease." Infection and Immunity 68(12): 7010-7017.

Casellas, F., S. Aguade, B. Soriano, A. Accarino, J. Molero and L. Guarner (1986). "Intestinal Permeability To Tc-99m-Diethylenetriaminopentaacetic Acid In Inflammatory Bowel-Disease." American Journal of Gastroenterology 81(9): 767-770.

Chang, J. X., S. Chen, L. P. Ma, L. Y. Jiang, J. W. Chen, R. M. Chang, L. Q. Wen, W. Wu, Z. P. Jiang and Z. T. Huang (2005). "Functional and morphological changes of the gut barrier during the restitution process after hemorrhagic shock." World J Gastroenterol 11(35): 5485-5491.

Chen, G.-Y., J. Tang, P. Zheng and Y. Liu (2009). "CD24 and Siglec-10 Selectively Repress Tissue Damage-Induced Immune Responses." Science 323(5922): 1722-1725.

Chen, L. W., W. J. Chang, P. H. Chen, W. C. Liu and C. M. Hsu (2008). "Tlr Ligand Decreases Mesenteric Ischemia and Reperfusion Injury-Induced Gut Damage through Tnf-Alpha Signaling." Shock 30(5): 563-570.

Cheville, N. F. (1994). Ultrastructural pathology: an introduction to interpretation. Ames, Iowa State University Press.

Choudhary, S., M. Kalita, L. Fang, K. V. Patel, B. Tian, Y. Zhao, C. B. Edeh and A. R. Brasier (2013). "Inducible tumor necrosis factor (TNF) receptor-associated factor-1 expression couples the canonical to the non-canonical NF-kappaB pathway in TNF stimulation." J Biol Chem 288(20): 14612-14623.

Coopersmith, C. M., P. E. Stromberg, C. G. Davis, W. M. Dunne, D. M. Amiot, 2nd, I. E. Karl, R. S. Hotchkiss and T. G. Buchman (2003). "Sepsis from Pseudomonas aeruginosa pneumonia decreases intestinal proliferation and induces gut epithelial cell cycle arrest." Crit Care Med 31(6): 1630-1637.

Coopersmith, C. M., P. E. Stromberg, W. M. Dunne, C. G. Davis, D. M. Amiot, 2nd, T. G. Buchman, I. E. Karl and R. S. Hotchkiss (2002). "Inhibition of intestinal epithelial apoptosis and survival in a murine model of pneumonia-induced sepsis." JAMA 287(13): 1716-1721.

Copeland, S., H. S. Warren, S. F. Lowry, S. E. Calvano and D. Remick (2005). "Acute inflammatory response to endotoxin in mice and humans." Clin Diagn Lab Immunol 12(1): 60-67.

Courtine, E., F. Pene, N. Cagnard, J. Toubiana, C. Fitting, J. Brocheton, C. Rousseau, S. Gerondakis, J.-D. Chiche, F. Ouaaz and J.-P. Mira (2011). "Critical Role of cRel Subunit of NF-kappaB in Sepsis Survival." Infect. Immun. 79(5): 1848-1854.

Croci, T., M. Landi, A. M. Galzin and P. Marini (2003). "Role of cannabinoid CB1 receptors and tumor necrosis factor-alpha in the gut and systemic anti-inflammatory activity of SR 141716 (rimonabant) in rodents." Br J Pharmacol 140(1): 115-122.

Crouser, E. D., M. W. Julian, D. M. Weinstein, R. J. Fahy and J. A. Bauer (2000). "Endotoxin-induced Ileal Mucosal Injury and Nitric Oxide Dysregulation Are Temporally Dissociated." Am. J. Respir. Crit. Care Med. 161(5): 1705-1712.

Dai, R., R. A. Phillips and S. A. Ahmed (2007). "Despite Inhibition of Nuclear Localization of NF-κB p65, c-Rel, and RelB, 17-β Estradiol Up-Regulates NF-κB Signaling in Mouse Splenocytes: The Potential Role of Bcl-3." The Journal of Immunology 179(3): 1776-1783.

de Chambrun, G. P., C. F. Manthey, C. S. McAllister, A. Till, M. F. Kagnoff, P. Desreumaux, D. Stupack, J. Y. Wang and L. Eckmann (2013). "21 Caspase 8 Maintains Epithelial Cell Adhesion and Intestinal Homeostasis In Vivo Through Regulation of Clathrin-Dependent Endocytosis and Autophagy." Gastroenterology 144(5): S-6.

Deitch, E. A., R. Berg and R. Specian (1987). "Endotoxin promotes the translocation of bacteria from the gut." Arch Surg 122(2): 185-190.

Deitch, E. A., R. D. Specian and R. D. Berg (1991). "Endotoxin-induced bacterial translocation and mucosal permeability: role of xanthine oxidase, complement activation, and macrophage products." Crit Care Med 19(6): 785-791.

Detmers, P. A., N. Thieblemont, T. Vasselon, R. Pironkova, D. S. Miller and S. D. Wright (1996). "Potential role of membrane internalization and vesicle fusion in adhesion of neutrophils in response to lipopolysaccharide and TNF." Journal of Immunology 157(12): 5589-5596.

Ding, J., D. Song, X. Ye and S. F. Liu (2009). "A Pivotal Role of Endothelial-Specific NF-κB Signaling in the Pathogenesis of Septic Shock and Septic Vascular Dysfunction." The Journal of Immunology 183(6): 4031-4038.

Dolowschiak, T., C. Chassin, S. Ben Mkaddem, T. M. Fuchs, S. Weiss, A. Vandewalle and M. W. Hornef (2010). "Potentiation of Epithelial Innate Host Responses by Intercellular Communication." Plos Pathogens 6(11).

Eberle, F., M. Sirin, M. Binder and A. H. Dalpke (2009). "Bacterial RNA is recognized by different sets of immunoreceptors." European Journal of Immunology 39(9): 2537-2547.

Eckelman, B. P., G. S. Salvesen and F. L. Scott (2006). "Human inhibitor of apoptosis proteins: why XIAP is the black sheep of the family." EMBO Rep 7(10): 988-994.

Eisenhoffer, G. T., P. D. Loftus, M. Yoshigi, H. Otsuna, C.-B. Chien, P. A. Morcos and J. Rosenblatt (2012). "Crowding induces live cell extrusion to maintain homeostatic cell numbers in epithelia." Nature 484(7395): 546-549.

El Marjou, F., K.-P. Janssen, B. Hung-Junn Chang, M. Li, V. Hindie, L. Chan, D. Louvard, P. Chambon, D. Metzger and S. Robine (2004). "Tissue-specific and inducible Cre-mediated recombination in the gut epithelium." genesis 39(3): 186-193.

Elmore, S. (2007). "Apoptosis: a review of programmed cell death." Toxicol Pathol 35(4): 495-516.

Eunok, I., R. Franz Martin, P. Charalabos and R. Sang Hoon (2012). "Elevated lipopolysaccharide in the colon evokes intestinal inflammation, aggravated in immune modulator-impaired mice." American Journal of Physiology-Gastrointestinal and Liver Physiology 303(4): G490-G497.

Ey, B., A. Eyking, G. Gerken, D. K. Podolsky and E. Cario (2009). "TLR2 mediates gap junctional intercellular communication through connexin-43 in intestinal epithelial barrier injury." J Biol Chem 284(33): 22332-22343.

Feinman, R., E. A. Deitch, A. C. Watkins, B. Abungu, I. Colorado, K. B. Kannan, S. U. Sheth, F. J. Caputo, Q. Lu, M. Ramanathan, S. Attan, C. D. Badami, D. Doucet, D. Barlos, M. Bosch-Marce, G. L. Semenza and D.-Z. Xu (2010). "HIF-1 mediates pathogenic inflammatory responses to intestinal ischemia-reperfusion injury." American Journal of Physiology - Gastrointestinal and Liver Physiology 299(4): G833-G843.

Fihn, B. M., A. Sjoqvist and M. Jodal (2000). "Permeability of the rat small intestinal epithelium along the villus-crypt axis: effects of glucose transport." Gastroenterology 119(4): 1029-1036.

Flint, N., F. L. Cove and G. S. Evans (1991). "A Low-Temperature Method for the Isolation of Small-Intestinal Epithelium Along the Crypt-Villus Axis." Biochemical Journal 280: 331-334.

Foster, D. M., S. H. Stauffer, M. R. Stone and J. L. Gookin (2012). "Proteasome Inhibition of Pathologic Shedding of Enterocytes to Defend Barrier Function Requires X-Linked Inhibitor of Apoptosis Protein and Nuclear Factor

kappaB." Gastroenterology.
Fouquet, S., V. H. Lugo-Martinez, A. M. Faussat, F. Renaud, P. Cardot, J. Chambaz, M. Pincon-Raymond and S. Thenet (2004). "Early loss of E-cadherin from cell-cell contacts is involved in the onset of Anoikis in enterocytes." J Biol Chem 279(41): 43061-43069.
Friederich, E., K. Vancompernolle, D. Louvard and J. Vandekerckhove (1999). "Villin Function in the Organization of the Actin Cytoskeleton: Correlation of In Vivo Effects to its Biochemical Activities In Vitro." Journal of Biological Chemistry 274(38): 26751-26760.
Gadjeva, M., Y. Wang and B. H. Horwitz (2007). "NF-κB p50 and p65 subunits control intestinal homeostasis." European Journal of Immunology 37(9): 2509-2517.
Garlanda, C., F. Riva, N. Polentarutti, C. Buracchi, M. Sironi, M. De Bortoli, M. Muzio, R. Bergottini, E. Scanziani, A. Vecchi, E. Hirsch and A. Mantovani (2004). "Intestinal inflammation in mice deficient in Tir8, an inhibitory member of the IL-1 receptor family." Proc Natl Acad Sci USA 101(10): 3522-3526.
Garside, P., C. Bunce, R. C. Tomlinson, B. L. Nichols and A. M. Mowat (1993). "Analysis of enteropathy induced by tumour necrosis factor alpha." Cytokine 5(1): 24-30.
Gassler, N., W. Roth, B. Funke, A. Schneider, F. Herzog, J. J. W. Tischendorf, K. Grund, R. Penzel, I. G. Bravo, J. Mariadason, V. Ehemann, J. Sykora, T. L. Haas, H. Walczak, T. Ganten, H. Zentgraf, P. Erb, A. Alonso, F. Autschbach, P. Schirmacher, R. Knüchel and J. Kopitz (2007). "Regulation of Enterocyte Apoptosis by Acyl-CoA Synthetase 5 Splicing." Gastroenterology 133(2): 587-598.
Gatt, M., B. S. Reddy and J. Macfie (2007). "Review article: bacterial translocation in the critically ill – evidence and methods of prevention." Alimentary Pharmacology & Therapeutics 25(7): 741-757.
Ge, Y., Ezzell R. M., and Warren H. S. (2000). "Localization of Endotoxin in the Rat Intestinal Epithelium." The Journal of Infectious Diseases 182(3): 873-881.
Gelberg, H. B. (2007). Alimentary System. In M. D. McGavin and J. F. Zachary (Eds.) *Pathologic Basis of Veterinary Disease* (4th ed. pp301-392). St.Louis: Elsevier Mosby.
Gerbe, F., J. H. van Es, L. Makrini, B. Brulin, G. Mellitzer, S. Robine, B. Romagnolo, N. F. Shroyer, J.-F. Bourgaux, C. Pignodel, H. Clevers and P. Jay (2011). "Distinct ATOH1 and Neurog3 requirements define tuft cells as a new secretory cell type in the intestinal epithelium." The Journal of Cell Biology 192(5): 767-780.
Gilmore, T. D. (2006). "Introduction to NF-kappaB: players, pathways, perspectives." Oncogene 25(51): 6680-6684.
Goldberg, R. F., W. G. Austen, X. Zhang, G. Munene, G. Mostafa, S. Biswas, M. McCormack, K. R. Eberlin, J. T. Nguyen, H. S. Tatlidede, H. S. Warren, S. Narisawa, J. L. Millán and R. A. Hodin (2008). "Intestinal alkaline phosphatase is a gut mucosal defense factor maintained by enteral nutrition." Proceedings of the National Academy of Sciences 105(9): 3551-3556.
Granger, D. N. (1988). "Role of xanthine oxidase and granulocytes in ischemia-reperfusion injury." Am J Physiol 255(6 Pt 2): H1269-1275.
Grossmann, J., K. Walther, M. Artinger, P. Rummele, M. Woenckhaus and J. Scholmerich (2002). "Induction of apoptosis before shedding of human intestinal epithelial cells." Am J Gastroenterol 97(6): 1421.
Guan, Y., A. J. Watson, A. M. Marchiando, E. M. Bradford, L. Shen, J. R. Turner and

M. H. Montrose (2011). "Redistribution of the tight junction protein ZO-1 during physiologic shedding of mouse intestinal epithelial cells." Am J Physiol Cell Physiol.

Guma, M., D. Stepniak, H. Shaked, M. E. Spehlmann, S. Shenouda, H. Cheroutre, I. Vicente-Suarez, L. Eckmann, M. F. Kagnoff and M. Karin (2011). "Constitutive intestinal NF-kappaB does not trigger destructive inflammation unless accompanied by MAPK activation." J Exp Med 208(9): 1889-1900.

Gunther, C., E. Martini, N. Wittkopf, K. Amann, B. Weigmann, H. Neumann, M. J. Waldner, S. M. Hedrick, S. Tenzer, M. F. Neurath and C. Becker (2011). "Caspase-8 regulates TNF-induced epithelial necroptosis and terminal ileitis." Nature 477(7364): 335-339.

Guo, S., R. Al-Sadi, H. M. Said and T. Y. Ma (2013). "Lipopolysaccharide Causes an Increase in Intestinal Tight Junction Permeability in Vitro and in Vivo by Inducing Enterocyte Membrane Expression and Localization of TLR-4 and CD14." The American Journal of Pathology 182(2): 375-387.

Guttman, J. A. and B. B. Finlay (2009). "Tight junctions as targets of infectious agents." Biochimica et Biophysica Acta (BBA) - Biomembranes 1788(4): 832-841.

Haegebarth, A. and H. Clevers (2009). "Wnt signaling, lgr5, and stem cells in the intestine and skin." Am J Pathol 174(3): 715-721.

Hahn, U., D. Schuppan, E. G. Hahn, H. J. Merker and E. O. Riecken (1987). "Intestinal cells produce basement membrane proteins in vitro." Gut 28 Suppl: 143-151.

Haimovitz-Friedman, A., C. Cordon-Cardo, S. Bayoumy, M. Garzotto, M. McLoughlin, R. Gallily, C. K. Edwards, E. H. Schuchman, Z. Fuks and R. Kolesnick (1997). "Lipopolysaccharide Induces Disseminated Endothelial Apoptosis Requiring Ceramide Generation." The Journal of Experimental Medicine 186(11): 1831-1841.

Han, J., C.-Q. Zhong and D.-W. Zhang (2011). "Programmed necrosis: backup to and competitor with apoptosis in the immune system." Nat Immunol 12(12): 1143-1149.

Han, X., M. P. Fink, R. Yang and R. L. Delude (2004). "Increased iNOS Activity is Essential for Intestinal Epithelial Tight Junction Dysfunction in Endotoxemic Mice." Shock 21(3): 261-270.

Harper, M. S., C. Carpenter, D. J. Klocke, G. Carlson, T. Davis and B. Delaney (2011). "E. coli Lipopolysaccharide: Acute oral toxicity study in mice." Food and Chemical Toxicology 49(8): 1770-1772.

Herdt, T. (1997). Gastrointestinal physiology and metabolism. In J. G. Cunningham (Ed.), *Textbook of Veterinary Physiology* (2nd ed. pp263-381). Philadelphia: W.B. Saunders.

Hirotani, T., M. Yamamoto, Y. Kumagai, S. Uematsu, I. Kawase, O. Takeuchi and S. Akira (2005). "Regulation of lipopolysaccharide-inducible genes by MyD88 and Toll/IL-1 domain containing adaptor inducing IFN-β." Biochem Biophys Res Commun 328(2): 383-392.

Hoekstra, M., S. J. A. Korporaal, Z. Li, Y. Zhao, M. van Eck and T. J. C. Van Berkel (2010). "Plasma lipoproteins are required for both basal and stress-induced adrenal glucocorticoid synthesis and protection against endotoxemia in mice." AJP - Endocrinology and Metabolism 299(6):E1038-43

Hornef, M. W., T. Frisan, A. Vandewalle, S. Normark and A. Richter-Dahlfors (2002). "Toll-like Receptor 4 Resides in the Golgi Apparatus and Colocalizes with Internalized Lipopolysaccharide in Intestinal Epithelial Cells." The Journal of Experimental Medicine 195(5): 559-570.

Hoshino, K., O. Takeuchi, T. Kawai, H. Sanjo, T. Ogawa, Y. Takeda, K. Takeda and

S. Akira (1999). "Cutting Edge: Toll-Like Receptor 4 (TLR4)-Deficient Mice Are Hyporesponsive to Lipopolysaccharide: Evidence for TLR4 as the Lps Gene Product." The Journal of Immunology 162(7): 3749-3752.

Huber, N. L., S. R. Bailey, R. M. Schuster, C. K. Ogle, A. B. Lentsch and T. A. Pritts (2010). "Remote Thermal Injury Increases LPS-Induced Intestinal IL-6 Production." Journal of Surgical Research 160(2): 190-195.

Husain, K. D. and C. M. Coopersmith (2003). "Role of intestinal epithelial apoptosis in survival." Curr Opin Crit Care 9(2): 159-163.

Ikeda, H., Y. Suzuki, M. Suzuki, M. Koike, J. Tamura, J. Tong, M. Nomura and G. Itoh (1998). "Apoptosis is a major mode of cell death caused by ischaemia and ischaemia/reperfusion injury to the rat intestinal epithelium." Gut 42(4): 530-537.

Jackson, G. D. F., W. Dai and W. A. Sewell (2000). "Bile mediates intestinal pathology in endotoxemia in rats." Infection and Immunity 68(8): 4714-4719.

Jarry, A., C. Bossard, C. Bou-Hanna, D. Masson, E. Espaze, M. G. Denis and C. L. Laboisse (2008). "Mucosal IL-10 and TGF-β play crucial roles in preventing LPS-driven, IFN-γ–mediated epithelial damage in human colon explants." The Journal of Clinical Investigation 118(3): 1132-1142.

Julian, M. W., S. Bao, D. L. Knoell, R. J. Fahy, G. Shao and E. D. Crouser (2011). "Intestinal epithelium is more susceptible to cytopathic injury and altered permeability than the lung epithelium in the context of acute sepsis." Int J Exp Pathol 92(5): 366-376.

Kaliannan, K., S. R. Hamarneh, K. P. Economopoulos, S. Nasrin Alam, O. Moaven, P. Patel, N. S. Malo, M. Ray, S. M. Abtahi, N. Muhammad, A. Raychowdhury, A. Teshager, M. M. Mohamed, A. K. Moss, R. Ahmed, S. Hakimian, S. Narisawa, J. L. Millan, E. Hohmann, H. S. Warren, A. K. Bhan, M. S. Malo and R. A. Hodin (2013). "Intestinal alkaline phosphatase prevents metabolic syndrome in mice." Proc Natl Acad Sci USA 110(17): 7003-7008.

Kaur, P. and C. S. Potten (1986). "Cell migration velocities in the crypts of the small intestine after cytotoxic insult are not dependent on mitotic activity." Cell Tissue Kinet 19(6): 601-610.

Kaur, P. and C. S. Potten (1986). "Circadian variation in migration velocity in small intestinal epithelium." Cell Tissue Kinet 19(6): 591-599.

Kawai, T. and S. Akira (2011). "Toll-like Receptors and Their Crosstalk with Other Innate Receptors in Infection and Immunity." Immunity 34(5): 637-650.

Kerr, J. F., A. H. Wyllie and A. R. Currie (1972). "Apoptosis: a basic biological phenomenon with wide-ranging implications in tissue kinetics." Br J Cancer 26(4): 239-257.

Kerr, J. F. R. (1971). "Shrinkage necrosis: A distinct mode of cellular death." The Journal of Pathology 105(1): 13-20.

Kiesslich, R., C. A. Duckworth, D. Moussata, A. Gloeckner, L. G. Lim, M. Goetz, D. M. Pritchard, P. R. Galle, M. F. Neurath and A. J. Watson (2012). "Local barrier dysfunction identified by confocal laser endomicroscopy predicts relapse in inflammatory bowel disease." Gut 61(8): 1146-1153.

Kiesslich, R., M. Goetz, E. M. Angus, Q. Hu, Y. Guan, C. Potten, T. Allen, M. F. Neurath, N. F. Shroyer, M. H. Montrose and A. J. Watson (2007). "Identification of epithelial gaps in human small and large intestine by confocal endomicroscopy." Gastroenterology 133(6): 1769-1778.

Kim, J. Y., M. Morgan, D. G. Kim, J. Y. Lee, L. Bai, Y. Lin, Z. G. Liu and Y. S. Kim (2011). "TNF alpha-induced noncanonical NF-kappa B activation is attenuated by RIP1 through stabilization of TRAF2." Journal of Cell Science 124(4): 647-656.

Kontgen, F., R. J. Grumont, A. Strasser, D. Metcalf, R. Li, D. Tarlinton and S.

Gerondakis (1995). "Mice lacking the c-rel proto-oncogene exhibit defects in lymphocyte proliferation, humoral immunity, and interleukin-2 expression." Genes Dev 9(16): 1965-1977.

Kontoyiannis, D., M. Pasparakis, T. T. Pizarro, F. Cominelli and G. Kollias (1999). "Impaired On/Off Regulation of TNF Biosynthesis in Mice Lacking TNF AU-Rich Elements: Implications for Joint and Gut-Associated Immunopathologies." Immunity 10(3): 387-398.

Kruzel, M. L., Y. Harari, C.-Y. Chen and G. A. Castro (2000). "Lactoferrin Protects Gut Mucosal Integrity During Endotoxemia Induced by Lipopolysaccharide in Mice." Inflammation 24(1): 33-44.

Kumar, V., A. K. Abbas, N. Fausto, S. L. Robbins and R. S. Cotran (2004) General Pathology. In Robbins and Cotran Pathologic Basis of Disease. Philadelphia:Saunders.

Lai, C. W., T. L. Sun, W. Lo, Z. H. Tang, S. Wu, Y. J. Chang, C. C. Wu, S. C. Yu, C. Y. Dong and L. W. Chen (2013). "Shedding-induced gap formation contributes to gut barrier dysfunction in endotoxemia." J Trauma Acute Care Surg 74(1): 203-213.

Lalles, J. P. (2010). "Intestinal alkaline phosphatase: multiple biological roles in maintenance of intestinal homeostasis and modulation by diet." Nutr Rev 68(6): 323-332.

Lau, K. S., A. M. Juchheim, K. R. Cavaliere, S. R. Philips, D. A. Lauffenburger and K. M. Haigis (2011). "In Vivo Systems Analysis Identifies Spatial and Temporal Aspects of the Modulation of TNF-alpha-induced Apoptosis and Proliferation by MAPKs." Sci. Signal. 4(165): ra16-.

Laubach, V. E., E. G. Shesely, O. Smithies and P. A. Sherman (1995). "Mice lacking inducible nitric oxide synthase are not resistant to lipopolysaccharide-induced death." Proceedings of the National Academy of Sciences 92(23): 10688-10692.

Lavrik, I. N., A. Golks and P. H. Krammer (2005). "Caspases: pharmacological manipulation of cell death." J Clin Invest 115(10): 2665-2672.

Leblond, C. P. and C. E. Stevens (1948). "The constant renewal of the intestinal epithelium in the albino rat." The Anatomical Record 100(3): 357-377.

Lee, J. S. (1977). "Epithelial cell extrusion during fluid transport in canine small intestine." Am J Physiol 232(4): E408-414.

Li, K., L. R. McGee, B. Fisher, A. Sudom, J. Liu, S. M. Rubenstein, M. K. Anwer, T. D. Cushing, Y. Shin, M. Ayres, F. Lee, J. Eksterowicz, P. Faulder, B. Waszkowycz, O. Plotnikova, E. Farrelly, S. H. Xiao, G. Chen and Z. Wang (2013). "Inhibiting NF-kappaB-inducing kinase (NIK): discovery, structure-based design, synthesis, structure-activity relationship, and co-crystal structures." Bioorg Med Chem Lett 23(5): 1238-1244.

Liu, J. J., K. L. Madsen, P. Boulanger, L. A. Dieleman, J. Meddings and R. N. Fedorak (2011). "Mind The Gaps: Confocal Endomicroscopy Showed Increased Density of Small Bowel Epithelial Gaps in Inflammatory Bowel Disease." Journal of Clinical Gastroenterology 45(3): 240-245.

Lobo, S. M., D. De Backer, Q. H. Sun, Z. Tu, G. Dimopoulos, C. Preiser, N. Nagy, B. Vray, V. Vercruy, R. G. G. Terzi and J. L. Vincent (2004). "Gut mucosal damage during endotoxic shock is due to mechanisms other than gut ischemia." Journal of Applied Physiology 96(2): 829-829.

Locksley, R. M., N. Killeen and M. J. Lenardo (2001). "The TNF and TNF Receptor Superfamilies: Integrating Mammalian Biology." Cell 104(4): 487-501.

Mabbott, N. A., D. S. Donaldson, H. Ohno, I. R. Williams and A. Mahajan (2013). "Microfold (M) cells: important immunosurveillance posts in the intestinal epithelium." Mucosal Immunol. 6:666-677

Madara, J. L. (1990). "Maintenance of the macromolecular barrier at cell extrusion sites in intestinal epithelium: physiological rearrangement of tight junctions." J Membr Biol 116(2): 177-184.

Majno, G. and I. Joris (1995). "Apoptosis, Oncosis, And Necrosis - An Overview Of Cell-Death." American Journal of Pathology 146(1): 3-15.

Malo, M. S., S. N. Alam, G. Mostafa, S. J. Zeller, P. V. Johnson, N. Mohammad, K. T. Chen, A. K. Moss, S. Ramasamy, A. Faruqui, S. Hodin, P. S. Malo, F. Ebrahimi, B. Biswas, S. Narisawa, J. L. Millan, H. S. Warren, J. B. Kaplan, C. L. Kitts, E. L. Hohmann and R. A. Hodin (2010). "Intestinal alkaline phosphatase preserves the normal homeostasis of gut microbiota." Gut 59(11): 1476-1484.

Marchiando, A. M., L. Shen, W. V. Graham, K. L. Edelblum, C. A. Duckworth, Y. Guan, M. H. Montrose, J. R. Turner and A. J. Watson (2011). "The Epithelial Barrier Is Maintained by In Vivo Tight Junction Expansion During Pathologic Intestinal Epithelial Shedding." Gastroenterology 140(4):1208-1218.e1-2.

Mari, M., A. Morales, A. Colell, C. Garcia-Ruiz, N. Kaplowitz and J. C. Fernandez-Checa (2013). "Mitochondrial glutathione: features, regulation and role in disease." Biochim Biophys Acta 1830(5): 3317-3328.

Marshall, J. C. (2005). "Lipopolysaccharide: An Endotoxin or an Exogenous Hormone?" Clinical Infectious Diseases 41(Supplement 7): S470-S480.

Mathison, J. C. and R. J. Ulevitch (1979). "The clearance, tissue distribution, and cellular localization of intravenously injected lipopolysaccharide in rabbits." J Immunol 123(5): 2133-2143.

Mayhew, T. M., R. Myklebust, A. Whybrow and R. Jenkins (1999). "Epithelial integrity, cell death and cell loss in mammalian small intestine." Histol Histopathol 14(1): 257-267.

McAllister, C. S., O. Lakhdari, G. Pineton de Chambrun, M. G. Gareau, A. Broquet, G. H. Lee, S. Shenouda, L. Eckmann and M. F. Kagnoff (2013). "TLR3, TRIF, and Caspase 8 Determine Double-Stranded RNA-Induced Epithelial Cell Death and Survival In Vivo." The Journal of Immunology 190(1): 418-427.

McDole, J. R., L. W. Wheeler, K. G. McDonald, B. Wang, V. Konjufca, K. A. Knoop, R. D. Newberry and M. J. Miller (2012). "Goblet cells deliver luminal antigen to CD103+ dendritic cells in the small intestine." Nature 483(7389): 345-349.

Meddings, J. (2008). "What role does intestinal permeability have in IBD pathogenesis?" Inflamm Bowel Dis 14 Suppl 2: S138-139.

Michalek, S. M., R. N. Moore, J. R. McGhee, D. L. Rosenstreich and S. E. Mergenhagen (1980). "The Primary Role of Lymphoreticular Cells in the Mediation of Host Responses to Bacterial Endotoxin." Journal of Infectious Diseases 141(1): 55-63.

Micheau, O. and J. Tschopp (2003). "Induction of TNF Receptor I-Mediated Apoptosis via Two Sequential Signaling Complexes." Cell 114(2): 181-190.

Mitchell, R. N. (2004). Hemodynamic Disorders, Thromboembolic Disease, and Shock. In V. Kumar, A. K. Abbas, and N. Fausto (Eds.) *Robbins and Cotran Pathologic Basis of Disease* (7th ed. pp 119-144). Philadelphia: Saunders.

Miura, S., D. Fukumura, I. Kurose, H. Higuchi, H. Kimura, Y. Tsuzuki, T. Shigematsu, J. Y. Han, M. Tsuchiya and H. Ishii (1996). "Roles of ET-1 in endotoxin-induced microcirculatory disturbance in rat small intestine." American Journal of Physiology - Gastrointestinal and Liver Physiology 271(3): G461-G469.

Mizoguchi, E., A. Mizoguchi, H. Takedatsu, E. Cario, J. De, C. Jin Ooi, R. J. Xavier, C. Terhorst, D. K. Odolsky and A. K. Bhan (2002). "Role of tumor necrosis factor receptor 2 (TNFR2) in colonic epithelial hyperplasia and chronic

intestinal inflammation in mice." Gastroenterology 122(1): 134-144.
Mollen, K. P., S. C. Gribar, R. J. Anand, D. J. Kaczorowski, J. W. Kohler, M. F. Branca, T. D. Dubowski, C. P. Sodhi and D. J. Hackam (2008). "Increased expression and internalization of the endotoxin coreceptor CD14 in enterocytes occur as an early event in the development of experimental necrotizing enterocolitis." Journal of Pediatric Surgery 43(6): 1175-1181.
Moolenbeek, C. and E. J. Ruitenberg (1981). "The "Swiss roll": a simple technique for histological studies of the rodent intestine." Lab Anim 15(1): 57-59.
Moore, R., S. Carlson and J. L. Madara (1989). "Villus contraction aids repair of intestinal epithelium after injury." American Journal of Physiology - Gastrointestinal and Liver Physiology 257(2): G274-G283.
Muglia, C., N. Mercer, M. A. Toscano, M. Schattner, R. Pozner, J. P. Cerliani, R. P. Gobbi, G. A. Rabinovich and G. H. Docena (2011). "The glycan-binding protein galectin-1 controls survival of epithelial cells along the crypt-villus axis of small intestine." Cell Death and Dis: e163.
Myers, R. K. and McGavin, M. D. (2007). Cellular and Tissue Responses to Injury. In M. D. McGavin and J. F. Zachary (Eds.), *Pathologic Basis of Veterinary Disease* (4th ed. pp3-62). St.Louis, Elsevier Mosby.
Nelson, D. E., A. E. Ihekwaba, M. Elliott, J. R. Johnson, C. A. Gibney, B. E. Foreman, G. Nelson, V. See, C. A. Horton, D. G. Spiller, S. W. Edwards, H. P. McDowell, J. F. Unitt, E. Sullivan, R. Grimley, N. Benson, D. Broomhead, D. B. Kell and M. R. White (2004). "Oscillations in NF-kappaB signaling control the dynamics of gene expression." Science 306(5696): 704-708.
O'Connor, L., A. Strasser, L. A. O'Reilly, G. Hausmann, J. M. Adams, S. Cory and D. C. Huang (1998). "Bim: a novel member of the Bcl-2 family that promotes apoptosis." EMBO J 17(2): 384-395.
Oldner, A., M. Goiny, A. Rudehill, U. Ungerstedt and A. Sollevi (1999). "Tissue hypoxanthine reflects gut vulnerability in porcine endotoxin shock." Crit Care Med 27(4): 790-797.
Ortega-Cava, C. F., S. Ishihara, M. A. K. Rumi, K. Kawashima, N. Ishimura, H. Kazumori, J. Udagawa, Y. Kadowaki and Y. Kinoshita (2003). "Strategic Compartmentalization of Toll-Like Receptor 4 in the Mouse Gut." The Journal of Immunology 170(8): 3977-3985.
Pålsson-McDermott, E. M. and L. A. J. O'Neill (2004). "Signal transduction by the lipopolysaccharide receptor, Toll-like receptor-4." Immunology 113(2): 153-162.
Pastores, S. M., D. P. Katz and V. Kvetan (1996). "Splanchnic ischemia and gut mucosal injury in sepsis and the multiple organ dysfunction syndrome." American Journal of Gastroenterology 91(9): 1697-1710.
Pentecost, M., G. Otto, J. A. Theriot and M. R. Amieva (2006). "Listeria monocytogenes invades the epithelial junctions at sites of cell extrusion." PLoS Pathog 2(1): e3.
Perrone, E. E., C. Chen, S. W. Longshore, O. Okezie, B. W. Warner, C.-C. Sun, S. M. Alaish and E. D. Strauch (2010). "Dietary bile acid supplementation improves intestinal integrity and survival in a murine model." Journal of Pediatric Surgery 45(6): 1256-1265.
Peschon, J. J., D. S. Torrance, K. L. Stocking, M. B. Glaccum, C. Otten, C. R. Willis, K. Charrier, P. J. Morrissey, C. B. Ware and K. M. Mohler (1998). "TNF Receptor-Deficient Mice Reveal Divergent Roles for p55 and p75 in Several Models of Inflammation." The Journal of Immunology 160(2): 943-952.
Pfeffer, K., T. Matsuyama, T. M. Kundig, A. Wakeham, K. Kishihara, A. Shahinian, K. Wiegmann, P. S. Ohashi, M. Kronke and T. W. Mak (1993). "Mice deficient for the 55kd tumor necrosis factor receptor are resistant to

endotoxic shock, yet succumb to L. monocytogenes infection." Cell 73(3): 457-467.

Piguet, P. F., C. Vesin, J. Guo, Y. Donati and C. Barazzone (1998). "TNF-induced enterocyte apoptosis in mice is mediated by the TNF receptor 1 and does not require p53." Eur J Immunol 28(11): 3499-3505.

Potten, C. S. (1990). "A comprehensive study of the radiobiological response of the murine (BDF1) small intestine." Int J Radiat Biol 58(6): 925-973.

Ramasamy, S., D. D. Nguyen, M. A. Eston, S. N. Alam, A. K. Moss, F. Ebrahimi, B. Biswas, G. Mostafa, K. T. Chen, K. Kaliannan, H. Yammine, S. Narisawa, J. L. Millan, H. S. Warren, E. L. Hohmann, E. Mizoguchi, H. C. Reinecker, A. K. Bhan, S. B. Snapper, M. S. Malo and R. A. Hodin (2011). "Intestinal alkaline phosphatase has beneficial effects in mouse models of chronic colitis." Inflamm Bowel Dis 17(2): 532-542.

Rodríguez, M., L. Cabal-Hierro, M. T. Carcedo, J. M. Iglesias, N. Artime, B. G. Darnay and P. S. Lazo (2011). "NF-κB Signal Triggering and Termination by Tumor Necrosis Factor Receptor 2." Journal of Biological Chemistry 286(26): 22814-22824.

Rosenblatt, J., M. C. Raff and L. P. Cramer (2001). "An epithelial cell destined for apoptosis signals its neighbors to extrude it by an actin- and myosin-dependent mechanism." Curr Biol 11(23): 1847-1857.

Roulis, M., M. Armaka, M. Manoloukos, M. Apostolaki and G. Kollias (2011). "Intestinal epithelial cells as producers but not targets of chronic TNF suffice to cause murine Crohn-like pathology." Proceedings of the National Academy of Sciences 108(13): 5396-5401.

Royet, J. and R. Dziarski (2007). "Peptidoglycan recognition proteins: pleiotropic sensors and effectors of antimicrobial defences." Nat Rev Microbiol 5(4): 264-277.

Ruemmele, F. M., J. F. Beaulieu, S. Dionne, E. Levy, E. G. Seidman, N. Cerf-Bensussan and M. J. Lentze (2002). "Lipopolysaccharide modulation of normal enterocyte turnover by toll-like receptors is mediated by endogenously produced tumour necrosis factor alpha." Gut 51(6): 842-848.

Sato, T. and H. Clevers (2013). "Growing Self-Organizing Mini-Guts from a Single Intestinal Stem Cell: Mechanism and Applications." Science 340(6137): 1190-1194.

Sato, T., R. G. Vries, H. J. Snippert, M. van de Wetering, N. Barker, D. E. Stange, J. H. van Es, A. Abo, P. Kujala, P. J. Peters and H. Clevers (2009). "Single Lgr5 stem cells build crypt-villus structures in vitro without a mesenchymal niche." Nature 459(7244): 262-265.

Schneider, C. A., W. S. Rasband and K. W. Eliceiri (2012). "NIH Image to ImageJ: 25 years of image analysis." Nat Meth 9(7): 671-675.

Seksik, P., L. Rigottier-Gois, G. Gramet, M. Sutren, P. Pochart, P. Marteau, R. Jian and J. Doré (2003). "Alterations of the dominant faecal bacterial groups in patients with Crohn's disease of the colon." Gut 52(2): 237-242.

Sha, W. C., H.-C. Liou, E. I. Tuomanen and D. Baltimore (1995). "Targeted disruption of the p50 subunit of NF-κB leads to multifocal defects in immune responses." Cell 80(2): 321-330.

Shaker, A. and D. C. Rubin (2010). "Intestinal stem cells and epithelial-mesenchymal interactions in the crypt and stem cell niche." Translational Research 156(3): 180-187.

Shanahan, F. (2002). "The host–microbe interface within the gut." Best Practice & Research Clinical Gastroenterology 16(6): 915-931.

Sherry, B., D. M. Jue, A. Zentella and A. Cerami (1990). "Characterization of high molecular weight glycosylated forms of murine tumor necrosis factor."

Biochem Biophys Res Commun 173(3): 1072-1078.
Shimazu, R., S. Akashi, H. Ogata, Y. Nagai, K. Fukudome, K. Miyake and M. Kimoto (1999). "MD-2, a molecule that confers lipopolysaccharide responsiveness on Toll-like receptor 4." The Journal of Experimental Medicine 189(11): 1777-1782.
Shindo, M., M. Majima, T. Ohno, K. Sugimoto and T. Ohwada (1996). "Induction mechanism of small intestinal lesions caused by intravenous injection of endotoxin in rats." Surgery Today 26(8): 610-617.
Sinclair, M. D. (2003). "A review of the physiological effects of alpha2-agonists related to the clinical use of medetomidine in small animal practice." Can Vet J 44(11): 885-897.
Skidmore, B. J., D. C. Morrison, J. M. Chiller and W. O. Weigle (1975). "Immunologic properties of bacterial lipopolysaccharide (LPS). The unresponsiveness of C3H/HeJ Mouse spleen cells to LPS-induced mitogenesis is dependent on the method used to extract LPS." J Exp Med 142(6): 1488-1508.
Smith, P. D., L. E. Smythies, M. Mosteller-Barnum, D. A. Sibley, M. W. Russell, M. Merger, M. T. Sellers, J. M. Orenstein, T. Shimada, M. F. Graham and H. Kubagawa (2001). "Intestinal Macrophages Lack CD14 and CD89 and Consequently Are Down-Regulated for LPS- and IgA-Mediated Activities." The Journal of Immunology 167(5): 2651-2656.
Sodhi, C., R. Levy, R. Gill, M. D. Neal, W. Richardson, M. Branca, A. Russo, T. Prindle, T. R. Billiar and D. J. Hackam (2011). "DNA attenuates enterocyte Toll-like receptor 4-mediated intestinal mucosal injury after remote trauma." American Journal of Physiology - Gastrointestinal and Liver Physiology 300(5): G862-G873.
Song, H. L., S. Lu and P. Liu (2005). "Tumor necrosis factor-alpha induces apoptosis of enterocytes in mice with fulminant hepatic failure." World J Gastroenterol 11(24): 3701-3709.
Song, J., S. E. Wolf, D. N. Herndon, X. W. Wu and M. G. Jeschke (2008). "Second hit post burn increased proximal gut mucosa epithelial cells damage." Shock 30(2): 184-188.
Steinbrecher, K. A., E. Harmel-Laws, R. Sitcheran and A. S. Baldwin (2008). "Loss of epithelial RelA results in deregulated intestinal proliferative/apoptotic homeostasis and susceptibility to inflammation." J Immunol 180(4): 2588-2599.
Stoney, R. J. and C. G. Cunningham (1993). "Acute Mesenteric Ischemia." Surgery 114(3): 489-490.
Su, L., S. C. Nalle, L. Shen, E. S. Turner, G. Singh, L. A. Breskin, E. A. Khramtsova, G. Khramtsova, P. Y. Tsai, Y. X. Fu, C. Abraham and J. R. Turner (2013). "TNFR2 Activates MLCK-Dependent Tight Junction Dysregulation to Cause Apoptosis-Mediated Barrier Loss and Experimental Colitis." Gastroenterology 145(2): 407-415.
Sun, S.-C. (2012). "The noncanonical NF-κB pathway." Immunological Reviews 246(1): 125-140.
Takahashi, T., M. Kinoshita, S. Shono, Y. Habu, T. Ogura, S. Seki and T. Kazama (2010). "The Effect of Ketamine Anesthesia on the Immune Function of Mice with Postoperative Septicemia." Anesthesia & Analgesia 111(4): 1051-1058.
Tawil, G. S. and S. El-Kholy (1959). "Serological types of Escherichia coli in association with infantile gastroenteritis." J Bacteriol 78(1): 13-17.
Theken, K. N., Y. Deng, M. A. Kannon, T. M. Miller, S. M. Poloyac and C. R. Lee (2010). "Activation of the acute inflammatory response alters cytochrome P450 expression and eicosanoid metabolism." Drug Metab Dispos. 39(1):

22-9
Tobias, P. S., K. Soldau and R. J. Ulevitch (1986). "Isolation of a lipopolysaccharide-binding acute phase reactant from rabbit serum." J Exp Med 164(3): 777-793.
Truett, G. E., P. Heeger, R. L. Mynatt, A. A. Truett, J. A. Walker and M. L. Warman (2000). "Preparation of PCR-quality mouse genomic DNA with hot sodium hydroxide and tris (HotSHOT)." Biotechniques 29(1): 52, 54.
Tuin, A., K. Poelstra, A. de Jager-Krikken, L. Bok, W. Raaben, M. P. Velders and G. Dijkstra (2009). "Role of alkaline phosphatase in colitis in man and rats." Gut 58(3): 379-387.
Vallabhapurapu, S. and M. Karin (2009). "Regulation and function of NF-kappaB transcription factors in the immune system." Annu Rev Immunol 27: 693-733.
Van Amersfoort, E. S., T. J. Van Berkel and J. Kuiper (2003). "Receptors, mediators, and mechanisms involved in bacterial sepsis and septic shock." Clin Microbiol Rev 16(3): 379-414.
Verburg, M., I. B. Renes, H. P. Meijer, J. A. Taminiau, H. A. Buller, A. W. Einerhand and J. Dekker (2000). "Selective sparing of goblet cells and paneth cells in the intestine of methotrexate-treated rats." Am J Physiol Gastrointest Liver Physiol 279(5): G1037-1047.
Vollmar, B. and M. Menger (2011). "Intestinal ischemia/reperfusion: microcirculatory pathology and functional consequences." Langenbeck's Archives of Surgery 396(1): 13-29.
Wagner, R., H. Gabbert and P. Höhn (1979). "The mechanism of epithelial shedding after ischemic damage to the small intestinal mucosa." Virchows Archiv B 30(1): 25-31.
Walton, K. L., L. Holt and R. B. Sartor (2009). "Lipopolysaccharide activates innate immune responses in murine intestinal myofibroblasts through multiple signaling pathways." Am J Physiol Gastrointest Liver Physiol 296(3): G601-611.
Wang, F., F. Wang, Z. Zou, D. Liu, J. Wang and Y. Su (2011). "Active deformation of apoptotic intestinal epithelial cells with adhesion-restricted polarity contributes to apoptotic clearance." Lab Invest 91(3): 462-471.
Wang, Y., H. Cui, A. Schroering, J. L. Ding, W. S. Lane, G. McGill, D. E. Fisher and H.-F. Ding (2002). "NF-kappaB2 p100 is a pro-apoptotic protein with anti-oncogenic function." Nat Cell Biol 4(11): 888-893.
Wang, Y., X. Tang, B. Yu, Y. Gu, Y. Yuan, D. Yao, F. Ding and X. Gu (2012). "Gene network revealed involvements of Birc2, Birc3 and Tnfrsf1a in anti-apoptosis of injured peripheral nerves." PLoS ONE 7(9): e43436.
Watson, A. J., S. Chu, L. Sieck, O. Gerasimenko, T. Bullen, F. Campbell, M. McKenna, T. Rose and M. H. Montrose (2005). "Epithelial barrier function in vivo is sustained despite gaps in epithelial layers." Gastroenterology 129(3): 902-912.
Watson, A. J. M. (2004). "Apoptosis and colorectal cancer." Gut 53(11): 1701-1709.
Watson, J. and R. Riblet (1974). "Genetic Control Of Responses To Bacterial Lipopolysaccharides In Mice: Evidence for a Single Gene that Influences Mitogenic and Immunogenic Respones to Lipopolysaccharides." The Journal of Experimental Medicine 140(5): 1147-1161.
Wright, N. A., J. Carter and M. Irwin (1989). "The measurement of villus cell population size in the mouse small intestine in normal and abnormal states: a comparison of absolute measurements with morphometric estimators in sectioned immersion-fixed material." Cell Tissue Kinet 22(6): 425-450.
Wright, S. D., R. A. Ramos, P. S. Tobias, R. J. Ulevitch and J. C. Mathison (1990). "CD14, a receptor for complexes of lipopolysaccharide (LPS) and LPS

binding protein." Science 249(4975): 1431-1433.
Wu, S., K. J. Rhee, M. Zhang, A. Franco and C. L. Sears (2007). "Bacteroides fragilis toxin stimulates intestinal epithelial cell shedding and gamma-secretase-dependent E-cadherin cleavage." J Cell Sci 120(Pt 11): 1944-1952.
Xia, Y., S. Chen, Y. Wang, N. Mackman, G. Ku, D. Lo and L. Feng (1999). "RelB Modulation of IκBα Stability as a Mechanism of Transcription Suppression of Interleukin-1α (IL-1α), IL-1β, and Tumor Necrosis Factor Alpha in Fibroblasts." Molecular and cellular biology 19(11): 7688-7696.
Xiang, X.-s., Y.-z. Zhao, N. Li, Q.-r. Li and J.-s. Li (2010). "Accumulation of DC in Lamina Propria Induced by FMS-Like Tyrosine Kinase 3 Ligand Aggravates the Intestinal Inflammatory Response During Endotoxemia." Inflammation 33(1): 34-45.
Yamaguchi, N., M. Oyama, H. Kozuka-Hata and J. Inoue (2013). "Involvement of A20 in the molecular switch that activates the non-canonical NF-kappaB pathway." Sci Rep 3: 2568.
Yang, Y., A. M. Wandler, J. H. Postlethwait and K. Guillemin (2012). "Dynamic Evolution of the LPS-Detoxifying Enzyme Intestinal Alkaline Phosphatase in Zebrafish and Other Vertebrates." Front Immunol 3: 314.
Yilmaz, Z. B., D. S. Weih, V. Sivakumar and F. Weih (2003). "RelB is required for Peyer's patch development: differential regulation of p52-RelB by lymphotoxin and TNF." EMBO J 22(1): 121-130.
Young, B., Lowe, J. S., Stevens, A. and Heath, J. W. (2006). In *Wheater's Functional Histology: A Text and Colour Atlas* (5th ed.). Philadelphia: Churchill Livingstone/Elsevier.
Youngner, J. S. (1972). "Bacterial lipopolysaccharide: oral route for interferon production in mice." Infection and Immunity 6(4): 646-647.

8. APPENDICES

8.1 Lipopolysaccharide Administration in Mice

Mouse strain	Gender	LPS type	Manufacturer	Dose	Route	Findings	Reference
C57BL/6	N/A	*Salmonella enterica* serovar Typhimurium	Difco Labs Westphal purified	60-350µg per mouse	IP	Microvascular endothelial apoptosis by 6h and mortality	Haimovitz-Friedman et al. 1997
C57BL/6	Male	*E. coli* O111:B4	Sigma	1mg/kg	IP	Decreased cyp450 and increased HETE by 6h	Theken et al. 2010
$CD14^{-/-}$ C57BL/6	N/A	N/A	Sigma	5mg/kg	IP	Up regulation of IL-6 at 3h and internalisation of CD14+TLR4	Mollen et al. 2008
C57BL/6	Female	*Salmonella minnesota* R595	List Biological Laboratories	50µg/kg	IV	Increased steroidogenesis	Hoekstra et al. 2010
Balb/c	Female	*E. coli* 055:B7	Sigma	60mg/kg	IP	Mortality after 12h	Xiang et al. 2010
C57BL/6	Male	*E. coli* O127:B8	Sigma	1mg/kg	IP	Intestinal apoptosis at 12h	Song et al. 2008
CF-1	Male	N/A	N/A	30mg/kg	IP	85% mortality at 48h. Vacuolation of intestinal epithelium with inflammatory infiltrate at 24h	Kruzel et al. 2000
C57BL/6	N/A	*E. coli* O55:B5	Sigma	60mg/kg	IP	Mortality at 24h	Garlanda et al. 2004
C57BL/6	Male	*E.coli*	N/A	10mg/kg	IP	SR141716 inhibition of TNF	Croci et al. 2003
Siglecg null C57BL/6	Male	*E.coli* 055:B5	Sigma	450µg per mouse	IP	Lethality from 18h	Chen et al. 2009
C57BL/6	Male	*E.coli* 0111:B4	N/A	2mg/kg	IP	Decreased tight junction staining from 6h	Han et al. 2004
CD-1	Male	*E.coli* 0111:B4	N/A	4mg/kg	IP	Intestinal apoptosis at 6h (H&E)	Alscher et al. 2001
C57BL/6	Male	*E.coli* O55:B5	Sigma	10mg/kg	IP	Intestinal apoptosis and villus shortening 24h	Perrone et al. 2010
C57BL/6	Male	*E. coli* 0111:B4	Calbiochem	10mg/kg	IP	Increased intestinal IL6 at 4h	Huber et al. 2010

8.2 Publications, Abstracts and Presentations during the Project

Publications

A Mouse Model of Pathological Small Intestinal Epithelial Cell Apoptosis and Shedding Induced by Systemic Administration of Lipopolysaccharide. Jonathan M. Williams, Carrie A. Duckworth, Alastair J. M. Watson, Mark R. Frey, Jennifer C. Miguel, Michael D. Burkitt, Robert Sutton, Kevin R. Hughes, Lindsay J. Hall, Jorge H Caamaňo, Barry J. Campbell, D. M. Pritchard. Disease Models and Mechanisms. 2013 Sep 12. [Epub ahead of print]. PMID: 24046352

Signaling mediated by the NF-κB sub-units NF-κB1, NF-κB2 and c-Rel differentially regulate Helicobacter felis-induced gastric carcinogenesis in C57BL/6 mice. Burkitt MD, Williams JM, Duckworth CA, O'Hara A, Hanedi A, Varro A, Caamaño JH, Pritchard DM. Oncogene 2013 Aug 26. doi: 10.1038/onc.2013.334. [Epub ahead of print].

Gastric Helicobacter infection induces iron deficiency in the INS-GAS mouse. Thomson MJ, Pritchard DM, Boxall SA, Abuderman AA, Williams JM, Varro A, Crabtree JE. PLoS One. 2012; 7(11):e50194. doi: 10.1371/journal.pone.0050194. Epub 2012 Nov 19.

Presentations and Abstracts

Lipopolysaccharide Induces Small Intestinal Epithelial Cell Apoptosis and Shedding by a TLR4 and TNFR1 Dependent Mechanism, Which Is Regulated by NFκB Signalling. Jonathan M. Williams, Carrie A. Duckworth, Barry J. Campbell, Mark R. Frey, Jennifer C. Miguel, Michael D. Burkitt, Alastair J. Watson, D. M. Pritchard. Gastroenterology 2013; Vol. 144, Issue 5, Supplement 1, Page S-668. Poster presentation at Digestive Disease Week, Conference, Orlando 2013.

Deletion of Specific NFκB Proteins Regulates Susceptibility to Developing Colitis Associated Cancer in C57BL/6 Mice As a Result of Altered Inflammatory and DNA Damage Responses. Abdalla Hanedi, Michael D. Burkitt, Jonathan M. Williams, Carrie A. Duckworth, Jorge Caamaňo, D. M. Pritchard. Gastroenterology 2013 Vol. 144, Issue 5, Supplement 1, Page S-136. Oral presentation at Digestive Disease Week Conference, Orlando 2013.

Pathological Epithelial Cell Shedding in the Small Intestine. Jonathan M. Williams, Carrie A. Duckworth, Mark R. Frey, Jennifer C. Miguel, Michael D. Burkitt, Alastair J. Watson, Jorge H Caamaño, Barry J. Campbell, D. M. Pritchard. Invited talk at The University of East Anglia, 06.11.12

Individual Nuclear Factor-κB Family Members Differentially Regulate Gastric Cytokine Responses to *Helicobacter Felis* Infection Leading to Altered Susceptibility to Developing Gastric Preneoplasia. Michael Burkitt, Jonathan Martin Williams, Andrea Varro, Jorge Caamaňo, D. Mark Pritchard. Poster presentation at United European Gastroenterology Week Conference, Amsterdam 2012.

Lipopolysaccharide induces small intestinal epithelial cell apoptosis and shedding which is regulated by NFκB signalling. JM Williams, CA Duckworth, BJ Campbell, DM Pritchard. Gut 2012;61:A342 doi:10.1136/gutjnl-2012-302514d.111. Poster presentation at Disease Disorders Federation Conference, Liverpool 2012.

Pathological Epithelial Cell Shedding in the Small Intestine. Jonathan M. Williams, Carrie A. Duckworth, Mark R. Frey, Jennifer C. Miguel, Michael D. Burkitt, Alastair J. Watson, Jorge H Caamaño, Barry J. Campbell, D. M. Pritchard. Oral presentation at Centre of Integrative Mammalian Biology Seminar, University of Liverpool 24.02.12.

LPS Induces Intestinal Epithelial Cell Shedding and Apoptosis. Jonathan M. Williams, Carrie Duckworth, Barry Campbell, D. Mark Pritchard. Poster presentation at Mouse Models of Disease - linking *in vivo* observations to pathology endpoints conference, Cambridge 2012.

8.3 A Mouse Model of Pathological Small Intestinal Epithelial Cell Apoptosis and Shedding Induced by Systemic Administration of Lipopolysaccharide.

Jonathan M. Williams, Carrie A. Duckworth, Alastair J. M. Watson, Mark R. Frey, Jennifer C. Miguel, Michael D. Burkitt, Robert Sutton, Kevin R. Hughes, Lindsay J. Hall, Jorge H Caamaňo, Barry J. Campbell, D. M. Pritchard. Disease Models and Mechanisms. 2013 Sep 12. [Epub ahead of print]. PMID: 24046352, doi: 10.1242/dmm.013284

Disease Models & Mechanisms 6, 1388-1399 (2013) doi:10.1242/dmm.013284

A mouse model of pathological small intestinal epithelial cell apoptosis and shedding induced by systemic administration of lipopolysaccharide

Jonathan M. Williams[1], Carrie A. Duckworth[1], Alastair J. M. Watson[2], Mark R. Frey[3], Jennifer C. Miguel[3], Michael D. Burkitt[1], Robert Sutton[4], Kevin R. Hughes[2,5], Lindsay J. Hall[2,5], Jorge H. Caamaño[6], Barry J. Campbell[1] and D. Mark Pritchard[1,*]

SUMMARY

The gut barrier, composed of a single layer of intestinal epithelial cells (IECs) held together by tight junctions, prevents the entrance of harmful microorganisms, antigens and toxins from the gut lumen into the blood. Small intestinal homeostasis is normally maintained by the rate of shedding of senescent enterocytes from the villus tip exactly matching the rate of generation of new cells in the crypt. However, in various localized and systemic inflammatory conditions, intestinal homeostasis can be disturbed as a result of increased IEC shedding. Such pathological IEC shedding can cause transient gaps to develop in the epithelial barrier and result in increased intestinal permeability. Although pathological IEC shedding has been implicated in the pathogenesis of conditions such as inflammatory bowel disease, our understanding of the underlying mechanisms remains limited. We have therefore developed a murine model to study this phenomenon, because IEC shedding in this species is morphologically analogous to humans. IEC shedding was induced by systemic lipopolysaccharide (LPS) administration in wild-type C57BL/6 mice, and in mice deficient in TNF-receptor 1 (*Tnfr1*$^{-/-}$), *Tnfr2* (*Tnfr2*$^{-/-}$), nuclear factor kappa B1 (*Nfκb1*$^{-/-}$) or *Nfκb2* (*Nfκb2*$^{-/-}$). Apoptosis and cell shedding was quantified using immunohistochemistry for active caspase-3, and gut-to-circulation permeability was assessed by measuring plasma fluorescence following fluorescein-isothiocyanate–dextran gavage. LPS, at doses ≥0.125 mg/kg body weight, induced rapid villus IEC apoptosis, with peak cell shedding occurring at 1.5 hours after treatment. This coincided with significant villus shortening, fluid exudation into the gut lumen and diarrhea. A significant increase in gut-to-circulation permeability was observed at 5 hours. TNFR1 was essential for LPS-induced IEC apoptosis and shedding, and the fate of the IECs was also dependent on NFκB, with signaling via NFκB1 favoring cell survival and via NFκB2 favoring apoptosis. This model will enable investigation of the importance and regulation of pathological IEC apoptosis and cell shedding in various diseases.

INTRODUCTION

The gut barrier consists of a single layer of intestinal epithelial cells (IECs) and the tight junctions between them. It allows absorption of nutrients from the intestinal lumen into the circulation, while preventing the entry of injurious microorganisms, toxins and antigens. In the small intestine, IECs are generated in the crypt, migrate up the villus and are shed at the villus tip (Leblond and Stevens, 1948). In mice, which exhibit whole IEC shedding similar to that which occurs in humans (Bullen et al., 2006), ~1400 IECs are estimated to be shed in this way from a single villus tip per day (Potten and Loeffler, 1990). The small intestine therefore has one of the highest cell turnover rates in the body, with an estimated 10^{11} and 2×10^{8} cells being shed per day from the small intestine of humans and mice, respectively (Potten and Loeffler, 1990). During the process of physiological cell shedding, the highly coordinated process of tight junction rearrangement that is required to allow the detachment and release of IECs from the epithelium maintains the gut barrier (Madara, 1990).

In various inflammatory conditions, however, the loss of IECs from the villus exceeds the rate of epithelial generation in the crypt. This process, which we have termed 'pathological IEC shedding' remains poorly understood. Such pathological IEC shedding might represent the earliest intestinal injury in a variety of intestinal diseases and is likely to have important consequences, potentially resulting in gap formation in the epithelium, permeability defects and villus shortening (villus atrophy). Indeed, increased numbers of shedding IECs with corresponding focal permeability defects and epithelial gaps have been observed in inflammatory bowel disease (IBD), including both Crohn's disease (CD) and ulcerative colitis (UC) (Kiesslich et al., 2012; Liu et al., 2011). It has also been shown that individuals at high risk of developing IBD exhibit increased gastrointestinal permeability (Hollander et al., 1986). Similarly, IL-10-deficient mice exhibit increased small intestinal permeability prior to the development of spontaneous colitis. In this animal model, colitis severity can be markedly reduced by administering a specific pharmacological inhibitor that reduces small intestinal permeability by preventing the opening of tight junctions, and is prevented completely by rearing animals in germ-free conditions

[1]Department of Gastroenterology, Institute of Translational Medicine, University of Liverpool, Liverpool, L69 3GE, UK
[2]Norwich Medical School, University of East Anglia, Norwich Research Park, Norwich, NR4 7TJ, UK
[3]Departments of Pediatrics, and Biochemistry and Molecular Biology, The Saban Research Institute at Children's Hospital Los Angeles, University of Southern California, Los Angeles, CA 90027, USA
[4]NIHR Liverpool Pancreas Biomedical Research Unit, 5th Floor UCD Block, Royal Liverpool University Hospital, Daulby Street, Liverpool, L69 3GA, UK
[5]Institute of Food Research, Norwich Research Park, Colney, Norwich, NR4 7UA, UK
[6]School of Immunity and Infection, University of Birmingham, Birmingham, B15 2TT, UK
*Author for correspondence (dmpritch@liverpool.ac.uk)

Received 13 June 2013; Accepted 15 August 2013

TRANSLATIONAL IMPACT

Clinical issue

Epithelial cell loss and defects in the epithelial barrier are common early events in the pathogenesis of acute intestinal or diarrheal diseases as well as chronic intestinal inflammatory disorders, such as Crohn's disease and ulcerative colitis. Increased intestinal epithelial cell (IEC) shedding, which is potentially associated with increased gut permeability, is thought to be a key contributor to these initial injuries. However, the molecular events underlying IEC shedding and disruption of intestinal barrier integrity during inflammatory disease states remain poorly understood. A robust animal model would greatly facilitate in-depth investigation of these processes. Mice exhibit a morphologically analogous form of small intestinal villus epithelial cell shedding to that observed in humans and have the potential to allow important mechanistic insights because of the availability of established transgenic and conditional mutant models.

Results

Utilizing the inflammatory response induced by systemic administration of lipopolysaccharide (LPS) in mice, the authors developed a new model for the investigation of IEC shedding. A threshold dose of ≥0.125 mg LPS/kg body weight delivered by intraperitoneal injection induced rapid and dynamic villus IEC apoptosis and shedding, which peaked at 1.5 hours post-administration. This coincided with significant villus shortening, fluid exudation into the gut and the onset of diarrhea. Activation of caspase-3 occurred concomitantly with IEC shedding in virtually all affected cells, suggesting that apoptosis is triggered within the epithelium prior to cells being shed. By examining the responses to LPS in transgenic mice, the authors showed that TNFR1 is essential for the induction of apoptosis and shedding. Furthermore, the fate of IECs is dependent on NFκB signaling, with signaling by NFκB1 favoring cell survival and signaling via NFκB2 favoring apoptosis.

Implications and future directions

Systemic LPS administration in mice provides an effective and reliable trigger of pathological IEC shedding that parallels that observed in human intestinal diseases. The authors' detailed characterization of affected mice confirms that villus epithelial apoptosis and cell shedding occurs with acute fluid exudation into the gut, leading to diarrhea. Furthermore, they provide evidence that TNFR1 and NFκB2-dominant signaling pathways are important in IEC apoptosis and shedding. By conducting an in-depth investigation of the kinetics, dose response and signaling mechanisms underlying these processes, they have established a novel and robust model that will facilitate further investigation of epithelial gap formation and barrier dysfunction in the inflamed intestinal epithelium. Further studies using this model are likely to provide insights into disease pathogenesis and support the development of more targeted treatments for inflammatory disorders.

(Arrieta et al., 2009). This suggests a crucial link between small intestinal permeability, luminal antigens and the development of chronic colitis.

Although recombinant tumor necrosis factor (TNF) has been previously shown to induce pathological intestinal villus epithelial cell shedding in mice (Kiesslich et al., 2007), the exogenous administration of this cytokine in isolation does not reflect the complexity of the mammalian inflammatory response that is present in most disease states. In addition, the concentrations of exogenous TNF required to induce IEC shedding are higher than found *in vivo*, making such experiments expensive and possibly yielding artefactual results. We have also found TNF to be an inconsistent stimulus of IEC shedding. We therefore sought to find a simple, inexpensive, rapid, reproducible and pathologically relevant stimulus to investigate the process of IEC shedding in detail in an animal model.

Lipopolysaccharide (LPS) is an integral component of Gram-negative bacteria and is a potent activator of the innate immune system. It represents a pathogen-associated molecular pattern (PAMP) recognized by Toll-like receptor 4 (TLR4) (Beutler et al., 2001), which initiates a systemic inflammatory response, with nuclear factor kappa B (NFκB) signaling pathways playing a central role in cell responses downstream of both TLR (Chow et al., 1999) and subsequent cytokine receptor ligation (Jacque et al., 2005). We therefore hypothesized that the mammalian systemic inflammatory response was capable of causing IEC apoptosis and shedding at the villus tip when triggered by LPS, and that this occurred prior to the onset of apoptosis in the crypt.

We have therefore examined in detail the earliest phase of LPS-induced murine gut injury. We demonstrate that intraperitoneally administered LPS is a simple, rapid and consistent stimulus of villus IEC apoptosis and shedding in the murine small intestine and that this occurs several hours prior to the onset of crypt apoptosis. This early response coincides with fluid effusion into the small intestinal lumen and diarrhea. We have subsequently characterized the dose response and the kinetics of this highly dynamic phenomenon. Using knockout mouse models, we have found that TNFR1-mediated signaling is essential for these events, with an NFκB2-dominant response favoring apoptosis. These data provide interesting insights into the control of IEC homeostasis in inflammatory disease, because the NFκB2 pathway has not previously been linked to IEC apoptosis and shedding.

RESULTS

Systemic LPS caused clinical signs and gross pathological changes from 1.5 hours, with fluid exudation into the intestinal lumen

To establish the time-dependent intestinal effects of LPS, we administered 10 mg phenol-extracted LPS (PE-LPS)/kg body weight by intraperitoneal (i.p.) injection to adult female wild-type (WT) mice, and euthanized them after 1, 1.5, 2, 3, 4 and 6 hours. Diarrhea was observed from 1.5-2 hours. At necropsy, there was serosal pallor of the small intestine (Fig. 1A), which exhibited distension with watery yellow fluid. These observations showed that LPS caused acute fluid exudation into the gut lumen with acute onset diarrhea.

LPS caused small intestinal villus IEC loss and shedding from 1.5 hours

We performed histopathological examination of hematoxylin and eosin (H&E)-stained sections to characterize intestinal injury. At 1.5 hours (Fig. 1A) there was marked villus shortening, clubbing and blunting. IECs at the villus tip exhibited variable separation and detachment from neighboring cells, often with a teardrop morphology and an apically positioned nucleus (consistent with cell shedding and apoptosis). Large numbers of shed IECs were present within the lumen. Comparable injury was not observed in the stomach, colon or other organs investigated (supplementary material Fig. S1). These observations suggest that LPS causes rapid and specific small intestinal villus epithelial injury, and that peak shedding correlates with the onset of clinical diarrhea.

LPS caused rapid villus shortening with IEC loss in the duodenum, jejunum and ileum

Because villus shortening is commonly utilized as a measure of small intestinal damage, we measured villus heights after LPS

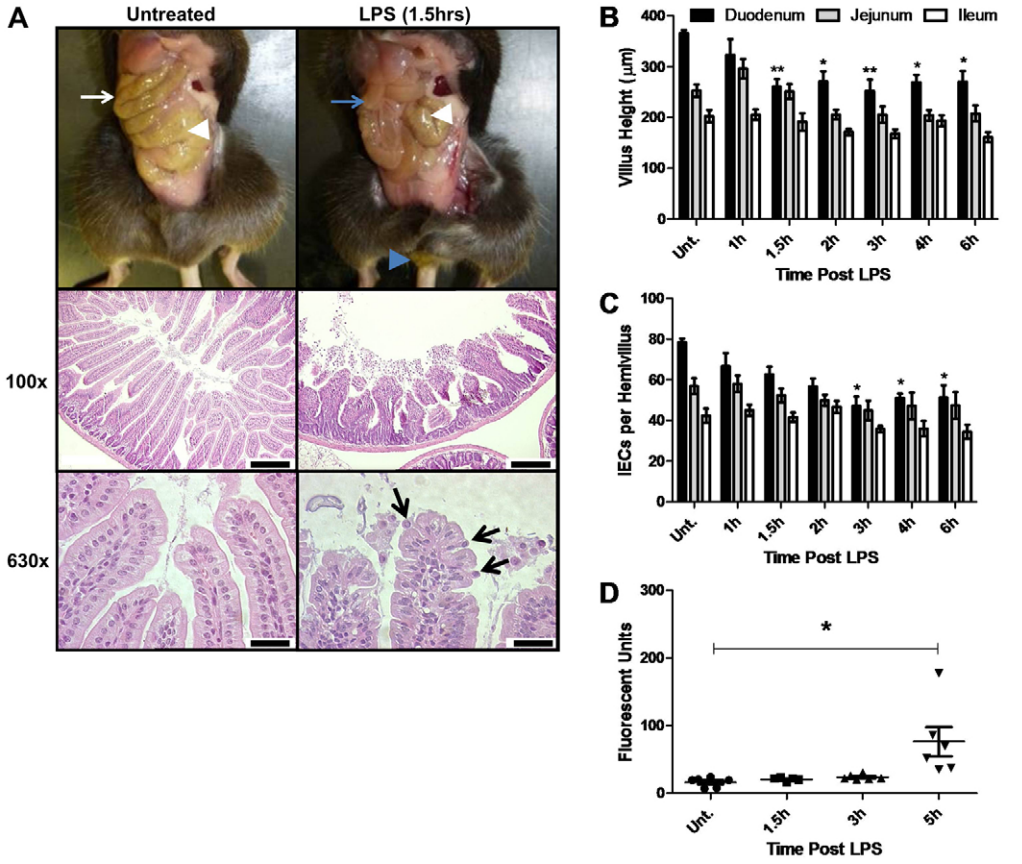

Fig. 1. LPS at 10 mg/kg body weight caused acute diarrhea, villus epithelial cell loss, villus shortening and increased gut permeability. (A) Small intestine of an untreated control (white arrow) and a WT mouse 1.5 hours after LPS treatment exhibiting a fluid-filled small intestine devoid of digesta (blue arrow) with diarrheic feces at anus (blue arrowhead). Caeca are indicated by white arrowheads. H&E-stained sections of duodenum (100×) show normal villi in an untreated control and shortened, blunted and clubbed villi with shed IECs in the lumen at 1.5 hours post-LPS. Scale bars: 200 μm. Villus tips (630×) are shown in an untreated control, and shedding IECs are seen at 1.5 hours post-LPS (arrows). Scale bars: 25 μm. (B) Villus heights for duodenum, jejunum and ileum (n=6). (C) Hemivillus IEC counts from base to apex for duodenum, jejunum and ileum (n=6). (D) Plasma fluorescence measured after 10 mg PE-LPS/kg body weight and gavage of FD4. n=6, one outlier excluded at 1.5 hours. *P<0.05, **P<0.01. Comparisons by ANOVA in A, and Kruskal-Wallis in B-D.

administration. In the duodenum at 1.5 hours after LPS administration, mean villus height was reduced by 29% (Fig. 1B) to 260.5±15.0 μm compared with villi from untreated mice (365.9±6.6 μm) (P<0.01: ANOVA). The reduction in villus height was still evident in treated versus non-treated mice through to 6 hours post-LPS (all P<0.05: ANOVA). A similar trend was also observed in both the jejunum and ileum, but differences did not reach statistical significance.

Villus shortening was associated with lower numbers of IECs lining the duodenal villi, with a 21% reduction in mean cell number observed at 1.5 hours post LPS administration compared with controls (62.7±3.7 versus 78.5±1.8 IECs in untreated mice), reaching significance at 3 hours, at which point a 40% decrease was observed (47.0±4.7 IECs, P<0.05: Kruskal-Wallis) (Fig. 1C). This correlated with large numbers of shed IECs within the intestinal lumen, suggesting that cell shedding occurs contemporaneously with villus shortening.

LPS significantly increased gut-to-circulation permeability by 5 hours

In order to measure gut-to-circulation permeability, mice were administered fluorescein-isothiocyanate-conjugated dextran (FD4) by oral gavage, followed by 10 mg LPS/kg body weight. At 5 hours post-LPS (5 hours FD4), there was a fivefold increase (P<0.05: Kruskal-Wallis) in plasma fluorescence, at 76.3±21.7 fluorescent units (Fig. 1D), compared with untreated mice (16.4±2.9 at 5 hours FD4), suggesting that gut barrier dysfunction allows large molecules to enter the bloodstream at around 5 hours post-LPS.

LPS caused activation of caspase-3 with concomitant apoptosis and shedding of villus IECs, and relatively spared the crypts

To investigate the type of cell death responsible for IEC shedding and loss from the villus, we performed immunohistochemistry (IHC) for active caspase-3. Large numbers of villus IECs exhibited positive immunolabeling as early as 1 hour, with almost universal immunolabeling of shed cells seen within the small intestinal lumen (Fig. 2A). Villus IECs were quantified by microscopy as 'apoptotic' or 'shedding' (as defined in Materials and Methods and summarized in Fig. 2B) and expressed as a percentage of total villus IECs counted.

Maximal active caspase-3 labeling of 12.5±1.7% villus IECs was found in the duodenum 1.5 hours after LPS (Fig. 2C), representing a 21-fold increase compared with untreated mice (0.6±0.2%, P<0.05: Kruskal-Wallis). Comparable IEC apoptosis and cell shedding were also observed at 1.5 hours after LPS treatment in the jejunum and ileum (12.1±2.4% and 11.2±1.3%, respectively). We therefore concluded that LPS caused dynamic villus IEC apoptosis and shedding, and that this occurred relatively uniformly throughout the small intestine. The almost universal positive labeling of IECs undergoing shedding additionally suggests that activation of the terminal pathway of apoptosis occurs prior to shedding in this model, rather than being triggered by detachment as occurs during the process of anoikis. Interestingly, crypt IEC apoptosis as interpreted by active caspase-3 IHC did not show a comparable magnitude of increase to that observed in villi at 1.5 hours (Fig. 2D), although there was an ~threefold increase by 6 hours post-LPS (1.2±0.3% versus

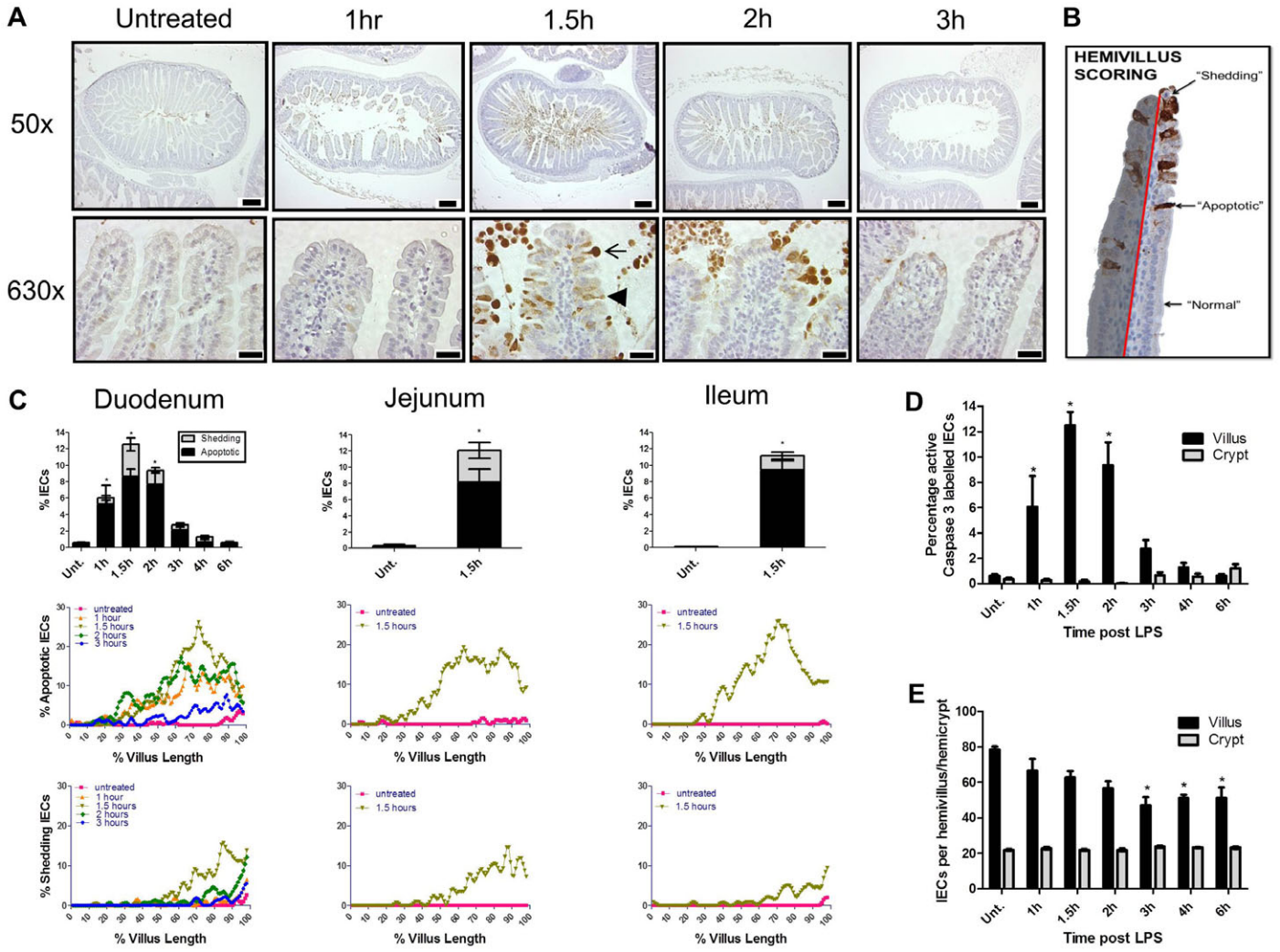

Fig. 2. LPS caused activation of caspase-3 with concomitant apoptosis and shedding of villus IECs, and relatively spared the crypts. (A) Duodenal sections labeled for active caspase-3 by IHC. Arrowhead indicates a positively labeled apoptotic IEC with unaltered morphology, and arrow indicates a positively labeled IEC with shedding morphology. Scale bars: 200 µm (50×), 25 µm (630×). (B) Example of a duodenal villus 1.5 hours following administration of 10 mg PE-LPS/kg body weight to a C57BL/6 female mouse. Individual cells were counted along the epithelial monolayer lining one side of a villus (delineated by red line) from base to tip, and therefore referred to as a 'hemivillus'. Cells were categorized as 'normal', 'apoptotic' or 'shedding'. A total of 18-20 hemivilli were analyzed for each intestinal segment for each individual animal. (C) Quantification of apoptotic and shedding IECs in the duodenum, jejunum and ileum (bar graphs), and cell positional quantification of 'apoptotic' or 'shedding' IECs in the duodenum, jejunum and ileum along villus length (line graphs; 0% villus length represents the villus base, 100% represents the villus tip). (D) Quantification of active-caspase-3-positive cells in villus versus crypt IECs. (E) Villus versus crypt IEC counts. *n*=6 female mice/group; **P*<0.05, comparisons by ANOVA.

0.4±0.1% in untreated). Accordingly, crypt counts did not alter significantly throughout the time course studied (Fig. 2E), in contrast to villus IEC counts.

LPS-induced apoptosis and cell shedding increased towards the villus tip

Administration of LPS (10 mg/kg body weight) increased the number of apoptotic and/or shedding IECs with similar distribution along the villus axis in the duodenum, jejunum and ileum (Fig. 2C). Apoptosis was markedly increased in the apical 50% of the villus, particularly at 1.5 hours, with a sharp increase in IEC shedding being observed at the villus tip, compared with controls.

LPS caused maximal apoptosis and shedding at a threshold dose

We administered 0.125-20 mg PE-LPS/kg body weight to WT mice and euthanized them after 1.5 hours to test whether LPS-induced IEC apoptosis and shedding was dose dependent. LPS at 0.125 mg/kg caused a minimal (5%) reduction in villus height [348.1±17.1 µm versus 399.0±35.5 µm in vehicle-treated control mice (Fig. 3A)] but with a tenfold observed increase in IEC apoptosis and cell shedding at 6.0±1.7% (P<0.05: ANOVA) (Fig. 3B). LPS doses ≥0.25 mg/kg body weight caused ~30% reduction in villus height compared with controls, and IEC apoptosis and cell shedding of ~12%. We concluded that LPS-induced small intestinal injury is initiated by a threshold dose of ~0.125 mg/kg body weight. Villus IECs therefore seem to be extremely sensitive to LPS-induced

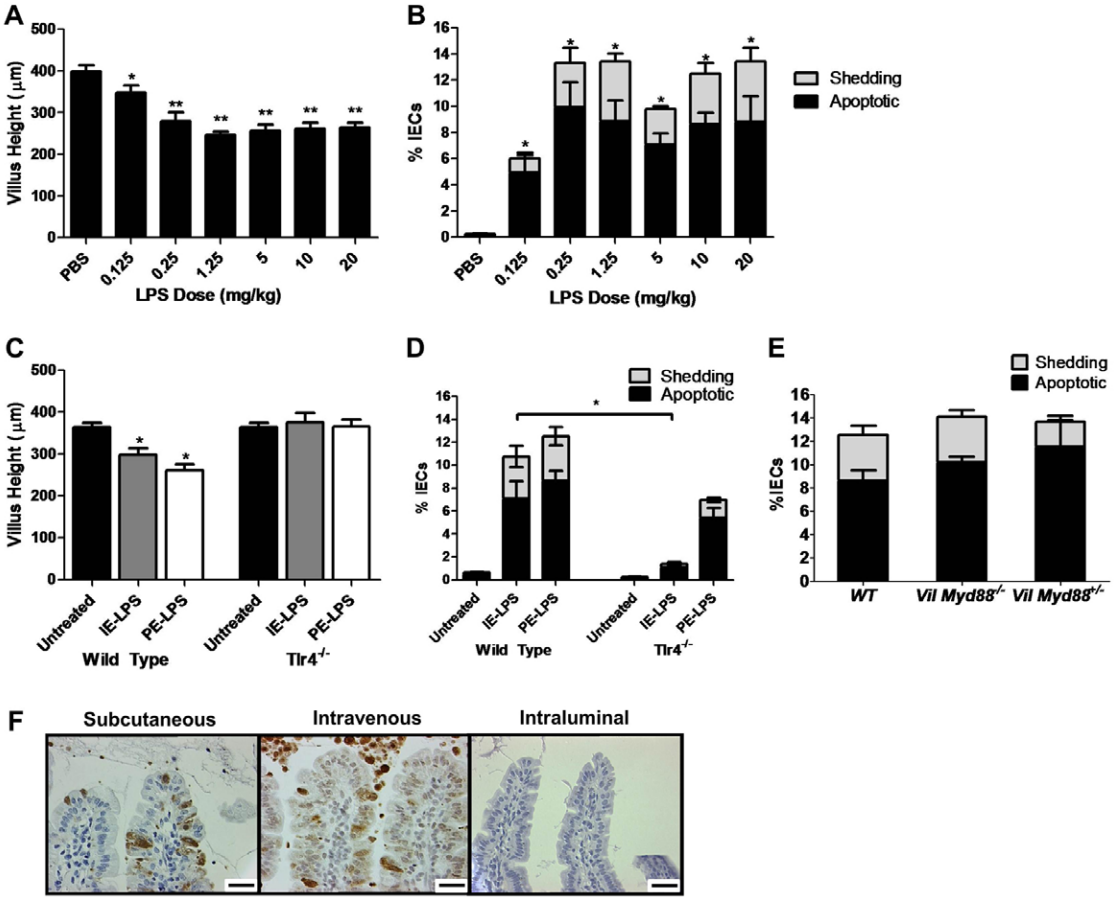

Fig. 3. LPS caused a plateau in apoptosis and shedding at a threshold dose through TLR4 signaling peripheral to epithelial cells. (A) Heights of duodenal villi 1.5 hours after PE-LPS administration at the indicated doses and (B) quantification of percentage apoptotic and shedding IECs by assessment of duodenal sections labeled for active caspase-3 by IHC. *n*=6 female mice/group for PBS, 0.125 mg/kg and 10 mg/kg, and *n*=4 female mice for all other groups. (C) Villus heights in WT or *Tlr4*$^{-/-}$ mice 1.5 hours after PE-LPS or IE-LPS treatment at 10 mg/kg, and (D) quantification of IEC apoptosis and shedding in IHC-labeled duodenal sections (*n*=6). (E) Quantification of apoptotic and shedding IECs in WT (*n*=6), *Vil-Cre Myd88*$^{-/-}$ (*n*=3) and *Vil-Cre Myd88*$^{+/-}$ (*n*=3) mice by assessment of duodenal sections labeled for active caspase-3 by IHC. (F) Small intestinal villi from WT female mice 1.5 hours post-PE-LPS by subcutaneous (s.c.) or intravenous (i.v.) routes exhibited villus IEC apoptosis and shedding, but not when LPS was instilled intraluminally [active caspase-3 IHC, duodenum shown for s.c. and i.v. LPS (*n*=3 per group), ileum shown for intraluminal administration instilled with 1 mg/ml LPS (*n*=4 per group)]. Scale bars: 25 μm. **P*<0.05, ***P*<0.01. Comparisons by ANOVA in A-C, and by Kruskal-Wallis and pairwise comparison of LPS-treated mice only in D.

apoptosis and cell shedding, whereas concomitant villus shortening only occurs at higher dosages of LPS.

LPS purity did not significantly affect IEC apoptosis and shedding

To assess whether the LPS purification and/or extraction method altered IEC apoptosis and shedding, we administered high-purity ion-exchange chromatography extracted LPS (IE-LPS; 10 mg/kg body weight) to WT mice for 1.5 hours. This preparation caused similar villus shortening to 10 mg PE-LPS/kg body weight (298.0±39.1 μm compared with 260.5±36.8 μm, respectively) (Fig. 3C). IEC apoptosis and shedding post IE-LPS administration were also significantly increased (10.8±2.8%) compared with untreated WT, as observed for PE-LPS (12.5±1.7%) (Fig. 3D).

LPS-induced apoptosis and cell shedding was significantly decreased in *Tlr4*$^{-/-}$ mice and was due to TLR ligation peripheral to IECs

Because TLR4 is necessary for the innate immune system to respond to LPS (Beutler et al., 2001), we investigated whether *Tlr4*$^{-/-}$ mice would exhibit LPS-induced small intestinal injury, to exclude the possibility of alternative mechanisms. IE-LPS (10 mg/kg body weight) caused negligible change in villus height in *Tlr4*$^{-/-}$ mice (Fig. 3C) and negligible IEC apoptosis and shedding compared with WT mice (Fig. 3D). However, it should be noted that, when *Tlr4*$^{-/-}$ mice were administered 10 mg PE-LPS/kg body weight, although this resulted in negligible change in villus height compared with untreated *Tlr4*$^{-/-}$ mice (Fig. 3C), moderate IEC apoptosis and shedding of 7.0±1.0% IECs was seen (Fig. 3D). To exclude the possibility that IEC apoptosis and shedding was affected by direct TLR ligation in IECs, we additionally tested the response of *Villin-Cre* (*Vil-Cre*) *Myd88*$^{-/-}$ mice, which lack the TLR signaling adapter molecule Myd88 in IECs, to systemic administration of 10 mg PE-LPS/kg body weight. These mice showed very comparable amounts of apoptosis and shedding (14.1±1.1% IECs) to their WT and heterozygous counterparts (Fig. 3E). Furthermore, we tested the small intestinal response to LPS by alternative routes of administration at 1.5 hours. We found that, although

intraperitoneal, intravenous or subcutaneous LPS administration caused IEC apoptosis and shedding, when LPS was delivered directly into the lumen of a ligated segment of small intestine in terminally anesthetized WT mice, this did not initiate apoptosis and shedding (Fig. 3F).

These results suggest that LPS-induced small intestinal injury is dependent on TLR4 signaling peripheral to IECs and that additional bacterial components in PE-LPS cause IEC shedding via TLR4-independent mechanisms.

Nfκb1$^{-/-}$ mice were more sensitive, and *Nfκb2*$^{-/-}$ mice more resistant, to LPS-induced intestinal injury

NFκB is a major transcriptional regulator downstream of TLR4. We therefore administered PE-LPS to *Nfκb1*$^{-/-}$ and *Nfκb2*$^{-/-}$ mice, to establish whether either of these subunits, integral to the canonical and non-canonical NFκB signaling pathways, respectively, is necessary for LPS-induced small intestinal injury. After administration of 10 mg LPS/kg body weight, similar villus shortening was seen in *Nfκb1*$^{-/-}$ and WT mice (Fig. 4A). This genotype also showed similar IEC apoptosis and shedding to WT mice (Fig. 4B). In contrast, *Nfκb2*$^{-/-}$ mice showed a significantly attenuated 11% villus height reduction in treated versus untreated, compared with 32% in treated versus untreated WT (P<0.05: Kruskal-Wallis) (Fig. 4A), and reduced IEC apoptosis and shedding compared with WT mice (Fig. 4B). Interestingly, when 0.125 mg LPS/kg body weight was administered, *Nfκb1*$^{-/-}$ mice showed greater villus shortening (supplementary material Fig. S2) of 27% in treated versus untreated (P<0.05: Kruskal-Wallis) compared with 5% shortening in treated versus untreated WT mice (Fig. 4A), and significantly greater IEC apoptosis and shedding at 12.9±1.7% IECs (P<0.05: Kruskal-Wallis) (Fig. 4C) compared with WT mice (5.5±1.3%). IEC apoptosis and shedding in *Nfκb2*$^{-/-}$ mice administered 0.125 mg LPS/kg body weight were negligible (0.8±0.2% IECs; P<0.05: Kruskal-Wallis) compared with WT mice. Together, these results suggest that LPS-induced intestinal injury is dependent on NFκB2, whereas NFκB1 might be necessary to suppress IEC apoptosis and shedding.

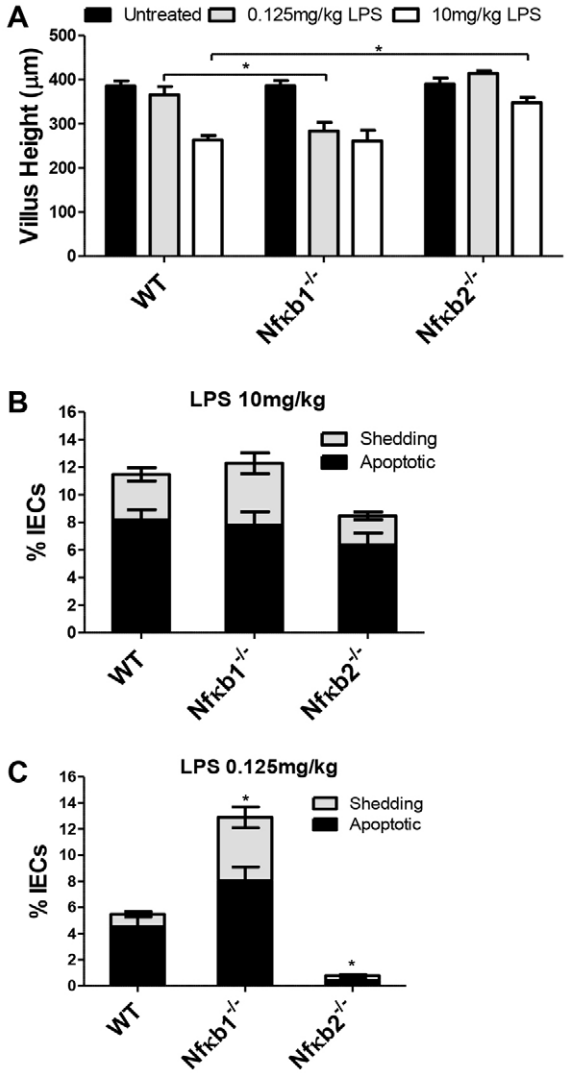

Fig. 4. *Nfκb1*$^{-/-}$ mice were more sensitive, and *Nfκb2*$^{-/-}$ mice more resistant, to LPS-induced small intestinal injury. (A) Villus heights of duodenal villi 1.5 hours after 0.125 mg/kg or 10 mg/kg PE-LPS in WT, *Nfκb1*$^{-/-}$ and *Nfκb2*$^{-/-}$ mice (comparisons between genotypes within same dosage groups only). (B,C) Quantification of apoptotic and shedding IECs in duodenal sections labeled for active caspase-3 in WT, *Nfκb1*$^{-/-}$ and *Nfκb2*$^{-/-}$ mice 1.5 hours after 10 mg/kg PE-LPS (B) and after 0.125 mg/kg PE-LPS (C). n=12-14 (male and female equally represented); *P<0.05, comparisons by Kruskal-Wallis.

LPS induced a significant increase in small intestinal *Tnf* mRNA

Because activation of caspase-3 does not categorically confirm that cell death has occurred by apoptosis, we performed an array analysis of 89 genes associated with various cell death pathways in PE-LPS-treated compared with untreated WT animals. We found that LPS predominantly altered expression of genes associated with apoptosis, rather than those associated with autophagy or necrosis (Fig. 5A). *Tnf* and *Cd40* showed marked upregulation, and we therefore analyzed these two proapoptotic genes by quantitative PCR (qPCR) using triplicate samples from individual animals (Fig. 5B). This showed a mean normalized gene expression ratio of +32.0 for *Tnf* mRNA (P<0.05: randomization test). qPCR also showed a non-significant increase of +2.1 for *Cd40*. These data, in conjunction with histopathological findings and activation of caspase-3, suggest that apoptosis is the predominant form of cell death occurring in LPS-induced small intestinal injury.

TNF caused small intestinal injury equivalent to LPS

Because TNF is a key mediator of endotoxic shock, and was markedly upregulated at the mRNA level in our array, we tested whether TNF would cause comparable enteric injury to LPS. At 1.5 hours, TNF (0.33 mg/kg body weight; i.p.) caused equivalent duodenal villus shortening (Fig. 6A) to that seen with 10 mg PE-LPS/kg body weight (268.4±20.9 μm and 260.5±15.0 μm, respectively). Although less IEC apoptosis and shedding were observed with TNF (7.0±1.0% IECs) compared with 10 mg PE-LPS/kg body weight (12.5±1.7% IECs) (Fig. 6B), this reflects a faster small intestinal response to exogenously administered TNF (supplementary material Fig. S3) than caused by LPS.

These data, together with significant induction of intestinal *Tnf* mRNA, suggest that TNF is central in the pathogenesis of LPS-induced small intestinal injury.

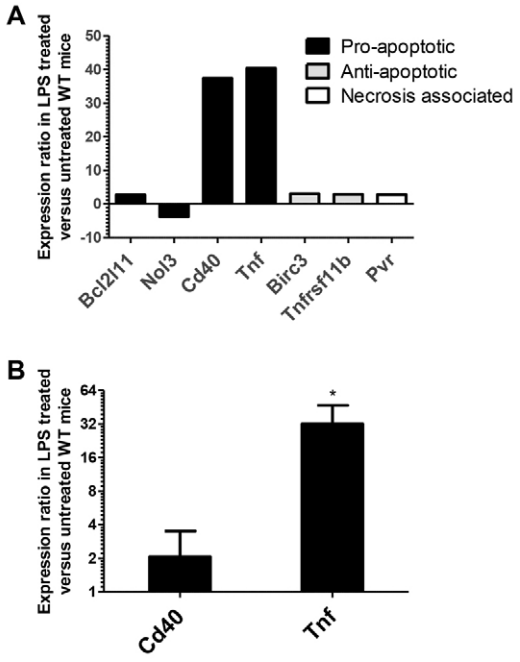

Fig. 5. LPS induced a significant increase in small intestinal *Tnf* mRNA. (A) qPCR array data for selected genes that exhibited a ≥twofold expression ratio out of 89 cell-death-pathway-associated genes assessed in pooled epithelial enriched extracts. (B) Mean gene expression ratio of PE-LPS-treated (10 mg/kg, 1.5 hours) versus untreated WT female mice for *Cd40* and *Tnf*. n=4, *P<0.05: randomization test.

Tnfr1$^{-/-}$ mice were completely resistant to LPS-induced apoptosis and cell shedding

We decided to further examine the role of TNF by testing whether the TNF receptors TNFR1 (p55) or TNFR2 (p75) were required to cause LPS-induced gut injury. When *Tnfr1*$^{-/-}$ mice were administered 10 mg PE-LPS/kg body weight for 1.5 hours, there was no villus shortening (Fig. 6C) and significantly less IEC apoptosis and shedding were seen relative to WT animals (0.1±0.1%, P<0.05: Kruskal-Wallis; Fig. 6D). By contrast, the same dose administered to *Tnfr2*$^{-/-}$ mice caused 68% of the response caused in WT, at 8.5±1.0% IEC apoptosis and shedding, although this did not cause a significant change in villus height (Fig. 6C). These findings suggest that TNFR1 signaling is required to drive LPS-induced IEC apoptosis and shedding, with potential enhancement by TNFR2.

Nfκb1$^{-/-}$ mice were highly sensitive, and *Nfκb2*$^{-/-}$ resistant, to TNF-induced small intestinal injury

NFκB is also a major exponent of downstream TNFR signaling. We therefore administered TNF to *Nfκb1*$^{-/-}$ and *Nfκb2*$^{-/-}$ mice. *Nfκb1*$^{-/-}$ mice were highly sensitive to TNF (supplementary material Fig. S2) and exhibited a significant reduction in villus height compared with TNF-treated WT mice (villus heights of 160.1±7.3 and 268.4±20.9 μm, respectively; P<0.05: ANOVA; Fig. 6E). This correlated with increased IEC apoptosis and shedding in *Nfκb1*$^{-/-}$ versus WT mice (9.9±0.7 and 7.0±1.0% IECs, respectively; P<0.05: ANOVA). Conversely, *Nfκb2*$^{-/-}$ mice were resistant to the TNF-induced reduction in villus height (340.1±15.1 μm) and IEC apoptosis and shedding (2.5±0.7%) compared with similarly treated WT animals (both P<0.05; Fig. 6F).

These data suggest that IEC apoptosis and shedding in response to LPS or TNF are regulated by a common NFκB signaling pathway, being suppressed by NFκB1 but promoted by NFκB2.

DISCUSSION

We present a detailed study of acute LPS-induced murine gut injury. Systemic LPS administration caused rapid IEC apoptosis and shedding in the murine small intestinal villus, and this resulted in shortening of the villus, fluid effusion into the small intestinal lumen and diarrhea.

We have characterized the dose response and kinetics of this highly dynamic phenomenon and demonstrate that it occurs within a tightly defined time period. All regions of the small intestine responded in a similar manner to LPS and in all cases apoptosis and cell shedding occurred in the apical 50% of the villus rather than exclusively at the tip. Using knockout mouse models, we confirmed that TLR4 signaling peripheral to the IEC was required, and that TNFR1-mediated signaling was essential for these events, with an NFκB2-dominant response favoring apoptosis.

Although there is an abundance of literature describing small intestinal crypt apoptosis several hours after the induction of endotoxic or septic shock (Cinel et al., 2002; Coopersmith et al., 2003; Guma et al., 2011), we present novel observations that the villus IECs respond much more rapidly than crypt IECs, and exhibit exquisite susceptibility to apoptosis and cell shedding in the earliest phases following LPS administration. The only other study to date that has examined small intestinal villus epithelial shedding in response to LPS studied this response from 5.5 hours post-LPS-administration by *in vivo* confocal microscopy, correlating gap formation with gut barrier dysfunction (Lai et al., 2013). This highlights the necessity of a detailed study of the kinetics of this response because, in our model, we found that the number of shedding events was profoundly reduced by 4 hours after LPS administration and the maximum response was observed as early as 1.5 hours. We found that, although multiple organ failure in the context of endotoxic shock has been extensively investigated, most commonly by biochemical parameters, obvious organ injury in terms of apoptosis was confined to the small intestine at the early time points examined herein. The reasons underlying this selective early injury to the villus IECs of the murine small intestine are not entirely clear. However, this phenomenon has been attributed to the greater sensitivity of the intestinal epithelium to mitochondrial damage than epithelia found in other commonly injured organ systems such as the lung. Interestingly, in the feline septic shock model in which this was demonstrated, other obvious hemodynamic derangements to which this effect might have been attributed, such as hypotension, intestinal hypoperfusion and hypoxia, were shown not to be responsible (Julian et al., 2011). Additionally, in our own studies, this small intestinal injury occurred by 1.5 hours not only when LPS was administered intraperitoneally, but also when given intravenously or subcutaneously, suggesting that this injury is not due to a localized phenomenon.

Clinically, we found that the onset of diarrhea correlated temporally with IEC apoptosis and shedding. This suggests that the shedding of IECs permits the net movement of fluid from the plasma into the intestinal lumen. This might be directly due to the rapid and uncoordinated shedding of IECs, potentially in

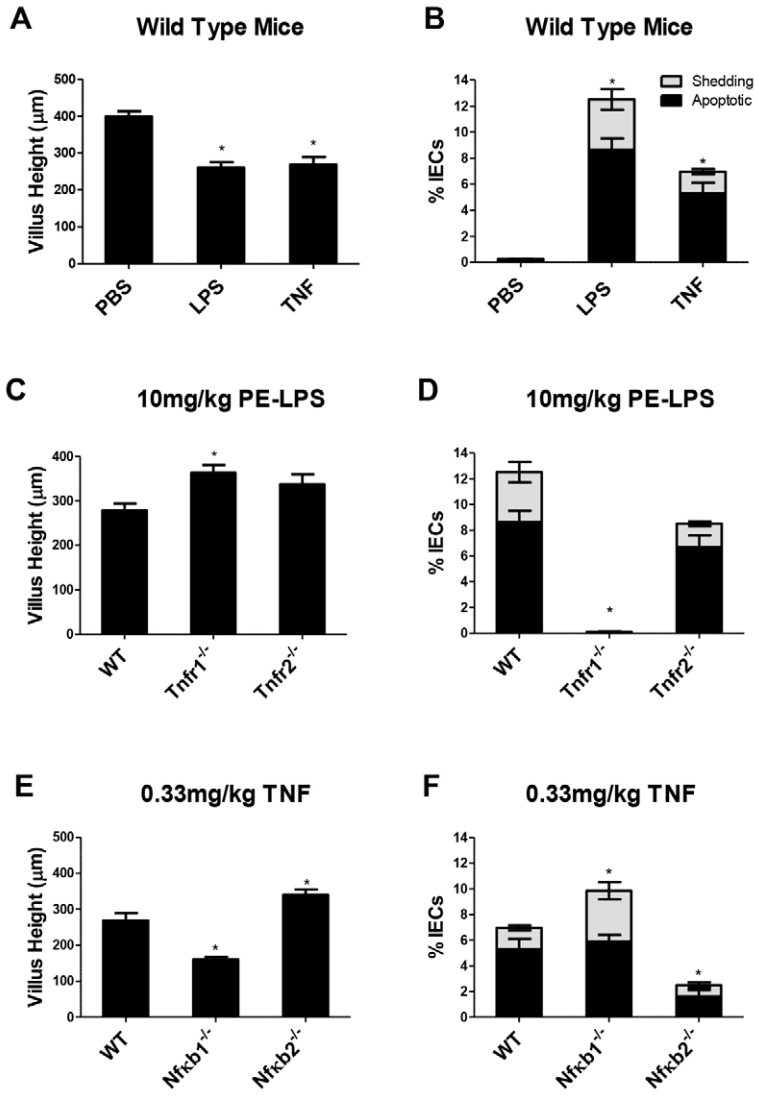

Fig. 6. LPS induced small intestinal IEC apoptosis and shedding via TNF and TNFR1, and was regulated by NFκB. Villus heights and IEC apoptosis and shedding 1.5 hours after 10 mg/kg PE-LPS or 0.33 mg/kg TNF in WT mice (A,B), after 10 mg/kg PE-LPS in WT, *Tnfr1*$^{-/-}$ and *Tnfr2*$^{-/-}$ mice (C,D), and after TNF administration in WT, *Nfκb1*$^{-/-}$ and *Nfκb2*$^{-/-}$ mice (E,F). *P<0.05; n=4-6 mice per group; comparisons by ANOVA, except in D (Kruskal-Wallis).

conjunction with increased vascular permeability, which causes disruption of both tight junctions and the paracellular space. Our own studies have previously shown that barrier loss in the intestine occurs at sites of excessive cell shedding (Kiesslich et al., 2012), and that the direction of fluid movement through epithelial defects is highly dependent on the osmotic and hydrostatic gradients across the epithelium. The concept of acute fluid exudation into the intestinal lumen after the administration of inflammatory stimuli has also been recognized in other studies utilizing LPS or TNF (Gadjeva et al., 2007; Kiesslich et al., 2012). It was not until 5 hours after LPS administration, however, that we found movement of larger molecules (FD4) from the lumen to the plasma. This is in agreement with findings from *in vivo* confocal microscopy that, from 5.5 hours after LPS administration, FD4 entered cell-free gaps and paracellular spaces (Lai et al., 2013).

In our model, a high-purity preparation of LPS caused villus IEC apoptosis and shedding through a TLR4-dependent mechanism, but PE-LPS of lower purity was capable of inducing a moderate response via TLR4-independent mechanisms, most likely due to ligation of alternative TLRs by residual impurities such as bacterial RNA. In support of other PAMPs causing this type of response, another recent study has demonstrated that the apoptosis in the intestinal villus by the viral PAMP, double-stranded RNA, occurred via TLR3 (McAllister et al., 2013). TLR3, in contrast to other TLRs, signals exclusively via the TRIF pathway rather than the Myd88 pathway (Kawai and Akira, 2011). As such, this agonist represents an unusual type of inflammatory response. It caused apoptosis by a TRIF-dependent and TNF-independent mechanism, which peaked at 2 hours post-administration, possibly reflecting delayed activation of the TRIF pathway compared with the Myd88 pathway (Pålsson-McDermott and O'Neill, 2004).

Most previous studies have found only low-level expression of TLR4 in IECs (Abreu, 2010). Therefore, rather than occurring in IECs themselves, initial recognition of systemically delivered LPS likely occurs via TLR4 ligation in monocytes and macrophages, which in turn rapidly secrete cytokines, including TNF (Beutler et al., 1985). To confirm this mechanism in our model, we administered LPS by i.p. injection to *Vil-Cre Myd88*$^{-/-}$ mice that specifically lacked intestinal TLR signal transduction (Fig. 3E). They showed comparable IEC apoptosis and shedding to their

heterozygous counterparts and WT mice of the same strain, demonstrating that peripheral TLR signaling is required for LPS-induced small intestinal injury.

LPS signaling is additionally dependent on delivery of LPS to the cell membrane in a bioactive form by lipopolysaccharide binding protein (LBP) and the adapter molecules CD14 (Wright et al., 1990) and MD-2 (Shimazu et al., 1999). TLR4 signaling might also therefore be fundamentally different in IECs, preventing what would be constant stimulation by the luminal Gram-negative bacterial population. Indeed, in cell culture of m-ICcl2 murine IECs, TLR4 was found to reside within the Golgi apparatus, rather than at the cell membrane (Hornef et al., 2002). In our studies, we found that LPS (1 mg/ml) instilled directly into the lumen of a ligated segment of small intestine for 1.5 hours did not cause apoptosis and cell shedding. Similarly, double-stranded RNA has failed to elicit apoptosis and shedding when administered orally (McAllister et al., 2013).

The rapid increase in plasma TNF concentration after LPS administration has been previously characterized (Copeland et al., 2005). In the current study, we also demonstrated a large fold change in *Tnf* mRNA abundance in small intestinal epithelial enriched extracts 1.5 hours after LPS administration. The significance of TNF as the crucial mediator in our model was further demonstrated by the fact that TNF administration caused very comparable IEC apoptosis and shedding as did LPS, consistent with previous results (Garside et al., 1993; Piguet et al., 1998). In the intestinal epithelium, and in intestinal cell lines, TNFR1 is expressed to a greater extent than TNFR2 (Lau et al., 2011; Mizoguchi et al., 2002), although the latter can be induced by inflammatory cytokines (Mizoguchi et al., 2002). TNFR1 has well-defined proapoptotic effects (Locksley et al., 2001) and, in our model, was essential for LPS-induced IEC apoptosis and shedding. This suggests that direct TNFR1 ligation occurs at the level of the IEC, although interactions in intermediary cell types, such as endothelial or myofibroblast cells, cannot be excluded. The role of TNFR2 has been less well characterized and interestingly the intestinal epithelial response to LPS was moderate in *Tnfr2*$^{-/-}$ mice, suggesting that this receptor does participate in LPS-induced IEC apoptosis, possibly by enhancing TNFR1 signals through degradation of TRAF2, resulting in termination of NFκB signaling (Rodríguez et al., 2011).

Mice deficient in NFκB1, an individual NFκB family member that signals via the canonical activation pathway, developed more IEC apoptosis and shedding in response to TNF than did WT mice. This is not surprising because TNFR1, as well as initiating apoptosis, also induces the expression of anti-apoptotic genes via NFκB (Wang et al., 1998). However, an interesting finding to emerge from our study was that mice deficient in NFκB2, an NFκB family member that signals via the alternative activation pathway, were more resistant to villus IEC apoptosis and shedding in response to TNF, compared with WT mice. This suggests that alternative NFκB2 pathway activation contributes to cell shedding and apoptosis. A possible mechanism to account for this effect could be due to the NFκB2 precursor acting as an inhibitor of NFκB activity (Basak et al., 2007; Fukushima et al., 2012). Absence of NFκB2 might therefore result in an extended expression of p65 (RelA)-induced anti-apoptotic genes (summarized in Fig. 7). The importance of p65 nuclear translocation in IECs that do not undergo shedding has been previously demonstrated in *Cryptosporidium parvum* infection (Foster et al., 2012). Alternatively, NFκB2-containing dimers might directly terminate the transcription of anti-apoptotic genes or induce the expression of proapoptotic genes.

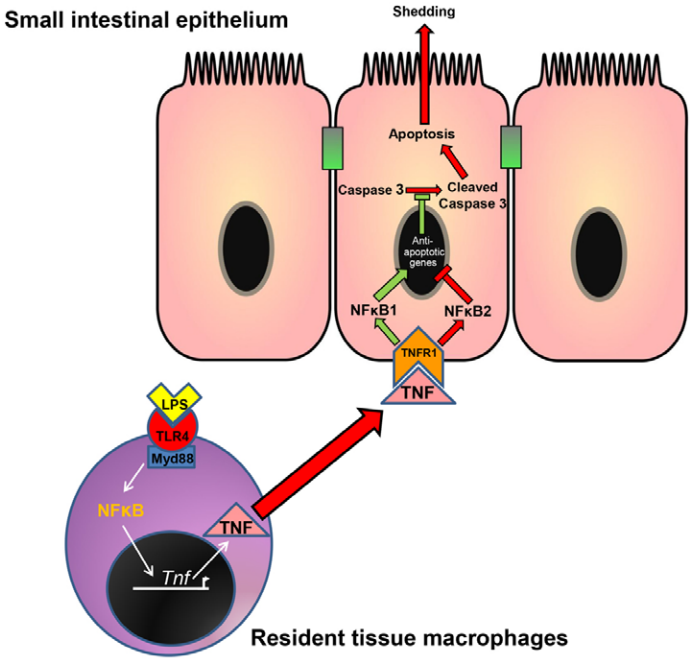

Fig. 7. Diagram summarizing the putative mechanism by which LPS induces apoptosis in IECs. Systemically delivered LPS is first recognized predominantly by resident TLR4-expressing mononuclear cells (monocytes/macrophages/dendritic cells), which produce TNF. TNF is released into the systemic circulation and binds with TNFR1 on IECs, triggering apoptosis and shedding if NFκB2 signaling dominates, or cell survival if NFκB1 signaling dominates.

In conclusion, we provide a detailed description of the early events and mechanisms that are responsible for acute, LPS-induced small intestinal injury. LPS therefore represents a robust, rapid and consistent stimulus for inducing pathological small intestinal epithelial cell apoptosis and shedding. Further study of this phenomenon could be highly relevant to our understanding of the initial pathogenesis of acute small intestinal disease states and diarrheal illnesses, and the intestinal manifestations of acute systemic disease states such as septic and endotoxic shock. Additionally, the very acute small intestinal lesions documented in this study might also contribute to development of chronic inflammation, such as is observed in IBD. Indeed, defective small intestinal permeability such as that which might occur in IEC shedding has been shown to contribute to the development of chronic colitis (Arrieta et al., 2009), meaning that this model might have relevance in CD or UC development. Ultimately, this could lead to the development of novel therapeutic strategies to ameliorate pathological villus epithelial cell apoptosis and shedding, and gut barrier dysfunction.

MATERIALS AND METHODS

Animals

Wild-type (WT) C57BL/6 mice supplied by Charles River (Margate, UK), and transgenic strains on a C57BL/6 background, including *Nfκb1*$^{-/-}$ and *Nfκb2*$^{-/-}$ mice (Caamaño et al., 1998; Sha et al., 1995)

and *Tlr4*$^{-/-}$ mice (Hoshino et al., 1999) (generated by Shizuo Akira and supplied by Mark Taylor) were maintained at the University of Liverpool. *Tnfr1*$^{-/-}$ and *Tnfr2*$^{-/-}$ mice (Peschon et al., 1998) were maintained at the Saban Research Institute at Children's Hospital Los Angeles. *Vil-Cre Myd88*$^{-/-}$ mice were maintained at the Disease Modelling Unit, University of East Anglia. All procedures were performed on adult mice (minimum age 9 weeks) under appropriate UK Home Office licenses or with approval and monitoring by the Children's Hospital Los Angeles Institutional Animal Care and Use Committee.

Generation of *Vil-Cre Myd88*$^{-/-}$ mice

Myd88$^{fl/fl}$, which express a truncated mutant Myd88 protein following removal of the floxed region, were bred with *Vil-Cre* mice, which conditionally express Cre recombinase under control of the villin promoter. Offspring were genotyped for the presence of WT *Myd88*, mutated *Myd88* and *Cre* alleles. Mice were on a C57BL/6 genetic background.

Lipopolysaccharide

LPS from *Escherichia coli* O111:B4 purified by phenol-extraction (PE-LPS) or ion-exchange chromatography (IE-LPS) (Sigma-Aldrich, Gillingham, UK) was diluted in sterile phosphate-buffered saline (PBS) and administered to mice by intraperitoneal (i.p.) injection.

TNF

Murine recombinant TNF (Peprotech Ltd, London, UK) was diluted in sterile water and administered by i.p. injection to mice at 0.33 mg/kg body weight.

Tissue processing

Following euthanasia, the intestinal tract was dissected *en bloc*. The intestinal lumina were flushed with PBS and immediately fixed in 10% neutral buffered formalin with selected organ samples. After 24 hours fixation, tissue was routinely processed and embedded in paraffin wax. Tissue sections (3-5 µm thickness) were prepared and stained either with H&E or used for immunohistochemistry (IHC).

Immunohistochemistry for apoptotic IECs

Tissue sections were treated with 1% hydrogen peroxide in methanol to block endogenous peroxidases, followed by heat-induced antigen retrieval in 0.01 M citrate acid buffer (pH 6) and incubation with a rabbit polyclonal anti-active-caspase-3 antibody (AF835: R&D Systems, Abingdon, UK). Peroxidase-labeled anti-rabbit EnVision™ (Dako, Cambridge, UK) and 3,3′-diaminobenzidine were used for visualization.

Quantification of active-caspase-3-positive cells

For quantification of apoptotic and shedding IECs, individual epithelial cells were counted from the base of the villus (above crypt level) to the mid-point of the villus tip in 18-20 well-orientated hemivilli at 400× magnification (delineated by red line in Fig. 2B). IECs were categorized according to the following criteria:

- 'normal' if there was no or weak diffuse non-specific brown staining and cells had a basally located basophilic nucleus;
- 'apoptotic' if there was defined positive staining that was confined to cytoplasmic or nuclear borders when compared with any background staining of neighboring IECs;
- 'shedding' if there was defined positive staining that was confined to cytoplasmic or nuclear borders and in addition there was apical elevation of the cytoplasmic membrane, and/or an apically positioned nucleus.

Crypt IECs were counted from the crypt base to the crypt-villus junction in 19-20 well-orientated duodenal hemicrypts per mouse. Crypt IECs were simply categorized as 'normal' or 'apoptotic' because no discernible evidence of shedding was observed within crypts.

Cell positional data

To allow comparison of cell positional data, villi were adjusted to a fixed length of 100 cells by using Wincrypts© software (Cancer Research Campaign 1999). Data are then represented as percentage of villus length, 0% therefore representing the villus base and 100% representing the villus tip.

Measurement of villus height

ImageJ (Schneider et al., 2012) was used to assess images captured by a Leica DMLA microscope, by setting the scale with a hemocytometer at 100× magnification. All images were captured at 100× magnification, and villi were measured by using the segmented line tool. Each segmented line was placed to originate at the base of the villus, above the level of adjoining crypts, and a segmented line extended to the villus tip, following any curvature of the villus. The mean of these segmented line lengths for ten well-orientated villi was calculated for each animal, and a mean value was then calculated for each group.

Gut permeability assessment

Fluorescein-isothiocyanate-conjugated dextran (FD4: Sigma-Aldrich, Gillingham, UK) was diluted to 22 mg/ml in PBS and administered at 20 ml/kg body weight by oral gavage ± i.p. injection of LPS. Plasma fluorescence was measured by a TECAN Infinite® F200 plate reader (excitation 485 nm, emission 535 nm) from blood collected post-mortem at 5 hours after gavage in order to allow FD4 to be distributed throughout the intestinal tract. Mice were euthanized via a rising CO_2 concentration and blood taken by cardiac puncture. To assess the effect of LPS on permeability, it was administered at set time points prior to the end of the experiment, i.e. at 1.5 hours, 3 hours and at the same time as FD4 for the 5-hour time point. Plasma was separated from heparinized whole blood by centrifugation at 5000 rpm for 2 minutes in a minicentrifuge.

Real-time PCR

Small intestinal extracts were isolated with chelation buffer solution as previously described (Flint et al., 1991), and RNA was isolated with a High Pure RNA Tissue Kit (Roche, Burgess Hill, UK). Reverse-transcription was performed with an RT^2 reverse-transcription kit (SABiosciences, Crawley, UK). An 89 gene Cell-Death Pathway Finder array (SABiosciences) was performed on a Roche LightCycler®480 followed by validation with replicate samples using TaqMan® gene expression assays for β-actin (Mm01205647_g1), TNF (Mm00443260_g1) and CD40 (Mm00441891_m1; Life Technologies, Paisley, UK). Cycling conditions were performed as per the manufacturer's instructions.

Data analysis

Data represent mean ± s.e.m. Comparisons were made between treatment groups and controls using SigmaPlot 12© (Systat Software, London, UK). Normally distributed data were assessed by ANOVA with Holm-Sidak post-hoc test, and non-parametric data were analyzed by ANOVA on ranks (Kruskal-Wallis) with Dunn's post-hoc test. $P<0.05$ was considered significant. REST© software was used for comparison of qPCR data from individualized samples by randomization test as previously described (Pfaffl et al., 2002). *n* numbers indicate the total number of mice studied.

ACKNOWLEDGEMENTS

The authors thank David Berry (University of Liverpool) for technical assistance, Mark Taylor and Alice Halliday (The Molecular and Biochemical Parasitology Group, Liverpool School of Tropical Medicine), Professor Shizuo Akira, and Associate Professor Satoshi Uematsu (Department of Host Defense, Research Institute for Microbial Diseases Osaka University, Japan) for the provision and use of *Tlr4*$^{-/-}$ mice. The authors also thank Simon Clare and Gordon Dougan, Wellcome Trust Sanger Institute, Cambridge, for the *Villin-Cre Myd88*$^{-/-}$ mouse strain.

COMPETING INTERESTS

The authors declare that they do not have any competing or financial interests.

AUTHOR CONTRIBUTIONS

J.M.W.: animal and laboratory procedures; data collection and analysis; histopathology; project development; composition of manuscript. C.A.D.: original conceptualization of project; animal and laboratory procedures; data analysis; manuscript preparation. A.J.M.W.: original conceptualization of project; grant and manuscript preparation. M.R.F.: animal and laboratory procedures; manuscript preparation. J.C.M.: animal and laboratory procedures; manuscript preparation. M.D.B.: laboratory procedures; data analysis; manuscript preparation. R.S.: data analysis, manuscript preparation. K.R.H.: animal and laboratory procedures; manuscript preparation. L.J.H.: animal and laboratory procedures; manuscript preparation. J.H.C.: provision of animal colonies; manuscript preparation. B.J.C.: original conceptualization of project; data analysis; grant and manuscript preparation. D.M.P.: original conceptualization of project; data analysis; grant and manuscript preparation.

FUNDING

J.M.W.'s PhD is funded by the Centre for Integrative Mammalian Biology and has also been supported by the *Journal of Comparative Pathology* Educational Trust. M.R.F. is supported by National Institutes of Health Grants K01DK077956 and R03DK090295 and a Senior Research Award from the Crohn's and Colitis Foundation of America. M.D.B. was funded by Wellcome Trust Research Training Fellowship 083823/Z/07/Z. J.H.C. was supported by the EU FP7 Integrated Project INFLACARE. This work was supported in part by a Biomedical Research Unit award from the National Institute for Health Research. K.R.H. gratefully acknowledges the support of the Biotechnology and Biological Sciences Research Council (BBSRC) Institute Strategic Programme grant for Gut Health and Food Safety BB/J004529/1. D.M.P. and B.J.C. are supported by SysmedIBD, which is funded by the European Commission within the 7th Framework Programme. A.J.M.W. and D.M.P. are supported by Wellcome Trust grant WT0087768MA. A.J.M.W. is also supported by BBSRC grant BB/J004529/1.

SUPPLEMENTARY MATERIAL

Supplementary material for this article is available at
http://dmm.biologists.org/lookup/suppl/doi:10.1242/dmm.013284/-/DC1

REFERENCES

Abreu, M. T. (2010). Toll-like receptor signalling in the intestinal epithelium: how bacterial recognition shapes intestinal function. *Nat. Rev. Immunol.* **10**, 131-144.

Arrieta, M. C., Madsen, K., Doyle, J. and Meddings, J. (2009). Reducing small intestinal permeability attenuates colitis in the IL10 gene-deficient mouse. *Gut* **58**, 41-48.

Basak, S., Kim, H., Kearns, J. D., Tergaonkar, V., O'Dea, E., Werner, S. L., Benedict, C. A., Ware, C. F., Ghosh, G., Verma, I. M. et al. (2007). A fourth IkappaB protein within the NF-kappaB signaling module. *Cell* **128**, 369-381.

Beutler, B., Greenwald, D., Hulmes, J. D., Chang, M., Pan, Y. C., Mathison, J., Ulevitch, R. and Cerami, A. (1985). Identity of tumour necrosis factor and the macrophage-secreted factor cachectin. *Nature* **316**, 552-554.

Beutler, B., Du, X. and Poltorak, A. (2001). Identification of Toll-like receptor 4 (Tlr4) as the sole conduit for LPS signal transduction: genetic and evolutionary studies. *J. Endotoxin Res.* **7**, 277-280.

Bullen, T. F., Forrest, S., Campbell, F., Dodson, A. R., Hershman, M. J., Pritchard, D. M., Turner, J. R., Montrose, M. H. and Watson, A. J. (2006). Characterization of epithelial cell shedding from human small intestine. *Lab. Invest.* **86**, 1052-1063.

Caamaño, J. H., Rizzo, C. A., Durham, S. K., Barton, D. S., Raventós-Suárez, C., Snapper, C. M. and Bravo, R. (1998). Nuclear factor (NF)-κ B2 (p100/p52) is required for normal splenic microarchitecture and B cell-mediated immune responses. *J. Exp. Med.* **187**, 185-196.

Chow, J. C., Young, D. W., Golenbock, D. T., Christ, W. J. and Gusovsky, F. (1999). Toll-like receptor-4 mediates lipopolysaccharide-induced signal transduction. *J. Biol. Chem.* **274**, 10689-10692.

Cinel, I., Buyukafsar, K., Cinel, L., Polat, A., Atici, Ş., Tamer, L. and Oral, U. (2002). The role of poly(ADP-ribose) synthetase inhibition in preventing endotoxemia-induced intestinal epithelial apoptosis. *Pharmacol. Res.* **46**, 119-127.

Coopersmith, C. M., Stromberg, P. E., Davis, C. G., Dunne, W. M., Amiot, D. M., II, Karl, I. E., Hotchkiss, R. S. and Buchman, T. G. (2003). Sepsis from Pseudomonas aeruginosa pneumonia decreases intestinal proliferation and induces gut epithelial cell cycle arrest. *Crit. Care Med.* **31**, 1630-1637.

Copeland, S., Warren, H. S., Lowry, S. F., Calvano, S. E., Remick, D.; Inflammation and the Host Response to Injury Investigators (2005). Acute inflammatory response to endotoxin in mice and humans. *Clin. Diagn. Lab. Immunol.* **12**, 60-67.

Flint, N., Cove, F. L. and Evans, G. S. (1991). A low-temperature method for the isolation of small-intestinal epithelium along the crypt-villus axis. *Biochem. J.* **280**, 331-334.

Foster, D. M., Stauffer, S. H., Stone, M. R. and Gookin, J. L. (2012). Proteasome inhibition of pathologic shedding of enterocytes to defend barrier function requires X-linked inhibitor of apoptosis protein and nuclear factor kappaB. *Gastroenterology* **143**, 133-144.e4.

Fukushima, H., Matsumoto, A., Inuzuka, H., Zhai, B., Lau, A. W., Wan, L., Gao, D., Shaik, S., Yuan, M., Gygi, S. P. et al. (2012). SCF(Fbw7) modulates the NFkB signaling pathway by targeting NFkB2 for ubiquitination and destruction. *Cell Rep* **1**, 434-443.

Gadjeva, M., Wang, Y. and Horwitz, B. H. (2007). NF-kappaB p50 and p65 subunits control intestinal homeostasis. *Eur. J. Immunol.* **37**, 2509-2517.

Garside, P., Bunce, C., Tomlinson, R. C., Nichols, B. L. and Mowat, A. M. (1993). Analysis of enteropathy induced by tumour necrosis factor alpha. *Cytokine* **5**, 24-30.

Guma, M., Stepniak, D., Shaked, H., Spehlmann, M. E., Shenouda, S., Cheroutre, H., Vicente-Suarez, I., Eckmann, L., Kagnoff, M. F. and Karin, M. (2011). Constitutive intestinal NF-κB does not trigger destructive inflammation unless accompanied by MAPK activation. *J. Exp. Med.* **208**, 1889-1900.

Hollander, D., Vadheim, C. M., Brettholz, E., Petersen, G. M., Delahunty, T. and Rotter, J. I. (1986). Increased intestinal permeability in patients with Crohn's disease and their relatives. A possible etiologic factor. *Ann. Intern. Med.* **105**, 883-885.

Hornef, M. W., Frisan, T., Vandewalle, A., Normark, S. and Richter-Dahlfors, A. (2002). Toll-like receptor 4 resides in the Golgi apparatus and colocalizes with internalized lipopolysaccharide in intestinal epithelial cells. *J. Exp. Med.* **195**, 559-570.

Hoshino, K., Takeuchi, O., Kawai, T., Sanjo, H., Ogawa, T., Takeda, Y., Takeda, K. and Akira, S. (1999). Cutting edge: Toll-like receptor 4 (TLR4)-deficient mice are hyporesponsive to lipopolysaccharide: evidence for TLR4 as the Lps gene product. *J. Immunol.* **162**, 3749-3752.

Jacque, E., Tchenio, T., Piton, G., Romeo, P.-H. and Baud, V. (2005). RelA repression of RelB activity induces selective gene activation downstream of TNF receptors. *Proc. Natl. Acad. Sci. USA* **102**, 14635-14640.

Julian, M. W., Bao, S., Knoell, D. L., Fahy, R. J., Shao, G. and Crouser, E. D. (2011). Intestinal epithelium is more susceptible to cytopathic injury and altered permeability than the lung epithelium in the context of acute sepsis. *Int. J. Exp. Pathol.* **92**, 366-376.

Kawai, T. and Akira, S. (2011). Toll-like receptors and their crosstalk with other innate receptors in infection and immunity. *Immunity* **34**, 637-650.

Kiesslich, R., Goetz, M., Angus, E. M., Hu, Q., Guan, Y., Potten, C., Allen, T., Neurath, M. F., Shroyer, N. F., Montrose, M. H. et al. (2007). Identification of epithelial gaps in human small and large intestine by confocal endomicroscopy. *Gastroenterology* **133**, 1769-1778.

Kiesslich, R., Duckworth, C. A., Moussata, D., Gloeckner, A., Lim, L. G., Goetz, M., Pritchard, D. M., Galle, P. R., Neurath, M. F. and Watson, A. J. (2012). Local barrier dysfunction identified by confocal laser endomicroscopy predicts relapse in inflammatory bowel disease. *Gut* **61**, 1146-1153.

Lai, C. W., Sun, T. L., Lo, W., Tang, Z. H., Wu, S., Chang, Y. J., Wu, C. C., Yu, S. C., Dong, C. Y. and Chen, L. W. (2013). Shedding-induced gap formation contributes to gut barrier dysfunction in endotoxemia. *J. Trauma Acute Care Surg.* **74**, 203-213.

Lau, K. S., Juchheim, A. M., Cavaliere, K. R., Philips, S. R., Lauffenburger, D. A. and Haigis, K. M. (2011). In vivo systems analysis identifies spatial and temporal aspects of the modulation of TNF-α-induced apoptosis and proliferation by MAPKs. *Sci. Signal.* **4**, ra16.

Leblond, C. P. and Stevens, C. E. (1948). The constant renewal of the intestinal epithelium in the albino rat. *Anat. Rec.* **100**, 357-377.

Liu, J. J., Madsen, K. L., Boulanger, P., Dieleman, L. A., Meddings, J. and Fedorak, R. N. (2011). Mind the gaps: confocal endomicroscopy showed increased density of small bowel epithelial gaps in inflammatory bowel disease. *J. Clin. Gastroenterol.* **45**, 240-245.

Locksley, R. M., Killeen, N. and Lenardo, M. J. (2001). The TNF and TNF receptor superfamilies: integrating mammalian biology. *Cell* **104**, 487-501.

Madara, J. L. (1990). Maintenance of the macromolecular barrier at cell extrusion sites in intestinal epithelium: physiological rearrangement of tight junctions. *J. Membr. Biol.* **116**, 177-184.

McAllister, C. S., Lakhdari, O., Pineton de Chambrun, G., Gareau, M. G., Broquet, A., Lee, G. H., Shenouda, S., Eckmann, L. and Kagnoff, M. F. (2013). TLR3, TRIF, and caspase 8 determine double-stranded RNA-induced epithelial cell death and survival in vivo. *J. Immunol.* **190**, 418-427.

Mizoguchi, E., Mizoguchi, A., Takedatsu, H., Cario, E., de Jong, Y. P., Ooi, C. J., Xavier, R. J., Terhorst, C., Podolsky, D. K. and Bhan, A. K. (2002). Role of tumor necrosis factor receptor 2 (TNFR2) in colonic epithelial hyperplasia and chronic intestinal inflammation in mice. *Gastroenterology* **122**, 134-144.

Pålsson-McDermott, E. M. and O'Neill, L. A. J. (2004). Signal transduction by the lipopolysaccharide receptor, Toll-like receptor-4. *Immunology* **113**, 153-162.

Peschon, J. J., Torrance, D. S., Stocking, K. L., Glaccum, M. B., Otten, C., Willis, C. R., Charrier, K., Morrissey, P. J., Ware, C. B. and Mohler, K. M. (1998). TNF receptor-deficient mice reveal divergent roles for p55 and p75 in several models of inflammation. *J. Immunol.* **160**, 943-952.

Pfaffl, M. W., Horgan, G. W. and Dempfle, L. (2002). Relative expression software tool (REST) for group-wise comparison and statistical analysis of relative expression results in real-time PCR. *Nucleic Acids Res.* **30**, e36.

Piguet, P. F., Vesin, C., Guo, J., Donati, Y. and Barazzone, C. (1998). TNF-induced enterocyte apoptosis in mice is mediated by the TNF receptor 1 and does not require p53. *Eur. J. Immunol.* **28**, 3499-3505.

Potten, C. S. and Loeffler, M. (1990). Stem cells: attributes, cycles, spirals, pitfalls and uncertainties. Lessons for and from the crypt. *Development* **110**, 1001-1020.

Rodríguez, M., Cabal-Hierro, L., Carcedo, M. T., Iglesias, J. M., Artime, N., Darnay, B. G. and Lazo, P. S. (2011). NF-kappaB signal triggering and termination by tumor necrosis factor receptor 2. *J. Biol. Chem.* **286**, 22814-22824.

Schneider, C. A., Rasband, W. S. and Eliceiri, K. W. (2012). NIH Image to ImageJ: 25 years of image analysis. *Nat. Methods* **9**, 671-675.

Sha, W. C., Liou, H.-C., Tuomanen, E. I. and Baltimore, D. (1995). Targeted disruption of the p50 subunit of NF-κ B leads to multifocal defects in immune responses. *Cell* **80**, 321-330.

Shimazu, R., Akashi, S., Ogata, H., Nagai, Y., Fukudome, K., Miyake, K. and Kimoto, M. (1999). MD-2, a molecule that confers lipopolysaccharide responsiveness on Toll-like receptor 4. *J. Exp. Med.* **189**, 1777-1782.

Wang, C.-Y., Mayo, M. W., Korneluk, R. G., Goeddel, D. V. and Baldwin, A. S., Jr (1998). NF-kappaB antiapoptosis: induction of TRAF1 and TRAF2 and c-IAP1 and c-IAP2 to suppress caspase-8 activation. *Science* **281**, 1680-1683.

Wright, S. D., Ramos, R. A., Tobias, P. S., Ulevitch, R. J. and Mathison, J. C. (1990). CD14, a receptor for complexes of lipopolysaccharide (LPS) and LPS binding protein. *Science* **249**, 1431-1433.